

**Metabolic dynamics and compartmentation
in the central metabolism of Chinese hamster ovary cells**

Dissertation

zur Erlangung des Grades

des Doktors der Naturwissenschaften

der Naturwissenschaftlich-Technischen Fakultät III

Chemie, Pharmazie, Bio- und Werkstoffwissenschaften

der Universität des Saarlandes

von

Judith Wahrheit

Saarbrücken

2014

Tag des Kolloquiums: 10.04.2015

Dekan: Prof. Dr. Dirk Bähre

Berichterstatter: Prof. Dr. Elmar Heinzle
Prof. Dr. Manfred Schmitt
Prof. Dr. Diethard Mattanovich

Vorsitz: Prof. Dr. Gert-Wieland Kohring

Akad. Mitarbeiter: Dr. Frank Hannemann

*"Dans la vie, il n'y a pas de solutions. Il y a des forces en marche:
il faut les créer et les solutions suivent"*

(Antoine de Saint-Exupéry, Vol de Nuit)

*"Imagination is more important than knowledge.
For knowledge is limited"*

(Albert Einstein)

*"Pour ce qui est de l'avenir, il ne s'agit pas de le prévoir,
mais de le rendre possible."*

(Antoine de Saint-Exupéry, La citadelle)

meiner Mama

Zusammenfassung

Die Arbeit zielte darauf ab, unser Wissen in Bezug auf metabolische Kompartimentierung im Stoffwechsel von Säugerzellen voranzubringen. Im Mittelpunkt stand die Untersuchung des Zentralmetabolismus und dessen Kontrolle in *Chinese hamster ovary* (CHO) Zellen. Eine notwendige Voraussetzung für diese Arbeit war die Entwicklung und Umsetzung einer Reihe von innovativen Methoden, u.a. die Analyse von extra- und intrazellulären Markierungsdynamiken, nicht-stationäre ^{13}C metabolische Flussanalyse, Bestimmung von kompartiment-spezifischen Enzymaktivitäten sowie Elementarmodenanalyse des mitochondrialen Stoffwechsels in selektiv permeabilisierten Zellen. Die Ergebnisse dieser Arbeit erweitern unser Verständnis der metabolischen Kontrolle an der Grenzfläche zwischen Zytosol und Mitochondrien, einschließlich der Kontrolle durch mitochondriale Transporter. Darüber hinaus werden Aspekte der Verknüpfung zwischen Glykolyse und TCA Zyklus, Mikrokompartimentierung und *Channeling*, Metabolitenaustausch zwischen Zellen und extrazellulärem Medium, sowie allgemein die Dynamik des Stoffwechsels beleuchtet. Die umfassenden Erkenntnisse tragen dazu bei, die Komplexität des Säugerstoffwechsels sowie die verschiedenen Spielarten von Stoffwechselkompartimentierung besser zu begreifen. Wissen über die Kontrolle des Stoffwechsels eröffnet neue Perspektiven zur Verbesserung von biotechnologischen Produktionsprozessen sowie zur Behandlung von schweren Krankheiten.

Abstract

The thesis aimed at advancing our knowledge about metabolic compartmentation in the metabolism of mammalian cells. The focus of the study was the central metabolism and its control in Chinese hamster ovary (CHO) cells. An essential part of the work was the development and implementation of innovative methods, e.g. the analysis of extra- and intracellular labeling dynamics, non-stationary ^{13}C metabolic flux analysis, determination of compartment-specific enzyme activities, and elementary mode analysis of the mitochondrial metabolism in selectively permeabilized cells. The results of this thesis increase our understanding of metabolic control at the cytosol-mitochondria interface, including control by mitochondrial transporters. In addition the work highlights aspects in the connection of glycolysis and TCA cycle, microcompartmentation and channeling, metabolite exchange between cells and extracellular medium, as well as metabolic dynamics in general. The comprehensive findings contribute to a deeper understanding of the complexity of mammalian metabolism and the various manifestations of metabolic compartmentation. Understanding the control of metabolism opens up new perspectives for improving biotechnological production processes and designing successful therapies for the treatment of severe diseases.

Extended abstract

The presented thesis provides an in-depth quantitative characterization of the central metabolism and its control in Chinese hamster ovary (CHO) cells. The work focused on studying the dynamics of metabolic compartmentation with a special emphasis on the connection between cytosolic glycolysis and mitochondrial TCA cycle. Different innovative experimental strategies and advanced computational methods were developed and implemented to approach the complexity of metabolic dynamics and compartmentation. The work is composed of seven subprojects that are structured into three major parts that build on each other.

In the first part, general characteristics of the CHO-K1 cell metabolism are described using **metabolite balancing** methods.

The combination of dynamic metabolic flux analysis (MFA) and determination of compartmental enzyme activities was used to investigate the CHO-K1 cell central metabolism in *chapter 2*. Different metabolic phases in CHO cell batch cultivation were distinguished and characterized by their dominating metabolic state, (i) overflow metabolism, (ii) balanced metabolism, and (iii) maintenance metabolism. The time-resolved analysis of specific metabolic ratios was demonstrated as useful strategy to assess metabolic efficiency and to monitor very sensitively metabolic shifts between different growth phases. Furthermore, we studied **metabolic control at the cytosol–mitochondria interface in different growth phases of CHO cells**. By integrating the information about *in situ* enzyme activities including their compartmental localization with *in vivo* metabolic fluxes, we were able to gain knowledge about metabolic regulation at overflow metabolism and balanced metabolism. We identified the hexokinase and the mitochondrial isocitrate dehydrogenase activities as rate-limiting steps in glycolysis and TCA cycle, respectively. Fine-tuning of glycolytic regulation was facilitated by a dynamic shift between glycolytic channeling and free diffusion of glycolytic intermediates. We propose that glycolytic channeling affects the availability of pyruvate for the mitochondria. In addition, we demonstrated that changing availabilities of TCA cycle substrates can be compensated and balanced by a tailored adjustment of the activities of aminotransferases and anaplerotic enzymes. Two follow-up studies presented in chapters 3 and 4 focused on investigating the availability of glutamine and pyruvate as the two most significant carbon sources for the mitochondrial metabolism in more detail.

In *chapter 3*, we analyzed the **dynamics of growth and metabolism controlled by glutamine availability**. A refined and improved dynamic metabolic flux analysis method was applied to capture metabolic dynamics in eight batch- and fed-batch cultivations with different glutamine supply (excess, sufficiency, scarcity, limitation). Varying glutamine availability resulted in global metabolic changes. We observed dose-dependent effects of glutamine in batch cultivation. Identifying metabolic links from the glutamine metabolism to specific metabolic pathways, we

showed that glutamine feeding results in its coupling to TCA cycle fluxes and in its decoupling from metabolic waste production. Furthermore, we analyzed the cellular responses upon mild or severe glutamine limitation and upon ammonia stress due to glutamine excess and provide a mechanistic explanation for the transition between these extreme states. Increased ammonia levels resulted in reduced growth rates. Mild glutamine limiting conditions stimulated growth and supported culture longevity. Glutamine limitation and ammonia stress were successfully compensated in CHO-K1 cells by flux rearrangements in the pyruvate and amino acid metabolism.

In *chapter 4*, we studied the **perturbation of the mammalian pyruvate metabolism and resulting rearrangement of central metabolic fluxes**. Two different biochemical effectors, dichloroacetic acid (DCA) and α -cyano-4-hydroxy-cinnamic acid (CHC), were used to either stimulate or inhibit the flux of pyruvate into the TCA cycle. Metabolic perturbation was successful at low CHC and DCA concentrations. High effector concentrations, in contrast, resulted in efficient metabolic compensation confirming the remarkable robustness and flexibility of CHO cells. However, an efficient compensation of CHC and DCA effects was strictly dependent on glutamine availability. Glutamine depletion provoked emergence of the anticipated effects at high CHC and DCA concentrations later in the cultivation. We demonstrated that the cellular energy state of CHO-K1 cells remained robust upon severe perturbation of the cellular pyruvate metabolism. However, susceptibility to low effector concentrations and at glutamine depletion reveals limitations of robustness.

In the second part of the thesis, we provide a more in-depth analysis of the CHO cell metabolism aiming at the resolution of very detailed metabolic networks with respect to compartmentation. This was achieved using highly informative ^{13}C labeling experiments in combination with **non-stationary ^{13}C metabolic flux analysis (INST-MFA)**.

In *chapter 5*, **non-stationary ^{13}C metabolic flux analysis in CHO cell batch culture using extracellular labeling** was successfully applied to **highlight metabolic reversibility and compartmentation**. We determined the mass isotopomer dynamics of eight extracellular metabolites derived from $[\text{U-}^{13}\text{C}_6]$ glucose as labeled substrate. The consideration of metabolic compartmentation and extracellular transport reversibility was essential to successfully describe the labeling dynamics. In parallel, we demonstrated that a simpler network neglecting metabolic compartmentation failed to reproduce the data. This highlights the importance of including metabolic compartmentation to obtain a meaningful representation of cellular physiology. Pivotal reactions in the connection of C3 and C4 pools (phosphoenolpyruvate carboxykinase, malic enzyme and pyruvate carboxylase) as well as simultaneous synthesis and degradation of several amino acids were successfully determined. Furthermore, the results of the parameter estimation confirm the idea of a mixed outcome of glycolysis by partial channeling and partial free diffusion of glycolytic intermediates as previously proposed in chapter 2. Most metabolites were reversibly exchanged with

the media. The reversibility of pyruvate and alanine production rates changed dynamically even if their net fluxes remained constant.

High resolution ^{13}C metabolic flux analysis in CHO cells using extra- and intracellular labeling dynamics derived from parallel labeling experiments using $[\text{U-}^{13}\text{C}_6]$ glucose and $[\text{U-}^{13}\text{C}_5]$ glutamine as substrates is presented in *chapter 6*. INST-MFA was applied to resolve the metabolic fluxes, reversibilities and intracompartmental concentrations in a complex metabolic network that included mitochondrial transport, metabolite compartmentation and channeling. Compared to the highly efficient reactor cultivation described in chapter 5, these shake flask cultivations were characterized by (1) a higher lactate/glucose ratio, (2) smaller TCA cycle flux, (3) lower connectivity between glycolysis and TCA cycle and (4) reduced catabolism of essential amino acids. On the other hand, a high pentose phosphate pathway activity, simultaneous catabolism and production of non-essential amino acids and excessive metabolite exchange with the extracellular media were observed consistently for both cultivation conditions. Malate and glutamate were cycled via several transporters between cytosol and mitochondria. The labeling dynamics of lactate and pyruvate indicate various metabolite channeling effects in the cytosol and the mitochondria as well as the existence of a mitochondrial lactate pool that serves most likely as intramitochondrial short-term redox buffer.

The last part of this thesis brings the focus on detailed **mitochondrial studies using selectively permeabilized cells**.

In *chapter 7*, we demonstrated a **high-throughput respiration screening** for functional *in situ* mitochondrial studies in permeabilized CHO cells. Determination of oxygen uptake rates verified transporter-mediated uptake and metabolization of mitochondrial substrates and allowed a distinction of substrates according to TCA cycle regulation. Metabolic regulation was different for reactions (i) in the first half, (ii) in the second half and (iii) at the initiation of the TCA cycle. Metabolization of substrates entering the first half was highly controlled by the energy state, while respiration on metabolites entering the second half of the cycle was less controlled. Metabolization of pyruvate was very strictly regulated by several independent mechanisms; energy state, phosphorylation as well as availability of CoA. A moderate stimulation of pyruvate metabolization could be accomplished by feeding both pyruvate and aspartate simultaneously.

The outcome of the respiration screening served as starting point for designing detailed mitochondrial studies presented in *chapter 8*. We accessed the mitochondrial metabolism of CHO cells by selective permeabilization and quantified mitochondrial uptake and production of several substrates without and with addition of ADP. **Elementary mode analysis of the mitochondrial metabolism** was applied to establish the contribution of different pathways to the metabolism of a substrate or substrate combination. Metabolic stimulation with ADP favored full metabolization of substrates to CO_2 while production of byproducts from partial TCA cycle was not enhanced.

Consistent with the findings of the respiration screening, the controlling effect of ADP was more pronounced when we supplied metabolites to the first part of the TCA cycle. Interestingly, mitochondrial aspartate uptake occurred only in combination with pyruvate but not alone suggesting a complex regulation of these reactions. Isocitrate dehydrogenase was confirmed as key control element of the TCA cycle.

The results of these different studies are synergistically discussed in the final conclusion (*chapter 9*) in order to provide a comprehensive picture of the central metabolism in CHO cells. Potential implications of these findings as well as future applications of the established novel methods are presented. The outlook proposes future steps towards increasing our knowledge about the compartmented mammalian metabolism (*chapter 10*).

Table of contents

	Zusammenfassung	5
	Abstract	5
	Extended abstract	6
1	General introduction	13
Part I	General characterization of the CHO cell metabolism using metabolite balancing methods	37
2	Metabolic control at the cytosol–mitochondria interface in different growth phases of CHO cells	39
3	Dynamics of growth and metabolism controlled by glutamine availability in Chinese hamster ovary cells	65
4	Perturbation of the mammalian pyruvate metabolism and resulting rearrangement of central metabolic fluxes in CHO cells	89
Part II	In-depth metabolic characterization of CHO cells using labeling studies and non-stationary ^{13}C metabolic flux analysis	109
5	Non-stationary ^{13}C metabolic flux analysis of Chinese hamster ovary cells in batch culture using extracellular labeling highlights metabolic reversibility and compartmentation	111
6	High resolution ^{13}C metabolic flux analysis in CHO cells	133
Part III	Detailed studies of mitochondrial metabolism using selectively permeabilized CHO cells	151
7	High-throughput respiration screening of single mitochondrial substrates using permeabilized CHO cells	153
8	Elementary mode analysis of the mitochondrial metabolism in selectively permeabilized CHO cells	173
9	Conclusion	195
10	Outlook and future prospects	213
11	References	214
12	Supplementary material	241
	Danksagung	269
	Curriculum Vitae	271

1 General introduction

1.1 Chinese hamster ovary cells – major workhorse of the biopharmaceutical industry and mammalian model system for more than 50 years

1.1.1 Applications and impact of mammalian cell cultures in research, production and therapy

Mammalian cell cultures are an indispensable tool in basic research, biotechnological production and therapeutic applications. Our current knowledge about cell function and physiology is mainly derived from studying basic biological questions *in vitro* using cultivated primary cells or stable cell lines (Freshney, 2010). Furthermore, cultured mammalian cells are increasingly used for toxicity assessment and drug screening thereby contributing to replace, reduce and refine animal testing in the development of drugs and cosmetics (Beckers et al., 2009; Niklas et al., 2009; Noor et al., 2009; Strigun et al., 2011a; Strigun et al., 2011b; Strigun et al., 2012). More recently, significant progress in cell culture technology, including specific media development and the use of scaffolds, allow mimicking the natural *in vivo* environment of cells and tissues and facilitate a longer maintenance of cell cultures (Gunness et al., 2013; Klein et al., 2014a). This makes them also amenable for long-term toxicity studies (Mueller et al., 2013; Mueller et al., 2014) as well as for tissue engineering approaches for the replacement or repair of damaged tissue (Berthiaume et al., 2011; Fisher and Mauck, 2013). Cell- and gene-based therapies provide new therapeutic strategies and have great potential in the targeted treatment of severe diseases (Fischbach et al., 2013; Ye et al., 2013). Biotechnological production is another major field of application for mammalian cells. Especially continuous cell lines play an important role in the industrial production of biopharmaceuticals and viruses. Viruses are produced for viral vaccines in human and veterinary use and for gene therapy using viral vectors (Genzel and Reichl, 2009). Vaccine production in cultured mammalian cells represents a safe and efficient alternative to more conventional vaccine production in chicken eggs. It is expected to become increasingly important in the future. The large scale manufacture of recombinant proteins using mammalian cell lines continues to revolutionize the medical sector (Wurm, 2004). Monoclonal antibodies and other proteins are produced for diagnostic and therapeutic use. The clinical applications of these therapeutic proteins open up new opportunities in the treatment of pathological conditions and give new hope to patients suffering from life-threatening diseases.

1.1.2 The global biopharmaceutical market

The biologics (biopharmaceutical, biologic medical product) sector represents the fastest growing market in pharmaceutical industry worldwide. In Germany, the biopharmaceutical market grew by 11% in 2012 (to ~ €6 billion) (Biotech-Report 2013, Verband forschender Arzneimittelhersteller and Boston Consulting Group, www.vfa.de). In the United States, the total sales of biologics even increased by 18.2% (to \$63.6 billion) in 2012 (Aggarwal, 2014). This is a more than seven-fold higher growth compared to the overall pharmaceutical industry. More than 200 biopharmaceutical products are currently on the market and many more are going to be launched in the coming years (Walsh, 2010a). Monoclonal antibodies are the best-selling class of biologics accounting for 38.5% of the total biopharmaceutical market in 2012 in the United States (Aggarwal, 2014). Future prospects for the biopharmaceutical industry are optimistic. While worldwide sales of biologics accounted for \$99 billion in 2009 (Walsh, 2010a), global sales of \$178.4 billion in 2017 were recently forecasted by the business information company Visiongain (www.visiongain.com).

1.1.3 Industrial production of recombinant therapeutic proteins in

Chinese hamster ovary cells

Mammalian cells are the primary cultivation system for the industrial production of biopharmaceuticals. In contrast to microbial production systems, mammalian cells are able to perform human-compatible post-translational modifications, such as proper assembling, folding and glycosylation, which are critical for activity, stability and safety of therapeutic proteins (Walsh, 2010b; Walsh and Jefferis, 2006). Chinese hamster ovary (CHO) cells are the most commonly used cell factories for the large-scale commercial production of recombinant proteins (e.g. antibodies, growth factors, hormones, blood factors) (Datta et al., 2013). Due to their favorable characteristics CHO cells outperform several other mammalian cell lines including hybridoma, myeloma, human-derived and embryonic-stem-cell-derived cell lines (e.g. NS0, BHK, HEK-293, Per.C6). CHO cells are easily adapted to grow in suspension in serum-free, chemically-defined media. The use of media containing undefined animal components (e.g. fetal calf serum) is undesirable in biopharmaceutical manufacturing because they exhibit high batch-to-batch variability leading to unpredictable results. Even more importantly, there are serious safety concerns since they bear the risk of virus or prion contamination. Furthermore, CHO cells have been demonstrated as safe host for the production of biologics. In particular, they do not allow replication of many human pathogenic viruses (HIV, influenza, hepatitis B, polio, herpes, measles etc.). A common disadvantage of using mammalian host cells for recombinant protein production is a low specific productivity compared to microbial systems. This can be overcome by a number of efficient gene amplification systems that are established for CHO cells (e.g. DHFR/methotrexate, glutamine synthetase/methionine sulfoxamine) (Wurm, 2004). In addition, they can be easily genetically modified, achieve very high cell densities and have the capacity for high expression levels reaching yields on the order of 5 g/liter and more

(Walsh, 2010a). Currently, about 70% of all biopharmaceuticals are produced in CHO cells (Datta et al., 2013; Jayapal et al., 2007). Although recent advances in cell culture technology and process development have achieved significant improvements in productivity, further optimization of host cell lines and production processes are required to meet the demand of a rapidly increasing market (Dietmair et al., 2011; Kim et al., 2012; Walsh, 2010a). So far, optimization strategies were mostly based on empirical findings and/or used screening methods in combination with design of experiments (DoE) principles. However, emerging new technologies and systems biology studies are expected to pave the way for more rational engineering and optimization strategies in the development of high-yielding producer cells in the future (Schaub et al., 2012).

1.1.4 A retrospect on the history of Chinese hamster ovary cells

Chinese hamsters have been introduced as laboratory species in 1919 and have been mostly used in epidemiological and radiation research. The first stable CHO cell line has been established in 1957 (Puck et al., 1958). Since then, they have been used in numerous studies of basic biological and biomedical research resulting in their terming as “the mammalian equivalent of the model bacterium *E. coli*” (Jayapal et al., 2007). Their immense adaptability to various culture conditions and ease in genetic manipulation made them an interesting system for heterologous protein production. In 1987, the first recombinant therapeutic protein manufactured in a mammalian system and approved by the Food and Drug Administration (FDA) was produced in CHO cells (tissue plasminogen activator, Activase, Genentech) (Kaufman et al., 1985). This marked the beginning breakthrough of CHO cells as major workhorse for the biopharmaceutical industry. After the foundation of the Consortium on Chinese hamster ovary cell genomics in 2006, the long-awaited draft genomic sequence of the ancestral CHO-K1 cell line has finally been published in 2011 (Xu et al., 2011). However, due to inherent genetic instability and intentional mutagenesis large genome rearrangements have occurred in different CHO cell lines since their first isolation in 1957. Even small variations in culture conditions, media composition, and process parameters (e.g. pH, $k_L a$) can induce clonal selection to CHO cell subpopulations (Wurm, 2007). In 2013, the genome sequences of the Chinese hamster (*Cricetulus griseus*) along with the sequences of seven CHO cell lines derived from the major CHO cell lineages have been published (Lewis et al., 2013). This provides a more complete picture of the genomic heterogeneity in different CHO cell lines and a sound starting point for further studies.

1.1.5 The emerging CHO cell systems biology era

Considering the immense importance of CHO cells as mammalian model system and industrial host cell line, knowledge about CHO cell physiology is surprisingly limited and rudimentary compared to other (microbial) cell factories (e.g. *Escherichia coli*, *Saccharomyces cerevisiae*) (Kildegaard et al., 2013). The availability of genomic resources for CHO cells (Lewis et al., 2013; Xu et al., 2011) opens up new opportunities for systems biology studies and optimization of biopharmaceutical protein production. The application of different ‘omics technologies, including genomics,

transcriptomics (Becker et al., 2011), proteomics (Baycin-Hizal et al., 2012), glycomics (North et al., 2010), metabolomics (Chong et al., 2012; Chong et al., 2011; Selvarasu et al., 2012) and fluxomics (Ahn and Antoniewicz, 2012; Niklas and Heinzle, 2012; Wahrheit et al., 2011), and the integration of these data sets into mathematical models will provide a fundamental understanding of the complex CHO cell physiology. This is expected to guide cell line development and metabolic engineering to further improve protein production in CHO cells.

1.2 The central carbon metabolism in Chinese hamster ovary cells

A simplified scheme of the metabolism in cultivated mammalian cells is depicted in Figure 1-1. Glucose and glutamine are the major carbon sources fueling catabolism. ATP and NADPH produced by catabolic processes drive anabolic reactions for biomass production and possibly synthesis of the product of interest (e.g. therapeutic proteins such as antibodies, hormones, growth factors, blood factors). The formation of the (amplified) recombinant protein product can impose a substantial and very specific metabolic burden regarding biosynthetic precursors, energy demand and required post-translational modifications (Klein et al., 2014b; Niklas et al., 2013). Mammalian cells are usually cultivated in very nutrient-rich culture media. High uptake rates of glucose, glutamine and other substrates exceeding anabolic requirements are correlated with the accumulation of by-products, such as lactate, ammonia and alanine. The following section will give a short overview about the central metabolic pathways in mammalian cells, highlight the cellular localization of metabolic activities and illustrate the current knowledge about characteristics that are specific for CHO cells.

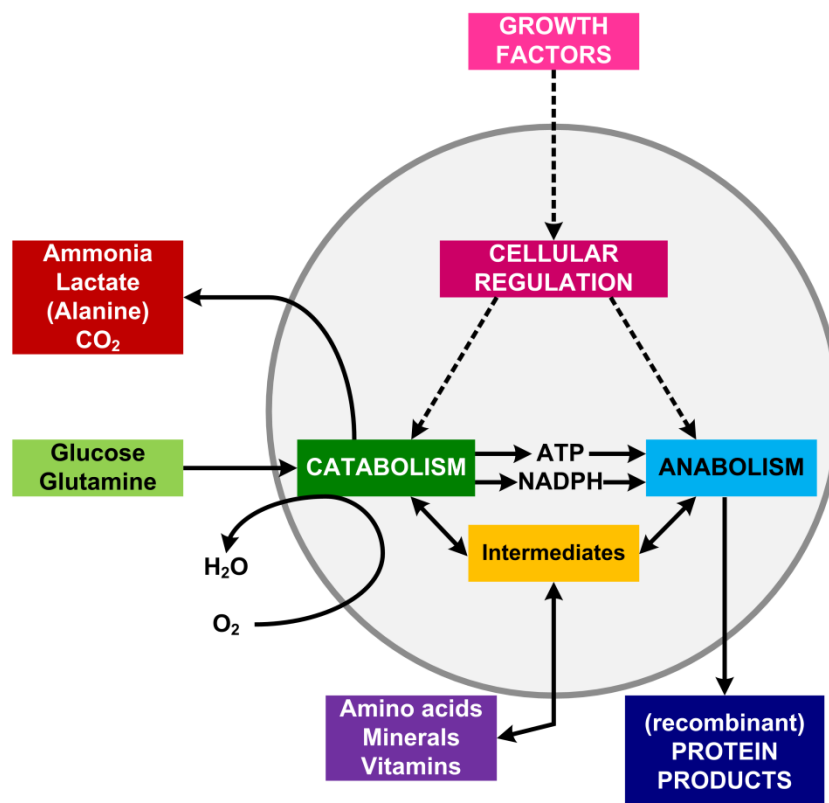


Figure 1-1. Scheme of the central metabolism in cultivated mammalian cells. The figure was inspired and modified from (Glacken, 1988).

1.2.1 Glycolysis and lactate metabolism

The glycolytic pathway converts glucose (and other hexoses) into 2 pyruvate generating 2 ATP and 2 NADH. It contains three irreversible steps with potential regulatory functions, namely the hexokinase (HK), the phosphofruktokinase (PFK) and the pyruvate kinase (PK). The HK has been proposed as the rate-limiting step of glycolysis in cultivated mammalian cells (Neermann and Wagner, 1996). Recently, the significance of the early glycolytic reactions in limiting the overall glycolytic flux has been confirmed using a kinetic model of the glucose metabolism in CHO cells (Chen et al., 2012). Besides the catabolic function of this pathway, glycolytic intermediates serve as precursors for anabolic processes, e.g. glucose-6-phosphate (G6P) for synthesis of carbohydrates, dihydroxyacetone phosphate (DHAP) for lipid synthesis, and 3-phosphoglycerate (3-PG) for serine and glycine synthesis. The final product of glycolysis, pyruvate, is transported into the mitochondria via the recently identified mitochondrial pyruvate carrier (MPC) (Bricker et al., 2012; Herzig et al., 2012). Eventually, pyruvate is oxidatively decarboxylated by the mitochondrial pyruvate dehydrogenase (PDH) to form acetyl-CoA which enters the tricarboxylic acid (TCA) cycle.

Since the glycolysis generates two reducing equivalents in the form of NADH, the oxidized form NAD^+ needs to be restored to sustain glycolytic activity. Under normal (aerobic) conditions, NAD^+

regeneration is achieved by the respiratory chain in the mitochondria which enables additional ATP synthesis. The inner mitochondrial membrane is impermeable to reducing equivalents NAD(P)H. The transfer of cytosolic NADH across the inner mitochondrial membrane is indirectly accomplished via the malate-aspartate shuttle (Figure 1-2) (Michal and Schomburg, 2012). Inside the mitochondria, NADH is oxidized by complex I of the respiratory chain (NADH dehydrogenase). The complete cycle further involves activities of cytosolic and mitochondrial malate dehydrogenase (MDH), cytosolic and mitochondrial aspartate aminotransferase (ASAT), and the malate/ α -ketoglutarate (OGC) and aspartate/glutamate (AGC) antiporters. An alternative system for transferring electrons into the mitochondria is the glycerol-3-phosphate shuttle (Michal and Schomburg, 2012). However, this shuttle system is thought to be of secondary importance due to its lower energetic efficiency and low expression in most tissues (Mracek et al., 2013).

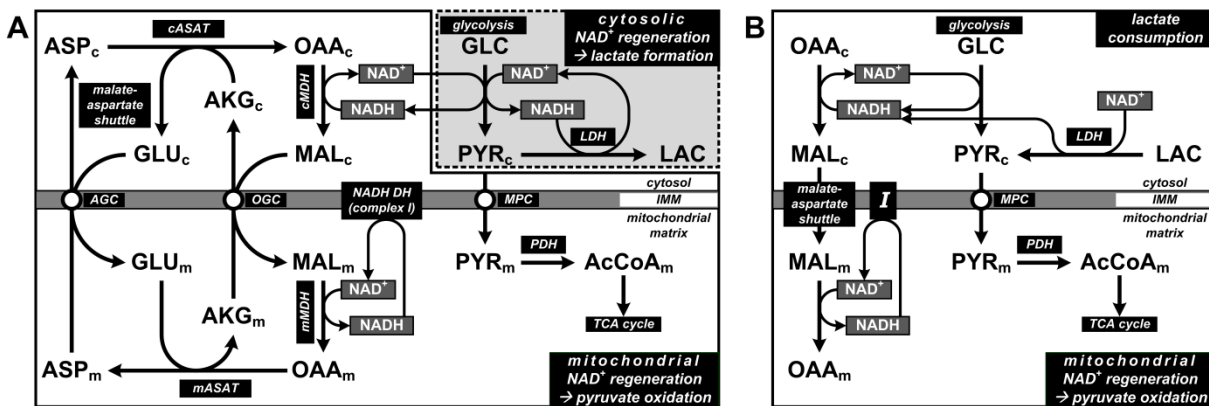


Figure 1-2. The function of the malate-aspartate shuttle for transfer of electrons across the inner mitochondrial membrane (IMM). (A) Competition of cytosolic and mitochondrial NAD⁺ regeneration at lactate production. (B) Dependence on mitochondrial NAD⁺ regeneration at lactate consumption; GLC – glucose, LAC – lactate, PYR – pyruvate, OAA – oxaloacetate, MAL – malate, AcCoA – acetyl-CoA, AKG – α -ketoglutarate, GLU – glutamate, ASP – aspartate, LDH – LAC dehydrogenase, PDH – PYR dehydrogenase, MDH – MAL dehydrogenase, ASAT – ASP aminotransferase, AGC – ASP/GLU carrier, OGC – MAL/AKG carrier, MPC – mitochondrial PYR carrier. Subscript m and c indicate mitochondrial and cytosolic.

However, most mammalian cell lines cultured under *in vitro* conditions, including CHO cells, exhibit aerobic glycolysis, also known as “Warburg effect” (Warburg, 1956). Aerobic glycolysis refers to a situation where glucose is preferentially converted to lactate as usually under hypoxic conditions although oxygen is available in sufficient amounts. The conversion of pyruvate to lactate via the lactate dehydrogenase (LDH) enables a direct cytosolic regeneration of NAD⁺ (Figure 1-2A, grey box). Since neither pyruvate nor NADH enter the mitochondrial metabolism, this happens at the expense of metabolic efficiency. As a consequence, the mitochondrial NAD⁺ regeneration using

the malate-aspartate shuttle (Figure 1-2A, white box) competes with this direct NADH oxidation via LDH (Figure 1-2A, grey box).

High glycolytic rates likely depend on a fast NAD^+ regeneration, thereby stimulating LDH activity and favoring aerobic glycolysis over pyruvate transport into mitochondria. It has been hypothesized that this represents an effective means to maximize growth under conditions of excess nutrient supply in highly proliferating cells (Vander Heiden et al., 2009). The theoretical maximum yield of lactate produced per glucose consumed is 2 mol/mol. A lactate/glucose ratio of 1.5 is often observed in CHO cell cultivations (Ahn and Antoniewicz, 2011; Ahn and Antoniewicz, 2013; Martinez et al., 2013; Neermann and Wagner, 1996). However, much higher metabolic efficiency with lactate/glucose ratios significantly lower than 1 (Carinhas et al., 2013; Goudar et al., 2010; Sheikholeslami et al., 2013b; Templeton et al., 2013) but also much lower metabolic efficiency with ratios close to 2 (Zamorano et al., 2010) have been reported depending on the particular cell clone, growth phase and culture condition. Lactate accumulation is related to increasing the osmolarity and decreasing the pH of the culture medium and thus represents a critical issue in industrial production processes. High lactate levels can inhibit cell proliferation and product formation (Lao and Toth, 1997) and can affect product quality (Li et al., 2012).

A remarkable feature of CHO cells is that they are able to switch from lactate production (Figure 1-2A) to lactate consumption (Figure 1-2B). Lactate accumulates during the early exponential growth phase while its reuptake can occur in later cultivation phases. This metabolic shift is usually correlated with a higher metabolic efficiency and desirable in terms of improved process performance and productivity (Martinez et al., 2013). However, the onset or absence of this metabolic shift to lactate consumption depends on various influencing factors. Several recent studies focused on an improved understanding and control of CHO cell lactate metabolism and its exploitation for process control. Changing glucose availability and altered expression levels of glycolytic enzymes (e.g. reduced expression levels of LDH, PK, PFK) are thought to be major influencing effectors (Baeza et al., 2011). Zagari et al. detected a correlation between high lactate production and an impaired mitochondrial oxidative capacity (Zagari et al., 2013a). Furthermore, it was shown that concentrations of the substrates glucose and glutamine (Zagari et al., 2013a) as well as specific media components (e.g. copper) (Luo et al., 2012) can modulate the lactate profile. Nolan et al. developed a kinetic model of CHO cell metabolism and successfully predicted the timing and magnitude of the lactate shift by including a redox variable (Nolan and Lee, 2011). Their simulation results suggest that the shift is triggered by an insufficient supply of NADH from the cytosol to the mitochondria, in other words, when the mitochondrial NADH demand exceeds the cytosolic NADH production. In a comprehensive gene expression study investigating a range of CHO cell clones with distinct lactate profiles cultivated in different cell culture media, the activity of the malate-aspartate shuttle (Figure 1-2) has been identified as a key factor to promote the switch from lactate production to its consumption in CHO cells (Zagari et al., 2013a). A low expression of

Aralar1, encoding the mitochondrial aspartate/glutamate carrier, (AGC, Figure 1-2A) and Timm8a1, involved in the correct localization of AGC, was correlated with a high lactate producing phenotype. The gene expression was strongly influenced by the media composition. Furthermore, the overexpression of either Aralar1 or Timm8a1 was sufficient to induce a switch to lactate consumption regardless of the media composition and the specific glucose uptake rate (Zagari et al., 2013a). As schematically depicted in Figure 1-2B, lactate consumption is strictly dependent on a mitochondrial NAD^+ regeneration and thus requires malate-aspartate shuttle activity to accomplish a transfer of cytosolic NADH into the mitochondria. The control of glycolysis and lactate metabolism is central to metabolic efficiency in CHO cells. Recent findings clearly illustrate the high complexity of its metabolic regulation and suggest that many components and their interplay are not yet understood or not even identified.

1.2.2 Pentose-phosphate pathway

The pentose-phosphate pathway (PPP) is an alternative cytosolic by-pass of glycolysis with mostly anabolic functions. It consists of the oxidative phase and the non-oxidative phase. In the oxidative PPP, G6P is irreversibly converted to ribose-5-phosphate (R5P) losing one carbon by CO_2 production and generating 2 NADPH. In the non-oxidative branch, R5P is reversibly converted to sugar phosphates with three to seven carbons and eventually to glyceraldehyde-3-phosphate and fructose-6-phosphate which reenter the glycolytic pathway. The PPP intermediate R5P is an essential precursor for the synthesis of nucleic acids (RNA, DNA). NADPH is required for reductive biosynthesis reactions (e.g. fatty acid synthesis) but also to reduce oxidized glutathione via glutathione reductase. Glutathione is an important antioxidant scavenging reactive oxygen species (ROS) and eventually preventing cellular damage. Thus, the PPP plays a crucial role both in cell proliferation and in the generation of reducing equivalents to counteract oxidative stress. The first enzyme of the oxidative branch, glucose-6-phosphate dehydrogenase (G6PDH), represents the rate-limiting step of PPP and is stimulated by high NADP^+ levels. G6PDH-deficient CHO cells are characterized by a higher susceptibility to apoptosis (Tuttle et al., 2000).

The determination of the carbon split between glycolysis and PPP requires the application of ^{13}C -tracer studies or accurate knowledge about cofactor balances (Niklas and Heinzle, 2012). However, mass balances of NADH and NADPH are generally not reliable due to the activity of transhydrogenases and the existence of enzymes that accept both NADH and NADPH as cofactor (e.g. glutamate dehydrogenase and different isoenzymes of isocitrate dehydrogenase). For classical studies on CHO cell metabolism using stoichiometric balancing, simplified metabolic models are applied to obtain a determined system. Usually, the non-oxidative PPP is neglected and the oxidative PPP is assumed to be limited to anabolic requirements of nucleic acids resulting in an underestimation of the actual PPP flux (Ahn and Antoniewicz, 2012). Goudar et al. compared the metabolic flux distribution obtained by metabolic flux analysis (MFA) using metabolite balancing

and ^{13}C MFA and determined the sensitivity to varying PPP fluxes. They concluded that the PPP flux has limited impact on most fluxes of the central metabolism which can be accurately determined by metabolite balancing alone (Goudar et al., 2010). In the few ^{13}C -MFA studies that are available for CHO cells, a wide range of PPP activities between 2% and 162% of the glucose uptake flux has been reported (Ahn and Antoniewicz, 2011; Ahn and Antoniewicz, 2013; Goudar et al., 2010; Sengupta et al., 2011; Templeton et al., 2013). A PPP flux exceeding the glycolytic flux was interpreted as substantial cycling of carbons between both pathways involving a conversion of fructose-6-phosphate to glucose-6-phosphate via phosphoglucose isomerase. These studies demonstrate the high variability of PPP activities in CHO cells depending on cultivation conditions, cell line and growth phase. High PPP fluxes might be accompanied by a significant loss of carbons due to CO_2 release. This should not be neglected in detailed investigations. An accurate estimation of the PPP activity is thus crucial for the determination of more complex metabolic networks.

1.2.3 Tricarboxylic acid cycle and amino acid metabolism

The tricarboxylic acid (TCA) cycle is a central metabolic pathway located in the mitochondria with both catabolic and anabolic functions. It requires NAD^+ regeneration by the respiratory chain and is therefore strictly aerobic. The cycle starts with the condensation of oxaloacetate (OAA) (C4-unit) and acetyl-CoA (C2-unit) to form citrate. Through a series of reactions, citrate is converted to OAA producing 2 CO_2 , 1 GTP, 3 NADH and 1 FADH_2 . The regenerated OAA restarts the TCA cycle by accepting another C2-unit from acetyl-CoA. The reducing equivalents NADH and FADH_2 are oxidized in the respiratory chain to drive ATP synthesis by oxidative phosphorylation. This represents the most efficient way to generate cellular energy. The phosphate/oxygen (P/O) ratio of oxidative phosphorylation describes the amount of ATP produced per oxygen atom reduced by the respiratory chain (Hinkle, 2005). P/O ratios of 2.5 ATP/NADH and 1.5 ATP/ FADH_2 , respectively, are consistent with most reports (Hinkle, 2005; Michal and Schomburg, 2012). A maximum of 32 mol ATP/mol glucose can be generated by complete glucose oxidation via oxidative phosphorylation while only 2 mol ATP/mol glucose are produced in aerobic glycolysis when glucose is converted to lactate (Michal and Schomburg, 2012). Constant concentrations of TCA cycle intermediates are crucial for the functioning of this metabolic pathway and are therefore strictly controlled by the cell. TCA cycle intermediates are removed from the cycle serving as precursors for the biosynthesis of other molecules, e.g. non-essential amino acids (NEAA). Citrate is exported from the mitochondria to the cytosol and cleaved by the ATP-dependent citrate lyase to provide cytosolic acetyl-CoA, e.g. for fatty acid synthesis. This carbon loss is balanced by anaplerotic reactions. On the other hand, a carbon excess in the TCA cycle has to be adjusted by cataplerotic reactions facilitating the exit of intermediates. The TCA cycle is strictly regulated by the cellular redox and energy state via the enzymes citrate synthase (CS), isocitrate dehydrogenase (IDH) and α -ketoglutarate dehydrogenase (AKGDH). In addition, the PDH supplying the CS

substrate acetyl-CoA plays a crucial role in TCA cycle regulation. Distinct metabolite pools in the mitochondria and the cytosol exist for TCA cycle intermediates, e.g. citrate, isocitrate and AKG. The cytosolic NADPH-dependent isoform of the IDH enzyme might be involved in cytosolic NADPH balance and α -ketoglutarate (AKG) supply. The compartmentation of these metabolites has not been taken into account in previous studies about CHO cell metabolism.

Amino acids can contribute to catabolism by degradation to pyruvate and TCA cycle intermediates. Besides pyruvate as major precursor for the C2-unit acetyl-CoA, glutamine is an important carbon source for the TCA cycle in mammalian cells. The mitochondrial enzyme glutaminase catalyzes the hydrolysis of glutamine to ammonia and glutamate which is further converted into the TCA cycle intermediate AKG by the mitochondrial glutamate dehydrogenase (GDH). Alternatively, AKG is generated by transfer of the amino group from glutamate either to pyruvate by alanine aminotransferases (ALAT) or to OAA by aspartate aminotransferases (ASAT). Both aminotransferases exist in a cytosolic and a mitochondrial isoform. The expression of different ASAT isoenzymes plays a crucial role in metabolic efficiency due to their involvement in the malate-aspartate shuttle (Figure 1-2). The cellular glutamine metabolism and additionally its non-enzymatic extracellular decomposition due to its non-stable nature represent the major sources of ammonia production (Tritsch and Moore, 1962). Accumulation of the toxic by-product ammonia can inhibit cell growth and negatively affect production and glycosylation of recombinant proteins (Yang and Butler, 2000; Yang and Butler, 2002). It is therefore a critical issue in industrial bioprocesses. In contrast to many other mammalian cell lines, CHO cells express low levels of glutamine synthetase (GS) and are therefore able to grow in glutamine-free medium (Zhang et al., 2006). Overexpression of the GS gene by co-transfection with the gene of interest is one of the most important gene selection systems in CHO cell engineering for production of recombinant proteins (Wurm, 2004). Essential amino acids (ESAA) have to be supplied in the cell culture medium to allow protein synthesis and partially contribute to catabolism. Non-essential amino acids (NEAA) can be simultaneously degraded and synthesized in CHO cells. This has been proven by incorporation of labeling into NEAA in ^{13}C -tracer studies (Ahn and Antoniewicz, 2012; Deshpande et al., 2009). However, the simultaneous consumption and production of amino acids has hardly been considered in metabolic studies so far.

1.2.4 Pyruvate metabolism and C3-C4 node

The metabolic reactions around the cellular pyruvate node are in the center of intermediary metabolism connecting glycolysis and TCA cycle and various other pathways (Figure 1-3). These key reactions take place in cytosol and mitochondria with separate metabolite pools in both cellular compartments. Pyruvate is taken up from the extracellular medium and/or is generated as end product of glycolysis from phosphoenolpyruvate (PEP) through PK (1) and has several metabolic fates. The highly regulated and irreversible PDH reaction catalyzes the conversion to acetyl-CoA

which enters the TCA cycle (2). Glycolysis and TCA cycle are further connected by reactions of malic enzyme (ME) (3), pyruvate carboxylase (PCX) (4) and PEP carboxykinase (PEPCK) (5). PDH and PCX are exclusively located in the mitochondria, while different isoforms with cytosolic or mitochondrial localization can potentially exist for ME and PEPCK (Michal and Schomburg, 2012). Furthermore, pyruvate can be reduced to lactate via LDH (6) and converted to alanine via alanine aminotransferase (ALAT) (7).

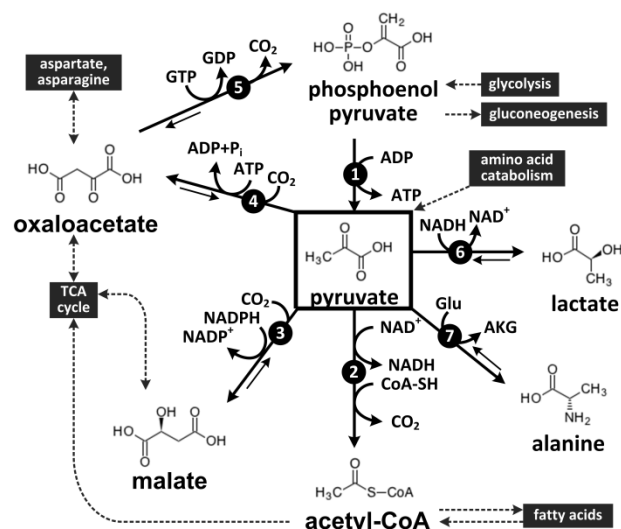


Figure 1-3. Metabolic reactions around the cellular pyruvate node. (1) pyruvate kinase, (2) pyruvate dehydrogenase, (3) malic enzyme, (4) pyruvate carboxylase, (5) phosphoenolpyruvate carboxykinase, (6) lactate dehydrogenase, (7) alanine aminotransferase. Potentially reversible reactions are indicated by an arrow in the opposite direction. Dashed arrows indicate connections to major metabolic pathways.

Neermann and Wagner were unable to detect significant activities of PDH, PEPCK and PCX in several CHO, BHK and hybridoma cell lines (Neermann and Wagner, 1996) indicating a low connection between glycolysis and TCA cycle. However, ^{13}C -tracer studies provide strong evidence for activity of these enzymes in CHO cells (Ahn and Antoniewicz, 2011; Ahn and Antoniewicz, 2013; Goudar et al., 2010). Dean and Reddy proved the expression of PEPCK and ME in CHO cells by Western Blot analysis (Dean and Reddy, 2013). Niklas et al. presented a valuable method for the high-throughput determination of compartmented enzyme activities using selective permeabilization techniques (Niklas et al., 2011a). They observed cytosolic and mitochondrial ME activity in an antithrombin-producing CHO cell line. PCX, ME and PEPCK play an essential role in anaplerosis of the TCA cycle. Furthermore, PCX and PEPCK are key enzymes initiating gluconeogenesis. The accurate determination of the compartmented reactions around the cellular pyruvate metabolism represents a significant challenge in the resolution of complex metabolic networks. Previous studies

of CHO metabolism usually present simplified descriptions of this highly branched metabolic hub in the intermediary metabolism.

1.3 Reconstruction of relevant network models for metabolic studies in CHO cells

The devil is in the details. This is especially true for detailed studies of mammalian metabolism which is highly complex particularly related to metabolite compartmentation and exchange (Wahrheit et al., 2011). Considering a relevant network structure is of utmost importance to calculate physiologically meaningful flux distributions. It is the first and potentially most important step in metabolic flux analysis (MFA). Although the number of MFA studies in mammalian systems rapidly increased in the last few years, published metabolic networks used for CHO cell studies are highly controversial and largely simplified. Given the high complexity of mammalian metabolism, certain assumptions might be necessary for model reduction (Zamboni, 2011). Quek et al. proposed a large list of model reductions based on literature supposing negligible activity for many enzymes (Quek et al., 2009). However, model reduction and oversimplification can produce misleading results and conclusions. Particular care has to be taken when introducing simplifications. A priori assumptions of negligible activity for certain enzymes followed by their exclusion from the metabolic model can only be an acceptable approach if evidence on the expression or activity level is available for the investigated cell clone and given condition (Wahrheit et al., 2011). Transferring knowledge derived from a different context, e.g. from another cell line or from a different environmental condition, is generally not valid.

Unfortunately, published model reductions for CHO cell network models seem rather arbitrary than reasonable and specific. It is common practice that cytosolic and mitochondrial metabolite pools are lumped assuming a rapid equilibrium between compartments (Templeton et al., 2013). Even if metabolic compartmentation is at least partially considered, there is no consensus with respect to localization and parallelization of pathways, reaction and transport reversibility as well as the occurrence of anaplerotic and gluconeogenic fluxes. In order to reconstruct a realistic metabolic network for CHO cells, one has to consider at least three compartments; the extracellular space, the cytosol and the mitochondria.

1.3.1 Enzyme localization

The analysis of compartmented metabolic networks is complicated by separation and parallelization of pathways. Metabolic pathways can span several compartments and the existence of isoenzymes creates parallel pathways in different subcellular locations (Wahrheit et al., 2011). Distinct metabolite pools in cytosol and mitochondria have different pool sizes and are involved in different pathways. In terms of ^{13}C -labeling experiments, one has to keep in mind that cytosolic and

mitochondrial metabolites are most likely differently labeled and exhibit different labeling dynamics (Figure 1-4A). There is general consensus about the cytosolic localization of glycolytic and PPP enzymes and the mitochondrial localization of the TCA cycle (Berg et al., 2012; Michal and Schomburg, 2012). However, reactions of the amino acid metabolism are sometimes misplaced or spuriously considered only in one compartment and in many cases experimental evidence for the enzyme localization is scarce. Based on current knowledge collected in various data bases (Brenda, Reactome, KEGG, UniProt), the glutaminase reaction is located in the mitochondria, while the glutamine synthesis takes place in the cytosol. However, most metabolic models published for CHO cells assume a cytosolic glutaminase localization (Ahn and Antoniewicz, 2011; Ahn and Antoniewicz, 2013; Sheikholeslami et al., 2013b; Templeton et al., 2013). Although, alanine and aspartate transaminases can be located in the cytosolic and the mitochondrial compartment (Michal and Schomburg, 2012), the existence of separate isoenzymes converting respective distinct metabolite pools in cytosol and mitochondria is rarely taken into account. Most published CHO cell models include only the cytosolic (Ahn and Antoniewicz, 2011; Ahn and Antoniewicz, 2013; Templeton et al., 2013) or only the mitochondrial isoenzymes of ALAT and ASAT (Sheikholeslami et al., 2013a; Sheikholeslami et al., 2014). CHO cells often conduct synthesis and degradation pathways of non-essential amino acids simultaneously as clearly proven by tracer studies (Ahn and Antoniewicz, 2012; Deshpande et al., 2009). The separation of these opposite pathways into distinct cellular compartments is a general means of metabolic regulation and should not be neglected. Compartmental enzyme activity determinations can help identifying the correct localization of enzymes (Niklas et al., 2011a). The isocitrate dehydrogenase (IDH) exists in three isoforms; the NAD^+ -dependent isoenzyme is located in the mitochondria (IDH3), while the NADP^+ -dependent isoforms exist in the cytosol (IDH1) and the mitochondria (IDH2), respectively (Henderson, 1965; Michal and Schomburg, 2012). Interestingly, it was found that the major part of total cellular IDH activity was located in the cytosol and not in the mitochondria in mammalian cells (Niklas et al., 2011a; Vriezen and van Dijken, 1998b). However, a cytosolic IDH reaction has so far never been considered in MFA studies of CHO cells (Ahn and Antoniewicz, 2012). This reaction is thought to have a crucial function in cytosolic NADPH balance and has been shown to be involved in cancer, diabetes, and oxidative stress (Dang et al., 2009; Ronnebaum et al., 2006; Turcan et al., 2012; Xu et al., 2004; Yan et al., 2009).

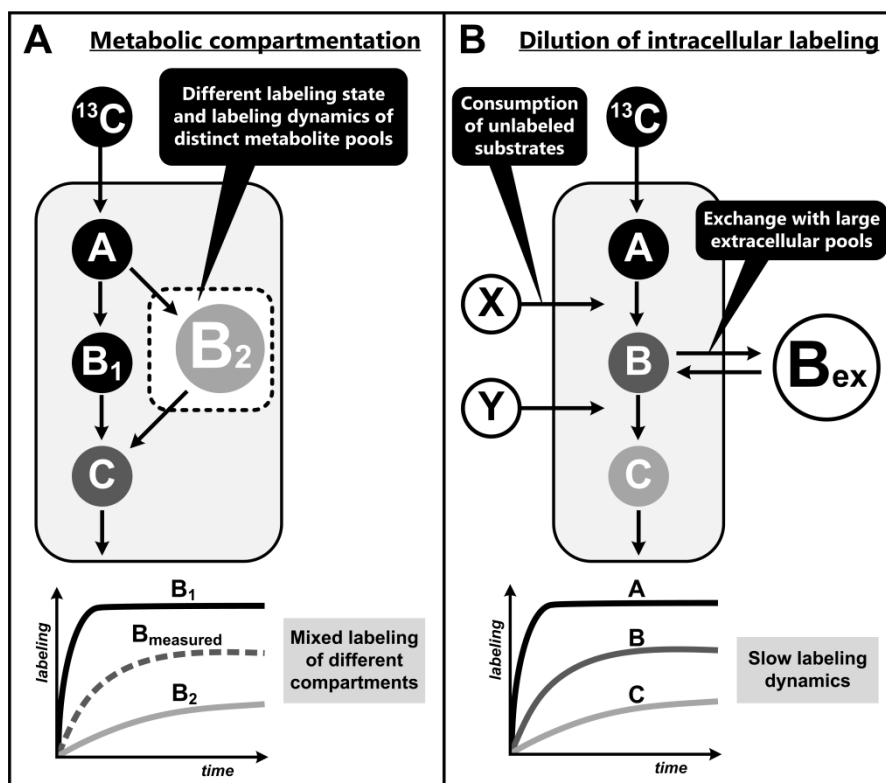


Figure 1-4. (A) Metabolic compartmentation results in distinct metabolite pools in different compartments (B_1 and B_2). Due to the disruptive nature of current metabolite extraction protocols it is not possible to separate and distinguish different metabolite pools. As a result, only the mixed labeling of all cellular pools of a specific metabolite can be determined (B_{measured}). (B) The consumption of multiple non-labeled substrates (X, Y) and the reversible exchange with significantly larger extracellular metabolite pools (B_{ex}) results in a dilution of intracellular labeling and slow labeling dynamics. ^{13}C -labeled metabolites are represented by black and grey circles, unlabeled metabolites by white circles.

1.3.2 Mitochondrial transport

A large set of specific transport systems links pathways, transfers precursors and cofactors, and mediates communication between interdependent compartments. The operation of mitochondrial carrier systems with regard to stoichiometry, specificity and reversibility is still a matter of discussion. Transport systems can be redundant and the relative contribution of different transporters is often uncertain. Many transport systems are poorly characterized or not even identified. Only very recently, the long awaited mitochondrial pyruvate carrier (MPC) gene has been identified (Bricker et al., 2012; Herzig et al., 2012). Some studies consider the MPC to be reversible with exchange fluxes thousand-fold exceeding the net import into the mitochondria (Ahn and Antoniewicz, 2011; Sheikholeslami et al., 2013b), while other studies include an irreversible pyruvate uptake (Ahn and Antoniewicz, 2013; Sheikholeslami et al., 2013a; Sheikholeslami et al., 2014). With respect to its coupling to the mitochondrial proton gradient (pyruvate enters the mitochondria via symport with a proton), it is likely that the import into mitochondria is irreversible.

Sheikholeslami et al. presented the first metabolic network of CHO cells that accounts for transport stoichiometry by including citrate/malate antiport via tricarboxylate carrier, malate transport via dicarboxylate carrier and aspartate transport via glutamate/aspartate antiport (Sheikholeslami et al., 2013b). However, in most MFA studies, metabolic compartmentation and mitochondrial transport is not considered. Much work remains to be done to shed light on some uncertainties regarding mitochondrial transport specificities and activities.

1.3.3 Reversible exchange with the extracellular medium

The extracellular space has to be treated as a distinct compartment, similar to the cellular compartments cytosol and mitochondria. CHO cells are cultivated in nutrient rich, complex media containing multiple carbon sources. Tracer studies revealed that a range of metabolites, e.g. lactate and pyruvate and many non-essential amino acids (NEAA), that are taken up at high net fluxes are in fact reversibly exchanged with the extracellular medium (Ahn and Antoniewicz, 2012). That implies that degradation and synthesis of NEAA have to be considered separately in the model. The consumption of non-labeled substrates and the high exchange fluxes with the extracellular medium significantly slow down the labeling dynamics in tracer studies (Figure 1-4B). Nevertheless, the reversible exchange of metabolites with the extracellular medium has not been included in previous studies of CHO metabolism.

1.3.4 Micro-compartmentation and metabolic channeling effects

Although the glycolytic pathway is entirely located in the cytosol, it is subject to metabolic compartmentation. The association of glycolytic enzymes into protein complexes and binding to cellular structures is involved in glycolytic regulation (Michal and Schomburg, 2012). Binding of the HK to the outer mitochondrial membrane substantially promotes glycolytic flux by providing preferential access to mitochondrially generated ATP. The channeling of intermediates results in a micro-compartmentation of the glycolytic pathway within the cytosolic compartment. Micro-compartmentation and channeling effects have also been proposed for the cellular pyruvate metabolism in CHO cells (Ahn and Antoniewicz, 2013).

1.4 Computational methods for the investigation of metabolic networks

The emerging systems biology era has substantially influenced the whole scientific world. Biology has moved from mere qualitative investigations to comprehensive quantitative descriptions followed by an integration of these quantitative data sets into mathematical models. In addition, instead of focusing on single aspects, biological studies aim more and more at gaining a holistic understanding of a biological system including dynamic interactions between single components. Metabolic fluxes integrate information of all upstream components of the cellular hierarchy (genome, transcriptome, proteome, metabolome) including their interactions and regulation on different levels. Therefore, the fluxome reflects the functional endpoint of a biochemical network (Figure 1-5A) (Sauer, 2006). Metabolic flux analysis (MFA) aims at quantifying the *in vivo* intracellular reaction rates of a metabolic network. It represents the most comprehensive way to quantify cell physiology and to provide a meaningful representation of the cellular phenotype. MFA has been extensively used in basic and applied research to characterize and understand physiological, pathological, or toxicological conditions as well as to identify therapeutic targets or to guide metabolic engineering and optimization of industrial production processes (Niklas and Heinzle, 2012; Niklas et al., 2010). The quantification of metabolic fluxes by MFA can be performed using simple metabolite balancing (Figure 1-5B) or by more sophisticated ^{13}C metabolic flux analysis (^{13}C MFA) (Figure 1-5C).

1.4.1 Metabolic flux analysis using metabolite balancing

Metabolic flux estimation using the metabolite balancing method (Figure 1-5B) only requires extracellular measurements of substrate uptake (S), product excretion (P) and biomass formation (BM). From these known (measurable) extracellular metabolic fluxes (r_m), the unknown intracellular flux distribution (r_c) can be calculated using a stoichiometric network model of the metabolism and material balances around the intracellular metabolite pools (Niklas and Heinzle, 2012). Metabolic flux estimation using metabolite balancing is the most commonly applied method for the investigation of mammalian systems. Due to the utilization of multiple carbon sources in mammalian cell cultures, a large number of extracellular measurements is usually available. In CHO cells, this classical MFA method has been used in various applications (Altamirano et al., 2006; Altamirano et al., 2001b; Burleigh et al., 2011; Carinhas et al., 2013; Goudar et al., 2006; Goudar et al., 2014; Nyberg et al., 1999b).

The application of metabolite balancing relies on metabolic steady state conditions which implies that the intracellular metabolite concentrations are constant with time ($dM/dt = 0$) (Figure 1-6, metabolic stationary state). In other words, at metabolic steady state, the sum of metabolite consumption rates equals the sum of their production rates. This is easily achieved in continuous cultivation experiments. Furthermore, a pseudo steady state assumption is usually valid at balanced

growth conditions, i.e. exponential growth and constant metabolite yields (Deshpande et al., 2009). However, for a range of mammalian cultivation systems (e.g. monolayer cultures), certain process modes (e.g. industrially relevant fed-batch cultivations), and generally at changing environmental conditions and cellular state, it is questionable if balanced growth and a (pseudo) metabolic steady state are truly achieved (Figure 1-6, metabolic instationary state). One possibility is to divide the cultivation profile into distinct metabolic phases for which balanced growth conditions are valid and calculate average rates for each separate phase (Niklas et al., 2011c).

An elegant way to deal with this challenge and circumvent the necessity of a metabolic steady state are dynamic approaches which calculate the evolution of metabolic fluxes over time (Antoniewicz, 2013b; Leighty and Antoniewicz, 2011; Llaneras and Pico, 2007b; Niklas et al., 2011c). Dynamic metabolic flux analysis (DMFA) methods are usually based on (1) data smoothing, e.g. using spline fitting, followed by (2) separation into very small time intervals, (3) taking derivatives of extracellular measurements and (4) successive application of classical MFA to calculate time-resolved fluxes (Niklas et al., 2011c). Special software tools, e.g. the user-developed Shape Language Modeling (SLM) tool for MATLAB (MathWorks), can be applied to include additional constraints and significantly improve the quality of fitting (e.g. avoid over-fitting). Other approaches of DMFA are based on a piecewise linear flux function describing the cultivation profile as a whole (Leighty and Antoniewicz, 2011) or on simulating the flux dynamics by including kinetic information and using a hybrid stoichiometric-kinetic model (Nolan and Lee, 2011).

The metabolite balancing method is very useful to resolve simple networks. However, more complex networks including cyclic pathways, alternative pathways, and reaction reversibilities cannot be resolved with metabolite balancing alone. In particular, information about metabolic compartmentation cannot be obtained by this simple MFA technique (Allen et al., 2009; Wahrheit et al., 2011; Zamboni, 2011). If the available extracellular measurements are insufficient, the metabolic network is underdetermined. Several variants of MFA and extensions of the metabolite balancing method have been proposed to calculate underdetermined parts in metabolic networks. Different constraints (e.g. on reaction reversibility, negligible enzyme activities) or specific objective functions (e.g. maximizing growth) assuming optimal behavior of an organism as applied in flux balancing analysis (FBA) can be introduced to reduce the solution space (Martinez et al., 2013; Orth et al., 2010). Furthermore, several groups proposed methods for the determination of upper and lower boundaries for non-calculable fluxes, sometimes referred to as flux spectrum approach (FSA) (Llaneras and Pico, 2007a; Llaneras and Pico, 2007b; Zamorano et al., 2010)

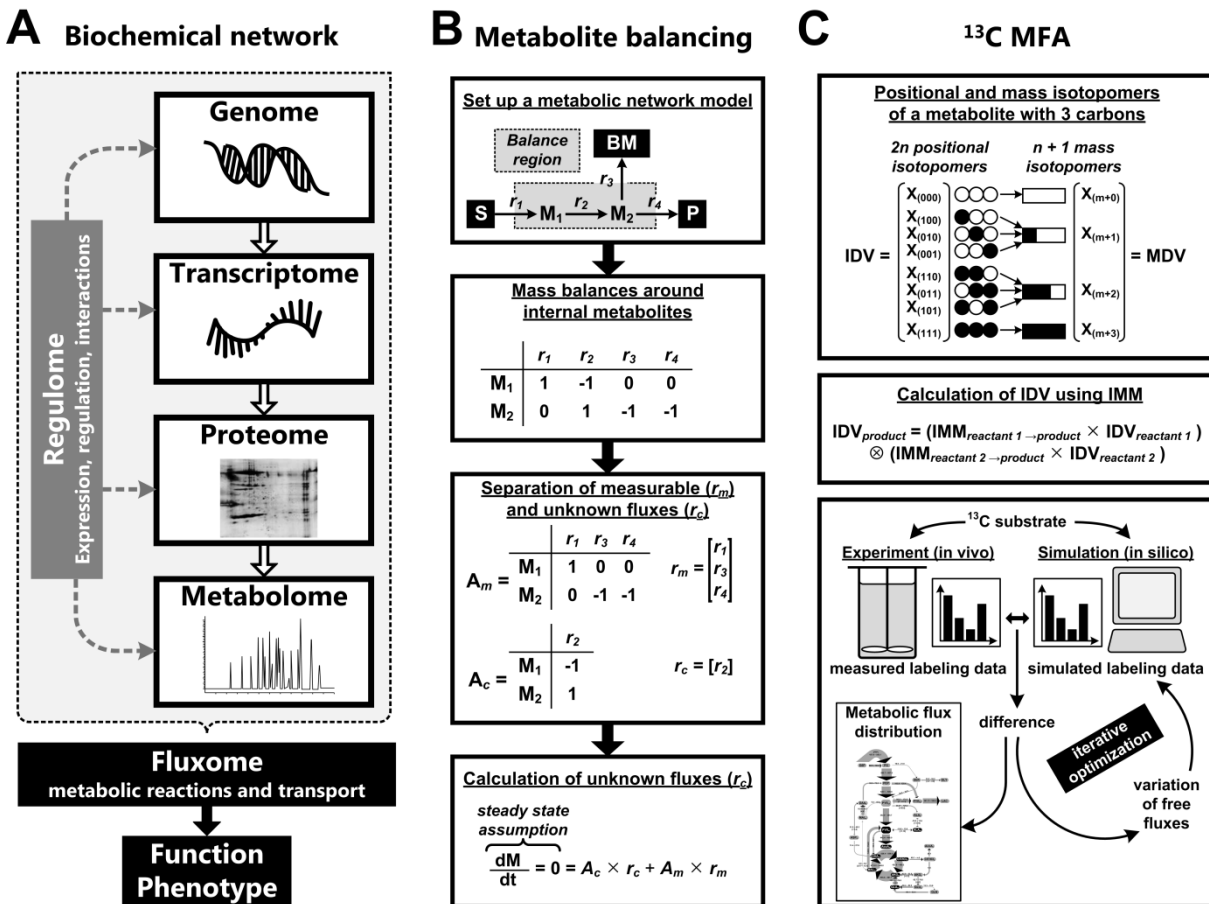


Figure 1-5. (A) The biochemical network is composed of the hierarchical components genome, transcriptome, proteome and metabolome. The fluxome reflects the integrated network response including regulation at the genomic, transcriptional, translational and metabolic level and eventually determines the cellular phenotype. (B) Different steps of metabolic flux analysis using the metabolite balancing method. S substrate, P product, BM biomass, M internal metabolite, r reaction rate, r_m measured fluxes, r_c calculated fluxes, A_m and A_c stoichiometric matrices of the measured and calculated fluxes, respectively. (C) ¹³C metabolic flux analysis (¹³C MFA). Positional and mass isotopomers constitute the labeling state of a metabolite. Isotopomer distribution vectors (IDV) and mass distribution vectors (MDV) mathematically quantify the fractions of positional and mass isotopomers as shown for an example of a metabolite with three carbons (Wittmann, 2002). Isotopomer mapping matrices (IMM) define the transition of isotopomers between reactants and products. \otimes refers to an element wise multiplication. The metabolic flux distribution is calculated by minimizing the deviation between measured and simulated ¹³C labeling patterns.

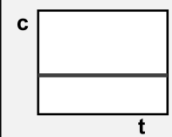
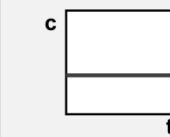
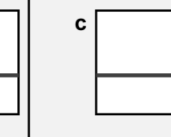
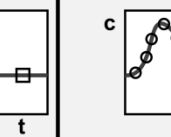
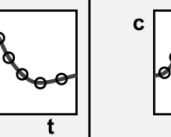
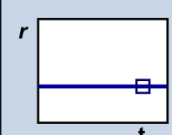
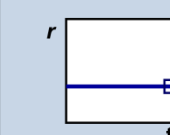
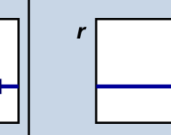
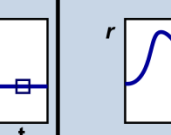
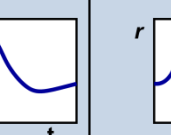
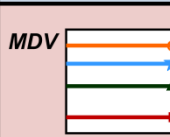
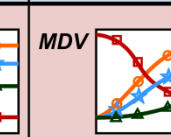
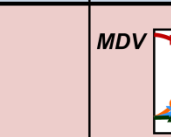
Metabolic state	stationary			instationary	
	no labeling	stationary	instationary	no labeling	instationary
Intracellular metabolite concentrations					
Fluxes					
Isotopomers					
MFA method	Metabolite balancing	¹³ C MFA	INST-MFA	Dynamic MFA	Dynamic ¹³ C MFA

Figure 1-6. Overview of different metabolic flux analysis (MFA) methods, experimental conditions with regard to metabolic and isotopic state and the characteristics of determined or assumed parameters: intracellular concentrations c , metabolic fluxes r , and isotopomers expressed as mass distribution vector (MDV). Metabolic stationary conditions (metabolic steady state) imply that intracellular metabolite concentrations and metabolic fluxes are constant with time ($dM/dt = 0$). If metabolite concentrations and fluxes are changing with time, the metabolic state is called instationary or dynamic. Metabolite balancing and dynamic MFA methods can be applied for metabolic flux calculation at metabolic stationary or instationary state, respectively, without the use of labeling. The application of ¹³C MFA requires the determination of ¹³C labeling patterns in specific readout metabolites. The isotopic state is stationary if the isotopomers of a metabolite are invariant with time. Metabolic steady state is a prerequisite for isotopic steady state. In this case, metabolic fluxes can be calculated by classical ¹³C MFA. At isotopic instationary state with dynamically changing isotopomers, flux calculation requires the application of either isotopically non-stationary MFA (INST-MFA) at metabolic stationary state or dynamic ¹³C-MFA at metabolic instationary conditions, respectively. The figure was adapted and extended from (Wahl et al., 2008).

1.4.2 ¹³C metabolic flux analysis

Additional information to resolve complex metabolic networks can be obtained from stable isotope labeling experiments. ¹³C-based metabolic flux analysis (¹³C MFA, Figure 1-5C) is an established standard method for the quantification of intracellular fluxes in detailed metabolic networks and has been widely applied for various different biological systems (Wiechert, 2001). This approach involves the feeding of substrates with one or more ¹³C-labeled carbons and the metabolization of the labeled substrate (tracer) by the cell (Zamboni et al., 2009). The distribution of ¹³C throughout the metabolic network is a function of the respective pathway activities resulting in specific labeling patterns of metabolites (Niklas and Heinzle, 2012). For classical ¹³C MFA, the labeling patterns are sampled at isotopic steady state (Figure 1-6, metabolic and isotopic stationary state). Thus, the metabolic flux distributions can be reconstituted from the isotopic enrichment in metabolic intermediates or macromolecules. The most commonly applied labeled substrates in ¹³C MFA of mammalian cells are different glucose and glutamine tracers (Metallo et al., 2009), since glucose and glutamine constitute the most important carbon sources in mammalian cell cultures (Eagle, 1955). It is essential to consider the atom-% purity of ¹³C-labeled compounds, e.g. for [U-¹³C₆] glucose with 99 atom-% isotopic purity the abundance of fully labeled glucose is not 99% but $0.99^6 = 94\%$ (Yang, 2013). Optimal design of isotope labeling experiments is crucial for the precision of ¹³C MFA-based flux estimates. The information of parallel labeling experiments can be combined to significantly improve the flux calculation (Antoniewicz, 2013a; Yang et al., 2006a; Yang et al., 2006b). The consumption of multiple carbon sources in mammalian cell cultures is a particular advantage in this respect (Wahrheit et al., 2011).

The labeling state of a metabolite is constituted by its isotopomers (Wittmann, 2002). Positional isotopomers define the exact position of labeled carbons, while mass isotopomers only describe the number of ¹³C atoms present in a specific molecule. A metabolite with n carbons has 2^n different positional isotopomers which sum up to $n + 1$ different mass isotopomers (Figure 1-5C). The fractions of positional and mass isotopomers are mathematically quantified by isotopomer distribution vectors (IDV) (Schmidt et al., 1997) and mass distribution vectors (MDV). The ¹³C labeling patterns of metabolites can be analyzed by nuclear magnetic resonance (NMR) spectroscopy (Teixeira et al., 2008; Zupke and Stephanopoulos, 1995) resolving positional isotopomers or mass spectrometry (MS) techniques, usually GC/MS, resulting in mass isotopomer data (Wittmann, 2002; Wittmann, 2007; Wittmann and Heinzle, 1999). GC/MS data has to be corrected for naturally occurring isotopes considering both the atoms of the analyte and derivatization residues, e.g. using correction matrices (van Winden et al., 2002; Wittmann and Heinzle, 1999; Yang et al., 2009).

The concept of atom mapping matrices (AMM) describes the carbon transition in a metabolic network in form of a $m \times n$ matrix where m is the number of carbons in the product and n is the

number of carbons in the reactant (Zupke and Stephanopoulos, 1994). The AMM concept has been further expanded to isotopomer mapping matrices (IMM) which map each positional isotopomer of a reactant to a product (Schmidt et al., 1997). The corresponding AMM is thereby converted into a $2^m \times 2^n$ IMM. The IDV of a product is calculated from the IMM and IDV of the reactants. The metabolic flux distribution is eventually determined by combination of isotopomer and metabolite balancing. Starting from initial random values that fulfill the constraints, the flux distribution is estimated based on minimizing the deviation between measured and simulated labeling patterns by applying suitable optimization routines (Figure 1-5C). More detailed descriptions on the concept of ^{13}C MFA can be found in relevant review articles (Sauer, 2004; Sauer, 2006; Wiechert, 2001; Zamboni et al., 2009; Zamboni and Sauer, 2009). Labeling experiments and ^{13}C MFA studies are still the exception in metabolic studies of CHO cells but are becoming more and more popular in the last few years (Ahn and Antoniewicz, 2013; Goudar et al., 2010; Sengupta et al., 2011; Sheikholeslami et al., 2013a; Sheikholeslami et al., 2013b; Sheikholeslami et al., 2014; Templeton et al., 2013).

1.4.3 Isotopically non-stationary metabolic flux analysis

In ^{13}C -labeling experiments of mammalian cell cultures, the utilization of several carbon sources and their reversible exchange with significantly larger extracellular metabolite pools results in considerable dilution of intracellular labeling and slows down the dynamics of label incorporation (Figure 1-4). The concept of non-stationary ^{13}C MFA (INST-MFA, isotopically non-stationary MFA) presented by the group of Wiechert (Wahl et al., 2008; Wiechert and Nöh, 2005; Wiechert and Nöh, 2013) is a powerful advancement of classical stationary ^{13}C MFA. While steady state ^{13}C MFA requires metabolic and isotopic steady state conditions (Figure 1-6, metabolic and isotopic stationary state), the INST-MFA method is applied to systems at metabolic steady state yet isotopic non-stationary conditions (Figure 1-6, metabolic stationary and isotopic instationary state). This approach uses the information of the transient period of label incorporation before isotopic steady state is reached. Following the isotopomer dynamics yields much richer information than the isotopic steady state (Nöh and Wiechert, 2011). This is particularly conducive for addressing very challenging questions, such as resolving the compartmented fluxes of a complex metabolic network. Metabolic compartmentation generally increases the number of alternative pathways, introduces a number of reversible transport reactions, and creates new cycles, thus increasing the degrees of freedom. Alternative pathways include shuttles involving the same metabolites and isoenzymes that catalyze the same reaction in different compartments (Wahrheit et al., 2011). INST-MFA can provide information about intracellular and intracompartamental concentrations, metabolic fluxes, reversibility, and network structure, however, requires demanding experimental techniques and sophisticated modeling efforts (Wahrheit et al., 2011). Additional parameters (e.g. metabolite pool sizes) have to be determined or estimated. This methodology offers new opportunities to investigate

the metabolism of more complex, higher organisms (in particular animal cells and plant cells), industrially relevant non-stationary bioprocesses and other biological systems where steady state ^{13}C MFA is not applicable but also when experiments at short time scales are preferred (Nöh et al., 2007; Nöh et al., 2006; Nöh and Wiechert, 2011). INST-MFA studies in mammalian cells are still very rare. Ahn and Antoniewicz determined metabolic fluxes in growth and non-growth phases of a CHO-K1 monolayer culture using intracellular labeling dynamics and INST-MFA (Ahn and Antoniewicz, 2011). However, there exists no INST-MFA study in mammalian suspension cells to date.

1.4.4 Metabolic pathway analysis using elementary mode analysis

Elementary mode analysis (EMA) is a mathematical tool for analyzing metabolic pathways. It allows for a more general characterization of cellular metabolism and metabolic network functionality than MFA. Similar to metabolite balancing, EMA only relies on the stoichiometric and thermodynamic properties of a metabolic network and does not require any kinetic information. A network with internal and external metabolites and reactions is reconstructed, where the steady state assumption is valid for internal metabolites (Figure 1-7A). However, MFA methods are applied to calculate a single *in vivo* flux distribution for a given condition, thus providing only one specific solution for the metabolic network under investigation (Figure 1-7B, asterisk). Different cultivation conditions will result in distinct metabolic flux distributions (different solutions). In contrast, EMA aims at identifying all possible solutions that can exist for a particular metabolic network, i.e. all elementary modes (EM) (Figure 1-7B, circles spanning the entire solution space or flux cone). An EM can be defined as “a unique, minimal set of enzymes to support steady state operation of a metabolic network with irreversible reactions to proceed in appropriate directions” (Trinh et al., 2009). Four elementary flux modes exist for the example network shown in Figure 1-7. For each metabolic network there exists a set of non-decomposable EM that describes all biochemically feasible pathways converting a certain substrate to a resulting product. In other words, EMA defines the capabilities of a metabolic genotype, while an actual metabolic flux distribution calculated by MFA determines the physiological phenotype for a specific condition. A steady state flux distribution can therefore be expressed as a non-negative linear combination of EM, i.e. a weighted average of all active EM.

EMA can be used to assess and predict inherent properties of the metabolic network structure for a wide range of applications. It assists in exploring the network topology and network functionality, e.g. concerning the flexibility of a network regarding redundancy and robustness. EMA can be applied to estimate metabolic capacities or limitations. The importance of individual reactions can be estimated based on the relative participation in a pathway. EMA can be used to find the optimal pathway for maximizing the product yield on specific substrates or to generally assess the potential of a producer strain. The identification of essential and expendable reactions, enzyme deficiencies,

and metabolic bottlenecks is another application. This is also useful in the analysis of network fragility and helps identifying metabolic engineering or drug targets. EMA allows the investigation of all physiologically relevant and meaningful states for a metabolic system. In CHO cell studies, EMA has been used to design predictive macroscopic models (Provost et al., 2006; Zamorano et al., 2013).

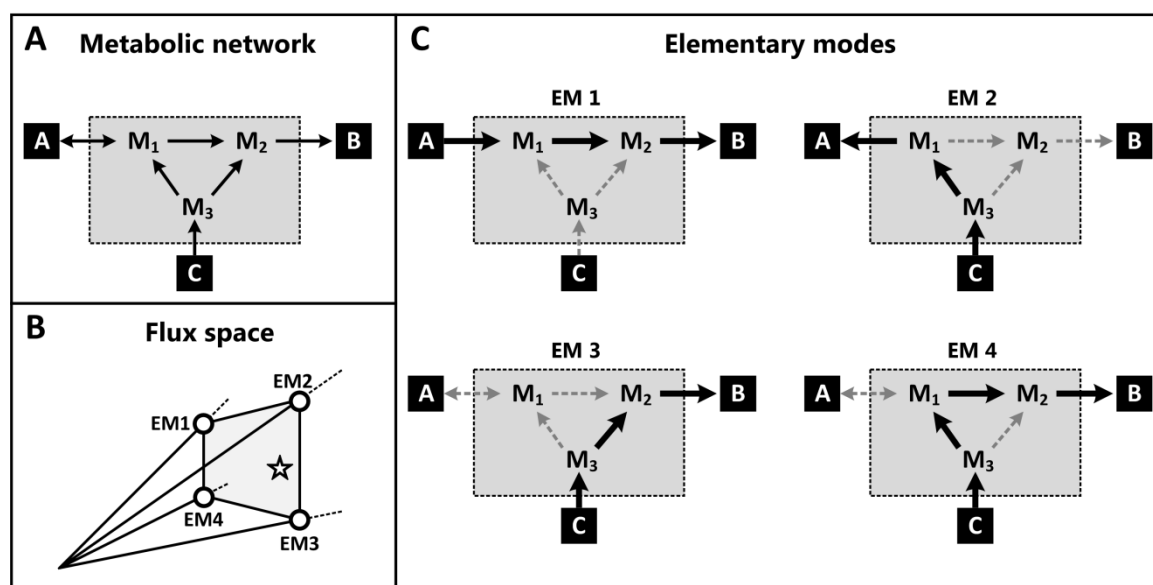


Figure 1-7. Elementary mode analysis. (A) A simple metabolic network composed of the internal metabolites M_1 , M_2 , and M_3 with $dM/dt = 0$ and the external metabolites A , B , and C that do not fulfill the steady state condition. (B) Geometric representation of the solution space. The flux cone represents all feasible metabolic pathways that can exist. It is spanned by four elementary modes (EM) as represented by circles. However, if there exist more EM they can also lie inside of the cone. The EM describe the capabilities of a metabolic network. A metabolic flux distribution under a given condition represented by the asterisk is a specific solution lying inside of the cone. It can be expressed by a linear combination of EM. (C) The four existing EM for the metabolic network shown in (A). The example was taken from (Papin et al., 2004).

1.5 Aim and outline of the thesis

The aim of the presented thesis was to increase the knowledge about metabolic dynamics and compartmentation in Chinese hamster ovary (CHO) cells. Compartmentation and inter-compartment transport substantially complicate the analysis of metabolic pathways. Especially the investigation of metabolic compartmentation in mammalian cells has been mostly neglected in the past. A major objective was the development and implementation of novel experimental techniques, theoretical concepts and computational methods in order to provide a sound basis for approaching this exceptionally challenging issue.

A special focus of the project was directed on the dynamics of cytosolic glycolysis and mitochondrial tricarboxylic acid (TCA) cycle and the metabolic reactions in the connection of these pathways. These include in particular the key reactions around the cellular C3-C4 node that involves conversions of pyruvate, phosphoenolpyruvate, malate and oxaloacetate, with distinct metabolite pools in cytosol and mitochondria. CHO cells have been chosen as an example organism considering their importance as mammalian model system and preeminent industrial relevance.

First, the applied CHO-K1 cell line was characterized by investigating the dynamics of *in vivo* metabolic fluxes and *in situ* enzyme activities during batch cultivation (**chapter 2**). Here, two powerful methods, dynamic metabolic flux analysis and time-resolved determination of compartmental enzyme activities, were combined to study metabolic shifts and metabolic control at the cytosol-mitochondria interface. In two follow-up studies, we explored the impact of the metabolism of glutamine (**chapter 3**) and pyruvate (**chapter 4**) as major substrates of the TCA cycle on the physiology of CHO-K1 cells by metabolic flux analysis using metabolite balancing.

The second part of the thesis aimed at a more in-depth understanding of the CHO cell metabolism. We applied non-stationary ^{13}C metabolic flux analysis based on different labeling studies using either only glucose (**chapter 5**) or glucose and glutamine in parallel (**chapter 6**) as tracer substrates. We were able to resolve the details of the highly complex metabolism of CHO cells. Here, a special emphasis was put on metabolic compartmentation including inter- and intracompartmental fluxes and concentrations, reaction and transport reversibilities and the distinction of amino acid synthetic and catabolic pathways.

The last section of the work focused on mitochondrial studies with selectively permeabilized cells. In a high-throughput respiration screening, we identified single mitochondrial substrates and could draw first conclusions about control of mitochondrial metabolic activities (**chapter 7**). These data served as starting point to design further in-depth studies. Using elementary mode analysis of functional mitochondria within permeabilized cells we explored the mitochondrial metabolic pathways in more detail (**chapter 8**).

Part I

**General characterization of the CHO cell
metabolism using metabolite balancing methods**

2 Metabolic control at the cytosol–mitochondria interface in different growth phases of CHO cells

2.1 Abstract

Metabolism at the cytosol–mitochondria interface and its regulation is of major importance particularly for efficient production of biopharmaceuticals in Chinese Hamster Ovary (CHO) cells but also in many diseases. We used a novel systems-oriented approach combining dynamic metabolic flux analysis and determination of compartmental enzyme activities to obtain systems level information with functional, spatial and temporal resolution. Integrating these multiple levels of information, we were able to investigate the interaction of glycolysis and TCA cycle and its metabolic control. We characterized metabolic phases in CHO batch cultivation and assessed metabolic efficiency extending the concept of metabolic ratios. Comparing *in situ* enzyme activities including their compartmental localization with *in vivo* metabolic fluxes, we were able to identify limiting steps in glycolysis and TCA cycle. Our data point to a significant contribution of substrate channeling to glycolytic regulation. We show how glycolytic channeling heavily affects the availability of pyruvate for the mitochondria. Finally, we show that the activities of transaminases and anaplerotic enzymes are tailored to permit a balanced supply of pyruvate and oxaloacetate to the TCA cycle in the respective metabolic states. We demonstrate that knowledge about metabolic control can be gained by correlating *in vivo* metabolic flux dynamics with time and space resolved *in situ* enzyme activities.

This chapter was published as

Wahrheit J, Niklas J, Heinzle E. (2014). Metabolic control at the cytosol–mitochondria interface in different growth phases of CHO cells. *Metabolic Engineering* 23 9-21.

2.2 Introduction

Although the knowledge of metabolic pathways is very broad, methods for analyzing metabolic control mechanisms in mammalian cells at a systems level are still very limited. A huge number of valuable studies exploring various individual aspects of mammalian metabolism and of its regulation can be found in the literature. Investigated cells range from different mammalian cell lines, e.g. Chinese hamster ovary (CHO) cells, Baby hamster kidney (BHK) cells, hybridoma cells, or myeloma cells, to primary cells or tissues. Usually, a single aspect, e.g. the metabolic flux distribution in a specific growth phase, is analyzed and sometimes different conditions, such as nutrient availability, genetic background, or different biological systems are compared. Such studies are well suited for a qualitative description of differences between distinct conditions. However, detailed quantitative understanding of mammalian metabolism and its control requires systems-oriented combined studies, e.g. of *in vivo* activity and its regulation.

Metabolic compartmentation is a major characteristic in all eukaryotes and represents an essential means of metabolic regulation (Wahrheit et al., 2011). The interaction of cytosolic glycolysis and mitochondrial TCA cycle is central for cellular energy generation and metabolic efficiency. It often represents a bottleneck in production processes (Niklas et al., 2012a; Niklas et al., 2012b; Niklas et al., 2011b) and is at least partially impaired in a wide range of diseases including diabetes, cancer and neurodegenerative disorders (Fernyhough et al., 2010; Haas, 2010; Rosenstock et al., 2010; Schrauwen and Hesselink, 2008; Stacpoole, 2012). Despite this central role in metabolism, many aspects of this metabolic hub are still unknown and remain the target of current studies. Although the existence of a specific mitochondrial pyruvate transporter has been demonstrated in the 1970s, the coding gene was only very recently identified (Bricker et al., 2012; Herzig et al., 2012). Increasing our knowledge in metabolic compartmentation and in particular in understanding the interconnection of glycolysis and TCA cycle at the cytosol–mitochondria interface will substantially advance the optimization of producer cell lines and biotechnological processes as well as the development of novel therapeutic approaches.

CHO cells have been used as a mammalian model system for more than 50 years (Jayapal et al., 2007; Puck et al., 1958) and have therefore been termed as “the mammalian equivalent of *E. coli*” (Puck, 1985). Furthermore, CHO cells are of substantial significance for the biopharmaceutical industry serving as the predominant cultivation system for the production of therapeutic proteins (Wurm, 2004).

In our study, we provide a comprehensive view on CHO central metabolism and its regulation. We used a unique combination of dynamic metabolic flux analysis (MFA) to obtain the time-resolved *in vivo* flux distribution and determination of compartmental *in situ* enzyme activities in different growth phases. This provides systems level information with functional, spatial and temporal resolution. In the first part of our study, we performed dynamic MFA to capture the dynamics of

growth and metabolism upon changing environmental conditions. The cellular adaptation to changing environmental conditions during a batch cultivation leads to metabolic shifts resulting in different growth phases with distinct metabolic states (Niklas et al., 2011c). We identified and characterized different metabolic phases addressing the following questions: (a) what distinguishes the distinct growth phases, (b) which metabolic characteristics determine the metabolic state of each phase, (c) what triggers the phase shifts, and (d) how do the cells respond to these metabolic shifts? Three distinct metabolic states were distinguished, namely overflow metabolism, balanced metabolism and maintenance metabolism.

In order to assess and predict metabolic efficiency at different metabolic states, we expand the concept of metabolic flux ratios. The lactate/glucose ratio is an often-used parameter to characterize the metabolism of mammalian cells (Ahn and Antoniewicz, 2011; Niklas et al., 2012a). We propose the TCA cycle/glycolysis ratio as additional indicator of metabolic efficiency. Furthermore, we analyze the dynamics of these metabolic flux ratios to monitor metabolic shifts.

The first two growth phases are further investigated in the second part by determining specific enzyme activities in distinct growth phases. Applying selective permeabilization techniques in combination with conventional enzyme assays, we were not only able to quantify total enzyme activity but even more important their compartmental distribution (Niklas et al., 2011a).

The last part of our study focused on analyzing the metabolic shift from phase I, characterized by inefficient overflow metabolism, to an efficient and balanced metabolism in phase II by integrating the different data sets. The correlation of *in situ* enzyme activities indicating possible maximum enzyme rates with *in vivo* metabolic rates representing the actual activities represents a powerful approach to gain insight into metabolic control. *In situ* enzyme activities and *in vivo* fluxome integrate information of all upstream functional levels (genome, transcriptome, and proteome), including regulatory events (Sauer, 2006). Additional important information about enzyme localization was obtained from compartmental enzyme activity assays (Niklas et al., 2011a). We integrated information about *in situ* and *in vivo* metabolic activities (functional resolution), metabolic state (time resolution), and compartmental localization of activities (spatial resolution). This allowed us to draw conclusions about metabolic efficiency, rate-limiting steps, glycolytic channeling, and metabolic interactions at the cytosol–mitochondria interface. We demonstrate that metabolic control in the central metabolism and eventually potential targets for process optimization and biomedical research can be identified by correlating *in vivo* metabolic flux dynamics with respective time and space resolved *in situ* enzyme activities.

2.3 Material and methods

2.3.1 Cell culture

The CHO-K1 cells were cultivated in protein free and chemically defined TC-42 medium (TeutoCell, Bielefeld, Germany) supplemented with 4 mM glutamine in 250 ml baffled shake flasks in a shaking incubator (2 inches orbit, 185 rpm, 37°C, 5% CO₂ supply). Two parallel cultivations of 100 ml volume were inoculated with 2×10^5 cells/ml. Cell density, cell viability and average cell diameter were determined using an automated cell counter (Invitrogen, Darmstadt, Germany).

2.3.2 Analytics

Quantification of glucose, organic acids and proteinogenic amino acids in supernatants were performed by HPLC as described previously (Strigun *et al.*, 2011b).

2.3.3 Metabolic flux analysis

Time resolved metabolic flux analysis was carried out using the method and metabolic network model described by Niklas *et al.* (2011c). The stoichiometric matrix of the metabolic network model is depicted in Supplementary Table S1.

2.3.4 Enzyme assays

For determination of specific enzyme activities in different growth phases, cells from two different cultures, the first one being between 48 h and 96 h cultivation time (phase I) and the second one between 96 h and 144 h after seeding (phase II), were harvested in parallel. Enzyme assays were performed in 96-well plates as described in Niklas *et al.* (Niklas *et al.*, 2011a) using selective permeabilization techniques for discrimination between cytosolic and mitochondrial activities. For each condition, complete permeabilization with Triton X-100, selective permeabilization with digitonin, and respective negative controls were performed with four technical replicates each. The change of absorbance at 340 nm was monitored over time for all NADH or NADPH dependent enzyme assays ($\epsilon_{340 \text{ nm}}=6.22 \text{ M}^{-1} \text{ cm}^{-1}$). For the citrate synthase assay, absorbance of dithionitrobenzoic acid (DTNB) at 412 nm was measured ($\epsilon_{412 \text{ nm}}=14.15 \text{ M}^{-1} \text{ cm}^{-1}$). In the applied 96-well format, layer thickness ($d=0.746 \text{ cm}$) was experimentally determined with NADH solutions at different concentrations using Lambert-Beer's law.

Assays for glucose-6-phosphate isomerase (PGI; EC:5.3.1.9), lactate dehydrogenase (LDH; EC:1.1.1.27), glucose-6-phosphate dehydrogenase (G6PDH; EC:1.1.1.49), fructose-1,6-bisphosphatase (FBPase; EC:3.1.3.11), NAD⁺- and NADP⁺-dependent isocitrate dehydrogenase (IDH_{NAD}; EC:1.1.1.41, and IDH_{NADP}; EC:1.1.1.42), malic enzyme (ME; EC:1.1.1.40), and glutamate dehydrogenase (GDH; EC:1.4.1.3) were carried out according to Niklas *et al.* (2011a). Assay solutions for other enzymes were as follow: Hexokinase (HK; EC:2.7.1.1): 1 mM MgCl₂, 6 mM

ATP, 1 mM NADP⁺, 10 mM glucose, 0.35 U glucose-6-phosphate dehydrogenase, and PBS. Phosphofructokinase (PFK; EC:2.7.1.11): 5 mM MgCl₂, 0.15 mM NADH, 0.05 mM ATP, 0.1 U aldolase, 0.6 U glycerol phosphate dehydrogenase, 9.4 U triose phosphate isomerase, 0.25 mM fructose-6-phosphate, and PBS. Pyruvatekinase (PK; EC:2.7.1.40): 15 mM MgCl₂, 0.25 mM NADH, 1 mM ADP, 1.2 U lactate dehydrogenase, 12 mM phosphoenolpyruvate, and PBS. After permeabilization the cell suspension was diluted 1:5 before used for this assay. Citrate synthase (CS; EC:2.3.3.1): 0.1 mM acetyl-Coenzyme A, 0.2 mM 5,5'-dithiobis-2-nitrobenzoic acid (DTNB), 0.5 mM oxaloacetate, and PBS. Phosphoenolpyruvate carboxykinase (PEPCK; EC:4.1.1.32): 1 mM MgCl₂, 0.15 mM NADH, 1 mM phosphoenolpyruvate, 1.5 mM GDP, 5 mM KHCO₃, >12 U malate dehydrogenase, and PBS. Alanine aminotransferase (ALAT; EC:2.6.1.2): 0.15 mM NADH, 0.02 mM pyridoxalphosphate, 200 mM alanine, 10 mM α-ketoglutarate, >17 U lactate dehydrogenase, and PBS. Aspartate aminotransferase (ASAT; EC:2.6.1.1): 0.15 mM NADH, 0.02 mM pyridoxalphosphate, 50 mM aspartate, 10 mM α-ketoglutarate, >12 U malate dehydrogenase, and PBS. Enzyme activities are related to dry cell mass [g] making those directly comparable to metabolic rates. The cellular dry weight was determined to be 290 pg/cell.

The total activity, $r_{T,i}$ was measured after permeabilization with Triton X-100. It comprises two different activities, $r_{D,i}$ and $r_{R,i}$, where i indicates the corresponding enzyme.

$$r_{T,i} = r_{D,i} + r_{R,i} \quad (1)$$

The activity $r_{D,i}$ represents the part of activity that is measured after selective plasma membrane permeabilization using digitonin. The activity $r_{R,i}$ corresponds to the cellular activity that is additionally measured after Triton X-100 treatment.

The isocitrate dehydrogenase activity that is available for the TCA cycle, IDH_{TCA} , was calculated as the sum of the activities $r_{R,IDHNAD}$ (NAD⁺-dependent isocitrate dehydrogenase, IDH_{NAD}) and $r_{R,IDHNADP}$ (NADP⁺-dependent isocitrate dehydrogenase, IDH_{NADP}).

$$r_{IDHTCA} = r_{R,IDHNAD} + r_{R,IDHNADP} \quad (2)$$

2.4 Results

2.4.1 Growth and extracellular metabolite profile of CHO-K1 cells

The growth profile could be divided into three phases with distinct specific growth rates (Figure 2-1A). During the first 96 h of cultivation (phase I), we observed exponential growth at a high specific growth rate ($\mu = 0.037 \pm 0.001 \text{ h}^{-1}$; $R^2 = 1.00$). During phase II, lasting from 96 to 144 h, the cells grew at a reduced rate ($\mu = 0.017 \pm 0.002 \text{ h}^{-1}$; $R^2 = 0.99$). The last phase (phase III) was characterized by further growth retardation. However, viability was kept constant for another 48 h.

These characteristic phases were clearly reflected in the extracellular metabolite profile (Figure 2-1B and Supplementary Figure 1). The major substrate in phase I was glucose. Glutamine, asparagine, serine and pyruvate were additionally consumed in substantial amounts. Mainly lactate, alanine, glycine, and much less glutamate were excreted as overflow products. At the end of phase I, glutamine was depleted. Besides glucose, lactate was the main substrate in phase II. Asparagine, aspartate, glutamate, and pyruvate were completely consumed during the second phase resulting in a lack of nutrients in phase III. Glucose and lactate were completely consumed during the last phase. In addition, alanine, which has been accumulated during former phases, was eventually taken up as well.

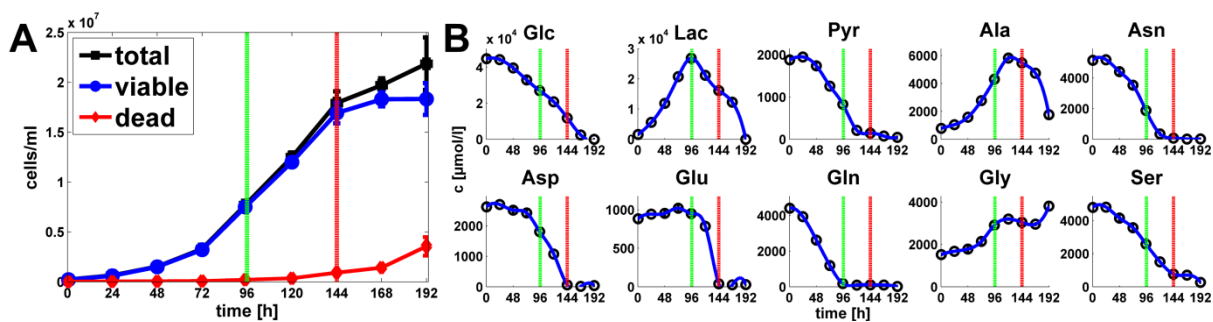


Figure 2-1. The cultivation profile of CHO-K1 batch cultivation. (A) Growth curve of CHO-K1. Total (black), viable (blue), and dead (red) cell densities [cells/ml] are plotted over the cultivation time [h]. (B) Extracellular metabolite profile of CHO-K1. Selected extracellular metabolite concentrations [$\mu\text{mol/l}$] over the cultivation time [h] are shown. The complete set of extracellular metabolites is provided in Supplementary Figure 1. The dashed vertical lines indicate the end of phase I (green) and II (red). Mean values and standard deviations from two parallel cultivations are shown. Abbreviations: Glc glucose, Lac lactate, Pyr pyruvate. For amino acids, the standard three-letter code is used.

2.4.2 Time-resolved metabolic flux distribution

Dynamic metabolic flux analysis (MFA) (Niklas et al., 2011c) was applied to calculate metabolic fluxes over time. Selected fluxes are shown in Figure 2-2. The complete set of extra- and intracellular fluxes is presented in Supplementary information (Supplementary Figures 2 and 3). Generally, rates are only shown starting from 24 h due to inherent difficulties and high uncertainty in determining rates from very small changes in concentrations. Even the application of spline fitting does not well enough solve this problem (Wahrheit et al., 2014a).

2.4.2.1 Glycolysis and pentose-phosphate pathway

Fluxes of glucose uptake, glycolysis, and lactate production were very high in the beginning but then decreased rapidly within the first phase. In phases II and III, lactate and glucose were consumed in parallel, although at much lower rates. Glycolytic rates were nearly constant in phase

II. Glucose depletion stopped glycolytic activity. PPP activity related to anabolic demand was estimated highest in the first 72 h matching the high specific growth rate during phase I. Afterwards it was constantly decreasing.

2.4.2.2 Pyruvate metabolism and TCA cycle

In phase I, pyruvate uptake rate, pyruvate transport into mitochondria, pyruvate dehydrogenase reaction, and TCA cycle fluxes were quite variable, reaching a maximum value within the first 48 h. Pyruvate consumption was lower in phase II and nearly 0 in phase III (Supplementary Figure 2). Mitochondrial pyruvate transport and TCA cycle fluxes were relatively constant in the second phase and only slightly decreasing towards the end of cultivation (Figure 2-2).

2.4.2.3 Amino acid metabolism

Conversion of pyruvate to alanine via alanine aminotransferase (ALAT) resulted in high excretion of alanine in the first two phases. In phase III, alanine was converted back to pyruvate. Between 48 and 144 h, flux from serine to pyruvate, comprising glycolytic intermediates from 1,3-bisphosphoglycerate to pyruvate, was negative indicating serine biosynthesis from 3-phosphoglycerate in addition to the high serine uptake in phases I and II. Glycine synthesis from serine, resulting in the formation of activated C₁-units, and glycine excretion rates were high and relatively constant within the first 72 h. Then they dropped until the end of phase II before slightly increasing again in phase III.

Glutamine and asparagine were initially taken up at high rates and further converted to glutamate and aspartate. They were feeding the TCA cycle by conversion into α -ketoglutarate and oxaloacetate via glutamate dehydrogenase (GDH) and aspartate aminotransferase (ASAT), respectively. However, at the end of phase I and in phase II, GDH worked in the direction of glutamate formation draining carbons from the TCA cycle (Figure 2-2).

After a relatively high initial uptake of the essential amino acids (arginine, histidine, threonine, leucine, isoleucine, valine, lysine, methionine, phenylalanine, tyrosine, and tryptophan) and proline, their consumption fluctuated around 0 indicating no significant contribution to catabolic processes. Despite an excess supply in the extracellular medium, their uptake was just matching the anabolic demand (Supplementary Figure 2).

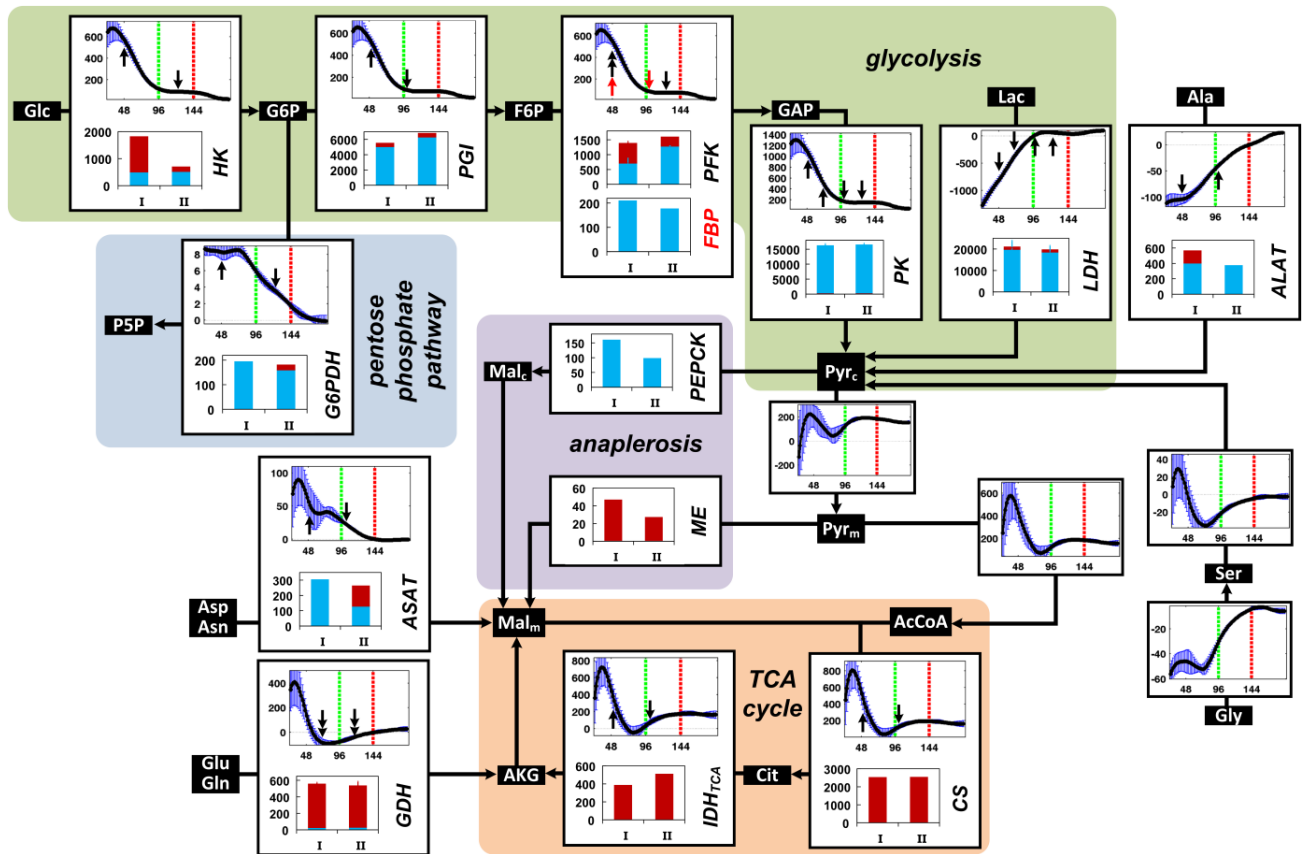


Figure 2-2. Time-resolved metabolic flux distribution and compartmental enzyme activities in the first two growth phases. Selected metabolic fluxes [$\mu\text{mol g}^{-1} \text{h}^{-1}$] over time [h] and enzyme activities [$\mu\text{mol g}^{-1} \text{h}^{-1}$] in phases I and II in the central metabolism of CHO-K1 are shown. All activities are related to dry cell mass [g]. The complete set of fluxes and *in vitro* enzyme activities are provided in Supplementary Figures 2, 3 and 4. Note that the timescale starts at 24 h because of high uncertainty of determination of initial slopes using splines. The arrows in the flux plots indicate the sampling times for the respective *in vitro* enzyme assays. Blue and red bars indicate activities $r_{D,i}$ and $r_{R,i}$ respectively. For definition of activities $r_{D,i}$ and $r_{R,i}$ see also Equation (1). The activity $r_{D,i}$ represents the part of activity that is measured after selective plasma membrane permeabilization using digitonin. The activity $r_{R,i}$ corresponds to the residual cellular activity that is additionally measured upon Triton X-100 treatment ($r_{R,i} = r_{T,i} - r_{D,i}$). Abbreviations: Glc – glucose, G6P – glucose-6-phosphate, P5P – pentose-5-phosphate, F6P – fructose-6-phosphate, GAP – glyceraldehyde-3-phosphate, Pyr – pyruvate, Lac – lactate, AcCoA – acetyl-CoA, Mal – malate, Cit – citrate, AKG – α -ketoglutarate, PEP – phosphoenolpyruvate, OAA – oxaloacetate. For amino acids, the standard three letter code is used. Subscript c and m indicate cytosolic and mitochondrial metabolite pools, respectively. HK – hexokinase, PGI – phosphoglucose isomerase, PFK – phosphofructokinase, FBP – fructose-1,6-bisphosphatase, PK – pyruvate kinase, ALAT – alanine aminotransferase, ASAT – aspartate aminotransferase, GDH – glutamate dehydrogenase, CS – citrate synthase, IDH_{TCA} – (mitochondrial part of) NAD- and NADP-dependent isocitrate dehydrogenases (see also Equation (2)), PEPCK – phosphoenolpyruvate carboxykinase, ME – malic enzyme.

2.4.3 Metabolic ratios

Time-resolved analysis of specific flux ratios allows the determination of the phase-shift timing and the identification of plateaus indicating stable metabolic states. The lactate/glucose ratio and the TCA cycle/glycolysis ratio were determined to assess metabolic efficiency (Figure 2-3A and B).

2.4.3.1 Lactate/glucose ratio

Glucose and lactate represent the most important carbon sources. On the other hand, lactate is also the most significant waste product. The lactate/glucose ratio ($v_{Lac\ ex\rightarrow Lac\ in}/v_{Glc\ ex\rightarrow Glc\ in}$) gives an indication about waste product formation relative to consumption of the major carbon sources (Figure 2-3A). In phase I, a nearly constant value of -1.5 indicates a stable metabolic state. The theoretical maximum ratio is 2 moles lactate per mole glucose. The value of -1.5 means that 75% of carbon originating from glucose was initially lost by lactate excretion and only 25% was further metabolized. After 72 h, a metabolic shift was induced. The lactate/glucose ratio changed the sign at 96 h determining the end of phase I. In phase II, glucose and lactate were consumed in parallel as shown by a positive ratio around 0.6 moles lactate per mole glucose. In this phase, glucose and lactate were simultaneously consumed in equal molar amounts. Therefore the carbon contribution from lactate was 50% that of glucose. At the end of phase II, decreasing availability of glucose led to an increasing contribution of lactate as carbon source as shown by an increasing lactate/glucose ratio in phase III.

2.4.3.2 TCA cycle/glycolysis ratio

The relative activities of TCA cycle and glycolysis as well as their coordinated interplay are crucial for cellular efficiency. The ratio of the fluxes from F6P to GAP ($v_{F6P\rightarrow GAP}$), representing glycolytic activity, and the formation of citrate ($v_{OAA\rightarrow Cit}$), an indicator for TCA cycle activity, provides information about the type of energy generation and about the connection of these pathways (Figure 2-3B). In phase I, the TCA cycle/glycolysis ratio showed a large variation between 1.3 and 0.2 mol/mol. This indicates a variable connection between both pathways. A ratio below 1 indicates a significant glycolytic contribution to energy generation. In the phases II and III, TCA cycle activity was clearly exceeding glycolytic activity as shown by a ratio higher than 1. A nearly constant value of 2.5 in phase II indicates a stable metabolic state with high connectivity between glycolysis and TCA cycle and mainly aerobic energy generation. The ratio was further increasing in phase III when extracellular glucose concentration and glycolytic activity dropped but TCA cycle fluxes were maintained at high rates.

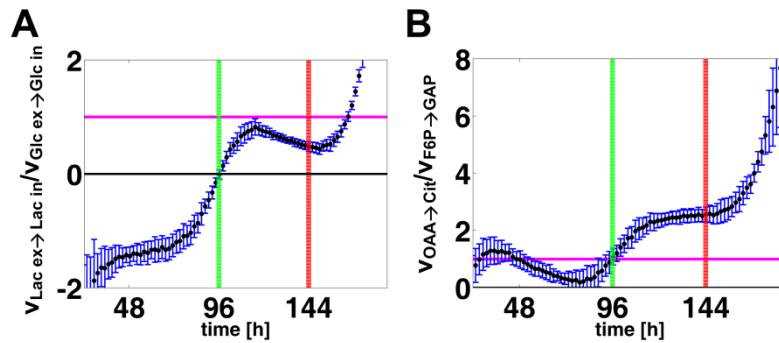


Figure 2-3. Metabolic ratios of selected metabolic fluxes. (A) Lactate/glucose ratio, the lactate uptake rate relative to the glucose uptake rate ($v_{Lac\ ex \rightarrow Lac\ in} / v_{Glc\ ex \rightarrow Glc\ in}$ [mol/mol]). (B) TCA cycle/glycolysis ratio, the TCA cycle activity relative to the glycolytic activity ($v_{OAA \rightarrow Cit} / v_{F6P \rightarrow GAP}$) [mol/mol]). Ratios and standard deviations were calculated by Monte Carlo simulation using the fluxes estimated by dynamic metabolic flux analysis. Note that the timescale starts at 24 h because of high uncertainty of determination of initial slopes.

2.4.4 *In vitro* enzyme activities and their compartmental localization in different growth phases

We applied selective permeabilization methods for discrimination of different enzyme activities (Niklas et al., 2011a) (Figure 2-2, Supplementary Figure 4). The total activity $r_{T,i}$ corresponds to the activity that was measured after Triton X-100 treatment. The activity $r_{D,i}$ is the fraction of activity that was measured after selective plasma membrane permeabilization with digitonin (Equation (1)). If $r_{D,i}$ is equal to $r_{T,i}$ the enzyme is cytosolic and the active center is freely accessible after digitonin treatment. The effects of digitonin treatment are weaker than those of Triton X-100 and leave intracellular structures including protein complexes intact. Residual activity $r_{R,i}$ is additionally measured after Triton X-100 treatment (see also Equation (1)). This activity is related to that fraction of enzymes that is not accessible after selective permeabilization with digitonin. This can be due to two reasons: (1) The enzyme is confined in a different compartment that is not permeabilized by digitonin treatment. In this case, the activity $r_{R,i}$ corresponds to the mitochondrial activity. (2) The enzyme is cytosolic but either the active site of the enzyme is not accessible or its activity is reduced by binding to intracellular structures. In this case, we define activity $r_{R,i}$ as concealed. When Triton X-100 is applied, such protein complexes dissociate permitting the measurement of the activity of the then solitary enzymes. Differences between the distinct metabolic phases are summarized in Table 2-1.

Table 2-1. Specific enzyme activities in phase II relative to activities measured in phase I. The total activity, $r_{T,i}$, is measured after permeabilization with Triton X-100. It comprises two different activities, $r_{D,i}$ and $r_{R,i}$, where i indicates the corresponding enzyme (Equation (1)). The activity $r_{D,i}$ represents the part of activity that is measured after selective plasma membrane permeabilization using digitonin. The activity $r_{R,i}$ corresponds to the cellular activity that is additionally measured after Triton X-100 treatment. The isocitrate dehydrogenase activity that is available for the TCA cycle, r_{IDHTCA} , was calculated as the sum of the activities $r_{R,IDHNAD}$ and $r_{R,IDHNADP}$ (Equation (2)). Abbreviations: HK – hexokinase, PGI – glucose-6-phosphate isomerase, PFK – phosphofructokinase, PK – pyruvate kinase, LDH – lactate dehydrogenase, G6PDH – glucose-6-phosphate dehydrogenase, FBP – fructose-1,6-bisphosphatase, CS – citrate synthase, IDH – isocitrate dehydrogenase, PEPCK – phosphoenolpyruvate carboxykinase, ME – malic enzyme, GDH – glutamate dehydrogenase, ALAT – alanine aminotransferase, ASAT – aspartate aminotransferase, and n.a. – no activity. Statistical significance as determined by two-tailed, unpaired student's t -test is indicated by asterisks

Enzyme	Activity relative to phase I [%]		
	$r_{T,i}$	$r_{D,i}$	$r_{R,i}$
HK	37 ***	104	11 *
PGI	125 **	119 *	208
PFK	115 *	151 **	68 *
PK	102	102	n.a.
LDH	93	93	91
FBP	84	84	n.a.
G6PDH	93	84	<i>Activation</i>
CS	102	n.a.	102
IDH _{NAD}	333 ***	n.a.	333 ***
IDH _{NADP}	121 **	118 **	126 *
IDH _{TCA}	134 **	n.a.	134 **
ME	56 **	n.a.	56 **
PEPCK	60 **	60 **	n.a.
GDH _{NAD(P)}	95	n.a.	95
ALAT	62 **	90	0 ***
ASAT	87	46 **	<i>Activation</i> ***

* $p < 0.05$.

** $p < 0.01$.

*** $p < 0.001$.

2.4.4.1 Total activities in glycolysis, gluconeogenesis and pentose-phosphate pathway

Hexokinase (HK) and phosphofructokinase (PFK) exhibited the lowest total activities of all glycolytic enzymes investigated (Figure 2-2). In phase II, HK activity was even reduced to 37% of phase I (1800 and 660 $\mu\text{mol g}^{-1} \text{h}^{-1}$ for phases I and II, respectively; Figure 2-2 and Table 2-1). In contrast, PFK activity was slightly increased by 15% (1300 and 1500 $\mu\text{mol g}^{-1} \text{h}^{-1}$ for PFK in phases I and II, respectively; Figure 2-2 and Table 2-1). The phosphoglucose isomerase (PGI) connecting the HK and the PFK reactions had a much higher activity (5500 and 6800 $\mu\text{mol g}^{-1} \text{h}^{-1}$, Figure 2-2). The PGI activity increased significantly by 25% in phase II (Table 2-1). The *in vitro* activity of the pyruvate kinase (PK) was similar in both phases (Table 2-1). It was at least ten times higher than the HK and PFK activities (15300 and 15500 $\mu\text{mol g}^{-1} \text{h}^{-1}$, Figure 2-2). The highest specific activity of all enzymes investigated in the central metabolism was observed for the lactate dehydrogenase (LDH) (20500 and 19200 $\mu\text{mol g}^{-1} \text{h}^{-1}$, Figure 2-2). No significant difference was detected between phases I and II (Table 2-1). The fructose-1,6-bisphosphatase activity (FBPase) representing the key enzyme of gluconeogenesis was low (190 and 140 $\mu\text{mol g}^{-1} \text{h}^{-1}$, Figure 2-2). The activity of glucose-6-phosphate dehydrogenase (G6PDH) catalyzing the first and irreversible reaction of the PPP was in the same range (190 and 180 $\mu\text{mol g}^{-1} \text{h}^{-1}$, Figure 2-2). Both activities were slightly but not significantly reduced in phase II (Table 2-1).

2.4.4.2 Localization of glycolytic enzymes

It is well established that glycolytic enzymes are located in the cytosol (Michal and Schomburg, 2012). However, they are partially bound to cellular structures (cellular membranes, the mitochondria, and the cytoskeleton) and are associated with each other (Michal and Schomburg, 2012). We found that for several glycolytic enzymes (HK, PGI, PFK, LDH; however not PK) the activity measured after Triton X-100 treatment, $r_{T,i}$ was higher than after digitonin treatment, $r_{D,i}$. This indicates that a significant part of activity is not detectable after digitonin treatment, $r_{R,i}$. In the case of HK and PFK, we found significant differences between the two growth phases (Figure 2-2 and Table 2-1). $r_{D,HK}$ and $r_{D,PFK}$ increased and $r_{R,HK}$ and $r_{R,PFK}$ decreased with time. About 72% in phase I but only 18% in phase II of the total HK activity was additionally measured after permeabilization with Triton X-100 (Figure 2-2). The fraction of residual PFK activity decreased constantly from 50% after 48 h to 18% after 120 h of cultivation (Figure 2-4).

It was found that although the total HK activity ($r_{T,HK}$) was largely reduced in the second phase, the ‘free’ part of activity ($r_{D,HK}$) was not significantly altered. Only the ‘concealed’ activity ($r_{R,HK}$) was significantly reduced to 11% (Table 2-1). The total PFK activity ($r_{T,PFK}$) was only slightly increased in phase II. However, the ‘free’ activity ($r_{D,PFK}$) was increased to 151% and the ‘concealed’ activity ($r_{R,PFK}$) reduced to 68% relative to phase I (Table 2-1). Concerning the distribution of ‘free’ ($r_{D,i}$) and

‘concealed’ ($r_{R,i}$) activities, no significant differences between the two growth phases were found for PGI and LDH (Table 2-1).

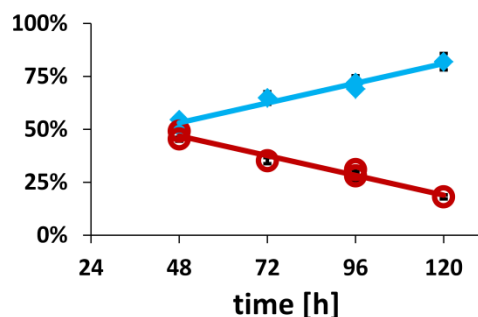


Figure 2-4. Relative distribution of the phosphofruktokinase activity at different time points during cultivation. Blue diamonds indicate the fraction of enzyme activity that was detected after digitonin treatment, $r_{D,PFK}$ (Equation (1)). Red circles indicate the fraction of activity that was additionally detected after Triton X-100 treatment, $r_{R,PFK}$ (Equation (1)).

2.4.4.3 TCA cycle and anaplerotic enzymes

Citrate synthase (CS) activity was only detected after Triton X-100 treatment ($r_{T,CS}=r_{R,CS}$) indicating a mitochondrial localization (2490 and 2450 $\mu\text{mol g}^{-1} \text{h}^{-1}$ for phases I and II, respectively; Figure 2-2). No significant difference was observed for the two growth phases (Table 2-1). For isocitrate dehydrogenase (IDH), different isoenzymes could be identified due to cofactor dependence (Supplementary Figure 4). NAD^+ -dependent IDH activity (IDH_{NAD}) was very low in both phases (20 and 66 $\mu\text{mol g}^{-1} \text{h}^{-1}$, Supplementary Figure 4). However, in the second growth phase, its activity was more than three times higher (Table 2-1). Corresponding to its exclusive mitochondrial localization (Michal and Schomburg, 2012), its activity was only measured after Triton X-100 treatment ($r_{T,\text{IDH}_{\text{NAD}}}=r_{R,\text{IDH}_{\text{NAD}}}$). NADP^+ -dependent IDH (IDH_{NADP}) activity was measured in different fractions after both treatments. This indicates localization in cytosol and mitochondria. The major part was located in the cytosol ($r_{D,\text{IDH}_{\text{NADP}}}=850$ and $1000 \mu\text{mol g}^{-1} \text{h}^{-1}$ for phases I and II, respectively). Only 30% of total cellular activity ($r_{T,\text{IDH}_{\text{NADP}}}=1200$ and $1450 \mu\text{mol g}^{-1} \text{h}^{-1}$) was found in mitochondria ($r_{R,\text{IDH}_{\text{NADP}}}=360$ and $450 \mu\text{mol g}^{-1} \text{h}^{-1}$). In phase II, the activity increased equally in both compartments so that the relative subcellular distribution did not change (Table 2-1). The sum of mitochondrial IDH activities, representing the TCA cycle activity (IDH_{TCA} in Figure 2-2, see also Equation (2)), was significantly increased by 34% in phase II (Table 1).

Low activities of phosphoenolpyruvate carboxykinase (PEPCK) and malic enzyme (ME) were found in both growth phases (Figure 2-2). For PEPCK almost identical activities were measured after Triton X-100 treatment and digitonin treatment ($r_{T,PEPCK}=r_{D,PEPCK}$). This indicates exclusive localization in the cytosol (150 and 90 $\mu\text{mol g}^{-1} \text{h}^{-1}$ in phases I and II). ME activity was only detected after Triton X-100 treatment indicating exclusive mitochondrial localization ($r_{T,ME}=r_{R,ME}$). Both activities were significantly reduced in phase II to 60% and 56%, respectively (Table 2-1).

2.4.4.4 Amino acid metabolism

It is well known that glutamate dehydrogenase (GDH) activity is exclusively found in mitochondria (Michal and Schomburg, 2012). This was confirmed in our experiments (Supplementary Figure 4). No significant difference was observed for the two growth phases (570 and 570 $\mu\text{mol g}^{-1} \text{h}^{-1}$ for $r_{R,GDHNAD}$ and 530 and 490 $\mu\text{mol g}^{-1} \text{h}^{-1}$ for $r_{R,GDHNADP}$, Figure 2-2, Table 2-1). Similar activities measured with NADH and NADPH indicate that there is only one isoenzyme using both cofactors as has been described in literature (Michal and Schomburg, 2012). Alanine (ALAT) and aspartate (ASAT) aminotransferase activities were quite different in distinct growth phases. In phase I, ALAT was active in both compartments. One third of total activity ($r_{T,ALAT}=540 \mu\text{mol g}^{-1} \text{h}^{-1}$) was located in mitochondria ($r_{R,ALAT}=150 \mu\text{mol g}^{-1} \text{h}^{-1}$, Figure 2-2). In phase II, only the cytosolic activity was maintained ($r_{D,ALAT}=350 \mu\text{mol g}^{-1} \text{h}^{-1}$, Figure 2-2), which was not significantly different from phase I ($r_{D,ALAT}=390 \mu\text{mol g}^{-1} \text{h}^{-1}$, Figure 2-2, Table 2-1). Mitochondrial activity was not detected any more. For ASAT, only a small difference in total cellular activities was observed ($r_{T,ASAT}$, 300 and 260 $\mu\text{mol g}^{-1} \text{h}^{-1}$, Figure 2-2, Table 2-1). However, in phase I, only cytosolic activity was measured while in phase II half of the total activity ($r_{T,ASAT}=260 \mu\text{mol g}^{-1} \text{h}^{-1}$, Figure 2-2) was located in mitochondria ($r_{R,ASAT}=130 \mu\text{mol g}^{-1} \text{h}^{-1}$, Figure 2-2).

2.4.5 Comparison of *in vitro* enzyme activities with respective *in vivo* fluxes

Specific *in vitro* activities represent the potential maximal activity. These were related to respective *in vivo* fluxes representing actual rates by determination of *in vitro/in vivo* ratios (Figure 2-5). Low ratios indicate that the enzyme is highly saturated and that the *in vivo* rate is only limited by the enzyme concentration. High ratios mean that, at least in Michaelis-Menten type kinetics, the enzyme operates in the first order region where *in vivo* rates depend on both the concentration of enzyme and substrates. The lower the ratio the higher is its contribution to metabolic control. Most enzymes showed a substantial overcapacity with *in vitro* activities largely exceeding the respective *in vivo* activities. However, for some reactions the *in vivo* activities were close to the specific *in vitro* activities. Of the five glycolytic enzymes investigated, HK and PFK had the lowest *in vitro/in vivo* ratios in both growth phases. This emphasizes their importance for glycolytic flux control. Ratios of all glycolytic enzymes were significantly higher in the second growth phase. The first reaction of the PPP catalyzed by the G6PDH had similar ratios in phases I and II. In phase I, CS and IDH_{TCA} had low *in vitro/in vivo* ratios of 5 and 1, respectively. The ratios of the GDH and the aminotransferases were also relatively low. The ALAT and ASAT reactions had quite similar ratios in both growth phases. The *in vitro/in vivo* ratios of the GDH and the TCA cycle enzymes were increased in phase II, but were still low. None of them showed such a high overcapacity as PGI, PK, or LDH.

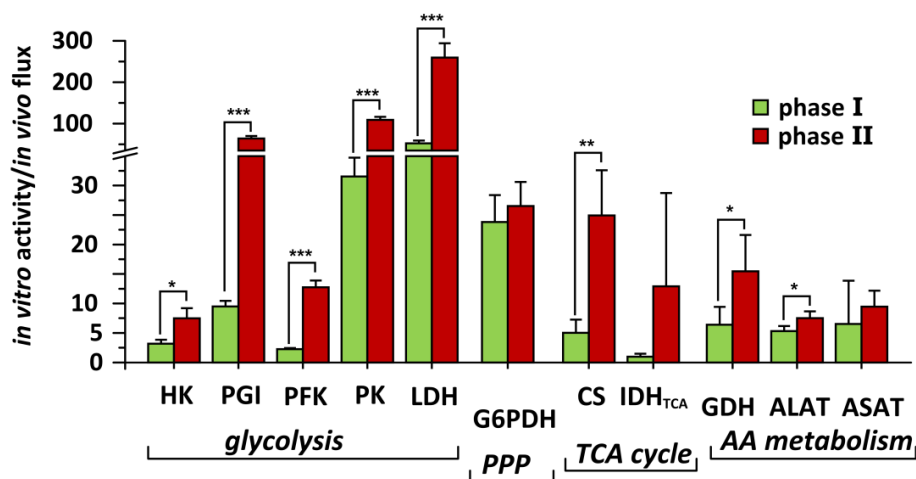


Figure 2-5. Ratios of specific *in vitro* enzyme activities and respective *in vivo* fluxes determined by dynamic metabolic flux analysis in growth phase I (green bars) and phase II (red bars). Glycolysis: $HK/v_{Glcex \rightarrow Glcin}$, $PGI/v_{G6P \rightarrow F6P}$, $PFK/v_{F6P \rightarrow GAP}$, $PK/v_{GAP \rightarrow Pyr}$, $LDH/v_{Lacex \rightarrow Lacin}$; PPP: $G6PDH/v_{G6P \rightarrow P5P}$; TCA cycle: $CS/v_{OAAm \rightarrow Citm}$, $IDH_{TCA}/v_{Citm \rightarrow AKGm}$; Amino acid (AA) metabolism: $GDH/v_{AKGm \rightarrow Glu}$, $ALAT/v_{Pyr \rightarrow Ala}$, $ASAT/v_{Asp \rightarrow OAA}$. The *in vitro/in vivo* ratios were calculated by Monte Carlo simulation including the standard deviations of the enzyme assays and the flux calculation, respectively. Statistical significance as determined by student's *t*-test is represented by asterisks: *** = $p < 0.001$, ** = $p < 0.01$, and * = $p < 0.05$.

2.5 Discussion

2.5.1 Metabolic flux dynamics and compartmental enzyme activities

The unique combination of dynamic MFA and determination of compartmental enzyme activities in distinct growth phases using selective permeabilization represents a novel approach for a quantitative and thorough analysis of metabolism.

Metabolite balancing is the most commonly used MFA method for the analysis of mammalian cells (Niklas and Heinzle, 2012). The applied time-resolved MFA method offers particular advantages over classical MFA techniques. It allows capturing the complete time-course of batch cultivation, thus monitoring metabolic shifts caused by environmental changes (Wahrheit et al., 2014a). Conventional stationary flux analysis using metabolite balancing methods often considers only a single growth phase, usually the exponential growth phase (Niklas et al., 2009), or distinct separate phases (Altamirano et al., 2006; Altamirano et al., 2001b), thereby neglecting the phase transitions.

In addition, we investigate metabolic flux ratios. The lactate/glucose ratio is a commonly applied parameter for characterizing the metabolism of mammalian cells (Ahn and Antoniewicz, 2011; Ahn and Antoniewicz, 2013). In our study, we extend the concept of metabolic ratios (1) by proposing additionally the TCA cycle/glycolysis ratio as a meaningful parameter to assess metabolic efficiency, and (2) by analyzing the dynamics of these metabolic ratios. The time-resolved analysis

of these metabolic flux ratios as sensitive parameters of metabolic changes represents a powerful tool for characterizing the central metabolism and metabolic efficiency in CHO batch cultivation.

Furthermore, we applied a simple, fast, and robust protocol that allows the determination of total enzyme activity levels as well as discrimination of mitochondrial and extra-mitochondrial enzymes (Niklas et al., 2011a). The applied selective permeabilization method allows a high throughput. It requires little cell material and does not require laborious isolation of mitochondria. Very few former studies differentiated between cytosolic and mitochondrial enzyme activities. Vriezen and van Dijken studied enzyme activities in mouse myeloma cells (Vriezen and van Dijken, 1998b). They used sonication and differential centrifugation to separate a particulate fraction containing the mitochondria and a soluble fraction containing cytosol and other cell components. To obtain necessary high cell numbers, sampling from a chemostat was done over a period of 16 h. Loss of enzyme activity may occur and could affect total activities and subcellular distribution patterns. The neglect of compartmental information can result in inaccurate assumptions about the availability of enzymes for certain pathways that would lead to biased conclusions. Including this information on the other hand allows deriving additional constraints for the set-up of metabolic network models and can provide information about limiting steps of metabolic pathways.

The combination of these two powerful methods represents the most important part of this study. Previous metabolic studies rarely considered more than one aspect. They focused rather on the description than on a thorough and comprehensive understanding of metabolism. The integration of multiple data sets as proposed in our study allows drawing conclusions about metabolic control (Figure 2-6).

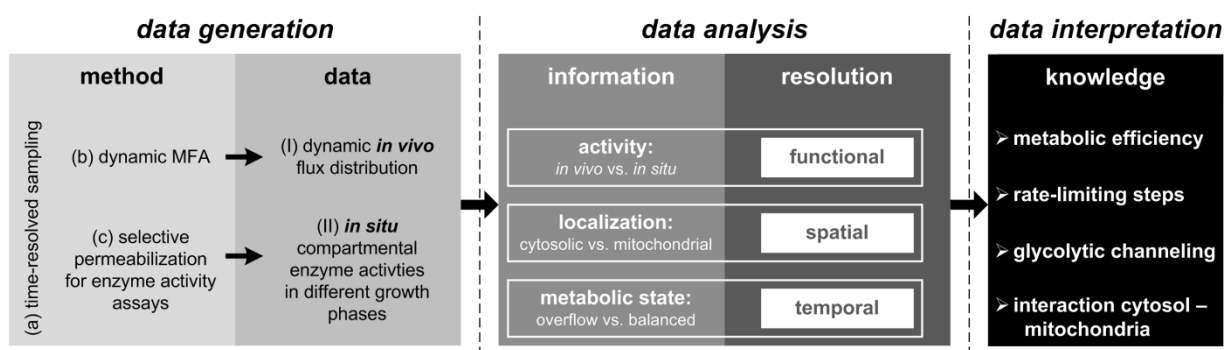


Figure 2-6. Scheme of the applied methodology. Step 1: Time-resolved measurements creating *in vivo* and *in situ* data. Step 2: Data analysis. Step 3: Data interpretation.

2.5.2 Metabolic shifts and metabolic efficiency

The successive consumption of available substrates during batch cultivation results in changing environmental conditions. This forces the cells to adapt their activities resulting in characteristic metabolic shifts and distinct growth phases. These different metabolic phases are characterized by distinct metabolic states with different metabolic efficiency. Since metabolic efficiency in this particular context is not a priori clearly defined, we determine the following features to characterize metabolic efficiency: (1) a low level or the absence of waste product excretion, *i.e.* no carbon spilling, (2) energy generation rather by aerobic pathways than by glycolysis, *i.e.* efficient energy generation, (3) a high connectivity between glycolysis and TCA cycle, *i.e.* a reliable carbon transfer between the two major pathways of central metabolism, and (4) matching catabolic and anabolic activities, *i.e.* no energy spilling. In Figure 2-7, the flow of energy is used as a measure for metabolic efficiency and is schematically depicted for the different metabolic phases. It was estimated by calculating the heat of combustion for consumed substrates, excreted waste products, and biomass production (Villadsen et al., 2011).

CHO cells are characterized by a remarkable adaptability to changing nutrient availability and high flexibility of metabolism due to their ability to utilize a wide range of substrates. The three growth phases were characterized by (1) overflow metabolism, (2) balanced metabolism and (3) maintenance metabolism.

When nutrients were abundant in phase I, the preferred substrates were glucose and glutamine taken up at high rates indicated by the thick arrow in Figure 2-7A. Such behavior is usually observed in CHO cells (Altamirano et al., 2000; Martinez et al., 2013) and other mammalian cell cultures like hybridoma or myeloma cells (Doverskog et al., 1997). High glycolytic and glutaminolytic rates led to an excess energy and carbon supply. This enabled a high anabolic activity as shown by excessive growth. However, the more complex anabolic processes cannot keep up with this excess catabolism. This results in a typical overflow metabolism characterized by energy spilling and significant waste product excretion. This has been observed already in earlier studies on CHO cells (Doverskog et al., 1997) and other organisms (Russell, 2007). The constant lactate/glucose ratio of -1.5 (Figure 2-3A) emphasizes the stability of this metabolic state. The observed value is in accordance with former studies of CHO cells (Ahn and Antoniewicz, 2011; Neermann and Wagner, 1996). In addition, we observed a low and variable TCA cycle/glycolysis ratio (Figure 2-3B) pointing to an unbalanced metabolism with a compromised connectivity between glycolysis and TCA cycle. This indicates a significant glycolytic contribution to ATP generation. In summary, the excess energy supply in phase I resulted in a high anabolic activity but also in high carbon and energy spilling activities (Figure 2-7A). The overflow metabolism represents the predominant activity determining the metabolic state and low metabolic efficiency in this phase.

Glutamine depletion resulted in a reduced specific growth rate in phase II (Figure 2-1) (Wahrheit et al., 2014a; Zhang et al., 2006) with almost matching catabolic and anabolic activities. The metabolism shifted from lactate excretion to lactate consumption as often observed in CHO cultures (Altamirano et al., 2006; Luo et al., 2012; Martinez et al., 2013; Zagari et al., 2013a). Lactate and glucose were consumed in approximately equal molar amounts (Figure 2-3A, lactate/glucose ratio ~ 1). In contrast to phase I, where the major substrates glucose and glutamine were introduced at very different entry sites of metabolism, glucose and lactate were both feeding the cytosolic pyruvate pool resulting in an efficient transport of cytosolic pyruvate into mitochondria. The high and constant TCA cycle/glycolysis ratio (Figure 2-3B) indicates a tight connection between glycolysis and TCA cycle. A metabolic shift from a low to a high connectivity between glycolysis and TCA cycle was also observed by Sengupta *et al.* studying the late non-growth phase of CHO cells (Sengupta et al., 2011). The moderate growth and altered substrate spectrum result in a balanced metabolism with high energy efficiency in the second phase (Figure 2-7B). Nearly all catabolically available energy is used for anabolic purposes.

Nutrient limitation initiated a shift to the last phase characterized by drastically reduced growth. Although various substrates were depleted (e.g. glutamine, asparagine, glutamate, aspartate, pyruvate), the culture viability was kept constant for another 48 h by efficient use of lactate and alanine as sole carbon sources. Lactate and alanine, both feeding the cellular pyruvate pools, were sufficient to maintain a high TCA cycle activity. A significant amount of produced energy was used for maintenance metabolism and heat which was the predominant metabolic activity in phase III (Figure 2-7C).

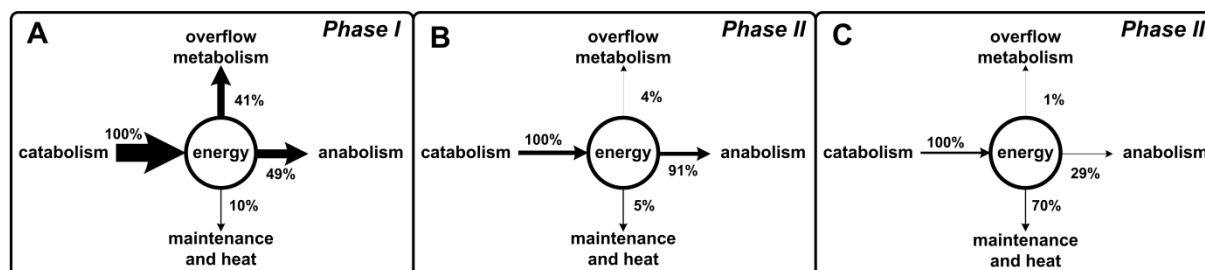


Figure 2-7. The flow of energy in the different growth phases. The flow of energy was estimated by calculating the heat of combustion for consumed substrates (catabolism), excreted waste products (overflow metabolism), biomass (anabolism), and maintenance metabolism (Villadsen et al., 2011). Line thickness of arrows indicates relative flux distributions.

2.5.3 Control points in the central metabolism

We apply the concept of *in vitro/in vivo* ratios to infer limiting steps in glycolysis and TCA cycle.

2.5.3.1 Hexokinase activity levels determine the glycolytic flux

The glycolytic pathway contains three irreversible enzyme reactions, HK, PFK, and PK. For HK and PFK specific activities were in a similarly low range and relatively low *in vitro/in vivo* ratios were measured in both phases (3 and 7 for HK, 2 and 13 for PFK). In contrast, PK showed a high overcapacity (32 and 109 for phases I and II, respectively) (Figure 2-5). This indicates a higher importance of HK and PFK and only a minor contribution of PK for controlling glycolytic flux. Similar observations were made in former studies of different CHO, BHK, hybridoma and myeloma cell lines (Neermann and Wagner, 1996; Vriezen and van Dijken, 1998a). In phase II, all glycolytic enzymes showed significantly higher *in vitro/in vivo* ratios (Figure 2-5). However, for HK the ratio was only slightly increased, from 3 in phase I to 7 in phase II. HK was the only glycolytic enzyme showing a significantly decreased total *in vitro* activity (37%, Table 2-1) matching the lower glycolytic flux in phase II (Figure 2-2). Based on these observations, we conclude that the HK reaction represents the rate-limiting step in the glucose metabolism of CHO-K1.

2.5.3.2 Mitochondrial isocitrate dehydrogenase activity is rate-limiting for TCA cycle fluxes

CS and IDH_{NAD} were exclusively found in the mitochondria. IDH_{NADP} had much higher *in vitro* activities than IDH_{NAD} and was active in both compartments. We found 70% of total IDH_{NADP} activity to be located in the cytosol which is in accordance with former studies of CHO cells (Niklas et al., 2011a) and mouse myeloma cells (Vriezen and van Dijken, 1998b). Cytosolic IDH_{NADP} activity cannot contribute to mitochondrial TCA cycle fluxes. Instead it could be involved in cytosolic NADPH supply. In phase I, we found an *in vitro/in vivo* ratio of 1 for IDH_{TCA} . This indicates that the available enzyme activity was just matching the actual *in vivo* activity. Furthermore, IDH_{TCA} activity was significantly increased in phase II (134%, Table 2-1) matching the higher TCA cycle activity *in vivo*, while CS activity was not significantly altered. Including information about activity localization, we were able to identify the mitochondrial IDH reaction as the rate-limiting step of the TCA cycle, although total cellular IDH activity was high.

2.5.4 Metabolic control and metabolic switches at the cytosol–mitochondria interface

The metabolic shift from an inefficient overflow metabolism in phase I to a highly efficient balanced metabolism in phase II was going along with a switch from a low to a high connectivity between glycolysis and TCA cycle. The most important fuels for the mitochondrial metabolism are pyruvate and glutamine. Pyruvate is mainly derived from glucose via glycolysis and in phase II

additionally from lactate due to a switch from net lactate production to net lactate consumption. Depletion of glutamine during phase I is compensated by consumption of glutamate and aspartate in phase II.

2.5.4.1 Fine-tuning of glycolytic regulation is achieved by micro-compartmentation of glycolytic enzymes and seems to affect pyruvate availability

Using two different permeabilization methods, we found that activities of several glycolytic enzymes measured upon complete permeabilization using Triton X-100 were higher than after selective plasma membrane permeabilization using digitonin. Protein complexes are well preserved after mild digitonin treatment resulting in lower apparent enzyme activities. Two different explanations are possible: (1) due to occlusion of the active site, it is not accessible for substrates used in the enzyme assay or (2) due to conformational changes induced by binding, the catalytic properties of the enzyme are altered. Reported varying release of proteins to the supernatant after treatment with different digitonin concentrations supports our findings. Soluble cytosolic proteins were released upon treatment with low digitonin concentrations while a particular cytoplasmic protein pool that was thought to associate with intracellular structures exhibited a restricted diffusion and was only released after complete cell disruption using much higher digitonin concentrations (Kelner et al., 1986).

As a consequence, two different enzyme activities, (1) ‘free’ activity representing the soluble, accessible part of enzymes ($r_{D,i}$) and (2) ‘concealed’ activity representing the part of enzymes that is organized into protein complexes or attached to cellular structures ($r_{R,i}$), have to be differentiated.

Significant differences observed for HK and PFK activities between distinct growth phases as well as the reproducibility indicate a physiological relevance. Our findings point to a significant contribution of protein association and substrate channeling to glycolytic regulation. Although there has been an ongoing debate whether or not substrate channeling plays a role in glycolytic regulation (Gutfreund and Chock, 1991; Ovadi, 1991; Ovadi and Saks, 2004; Spivey and Ovadi, 1999; Wu et al., 1991), increasing evidence supports the concept of a cytosolic sub-compartment with restricted diffusion. Different groups have shown that glycolytic channeling can be preserved in dextran sulfate permeabilized mouse fibroblasts (L-929 cells) (Clegg and Jackson, 1990) and permeabilized vascular smooth muscle cells from hog (Hardin and Finder, 1998). Comparing intact, dextran sulfate permeabilized and sonicated L-929 cells, Jackson *et al.* showed that the glycolytic activity increased with increasing degree of cell disruption (Jackson et al., 1990). The permeabilized cells more closely reflected the *in vivo* situation in intact cells. The rates were much lower than in sonicated cells which were characterized by freely diffusing enzymes and intermediates. Based on

experiments with ^{14}C labeled glucose, they proposed a ‘leaky’ form of glycolytic channeling which allows some release and entry of intermediates into the pathway (Clegg and Jackson, 1990).

However, instead of a ‘leaky’ channeling we rather postulate a mixed response of attached and soluble enzymes. Glycolytic regulation via metabolite channeling is continuously changing during cultivation. It is likely that both forms, attached and soluble enzymes, exist in a dynamic, but relatively slow equilibrium. The extent to which protein association occurs depends on the metabolic state (Batke, 1989). Two different situations can occur: (a) glycolytic channeling characterized by a direct transfer of intermediates from one active site to the next without leaving the glycolytic chain or (b) free diffusion of glycolytic intermediates (Figure 2-8). Both states seem to coexist at all times throughout cultivation. However, either glycolytic channeling or free diffusion is more or less favored depending on the metabolic state. The relative distribution of soluble and attached enzymes is likely to be a powerful mechanism for metabolic flux regulation (Graham et al., 2007).

Since the 1970s much evidence has been presented that glycolytic enzymes can be associated with each other (MacGregor et al., 1980; Mowbray and Moses, 1976; Ovadi et al., 1986; Tompa et al., 1986) or with subcellular structures like the mitochondria (Sagrista and Bozal, 1987b; Wilson, 1982) or the cytoskeleton (Roberts et al., 1988; Westrin and Backman, 1983). For HK, between 72% (phase I) and 18% (phase II) of the total activity was found to be ‘concealed’ upon digitonin treatment. Vriezen and van Dijken studied enzyme localization in mouse myeloma cells by separating a particulate (mitochondrial) and a soluble (cytosolic) fraction using differential centrifugation (Vriezen and van Dijken, 1998b). They found 20% of total HK activity in the particulate fraction which they suggested to be attached to the outer mitochondrial membrane. In our study, up to 50% of total PFK activity could not be detected after digitonin treatment. Campanella *et al.* studied the location of glycolytic enzymes in human erythrocytes using confocal microscopy (Campanella et al., 2005). In their study, 50% of PFK protein was bound to cellular structures. Thus, the extent to which we observe this ‘concealed’ activity seems to be in a representative range.

The ‘concealed’ part of HK activity was mainly found in phase I when glucose was highly abundant. A shift from the free cytosolic HK to the mitochondrially-bound and more active form of HK was shown to be induced by high glucose concentrations in rat pancreatic islets (Rabuzzo et al., 1997). On the other hand, dissociation of HK from mitochondria was induced by elevated lactate levels in different tissues from mouse (Leite et al., 2011). At low glycolytic rates in phase II, this activity was significantly reduced to 11% relative to phase I. Several HK isoenzymes are known differing in catalytic and regulatory properties as well as in their localization (Wilson, 2003). In studies of rat brain it was shown, that HK that is bound to the outer mitochondrial membrane binds as a tetramer (Xie and Wilson, 1990). It is functionally coupled to the adenine nucleotide

translocase (ANT) via binding to the voltage-dependent anion channel (VDAC) (Beutner et al., 1998; Beutner et al., 1996; Buhler et al., 1998; Hashimoto and Wilson, 2000; Vyssokikh and Brdiczka, 2003) (Figure 2-8). As a consequence, bound HK selectively uses intra-mitochondrial ATP as substrate and does not respond to extra-mitochondrial ATP (Wilson, 2003). Our results are in accordance with these findings since the activity of mitochondrially-bound HK would not be detectable in the enzyme assay due to inaccessibility of ATP contained in the reaction buffer. Similarly, the ‘concealed’ part of PFK activity was higher during overflow metabolism and decreasing over time (Figure 2-4).

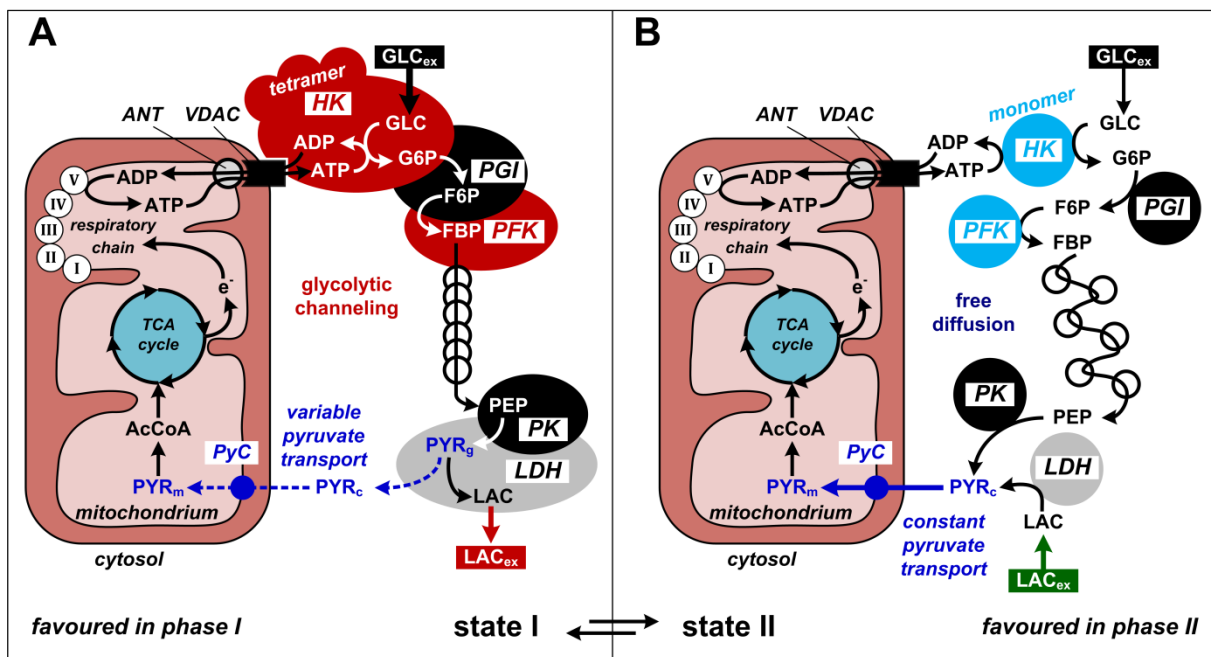


Figure 2-8. Pyruvate transport into the mitochondria at glycolytic channeling and free diffusion. (A) Glycolytic channeling. High glucose concentrations induce binding of hexokinase HK as tetramers to the outer mitochondrial membrane. This favors association of glycolytic enzymes and glycolytic channeling. Via binding of HK to the voltage-dependent anion channel VDAC, HK is functionally coupled to the adenine nucleotide translocase (ANT). This provides preferential access to mitochondrially generated ATP and stimulates glycolytic flux. Glycolytic channeling results in formation of a distinct cytosolic pyruvate pool (PyR_g) that is preferentially converted into lactate. The mitochondrial pyruvate carrier (PyC) has restricted access to cytosolic pyruvate (PyR_c) resulting in a variable pyruvate transport into the mitochondria. (B) Free diffusion. At lower glucose and elevated lactate concentration, the soluble form of glycolytic enzymes and free diffusion of glycolytic intermediates is favored. Cytosolic pyruvate is additionally fed by consumption of extracellular lactate and is freely available to the mitochondrial pyruvate carrier (PyC) resulting in a constant pyruvate transport into the mitochondria.

It still needs to be determined which cellular stimuli control the relative distribution of soluble and attached enzymes. The most remarkable difference between phase I and phase II is the switch from net lactate production to net lactate consumption. A continuous drop in pH of culture supernatant during phase I and subsequent increase of pH in phase II was directly correlated to the lactate profile. The accumulation of lactate in the cells would lead to an acidification of the cytosol. Clegg and Jackson have shown that the glycolytic rates in dextran sulfate permeabilized cells are highly pH dependent and decrease with decreasing pH (Clegg and Jackson, 1990). Furthermore, it has been shown that the assembly of glycolytic enzymes is oxygenation-dependent in murine erythrocytes (Campanella et al., 2008). Graham *et al.* found that the proportion of glycolytic enzymes associated with the mitochondria correlates with the respiration rate in *Arabidopsis* cells (Graham et al., 2007). Inhibition of respiration reduced the degree of association while stimulation of respiration increased mitochondrial association of glycolytic enzymes. A decreased mitochondrial membrane potential and a decreased mitochondrial oxidative capacity has also been correlated with the lactate metabolism in CHO cells (Zagari et al., 2013a). HK binding to the outer mitochondrial membrane was found to be affected by the mitochondrial membrane potential (Vyssokikh and Brdiczka, 2003). In addition, it was shown that high glucose levels induce the binding of HK to mitochondria (Rabuzzo et al., 1997) while high lactate levels induce the dissociation of HK from mitochondria (Leite et al., 2011). These studies demonstrate that the association of enzymes can be regulated by the metabolic state and vice versa. The fact, that we observed these changes in the relative subcellular distribution of soluble and attached enzymes only for HK and PFK is in accordance with the results of the *in vitro/in vivo* ratios where we identified HK and PFK as most important enzymes of glycolytic control (Figure 2-5). We conclude that the glycolytic flux is not only determined by total activity levels of HK and PFK but also by their relative involvement in substrate channeling.

We hypothesize that the extent of glycolytic channeling affects the pyruvate availability and eventually the connectivity between glycolysis and TCA cycle (Figure 2-8). We propose the following mechanism: High glucose concentrations induce HK binding to mitochondria. This triggers the association of glycolytic enzymes. Glycolytic flux is stimulated by an improved supply of ATP to HK due to the preferential use of mitochondrially generated ATP and by a more active HK isoform. Cytosolic pyruvate might be only partly released from the glycolytic chain and is instead directly channeled into lactate providing NAD^+ for glycolysis to maintain the redox balance. Eventually, this leads to a high excretion of lactate and overflow metabolism. The existence of two cytosolic pyruvate pools with one pool tightly connected to the glycolytic chain (Pyr_g , Figure 2-8) and thus not directly available to the mitochondrial pyruvate carrier (PyC, Figure 2-8) has been hypothesized in former studies with isolated perfused rat heart (Peuhkurinen et al., 1983) and rat hind limbs (Schadewaldt et al., 1983). As a consequence, this would result in a compromised pyruvate transport into mitochondria when glycolytic channeling is favored during overflow metabolism in phase I. Lactate accumulation during phase I results in a drop of cytosolic pH and

affects the mitochondrial membrane potential. This might shift the metabolic state to a situation where free diffusion is more favored. In phase II, free diffusion of glycolytic intermediates is favored and the cytosolic pyruvate pool is additionally fed by consumption of lactate. At the same time we observe a high connectivity between glycolysis and TCA cycle due to constant pyruvate transport into mitochondria. The exact molecular mechanism of this regulation remains, however, unclear.

2.5.4.2 The aminotransferases together with malic enzyme and phosphoenolpyruvate carboxykinase support the carbon supply into the TCA cycle

The two major inputs into the TCA cycle are via the pyruvate dehydrogenase reaction generating acetyl-CoA (C2-unit) from pyruvate and the GDH generating AKG from glutaminolysis that is further converted to oxaloacetate (OAA) (C4-unit). To obtain a balanced TCA cycle, equimolar amounts of C2- and C4-units have to be available to form citrate. However, due to glycolytic channeling during overflow metabolism as well as because of glutamine limitation and lactate consumption during balanced metabolism, availabilities of C2- and C4-units are changing from phase I to phase II.

During overflow metabolism in phase I, cytosolic pyruvate was mainly converted to lactate and alanine. Pyruvate transport into mitochondria was variable resulting in a low connectivity between glycolysis and TCA cycle. High glutaminolytic rates provide an excess supply of C4-units. This would result in a relative depletion of mitochondrial pyruvate and eventually reduce or even stop TCA cycle fluxes. In phase I, ALAT was active in both compartments but ASAT was only detected in the cytosol. The *in vivo* fluxes, e.g. significant consumption of asparagine and aspartate, indicate that ASAT is working in the direction of OAA formation. However, OAA could not directly enter the mitochondrial TCA cycle, since ASAT was only active in the cytosol. It can however be reduced to malate that can be transported into the mitochondria where it can oxidatively decarboxylate to pyruvate by mitochondrial ME. The high alanine excretion in phase I clearly indicates that the cytosolic ALAT catalyzes the formation of alanine. However, since cytosolic and mitochondrial isoforms were active, both reactions, alanine formation and pyruvate formation, can potentially take place in different compartments. In order to prevent the TCA cycle from slowing down dramatically, mitochondrial ALAT together with the mitochondrial ME, both fueling the mitochondrial pyruvate pool, can compensate for an insufficient pyruvate transport capacity from the cytosol. Cytosolic PEPCK and ASAT further support these metabolic reactions (Figure 2-9A).

In phase II, lactate was no longer excreted but consumed, now fueling the cytosolic pyruvate pool. In addition, free diffusion of glycolytic metabolites was favored resulting in freely available cytosolic pyruvate derived from glycolysis. Pyruvate was efficiently transported into mitochondria

resulting in a constant connection between glycolysis and TCA cycle. Additional feeding of the mitochondrial pyruvate pool might not be necessary. Accordingly, we observed reduced activities for all enzymes involved in such pyruvate supply; cytosolic ASAT, cytosolic PEPCK and mitochondrial ME activity were significantly decreased and a complete inactivation was observed for the mitochondrial ALAT (Figure 2-9B). However, glutamine limitation in phase II leads to a relative shortage of C4-units compared to the high C2-unit supply. We observed an activation of mitochondrial ASAT providing mitochondrial OAA now directly feeding into the TCA cycle. This compensates for the reduced carbon input at AKG that supplied C4-units in phase I (Figure 2-9B).

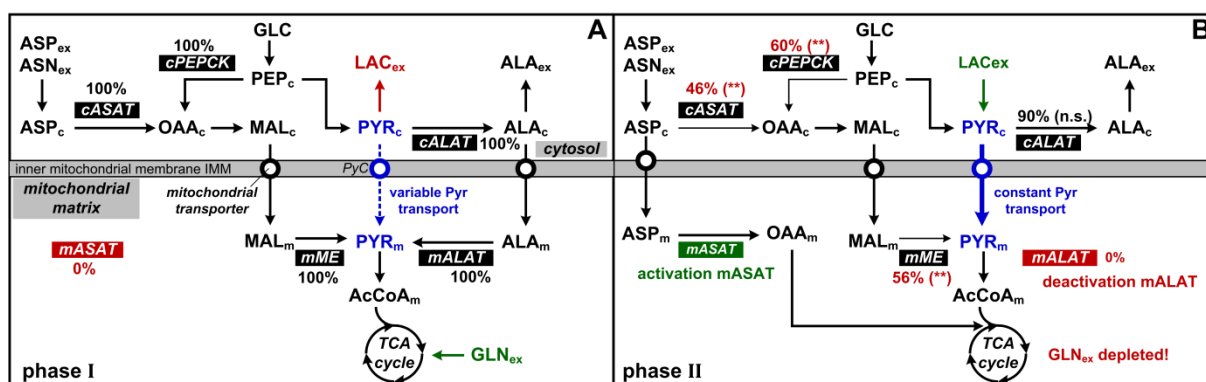


Figure 2-9. Carbon supply into the TCA cycle at overflow metabolism in phase I and after glutamine limitation in phase II. (A) Overflow metabolism. High lactate excretion and variable pyruvate transport into the mitochondria lead to a relative shortage of C2-units. The mitochondrial pyruvate pool is additionally fed by the combined action of cytosolic aspartate amino transferase cASAT, cytosolic phosphoenolpyruvate carboxykinase cPEPCK, mitochondrial malic enzyme mME, and mitochondrial alanine amino transferase mALAT. This supports C2-unit supply into the TCA cycle to match the high carbon input due to excess glutaminolysis. (B) Balanced metabolism. Lactate consumption enables an efficient pyruvate transport into the mitochondria. Anaplerotic enzymes involved in fueling the mitochondrial pyruvate pool in phase I have significantly reduced activities. A relative shortage of C4- units due to glutamine depletion in phase II is compensated by activation of mitochondrial aspartate amino transferase mASAT to feed OAA directly into the TCA cycle. Statistical significance as determined by student's t-test is represented by asterisks: *** = $p < 0.001$, ** = $p < 0.01$, * = $p < 0.05$, n. s. not significant.

2.6 Conclusions and future applications

In this study, we propose a novel approach for the quantitative analysis of metabolic dynamics in CHO cultivation. The presented methodology is transferable to all kinds of different biological systems and scientific issues.

With the extended concept of time-resolved analysis of metabolic flux ratios as sensitive parameters of physiological changes, we provide a useful tool for a schematic characterization of the metabolic state and metabolic efficiency. Metabolic efficiency reflects a healthy state of cellular metabolism

and represents a target for optimization in industrial production processes. The assessment and prediction of metabolic efficiency is therefore of equal importance for biotechnological and biomedical questions.

We further demonstrate that knowledge about metabolic control can be generated by integrating several data-sets with resolution in different dimensions; (1) time resolution, *i.e.* phase I vs. phase II, (2) spatial resolution, *i.e.* cytosolic vs. mitochondrial localization of activities, and (3) functional resolution, *i.e.* *in situ* vs. *in vivo* activity. Using this systems-oriented approach, we were able to identify the HK reaction and the mitochondrial IDH reaction as rate-limiting steps in glycolysis and TCA cycle, respectively. Our findings strongly indicate that the dynamics of substrate channeling play a crucial role in glycolytic regulation in CHO cells and affect the intracellular pyruvate availability. Finally, our data point to a coordinated interplay of transaminases and anaplerotic enzymes to compensate an unbalanced carbon input into the TCA cycle. These conclusions could only be drawn by correlating different levels of information.

The identification of rate-limiting steps as well as understanding metabolic implications of different metabolic efficiencies, in particular at the cytosol–mitochondria interface as most important hub in the central metabolism, helps characterizing cellular phenotypes, different producer strains or pathophysiological conditions. The acquired knowledge can be used to understand disease mechanisms or toxic effects, to develop medical therapies or identify metabolic targets for process optimization to achieve an improved biopharmaceutical production (e.g. by genetic engineering, media optimization, feeding strategies).

2.7 Acknowledgments

We thank the Institute of Cell Culture Technology (University Bielefeld, Germany) for supplying the CHO-K1 cells and the BMBF (German Federal Ministry of Education and Research) project SysCompart (project ID 031555D), part of the Systems Biology program, New Methods in Systems Biology (SysTec), for funding.

2.8 Supplementary material

Supplementary material associated with this chapter is available online:

<http://dx.doi.org/10.1016/j.ymben.2014.02.001>

3 Dynamics of growth and metabolism controlled by glutamine availability in Chinese hamster ovary cells

3.1 Abstract

The physiology of animal cells is characterized by constantly changing environmental conditions and adapting cellular responses. Applied dynamic metabolic flux analysis captures metabolic dynamics and can be applied to industrially relevant cultivation conditions. We investigated the impact of glutamine availability or limitation on the physiology of CHO-K1 cells in eight different batch- and fed-batch cultivations. Varying glutamine availability resulted in global metabolic changes. We observed dose-dependent effects of glutamine in batch cultivation. Identifying metabolic links from the glutamine metabolism to specific metabolic pathways, we show that glutamine feeding results in its coupling to tricarboxylic acid (TCA) cycle fluxes and in its decoupling from metabolic waste production. We provide a mechanistic explanation of the cellular responses upon mild or severe glutamine limitation and ammonia stress. The growth rate of CHO-K1 decreased with increasing ammonia levels in the supernatant. On the other hand, growth, especially culture longevity, was stimulated at mild glutamine limiting conditions. Flux rearrangements in the pyruvate and amino acid metabolism compensate glutamine limitation by consumption of alternative carbon sources and facilitating glutamine synthesis and mitigate ammonia stress as result of glutamine abundance.

This chapter was published as

Wahrheit J, Nicolae A, Heinzle E. (2014) Dynamics of growth and metabolism controlled by glutamine availability in Chinese hamster ovary cells. *Applied Microbiology and Biotechnology* 98 1771-1783.

3.2 Introduction

Metabolic studies of mammalian cells are increasingly important in biological, biomedical and biotechnological research. An in-depth analysis of mammalian metabolism is crucial for the understanding of physiological, pathophysiological and toxicological mechanisms. This is required to identify potential drug targets or biomarkers as well as to determine a strategy for metabolic engineering, media optimization and feeding in the development of efficient large-scale production processes (Niklas and Heinzle, 2012).

In mammalian cells, the glutamine metabolism is of particular interest due to its importance as cellular energy, carbon and nitrogen source (Neermann and Wagner, 1996; Newsholme et al., 2003a; Newsholme et al., 2003b). The glutamine metabolism represents also the primary source for ammonia (Glacken, 1988; Kurano et al., 1990; Street et al., 1993). The formation of metabolic by-products such as lactate and ammonia is a common issue in the cultivation of mammalian cells that can have a significant impact on the whole cultivation performance (Ozturk et al., 1992; Schneider et al., 1996). In particular the accumulation of the toxic waste product ammonia can inhibit growth and, in the case of industrial producer strains, can affect productivity and product quality (Chen and Harcum, 2006; Hassell et al., 1991; Priesnitz et al., 2012; Yang and Butler, 2000; Yang and Butler, 2002).

Metabolic flux analysis (MFA) is the method of choice for detailed quantitative metabolic studies. Classical approaches require metabolic steady-state conditions. However, metabolic steady-state is usually not attained under industrially relevant conditions, i.e. batch or fed-batch cultivations. The successive consumption and depletion of substrates and the accumulation of specific side-products result in the development of different metabolic phases and metabolic shifts (Niklas et al., 2011c). One possibility to deal with this issue is to divide the cultivation profile into several phases and perform a separate analysis (Niklas et al., 2012a; Niklas et al., 2011c). Often an adjustment of the cultivation conditions, e.g. by a special media design, is necessary to achieve steady-state conditions in mammalian cell cultures (Deshpande et al., 2009).

Dynamic metabolic flux analysis represents an elegant way to circumvent several of these difficulties and drawbacks. Since extracellular steady-state conditions are not a requirement, this time-resolved MFA method can be applied to batch- and fed-batch cultivations. It provides the unique possibility to capture metabolic dynamics and metabolic shifts by monitoring the complete time-course of cultivation including the phase transitions between different metabolic phases. Furthermore, dynamic MFA enables the direct comparison of very different conditions with different growth behavior and allows the determination of the exact timing of metabolic events.

We tested different glutamine start concentrations and different glutamine feeding profiles to study the glutamine metabolism in Chinese hamster ovary (CHO) cells using dynamic MFA. The aim of

the study was to obtain an in-depth representation of the metabolic changes in CHO-K1 cells as a result of (a) excess glutamine supply, (b) controlled glutamine supplementation, (c) glutamine limitation, (d) glutamine depletion, and (e) ammonia accumulation. A more detailed understanding of physiological and metabolic implications of varying glutamine supply will provide a strong basis for design and development of novel producer cells, bioprocesses, as well as therapeutic strategies.

3.3 Material and methods

3.3.1 Cell culture and experimental set-up

The CHO-K1 cell line was kindly provided by the group of cell culture technology of the University Bielefeld. The cells were growing in suspension under serum and protein free conditions in the chemically defined medium TC-42 (TeutoCell AG, Bielefeld, Germany) at 37°C with 5% CO₂ supply in a shaking incubator (185 rpm, 2 inches shaking orbit, Innova 4230, New Brunswick Scientific, Edison, NJ, USA). The pre-culture was performed in a 250 ml baffled shake flask (Corning, NY, USA) with a volume of 100 ml in TC-42 supplemented with 4 mM glutamine. The main cultures were carried out in 50 ml filter-tube bioreactors (TPP, Trasadingen, Switzerland) at a start cell density of 2×10^5 cells/ml and a start volume of 20 ml. For the different test conditions TC-42 medium without glutamine or supplemented with different glutamine concentrations was prepared. For the fed-batch cultivations a stock solution of 200 mM glutamine resolved in dest. H₂O was prepared as feeding solution. Six different batch cultivations with 0 mM, 1 mM, 2 mM, 4 mM, 6 mM or 8 mM glutamine start concentrations and two different fed-batch cultivations starting at 1 mM glutamine and feeding 1 mM every 24 h or starting at 2 mM and feeding 2 mM every 48 h were performed. In total, 8 mM glutamine was added to the fed-batch cultivations. An example for reproducibility of growth and metabolite profiles is shown in the supplementary material in Figure S1. Samples of 500 µl were taken every day. 50 µl of the sample was diluted with PBS and mixed with Trypan Blue for determination of cell density, cell viability and average cell diameter using an automated cell counter (Invitrogen, Darmstadt, Germany). The average cell volume was estimated from the average cell diameter assuming a sphere. Differences of cell diameters during the cultivation were very small and not taken into account. The sample was centrifuged (10,000 rpm, 5 min, Biofuge pico, Heraeus Instruments, Hanau, Germany), 300 µl of the supernatant transferred into fresh tubes and stored at -20°C for further analysis. The rest of the sample was used for pH determination (MP 220 pH Meter, Mettler-Toledo, Giessen, Germany).

3.3.2 Quantification of metabolites

Quantification of glucose, organic acids and amino acids via HPLC was carried out as described recently (Strigun et al., 2011b). Ammonia was quantified using an ammonia assay kit (Sigma-Aldrich, Steinheim, Germany) in 96-well plates. 10 μl of sample was mixed with 100 μl of assay reagent, mixed on a plate shaker for 5 min and the absorbance measured at 340 nm in a micro plate reader. Then, 1 μl of glutamate dehydrogenase was added to each well, the plate mixed on a plate shaker for 5 min and the absorbance measured at 340 nm. Standards with different ammonia concentrations (2-10 mg/l) were used for calibration. Urea was measured via HPLC as described earlier (Clark et al., 2007).

3.3.3 Dynamic metabolic flux analysis

The continuous time course of the metabolic fluxes was computed similar to Niklas et al. (Niklas et al., 2011c) following the steps: 1. interpolation of the extracellular concentrations of metabolites and the cell density with a continuously derivable function, 2. computing the extracellular rates, 3. computing intracellular fluxes based on a stoichiometric model. Cell density and extracellular concentrations of metabolites from each cultivation were interpolated using SLM (Shape Language Modeling), a user-developed fitting tool that uses customized splines (Matlab 2012b, The Mathworks, Natick, MA, USA). To avoid overfitting and biological nonsense, all fitted values were constrained to positive values, not more than 3 splines per curve were used and, except where observed to be otherwise, all curves were monotonous. Glutamine and glutamate concentrations were fitted for each fed-batch phase, while for the rest of metabolites the interpolated concentration curves were derivable for the whole cultivation time interval.

Water evaporation was taken into account by correcting the concentration values prior to interpolation using the experimentally determined evaporation rate. Both the evaporation rate and glutamine degradation kinetics were determined experimentally in a cell-free setup identical to the one employed during the cultivation.

Extracellular fluxes were calculated in [$\text{mmol/L} \times \text{h}$] units using the numerically differentiated

concentration slopes $\frac{dC_i}{dt}$:

$$v_{u,i} = -\frac{dC_i}{dt} \cdot \frac{1}{X} \cdot \frac{1}{V_{cell}} \quad (1)$$

and by considering the spontaneous degradation of glutamine:

$$v_{u,GLN} = -\frac{dC_{GLN}/dt + kd_{GLN} \cdot C_{GLN}}{X \cdot V_{cell}} \quad (2)$$

where $v_{u,i}$ is the uptake rate of metabolite i , C_i is the fitted extracellular concentration, kd_{GLN} is the first order degradation constant of glutamine, X is the fitted cell density and V_{cell} is the volume of one cell. Biomass fluxes were calculated using the time-dependent growth rate:

$$v_{bio,i} = Y_{i/X} \cdot \frac{dX/dt}{X} \cdot \frac{1}{V_{cell}} \quad (3)$$

where $v_{bio,i}$ is the biomass rate for metabolite i and $Y_{i/X}$ is the biomass yield coefficient.

The stoichiometric model of the CHO-K1 metabolism was built based on pathway data presented by Ahn and Antoniewicz (Ahn and Antoniewicz, 2012) and adapted to accommodate experimental observations (Supplementary material, Figure S2). It comprises the main pathways in the central carbon metabolism: biomass production using proteins, fatty acids and carbohydrates; glycolysis, pentose phosphate pathway (PPP), tricarboxylic acid (TCA) cycle and amino acids syntheses and catabolism. Aminotransferase reactions were always coupled with the conversion of α -ketoglutarate (AKG) to glutamate. The stoichiometric model was simplified in the following way: compartmentation was neglected, anaplerotic reactions were lumped into one flux connecting phosphoenolpyruvate (PEP) with oxaloacetate (OAA), serine production and degradation reactions were modeled as one reversible flux between serine and pyruvate. The intracellular fluxes were calculated using the external fluxes according to the network stoichiometry:

$$v_c = -inv(G_c) \times (G_m \times v_m) \quad (4)$$

where v_c and v_m are the arrays of intracellular and extracellular fluxes, G_c and G_m are the corresponding stoichiometric matrices specified in the supplementary material (Table S1 and Table S2). The matrix that corresponds to intracellular fluxes must be invertible. Consequently, the stoichiometric model was modified as described above.

After making all listed simplifications, the PPP flux could still not be calculated directly but had to be fixed in order to obtain an invertible G_c . The PPP flux was sampled randomly at each time point with a time interval less than one hour and had to fulfill predefined biological constraints (Supplementary material Table S3) and the constraints imposed by the whole network. A somewhat similar approach but applying elementary modes was recently described and shows that many fluxes can be determined within narrow intervals whereas others cover a fairly broad range (Zamorano et al., 2010). The resulting fluxes containing the noise generated by random sampling of the PPP flux were smoothed by spline fitting and thus time-varying flux values were obtained. Considering that the flux space is greatly reduced by the known fluxes and constraints, e.g. reversibility of reactions (Wiback et al., 2004), the averaging is expected to have little impact on non-glycolytic fluxes, e.g. TCA cycle and glutamine metabolism, that are not closely connected to the PPP carbon flux.

3.4 Results

3.4.1 Influence of glutamine on growth and culture longevity of CHO-K1

The impact of the glutamine availability on the growth behaviour of CHO cells was analysed by (1) the time course of the specific growth rate μ , (2) the maximum viable cell density reached during the cultivation period, (3) viability, and (4) the viability-pH profile (Figure 3-1). Furthermore, the specific growth rates μ were correlated to the extracellular glutamine rate over time (Figure 3-2). Generally, rates are only shown starting from 20 h due to inherent difficulties to determine initial rates using splines. The profiles of the specific growth rates of all cultivations had a similar pattern, starting at maximum values and rapidly decreasing afterwards (Figure 3-1B and 1F). Interestingly, identical initial μ were determined for the cultivations with start concentrations of 4, 6, and 8 mM glutamine reaching a maximum specific growth rate of 0.07 h^{-1} (Figure 3-1B). With increasing glutamine start concentration (0 mM to 8 mM glutamine) the specific growth rate μ was initially higher but dropped faster (Figure 3-1B). At the beginning of the cultivation, The specific growth rate μ increased linearly with increasing glutamine uptake rates (Figure 3-2A, 24 h). For later time-points (Figure 3-2B-E, 48-120 h), there was still a linear relationship between μ and the extracellular glutamine rates. However, we observed a clustering in two groups, (1) low glutamine concentrations, 0 to 2 mM glutamine and (2) high glutamine concentrations, 4 to 6 mM glutamine. After 48 h of cultivation, we determined higher specific growth rates for lower glutamine concentrations (Figure 3-2B and 2C). After glutamine depletion, there was no correlation, as it was the case for 0 to 2 mM glutamine after 96 h (Figure 3-2D and 2E). The lowest viable cell density was obtained in the glutamine-free cultivation (Figure 3-1A). The highest viable cell densities were found in the batch cultivation with 1 mM glutamine start concentration and in the 8×1 mM fed-batch cultivation (Figure 3-1E). Culture longevity, as indicated by longer maintenance of high viability and a slower decrease of the specific growth rate, was superior at low glutamine and glutamine-free conditions. Specific growth rates decreased faster at high glutamine levels (Figure 3-1B and Figure 3-2B-E). In the glutamine-free cultivation, the specific growth rate μ was the lowest of all tested at the beginning and highest after about 110 h of cultivation where it remained constant until the end of cultivation. Cell viability dropped earlier for cultivations with high glutamine levels and latest for 0 mM and 1 mM batch and 8×1 mM fed-batch cultivations (Figure 3-1C and 1G). Interestingly, viability was always high above a pH value of 6.8 (Figure 3-1D and 1H). Upon reaching a pH value of about 6.8, viability dropped sharply in all cultures, irrespective of actual ammonia levels (Supplementary Material Figure S3B). After reaching a pH value of about 6.8, pH does not any more decrease monotonically as is also indicated in the pH-ammonia plot (Supplementary Material, Figure S3A and B). Interestingly, the cultivation without supply of glutamine does not reach this pH value and viability does not drop as in the other cultures. Towards the end of cultivation ammonia concentration increases in all cases (Figure 3-3) and is negatively

correlated with pH (Supplementary Material Figure S3A). Plots of specific growth versus ammonia concentration showed that in each case it decreased with increasing ammonia concentration (Supplementary Material Figure S3C). Remarkably, viability dropped sharply but at different ammonia concentrations (Supplementary Material Figure S3B). These results indicate that ammonia accumulation is not the primary cause for a decline in pH, viability and growth rate. However, there was a clear linear correlation between the pH and the extracellular lactate concentration (Supplementary Material Figure S3D). Viability dropped when a lactate concentration of 30 mM was reached.

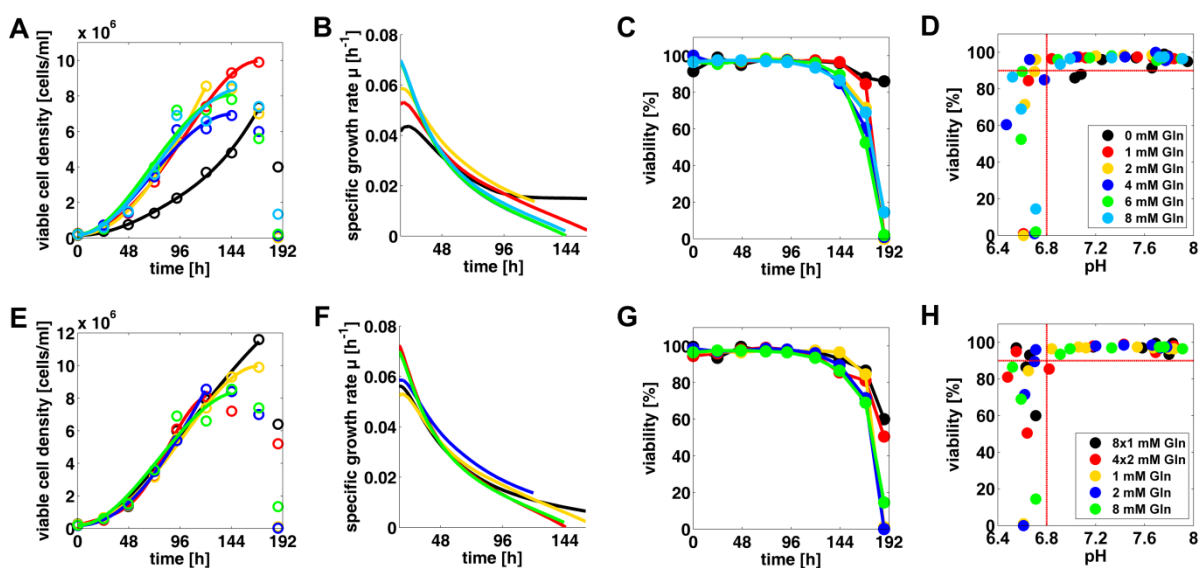


Figure 3-1. Growth profiles of CHO-K1 at different glutamine availabilities. Different batch cultivations with 0 mM, 1 mM, 2 mM, 4 mM, 6 mM or 8 mM glutamine start concentrations (Top, **A-D**) and different fed-batch cultivations with feeding of 1 mM every 24 h (8×1 mM) or of 2 mM every 48 h (4×2 mM) compared to respective batch cultivations with 1 mM, 2 mM, or 8 mM glutamine start concentrations without additional feeding of glutamine (Bottom, **E-H**). (**A**) and (**E**) Viable cell densities [cells/ml] over time [h]. (**B**) and (**F**) Specific growth rates μ [h^{-1}] over time [h] (note that the timescale starts at 20 h because of high uncertainty of determination of initial slopes using splines). (**C**) and (**G**) Cell viability [%] over time [h]. (**D**) and (**H**) Cell viability [%] relative to the respective culture pH that decreased with time (not shown).

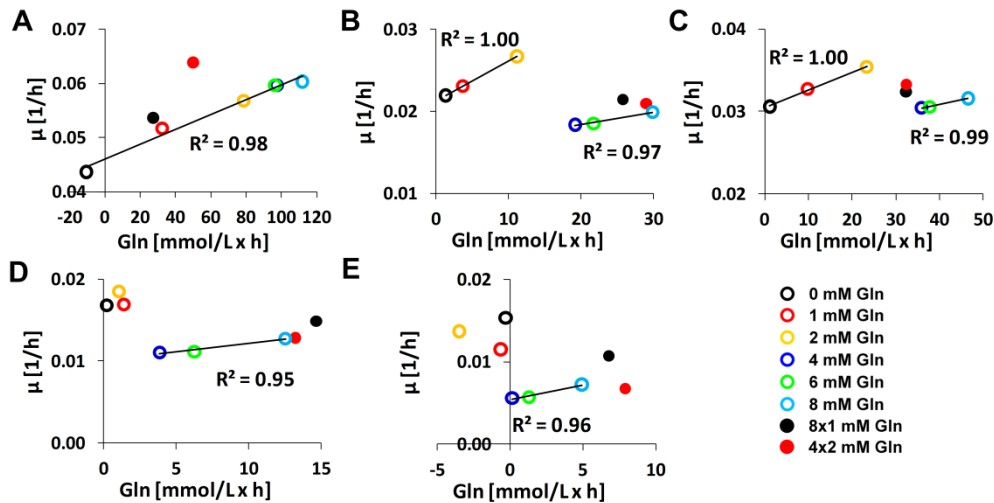


Figure 3-2. Correlation between the specific growth rates μ and the extracellular glutamine rates of different batch cultivations after (A) 24 h, (B) 48 h, (C) 72 h, (D) 96 h and (E) 120 h. Positive glutamine rates indicate glutamine uptake, negative rates glutamine excretion. In a, the linear correlation between specific growth rates and glutamine uptake rates for the six different batch cultivations are shown. In (B) and (C), a linear correlation between cultivations with low glutamine concentrations, 0 mM, 1 mM, and 2 mM glutamine, and between cultivations with high glutamine concentrations, 4 mM, 6 mM, and 8 mM glutamine, are determined separately. In (D) and (E), the linear correlation between cultivations with high glutamine concentrations is shown. No linear correlation was determined for cultivations with low glutamine concentrations since glutamine was depleted at 96 h (D) and 120 h (E). The fed-batch cultivations are not included in the determination of correlation and are only shown for comparison.

3.4.2 Dynamics of extracellular metabolite concentrations

Selected extracellular metabolites are presented in Figure 3-3, the complete extracellular metabolite profiles are depicted in the supplementary material (Figure S4 and S5). With the exception of glutamine, none of the measured extracellular media components was depleted during the cultivation. This provides clear evidence that no nutrient limitation occurred (Supplementary Material Figure S6 and S7). No urea could be detected in the supernatants. Glucose uptake and lactate excretion were similar in all glutamine supplemented cultures but significantly lower in the glutamine-free cultivation. Pyruvate uptake was first comparable for all conditions. After 96 h of cultivation, pyruvate uptake was lower in the glutamine-free cultivation. Glutamine uptake, alanine excretion and ammonia accumulation increased with increasing glutamine start concentration. In the fed-batch cultivations, alanine and ammonia excretion were lower than in the batch cultivation with a single dose of 8 mM glutamine. Serine uptake was similar in all cultivations. Asparagine uptake was similar for all glutamine supplemented cultures but delayed for the glutamine-free cultivation. Aspartate was not taken up initially but significantly consumed after 48 h in glutamine supplemented cultures and after 96 h in the glutamine-free cultivation. Aspartate uptake was decreasing with increasing glutamine start concentration.

Glycine and glutamate were first excreted, then consumed and eventually excreted again. Glycine excretion and the following re-uptake were highest at 0 mM glutamine and decreased with increasing glutamine concentration. For high glutamine levels, glycine re-uptake was almost negligible. The shift from glycine excretion to glycine re-uptake was delayed with decreasing glutamine concentration. Glutamate excretion increased with increasing glutamine start levels but was highest in the glutamine-free cultivation. Consumption of glutamate was more significant and started earlier at lower glutamine start levels. Glutamate reuptake was delayed in the glutamine-free cultivation. For the fed-batch cultivation an intermediate response between low and high glutamine start concentrations was observed.

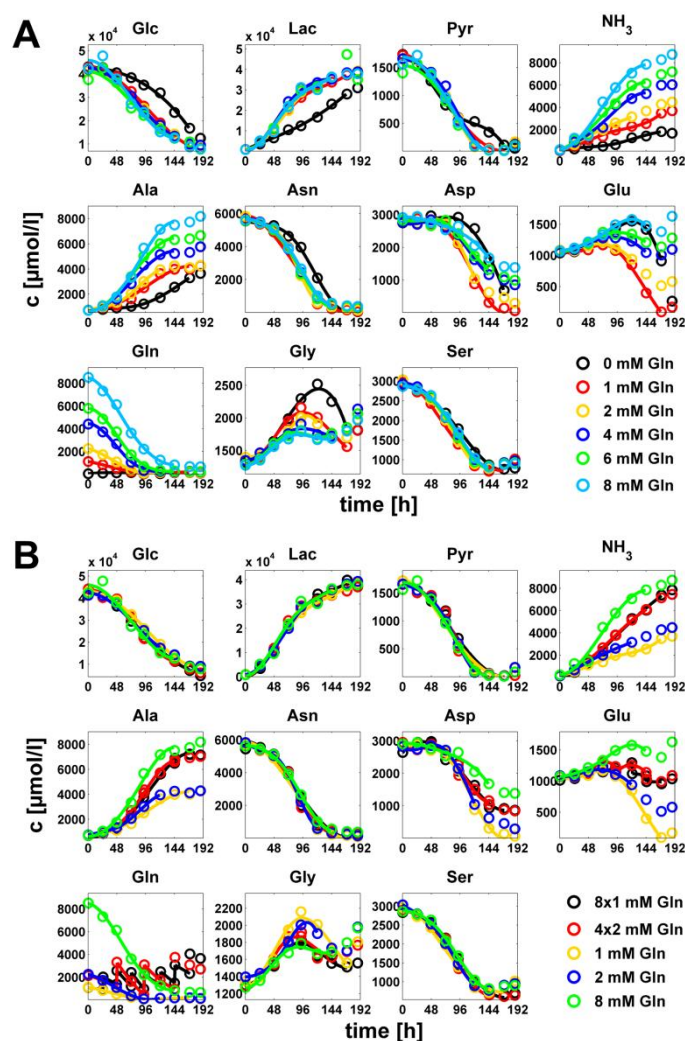


Figure 3-3. Extracellular metabolite profiles of CHO-K1 at different glutamine availabilities. (A) Different batch cultivations with 0 mM, 1 mM, 2 mM, 4 mM, 6 mM or 8 mM glutamine start concentrations. (B) Different fed-batch cultivations with feeding of 1 mM every 24 h (8×1 mM 24 h) or 2 mM every 48 h (4×2 mM 48 h) compared to respective batch cultivations with 1 mM, 2 mM, or 8 mM glutamine start concentrations without additional feeding of glutamine. Abbreviations: Glc glucose, Lac lactate, Pyr pyruvate, for amino acids the standard three letter code is used.

3.4.3 Changes in the dynamic flux distribution upon different glutamine availabilities

Selected fluxes in the central energy metabolism and the amino acid metabolism are shown in the flux maps in Figure 3-4. The complete set of calculated fluxes is shown in the supplementary material (Figure S8-S10 for batch cultivations and Figure S11-S13 for fed-batch cultivations). Glycolytic rates started at high values and decreased rapidly over time. The different glutamine batch- and fed-batch conditions did not significantly affect glycolytic fluxes. Only the glutamine-free culture maintained higher rates after 96 h compared to glutamine-supplemented cultures. The pyruvate uptake rate was substantially increased in the glutamine-free culture and initially slightly increased for the 1 mM batch cultivation compared to higher glutamine levels. After 96 h of cultivation, pyruvate uptake rates were similar for all conditions.

The serine uptake rate increased with decreasing glutamine concentration. In addition, serine was initially produced from 3-phosphoglycerate, as indicated by a negative flux from serine to pyruvate. Serine synthesis was highest in the glutamine-free culture and at high glutamine concentrations. Later in the cultivation, serine was still produced in cultivations with low glutamine start concentrations, but slightly degraded to pyruvate at high glutamine start levels and at glutamine-free conditions. Glycine excretion rate increased with decreasing glutamine concentrations. Later, glycine is still produced from serine but not excreted any longer. Alanine and ammonia excretion rates increased with increasing glutamine concentration. In the two fed-batch cultivations, these rates were significantly lower than in the 8 mM batch cultivation.

Glutamine uptake rates and glutamine degradation to glutamate increased with increasing glutamine levels. Glutamate was further converted to α -ketoglutarate (AKG) feeding the tricarboxylic acid (TCA) cycle. At glutamine-free conditions, the glutamate dehydrogenase reaction was initially reversed to produce glutamate for glutamine synthesis draining carbons from the TCA cycle. Glutamine was first slightly produced in the glutamine-free cultivation and later taken up again. As a result, glutamate excretion rates were much higher in the glutamine-free culture than in glutamine supplemented cultures through most part of the cultivation. Glutamate excretion rates in glutamine supplemented cultures were initially not significantly different for different glutamine concentrations. In cultures with low glutamine start levels where glutamine limitation was reached, glutamate was consumed later in the cultivation. At high glutamine start concentrations and in the fed-batch cultivations, glutamate was continuously excreted.

Fluxes from AKG to oxaloacetate (OAA) were at least initially affected by the glutamine supply resulting in increased rates with increasing glutamine levels. The reflux from TCA cycle to glycolysis via reactions of malic enzyme, phosphoenolpyruvate (PEP) carboxykinase, and pyruvate carboxylase represented as a combined flux from OAA to PEP was strongly affected by the glutamine supply. The flux was increasing with increasing glutamine concentrations removing

carbons from the TCA cycle. As a consequence, TCA cycle fluxes from OAA to AKG were not dose-dependently affected by increasing glutamine consumption rates. However, at the beginning of the cultivation these fluxes were highest for the highest glutamine start concentration, 8 mM glutamine. In the glutamine-free cultivation, the anaplerotic flux from PEP to OAA was initially feeding carbons into the TCA cycle. Later in the cultivation, after about 60 h, this flux was reversed as observed in all glutamine supplemented cultures. In later phases of the cultivation, TCA cycle fluxes were highest for the glutamine-free cultivation (Figure 3-4A) and the 4×2 mM fed-batch cultivation (Figure 3-4B). Overall less variation of TCA cycle fluxes and the flux from OAA to PEP was observed in the fed-batch cultures compared to batch cultivations.

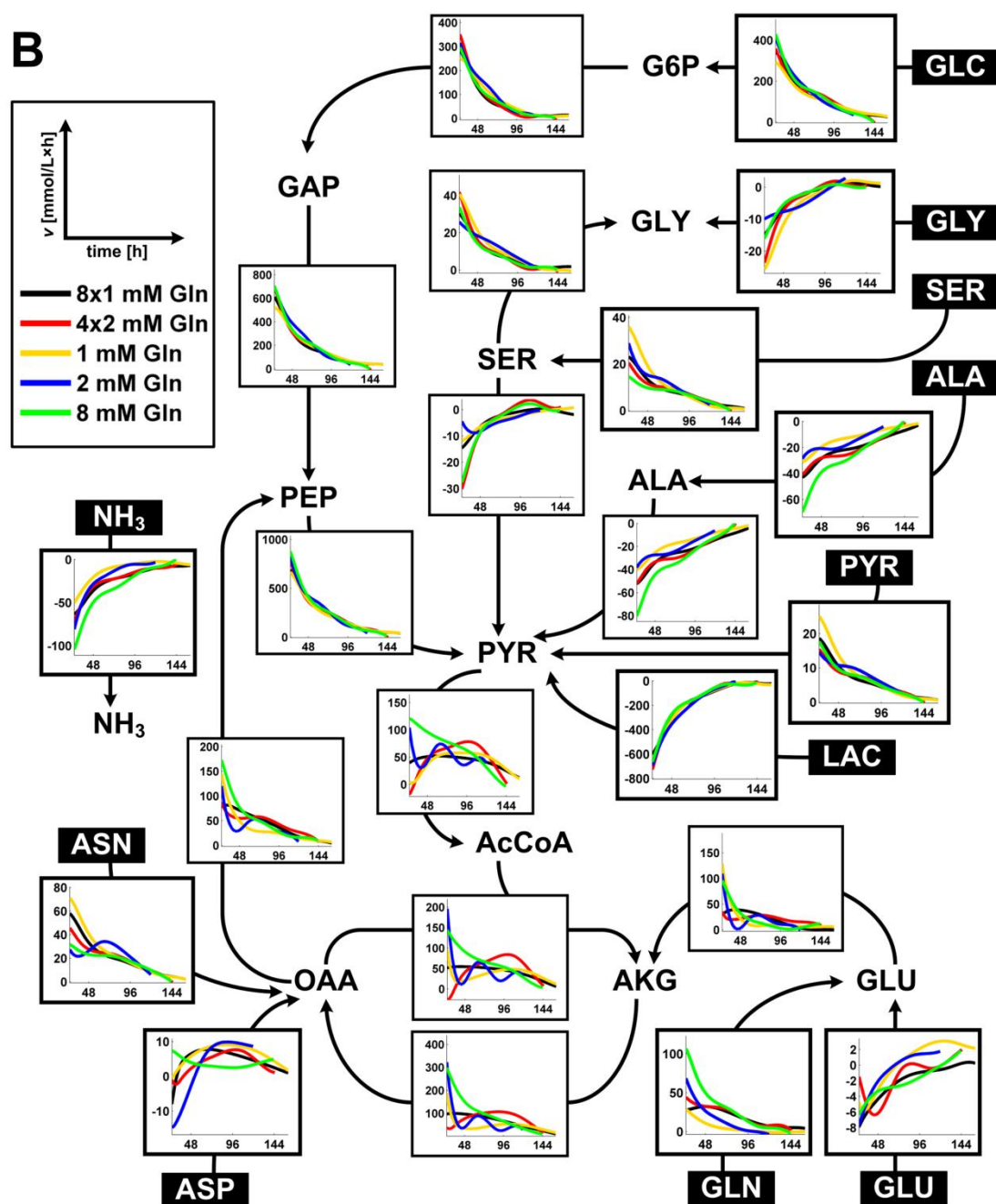


Figure 3-4. (B) Flux maps of CHO-K1 at different glutamine availabilities. Shown are the metabolic rates related to the cell volume [mmol/(L × h)]. Different fed-batch cultivations with feeding of 1 mM every 24 h (8 × 1 mM 24 h) or of 2 mM every 48 h (4 × 2 mM 48 h) compared to respective batch cultivations with 1 mM, 2 mM, or 8 mM glutamine start concentrations without additional feeding of glutamine. Abbreviations: Glc glucose, G6P glucose-6-phosphate, F6P fructose-6-phosphate, GAP glyceraldehyde-3-phosphate, PEP phosphoenolpyruvate, Pyr pyruvate, Lac lactate, AcCoA acetyl-CoA, AKG α -ketoglutarate, OAA oxaloacetate, for amino acids, the standard three letter code is used. Negative values indicate fluxes in the opposite direction of the arrow. This is generally possible for all reactions not constrained as specified in Table S3 of the Supplementary Material. Note that the timescale starts at 20 h because of high uncertainty of determination of initial slopes using splines.

3.4.4 Metabolic links from glutamine metabolism to specific metabolic pathways

Extra- and intracellular fluxes were related to the extracellular glutamine flux in order to identify metabolic links. A linear correlation reveals a metabolic interdependence (coupling) indicating that this metabolic pathway can be at least partially controlled by the glutamine uptake. Coefficients of determination (R^2) are plotted in a heat map for the eight different test conditions (Figure 3-5). Deviations from linearity and relatively small changes of the respective fluxes will result in a bad correlation, i.e. a low R^2 value.

3.4.4.1 Glutamine-free cultivation

In the glutamine-free cultivation, the extracellular glutamine flux (changing from glutamine excretion to glutamine uptake) was only correlated to the glutamine synthesis or glutaminase reaction, respectively, and the ammonia excretion. For all other metabolic fluxes no correlation was observed.

3.4.4.2 Glutamine batch cultivations

In the glutamine supplemented batch cultures, we observe a linear correlation with the formation of alanine and serine from pyruvate, formation of glycine from serine as well as all extracellular uptake and excretion rates except asparagine at 2 mM glutamine. The degradation of asparagine to aspartate and its conversion to oxaloacetate were strongly connected only to the glutamine uptake at 1 mM glutamine concentration. Only little correlation was found for higher glutamine concentrations. The correlation of glutamate dehydrogenase activity with glutamine uptake was increasing with increasing glutamine concentration.

A good correlation was also found with the glycolytic fluxes and with the gluconeogenic flux from TCA cycle to glycolysis (OAA to PEP). In contrast, the pyruvate dehydrogenase reaction and the TCA cycle fluxes were much less connected to the glutamine uptake. However, coupling was strengthened with increasing glutamine concentrations and a strong connection was observed at 8 mM glutamine.

3.4.4.3 Glutamine fed-batch cultivations

Striking differences could be found between the batch and the fed-batch cultivations. In contrast to batch cultivations, the glutamine uptake rate was decoupled from glycolysis and all extracellular fluxes. The extracellular glutamine flux was also decoupled from formation of alanine, serine and glycine. This effect was more significant in the cultivation where glutamine was fed every day (8×1 mM) than in the cultivation with feeding every second day (4×2 mM). In the cultivation with daily feeding, the connection of the glutamine uptake with the glutamate dehydrogenase flux and with the anaplerotic flux (OAA to PEP) was maintained. In addition, the TCA cycle fluxes were

connected to the glutamine uptake as it was the case for the batch cultivation with a glutamine start concentration of 8 mM.

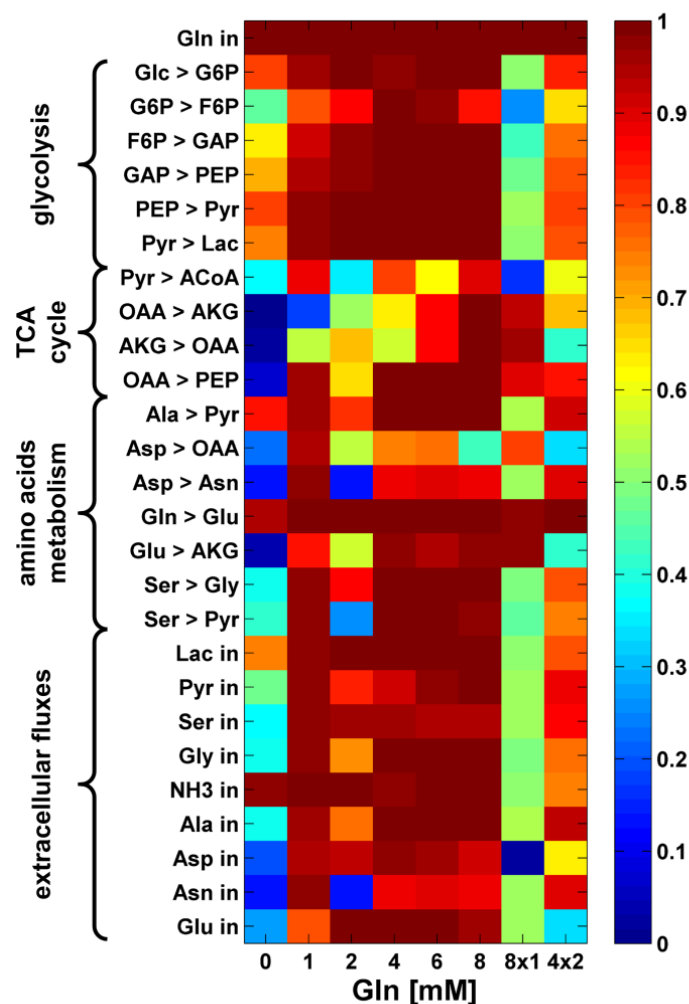


Figure 3-5. Correlation of extracellular uptake fluxes and intracellular fluxes of glycolysis, TCA cycle, and amino acid metabolism with glutamine uptake fluxes (Gln in). Metabolic fluxes determined using splines are related with the extracellular glutamine rates for the cultivation period between 20 and 120 h. Linear correlations are determined by the coefficient of determination (R^2) indicated by the color scale. The different cultivation conditions with varying glutamine supply are shown on the x-axis.

3.5 Discussion

3.5.1 Global metabolic changes controlled by the glutamine availability

We provide a comprehensive analysis of the glutamine metabolism in CHO cells and the metabolic changes controlled by varying glutamine availabilities using dynamic metabolic flux analysis (MFA). To our knowledge, this is the first study investigating the complete range of glutamine availabilities that can occur in animal cell cultivation, including dose-dependent effects of glutamine, mild or severe glutamine limitation, and controlled supplementation of glutamine. Numerous studies investigated the glutamine metabolism in different mammalian cell lines, e.g. in hybridoma (Kurokawa et al., 1994; Ljunggren and Haggstrom, 1994), myeloma (Ljunggren and Haggstrom, 1992), HEK 293 (Nadeau et al., 2000), PER.C6 cells (Maranga and Goochee, 2006), however studies of the glutamine metabolism in CHO cells are rather limited (Rajendra et al., 2012; Sanfeliu and Stephanopoulos, 1999). Most studies focused only on the comparison of two conditions, i.e. high glutamine batch and low glutamine fed-batch cultivations, but do not cover a larger range of glutamine availabilities. Moreover, intracellular metabolic fluxes have rarely been considered in previous studies (Burleigh et al., 2011; Nadeau et al., 2000; Nyberg et al., 1999a) and never using dynamic MFA.

In addition, our study allows investigating the effects of ammonia accumulation due to its direct connection to glutamine metabolism. The effects of increased ammonia concentrations on CHO (Chen and Harcum, 2006; Lao and Toth, 1997) and other mammalian cell cultures (Mirabet et al., 1997; Ozturk et al., 1992; Priesnitz et al., 2012; Schneider et al., 1996) have been studied by numerous groups in the past. Most studies supplemented the culture with elevated ammonia concentrations to test the effect of ammonia stress on cell cultures. However, since cell culture media do usually not contain ammonia this is an artificial condition with limited relevance. We propose to study the effects of ammonia accumulation by varying the glutamine concentration as a more valid condition for cell cultures.

According to the glutamine supply applied in the eight different test conditions, four distinct situations together with early and late effects can be distinguished: (1) glutamine-free cultivation with a constant glutamine limitation from the start (Figure 3-6, no glutamine), (2) low glutamine start levels leading to early glutamine depletion during the cultivation (Figure 3-6, low glutamine), (3) high glutamine start levels when no or only late glutamine limitation occurs (Figure 3-6, high glutamine), and (4) controlled feeding of low glutamine concentrations completely avoiding glutamine limitation (Figure 3-6, feeding glutamine).

Changing glutamine availabilities impose (1) different extreme situations on the cells, (1a) glutamine abundance and (1b) glutamine limitation, triggering (2) different cellular responses. The cells respond by (2a) adjusting their anabolic activities and their growth behaviour, (2b) rearranging

their metabolic fluxes in order to attenuate these extreme situations, which in turn results in (2c) adaptation of waste product excretion and substrate consumption leading to (3) alteration of the environmental conditions eventually imposing (1) new constraints on the cells. The dynamic interdependence of different extreme states with corresponding cellular responses to them and transition of different states into each other is schematically depicted in Figure 3-7.

3.5.2 The glutamine availability affects waste product excretion and substrate consumption

The extracellular metabolite profile gives a first indication of the metabolic changes induced by the glutamine availability. Lactate, alanine, and ammonia were excreted as waste products, glutamate and glycine were first excreted, then taken up and eventually excreted again, and glucose, pyruvate and all other amino acids were consumed during the whole cultivation period. The glutamine availability affects waste product excretion and substrate consumption by (a) supporting significant waste production of specific metabolites at glutamine abundance and (b) inducing the consumption of alternative carbon sources to compensate for glutamine limitation.

In the batch cultivations from 1 mM to 8 mM glutamine, we observe a clearly dose-dependent effect of glutamine on substrate consumption and product excretion. Excretion of ammonia, alanine, and glutamate increased dose-dependently with increasing glutamine consumption as expected due to their direct connection to glutamine metabolism (Doverskog et al., 1997). In contrast, glycine excretion was dose-dependently increased with decreasing glutamine concentration. Our findings are in accordance with previous studies on myeloma and hybridoma cells where glutamine limitation resulted in reduced production of ammonia and alanine, but increased glycine production (Ljunggren and Haggstrom, 1992; Ljunggren and Haggstrom, 1994). Reuptake and consumption of glutamate, aspartate and glycine was more significant, the lower the glutamine start concentration and the earlier glutamine depletion occurred. At glutamine depletion, these amino acids seem to be efficient substrates to compensate for glutamine limitation.

Interestingly, the outcome of the glutamine-free cultivation was not always an extrapolation of the dose-dependent effects observed for the different glutamine supplemented batch cultivations. On the contrary, a mixed response was observed for the glutamine-free cultivation. Excretion of alanine and ammonia were lowest in the glutamine-free cultivation but that of glycine was highest. However, excretion of glutamate was as high as in the 8 mM batch cultivation. Consumption of glutamate, aspartate, and glycine occurred as late as for the 8 mM batch cultivation but was larger than for the 1 mM batch cultivation. Our findings demonstrate that severe and mild glutamine limiting conditions have to be considered separately since they lead to very distinct metabolic effects.

The extracellular metabolite profiles of the two fed-batch cultivations were consistent with the different glutamine supplemented batch cultivations. Concerning the consumption of substrates and excretion of products an intermediate response between the 1 mM and 2 mM batch cultivations and the 8 mM batch cultivation was observed for the fed-batch cultivations. Waste product excretion was less significant than in the respective batch cultivations. Reduced waste product excretion in glutamine limited fed-batch cultivations compared to high glutamine batch cultivations was commonly observed in different cell lines (Ljunggren and Haggstrom, 1992; Ljunggren and Haggstrom, 1994; Maranga and Goochee, 2006).

3.5.3 Flux rearrangements in the pyruvate and amino acid metabolism compensate glutamine limitation and mitigate ammonia stress

Depending on the availability of glutamine the cells have to cope with different extreme situations, (a) glutamine abundance increasing ammonia stress and (b) glutamine limitation (Figures 3-6 and 3-7). When glutamine was abundant, it was preferentially consumed as major carbon source besides glucose. With increasing glutamine availability glutamine consumption and ammonia production rates increased. Ammonia stress triggered several cellular adaptations. We observed an increased production of alanine and serine serving as nitrogen sinks (Figure 3-6). The latter is correlated with a reduction of serine uptake. Glutamate excretion reduced production of ammonia by removing the substrate of glutamate dehydrogenase (Figures 3-6 and 3-7). However, the glutamate excretion rate was initially not significantly different in batch cultivations from 1 mM to 8 mM glutamine indicating that this is not the primary mechanism to reduce ammonia stress as proposed previously by Priesnitz et al. for the human cell line AGE1.hn (Priesnitz et al., 2012). Furthermore, we found an increased excretion of the two major side products of glutaminolysis, ammonia and alanine. Changes in the amino acid metabolism upon ammonia stress in animal cells have been found also before by several groups for CHO cells (Hansen and Emborg, 1994b) and other mammalian cell lines (Miller et al., 1989; Ozturk et al., 1992; Priesnitz et al., 2012). These adaptations either support ammonia fixation or reduce ammonia release by increased production or decreased uptake and degradation of specific amino acids, respectively.

Glutamine depletion resulted in a mild form of glutamine limitation (Figure 3-7). The cells had time to adapt to decreasing glutamine concentrations by activating compensation mechanisms. Glutamine depletion was first compensated by increased consumption of pyruvate, serine and partially asparagine and later by consumption of glutamate and aspartate (Figures 3-6 and 3-7). A severe and complete glutamine limitation as induced in the glutamine-free cultivation was also compensated by increased consumption of pyruvate and serine. In addition, the cells needed to synthesize glutamine from glutamate via glutamine synthetase. As a consequence, the glutamate dehydrogenase flux was reversed to produce glutamate for cellular glutamine synthesis (Figures 3-6 and 3-7). Since AKG was removed from the TCA cycle in favour of glutamine synthesis, the TCA cycle was additionally

fed via the anaplerotic flux from PEP to OAA to compensate for the lack of carbons in the TCA cycle (Figures 3-6 and 3-7). In later phases of the cultivation, the glutamine limited cultures had higher TCA cycle fluxes than the cultures with high glutamine start levels. This was achieved by an efficient management of glutamine limitation with successive recruitment of alternative substrates.

These compensation mechanisms, however, partially resulted in additional waste production. Activation of the glutamine synthesis pathway was accompanied by substantial glutamate excretion in the glutamine-free cultivation. Increased uptake of pyruvate and serine led to increased glycine production. Increased production of glycine in glutamine limited fed-batch cultivations was previously found for myeloma cells. However, they provided no explanation for this observation (Ljunggren and Haggstrom, 1992). Genzel et al. showed that pyruvate can be used as a replacement for glutamine in different adherent cell lines. Similar to our study, they observed increased excretion of glycine at growth on pyruvate (Genzel et al., 2005).

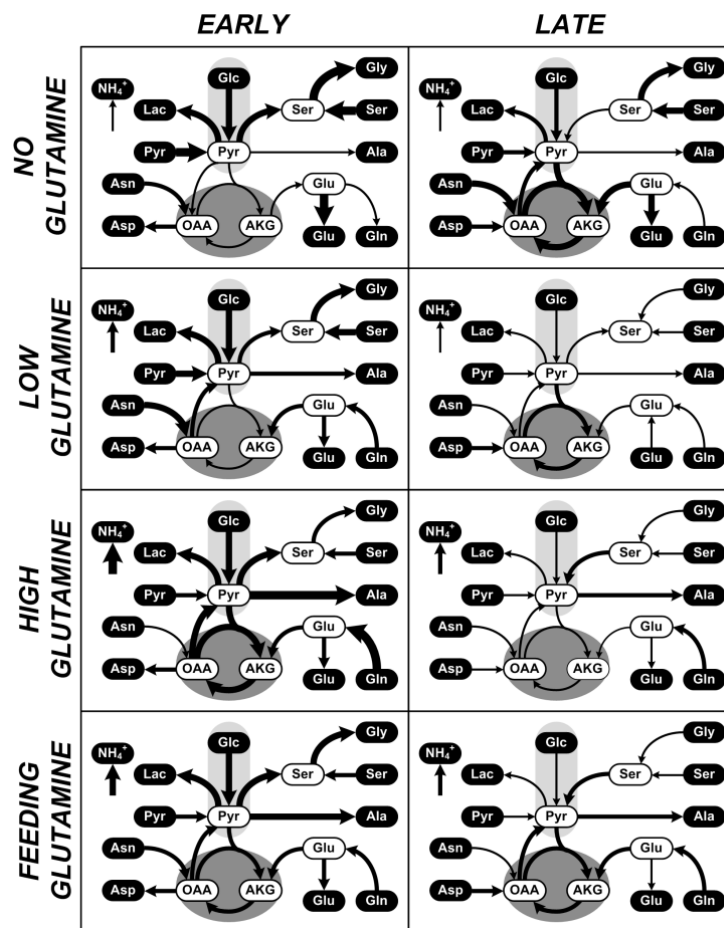


Figure 3-6. Schematic representation of metabolic flux dynamics in the central metabolism. Four different situations, no glutamine, low or high glutamine start concentrations, or feeding glutamine (top to bottom) with distinction of early (left) and late (right) effects can be distinguished. Abbreviations: Glc glucose, Pyr pyruvate, Lac lactate, AKG α -ketoglutarate, OAA oxaloacetate, for amino acids, the standard three letter code is used, the thickness of the arrows indicate relative values for each individual flux.

3.5.4 Low glutamine levels cause moderate growth and improved culture longevity

Growth and culture longevity of CHO-K1 were strongly influenced by the glutamine availability. Culture longevity can be seen by longer maintenance of high viability and relatively high specific growth rates. A time-resolved description of growth as applied in our study allows the distinction of early and late effects. In accordance with previous investigations on hybridoma and myeloma cells, specific growth rates reached maximum values early during the cultivation and decreased thereafter (Ljunggren and Haggstrom, 1992; Ljunggren and Haggstrom, 1994). Glutamine had an initial growth stimulating effect. The initial specific growth rates increased linearly with increasing glutamine uptake rates. However, identical maximal growth rates observed for 4, 6, and 8 mM glutamine start concentration indicate that there is an upper limit for μ and that the growth rate cannot be arbitrarily increased by raising the glutamine concentration. Identical specific growth rates in CHO batch cultivations with 4 mM and 8 mM glutamine start concentrations have also been described by Burleigh et al. (Burleigh et al., 2011). In contrast to hybridoma or myeloma cells, CHO cells are able to grow under glutamine-free conditions due to endogenous glutamine synthetase activity (Bebbington et al., 1992; Mercille and Massie, 1994; Street et al., 1993; Zhang et al., 2006). The glutamine synthetase catalyzes the ATP-hydrolyzing condensation of glutamate and ammonia to form glutamine. However, the initial growth rate in the glutamine-free cultivation was largely reduced compared to glutamine supplemented cultures which has been described before for CHO cells (Burleigh et al., 2011; Sanfeliu and Stephanopoulos, 1999).

Excessive growth and glutamine degradation at the beginning of cultivation resulted in acidification of the culture medium and in ammonia accumulation. Both, high ammonia concentrations (Hassell et al., 1991; Kurano et al., 1990) and a low pH (Trummer et al., 2006) have been shown to inhibit growth. As a consequence culture longevity was compromised at high glutamine start levels. At lower glutamine start concentrations as well as in the 8×1 mM fed-batch cultivation, viability and pH dropped later and specific growth rates decreased less. Interestingly, we found a high and constant late specific growth rate for the glutamine-free cultivation. A previous study investigating CHO batch cultivations at 0 mM, 4 mM and 8 mM glutamine made a similar observation. In contrast to the glutamine supplemented cultures, they found a high and constant specific growth rate in the glutamine-free cultivation (Burleigh et al., 2011). Improved culture longevity at glutamine limiting conditions was observed by several groups (Sanfeliu and Stephanopoulos, 1999; Wong et al., 2005). Sanfeliu and Stephanopoulos found that glutamine limitation initiated a slower rate of cell cycling protecting the cells from entering apoptosis (Sanfeliu and Stephanopoulos, 1999). The high production of glycine and C1 units, two key metabolites of biomass synthesis, observed in glutamine limited cultures might also stimulate growth. Glycine synthesis has been strongly correlated with elevated proliferation rates in various cancer cells (Jain et al., 2012). As a result of

this improved culture longevity, highest viable cell densities were observed in glutamine limited cultivations, i.e. in the 1 mM batch and the 8×1 mM fed-batch cultivation.

Varying glutamine availabilities trigger different cellular responses. We propose the following cellular mechanism to explain early and late effects of (a) glutamine abundance and (b) glutamine limitation on the growth behaviour of CHO cells (Figure 3-7):

(a) When glutamine is abundant, growth is first stimulated. The growth stimulation is antagonized by increasing ammonia accumulation. Elevated ammonia concentrations lead to growth inhibition in later stages of the cultivation. (b) At complete glutamine limitation, the cells need time to adapt their metabolism towards glutamine synthesis resulting in an early growth inhibition. However, as proposed by Sanfeliu and Stephanopoulos, glutamine limitation inhibits the onset of apoptosis improving culture longevity (Sanfeliu and Stephanopoulos, 1999). In addition, glutamine limitation was accompanied by increased glycine production rates which might further support growth later in the cultivation.

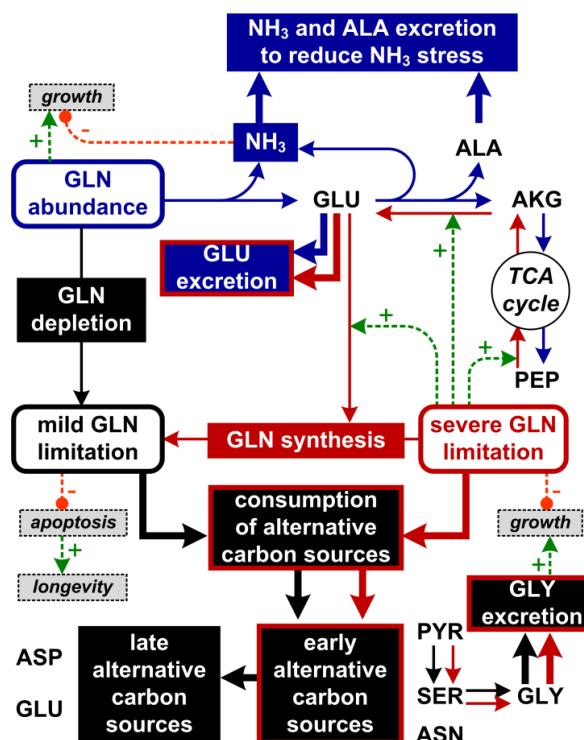


Figure 3-7. Cellular responses to ammonia stress and glutamine limitation. Three general conditions of glutamine availability triggering different cellular responses are described. Glutamine abundance (blue) results in ammonia stress. At severe glutamine limiting conditions (red) the cells need to synthesize glutamine. Mild glutamine limiting conditions (black) as a result of (i) controlled feeding or (ii) depletion after glutamine abundance or (iii) glutamine synthesis as response to severe glutamine limitation trigger the consumption of alternative carbon sources for compensation.

3.5.5 Glutamine feeding results in coupling to TCA cycle fluxes and decoupling from metabolic waste production eventually preventing cellular stress

The identification of metabolic links between the glutamine metabolism and specific metabolic activities (Figure 3-5) revealed a direct connection between the glutamine supply and all metabolic waste producing reactions. Thus, high glutamine availability triggered the production and excretion of significant amounts of waste products.

On the other hand, a high glutamine concentration was needed to create a link to the TCA cycle. The glutamate excretion partially prevented corresponding carbon input into the TCA cycle at lower glutamine concentrations. A substantial reflux from TCA cycle to glycolysis (OAA \rightarrow PEP) additionally removed carbons from the TCA cycle. Interestingly, the pyruvate dehydrogenase reaction was completely decoupled from the glutamine input. In a previous study of CHO cells, a similar observation was made. The TCA cycle fluxes from AKG to OAA were influenced by the glutamine uptake, however, the TCA cycle fluxes from OAA to AKG were impaired because carbons were removed from the TCA cycle at the site of OAA (Burleigh et al., 2011).

Controlled glutamine availability as achieved in fed-batch cultivations establishes a link between glutamine degradation and TCA cycle fluxes. A reduced glutamine supply decoupled the glutamine metabolism from glycolysis and waste producing pathways. By preventing an excessive glutamate excretion and reducing the carbon loss via the reflux from OAA to PEP the glutamine input is efficiently coupled to the glutamate dehydrogenase reaction and TCA cycle fluxes, eventually realizing moderate but stable TCA cycle activity. At the same time, cellular stress either due to excess glutamine supply resulting in ammonia accumulation or due to glutamine limitation is successfully avoided.

In summary, we propose a dynamic metabolic flux analysis method that takes into account the dynamic changes of growth and metabolism, thus providing a more valid description of cellular physiology than stationary methods. The proposed methodology is well suited for future applications in biomedical research and development of bioprocesses. It can be applied in the screening of cell clones and selection of efficient producer strains as well as in testing different media and feeding profiles. Furthermore, the method can assist in characterizing physiological conditions and disease phenotypes.

In this study, we investigated the impact of glutamine availability or limitation on the physiology of CHO-K1 cells. Varying glutamine availabilities resulted in global metabolic changes. We observed dose-dependent effects of glutamine in batch cultivation and an intermediate response with reduced waste product excretion in fed-batch cultivation. Identifying metabolic links from the glutamine metabolism to specific metabolic pathways, we could show that glutamine feeding results in decoupling from metabolic waste production and as a result in coupling to TCA cycle fluxes. In addition, we propose a mechanistic scheme explaining the cellular responses upon mild or severe

glutamine limitation and glutamine abundance and how these extreme situations are linked with each other. Flux rearrangements in the pyruvate and amino acid metabolism facilitate glutamine synthesis in the glutamine-free cultivation, compensate glutamine limitation by consumption of alternative carbon sources and mitigate ammonia stress as a result of glutamine abundance.

3.6 Acknowledgments

We thank Pavanteja Talluri for experimental assistance, the Institute of Cell Culture Technology (University Bielefeld, Germany) for supplying the CHO-K1 cells and the BMBF (German Federal Ministry of Education and Research) project SysCompart (project ID 031555D), part of the Systems Biology program, New Methods in Systems Biology (SysTec), for funding.

3.7 Supplementary material

Supplementary material associated with this chapter is available online:

<http://link.springer.com/article/10.1007%2Fs00253-013-5452-2>

4 Perturbation of the mammalian pyruvate metabolism and resulting rearrangement of central metabolic fluxes in CHO cells

4.1 Abstract

Chinese hamster ovary (CHO) cells are famous for their extraordinary robustness and flexibility making them a popular industrial host cell line and mammalian model system. Cellular pyruvate metabolism represents the major metabolic hub bridging glycolysis with tricarboxylic acid (TCA) cycle. We perturbed its metabolism applying dichloroacetic acid (DCA) and α -cyano-4-hydroxycinnamic acid (CHC) to either stimulate or inhibit the flux of pyruvate into the TCA cycle. The response was analyzed using metabolic flux analysis.

Inhibition or stimulation of pyruvate metabolism was successful at low CHC and DCA concentrations. However, high effector concentrations resulted in efficient metabolic compensation by readjustment of (1) the glutamate dehydrogenase/pyruvate dehydrogenase activity ratio, (2) the fluxes connecting C4 and C3 pools, and (3) feedback regulation of glycolysis. Efficient compensation of CHC and DCA effects was strictly dependent on glutamine availability. Glutamine depletion provoked emergence of the anticipated effects later in the cultivation.

Growth and cellular energy state of CHO cells remained robust upon severe perturbation of the mitochondrial pyruvate metabolism due to efficient overcompensation. However, metabolic inhibition or stimulation (i) at low effector concentrations and (ii) at glutamine depletion demonstrates the cell's limits of robustness. Knowing conditions of limited robustness helps to avoid undesired excursion of production processes. On the other hand, leading the cells into a susceptible state can be a powerful therapeutic strategy.

This chapter is in preparation for submission

Wahrheit J, Nonnenmacher Y, Nicolae A, Heinzle E. Perturbation of the Mammalian Pyruvate Metabolism and Resulting Rearrangement of Central Metabolic Fluxes in CHO Cells

4.2 Introduction

Pyruvate (Pyr) represents a key branch point of the intermediary metabolism playing a pivotal role in several metabolic pathways (Modak et al., 2002; Zeng et al., 2002). As it is the end product of glycolysis and a major substrate for the tricarboxylic acid (TCA) cycle, alterations in the Pyr metabolism commonly lead to an impaired connection between these pathways. Such metabolic alterations have been associated with diabetes, cancer and other pathological states (Gray et al., 2013; Hanahan and Weinberg, 2011; Kahn et al., 2006; Wu and Zhao, 2013).

We investigate control of this major hub of the central metabolism by manipulating the mitochondrial Pyr metabolism of CHO-K1 cells in opposite directions. Two different biochemical inhibitors, with (a) an inhibiting and (b) a potentially stimulating effect, were applied (Figure 4-1). (a) The recently identified mitochondrial pyruvate carrier (MPC) (Bricker et al., 2012; Herzig et al., 2012) was blocked by its specific inhibitor α -cyano-4-hydroxy-cinnamic acid (CHC) (Halestrap, 1975). (b) The pyruvate dehydrogenase (PDH) was indirectly stimulated by addition of dichloroacetic acid (DCA) (Sutendra and Michelakis, 2013). DCA is an established inhibitor of the PDH-inhibiting regulatory enzyme pyruvate dehydrogenase kinase (PDK). After application of CHC or DCA, the utilization of Pyr in the mitochondria, or in other words, the connection between glycolysis and TCA cycle, should be either inhibited or promoted, respectively. Both applied substances, CHC and DCA, have independently been proposed as promising anti-cancer agents (Kumar et al., 2013; Michelakis et al., 2008; Miranda-Goncalves et al., 2013). CHO cells share many common features with cancer cells and other pathologically impaired cells; amongst others these are: aerobic glycolysis (Warburg effect), increased glutaminolysis, chromosome instability leading to genetic heterogeneity, a fast (uncontrolled) proliferation, and most importantly an extreme robustness against internal and external perturbations (Altamirano et al., 2013). As demonstrated by their long history as mammalian model organism (Jayapal et al., 2007), they are a useful system to study general characteristics of this specific metabolic phenotype. Additionally, CHO cells are the most important cell factory in the industrial production of therapeutic proteins (Wurm, 2004).

Biological systems are very robust against general perturbations but tend to be extremely vulnerable against certain specific perturbations (Kitano, 2004). Generally, robustness is achieved at the expense of reduced overall performance or of the emergence of fragility under certain conditions. The mammalian energy metabolism can be maintained by glycolysis or by oxidative phosphorylation. The balance between these pathways is adjusted according to available resources. A metabolic shift to aerobic glycolysis, as it occurs in many diseases, e.g. in cancer metabolism, demonstrates cellular robustness, however, at the cost of metabolic efficiency.

Our study aimed at analyzing the impact of CHC and DCA on growth and (energy) metabolism of CHO-K1 cells. We applied metabolic flux analysis (MFA) to investigate the implication of these metabolic perturbations on the intracellular metabolic flux distribution. The following questions were considered: (i) Are CHO-K1 cells able to cope with a significant perturbation of the cellular pyruvate metabolism? (ii) What are the means by which robustness is achieved, i.e. how do the cells compensate such perturbations? (iii) What are the limits of perturbation tolerated by the cells, i.e. under which conditions do the cells lose their robustness? Maintaining cellular robustness and metabolic efficiency is crucial for industrial processes. On the other hand, limited robustness can be desirable state to achieve when treating pathological conditions, e.g. cancer cells. Studying cellular robustness and its limits will help us understanding the control of a major metabolic branch point in the intermediary metabolism and guide design of medical therapies and efficient biotechnological production processes.

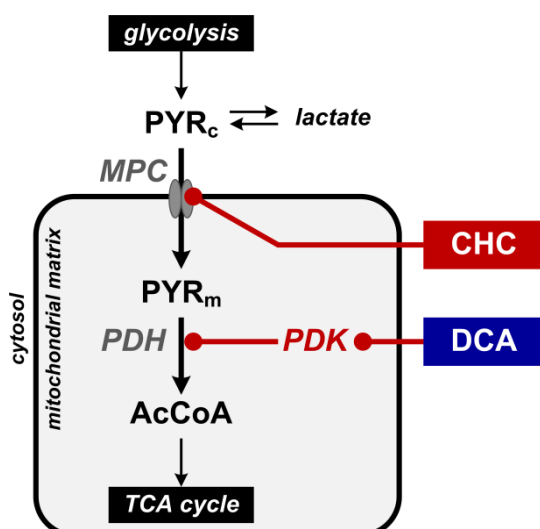


Figure 4-1. Scheme of CHC and DCA effects on the pyruvate metabolism. Cytosolic pyruvate (PYR_c) is transported into the mitochondrial matrix via the mitochondrial pyruvate carrier (MPC). Mitochondrial pyruvate (PYR_m) is further converted into acetyl-CoA (AcCoA) via the pyruvate dehydrogenase (PDH) reaction. The PDH is inhibited by phosphorylation through the PDH kinase (PDK). Inhibition of the mitochondrial pyruvate metabolism is achieved by application of the specific MPC inhibitor α -cyano-4-hydroxy cinnamic acid (CHC). Stimulation of the mitochondrial pyruvate metabolism is achieved by inhibition of the PDK using dichloroacetic acid (DCA)

4.3 Materials and methods

4.3.1 Cell culture

Cultivation of the CHO-K1 cells was performed in baffled shake flasks (250 ml, Corning, New York, USA) in a shaking incubator (Innova 4230, New Brunswick Scientific, Edison, NJ, USA) at 135 rpm (2 inches orbit), 37°C and 5% CO₂. The cells were cultivated in chemically defined, protein-free TC-42 medium (TeutoCell, Bielefeld, Germany), supplemented with 6 mM L-glutamine (Sigma-Aldrich, Steinheim, Germany) from a 240 mM stock solution in dH₂O.

4.3.2 Toxicity screening of α -cyano-4-hydroxy cinnamic acid (CHC) and dichloroacetic acid (DCA) in CHO-K1 cells

CHO-K1 cells in the early exponential phase were harvested by centrifugation (5 min, $125 \times g$, Labofuge 400R, Function Line, Heraeus Instruments, Hanau, Germany) and resuspended in TC-42 medium (supplemented with 6 mM L-glutamine). The cell number was determined using an automated cell counter (*Countess[®] Automated Cell Counter*, Invitrogen, Karlsruhe, Germany) and set to 2×10^5 cells/ml. 100 μ l of the cell suspension were transferred into the wells of a 96-well *OxoPlate* (PreSens, Regensburg, Germany). Tested substances α -cyano-4-hydroxycinnamic acid (CHC) and dichloroacetic acid (DCA) have been added from 2-fold concentrated stock solutions resolved in TC-42 medium to obtain a final volume of 200 μ l and a cell density of 1×10^5 cells/ml. Tested concentrations were in a range of 10 nM - 5 mM and 50 μ M - 100 mM for CHC and DCA, respectively, prepared by serial dilution with TC-42 medium. Six replicates were carried out for each concentration. Since the 500 mM stock solution of CHC was prepared in DMSO, an additional control containing 1% DMSO was carried out, representing the highest DMSO concentration used in the screening of CHC. Dissolved oxygen concentration was monitored every 10 min for 70 h using a fluorescence reader with integrated incubation unit (FLUOstar, BMG Labtechnologies, Offenburg, Germany), placed in an airtight box at 5% CO₂ and 37°C. Before each measurement, the plate was shaken for 300 s (140 rpm, 4 mm orbit) to prevent sedimentation of the cells. Every 24 h one of the replicates of each concentration was removed from the plate. 30 μ l of each suspension were used immediately for determination of cell densities and cell viability using an automated cell counter (*Countess[®] Automated Cell Counter*, Invitrogen, Karlsruhe, Germany). The rest was centrifuged and the supernatants were frozen at -20°C for subsequent analysis.

4.3.3 CHO-K1 cell cultivation during treatment with α -cyano-4-hydroxy cinnamic acid (CHC) and dichloroacetic acid (DCA)

CHO-K1 cells in the early exponential phase were harvested and resuspended in TC-42 medium containing selected concentrations of DCA or CHC. The cell number was determined using an automated cell counter (*Countess[®] Automated Cell Counter*, Invitrogen, Karlsruhe, Germany). The cells were seeded into 250 ml baffled shake flasks (Corning, New York, USA) to obtain a final volume of 100 ml TC-42 containing the selected concentrations of CHC (1 and 3 mM) or DCA (3, 5 and 10 mM) and a viable cell density of 4×10^5 cells/ml. CHC was added from 100 \times stock solutions in DMSO, resulting in a DMSO concentration of 0.5% in every CHC-containing culture. A control cultivation containing the same concentration of DMSO (but no CHC) was also performed. The pH of all media was determined in advance and set to 7.8 by addition of 30% NaOH. The different media were sterile filtered prior to use (pore size: 0.2 μ m).

Samples of 400 μl were taken every 24 hours. 30 μl were immediately used for the determination of growth parameters (cell densities, average cell diameter and viability). The rest of the sample was centrifuged (5 min, $6000 \times g$, Biofuge pico, Heraeus Instruments, Hanau, Germany) and 200 μl of the supernatant were frozen at -20°C for subsequent analysis. The remaining supernatant was used for determination of the pH value (pH-Meter, Mettler-Toledo, Giessen, Germany).

4.3.4 Quantification of extracellular metabolites

Quantification of glucose, organic acids and proteinogenic amino acids in supernatants were performed by HPLC as described previously (Strigun et al., 2011b). Since DCA co-eluted with glucose in the HPLC analysis, the glucose concentration in culture supernatants containing DCA was determined using a D-glucose UV assay kit (Roche, Darmstadt, Germany) according to kit instructions.

4.3.5 Quantification of cellular ATP concentration

Quantification of intracellular ATP in a luminometer (GloMax[®] 96 Microplate Luminometer, Promega Corporation, Madison, WI, USA) was performed using the *CellTiter Glo[®] Luminescent Cell Viability Assay* (Promega Corporation, Madison, WI, USA) according to kit instructions.

4.3.6 Metabolic flux analysis

Metabolic fluxes were calculated using Matlab R2012b (The Mathworks, Natick, MA, USA) applying stationary metabolic flux analysis using metabolite balancing as described in literature (Niklas and Heinzle, 2012; Niklas et al., 2011c). The stoichiometry of the applied metabolic network model is given as stoichiometric matrix in the supplementary material (Table S1 and Table S2). A scheme of the metabolic network model is depicted in Supplementary Figure S1. Fatty acids and storage carbohydrates composition of the cell was taken from Altamirano et al. (Altamirano et al., 2001b). The amino acid composition of proteins was determined as described previously (Niklas et al., 2009). The biomass composition can be found in the supplementary material (Table S3). Metabolic rates [$\text{mmol}/(\text{L} \times \text{h})$] were related to the cell volume. The average cell volume was estimated from the average cell diameter assuming a sphere. Differences of cell diameters during the cultivation and between different cultivations were very small ($\sim 3\%$) and not further considered.

4.4 Results and Discussion

4.4.1 Determination of effective CHC and DCA concentrations

A wide range of CHC and DCA concentrations was tested in terms of toxicity and influence on metabolism. We performed a toxicity screening in 96-well OxoPlates using respiration analysis and calculated EC_{50} values as described before (Niklas et al., 2009; Noor et al., 2009). After 70 h of cultivation, we determined EC_{50} values of 3.5 mM and 13 mM for CHC and DCA, respectively (supplementary Figure S2A and S2B). For both effectors, we observed an influence on extracellular pyruvate (Pyr) and lactate (Lac) compared to control cultivations at concentrations of 1 mM and above (supplementary Figure S2C to S2F). Based on these results, we selected effective concentrations of 1 mM ($EC_{0.002}$) and 3 mM CHC (EC_{20}) as well as 3 mM ($EC_{0.04}$), 5 mM ($EC_{0.6}$), and 10 mM DCA (EC_{20}) for further studies. Selected concentrations were in a similar range as applied before in cell cultures (Lefort et al., 2013; McKenna et al., 2001; Simpson et al., 2006).

4.4.2 Cultivation profiles of CHO-K1 cells with CHC or DCA treatment

The growth and pH profiles, cellular ATP concentration over time as well as the profiles of selected extracellular metabolites are depicted in Figure 4-2. The complete set of measured extracellular metabolites can be found in the Supplementary Figures S3 and S4.

The cells treated with 0.5% DMSO (solvent control) and 1 mM CHC showed a similar growth behavior to that of the control cultivation. However, the maximum viable cell density (VCD) reached during cultivation was reduced by 7% (DMSO) and 12% (1 mM CHC), respectively, compared to the control (20.5×10^6 cells/ml). At 3 mM CHC, growth was significantly slowed after 48 h of cultivation and reached a plateau maintaining a constant VCD after 96 h. The maximum VCD was decreased by 50% (Figure 4-2A). There was a slight tendency of faster growth on 3 mM DCA and slower growth on 10 mM DCA, however, growth was not significantly different to the control cultivation (Figure 4-2B).

Three metabolic phases could be distinguished. The first metabolic phase was characterized by glutamine (Gln) consumption and Lac excretion and lasted from 0 to 72 h (phase I). The second phase from 72 to 120 h was initiated by Gln depletion and Lac reuptake (phase II). A shift from Lac production to consumption is a commonly observed characteristic of CHO cells (Martinez et al., 2013; Wahrheit et al., 2014b; Zagari et al., 2013a). After 120 h the VCD decreased significantly (phase III). The most significant changes in the metabolite profile were observed for extracellular Pyr, Lac, and alanine (Ala) which are directly connected to the cellular Pyr metabolism. We observed a delayed Pyr uptake at 1 mM CHC. At 3 mM CHC, Pyr was even significantly excreted within the first 72 h and then consumed. Lac excretion was slightly delayed for 1 and 3 mM CHC (Figure 4-2A) and decreased significantly with increasing DCA concentrations (Figure 4-2B). At

3 mM CHC, Lac excretion persisted in phase II and III thereby completely omitting the Lac shift. Compared to untreated control cultivations, the maximally reached Lac concentration was increased by 40% at 3 mM CHC treatment and reduced by 16%, 20% and 26% for 3, 5, and 10 mM DCA, respectively. The pH profile was correlated with the Lac profile. The culture pH decreased during Lac excretion and increased during Lac consumption. Accordingly, the pH decreased constantly at 3 mM CHC (Figure 4-2A). Ala was initially excreted but consumed after 96 h. Ala excretion decreased with increasing CHC and DCA concentrations. At 3 mM CHC, Ala was not taken up at the end of the cultivation but constantly excreted. Glycine (Gly) excretion decreased dose-dependently at DCA treatment and was clearly larger during the plateau phase at 3 mM CHC. Uptake of glucose (Glc) and serine (Ser) (Figure 4-2A) as well as of other amino acids was reduced at 3 mM CHC later in the cultivation matching the reduced growth (Supplementary Figure S3).

The cellular ATP concentration increased dose-dependently upon DCA treatment within the first 48 h of cultivation but was not significantly different from the control afterwards (Figure 4-2B). At 3 mM CHC, the cellular ATP content was unchanged during the first 72 h of cultivation. It was, however, significantly reduced during the plateau phase starting at 96 h of cultivation (Figure 4-2A). At a concentration of 1 mM CHC, ATP levels were not affected.

While we observed mostly dose-dependent effects for the three DCA test concentrations, there was a prominent metabolic shift between the two CHC test cultivations. As is clearly evident from the profiles of pH, Lac, Pyr and Ala, the metabolic behavior was very different at low and high CHC concentrations.

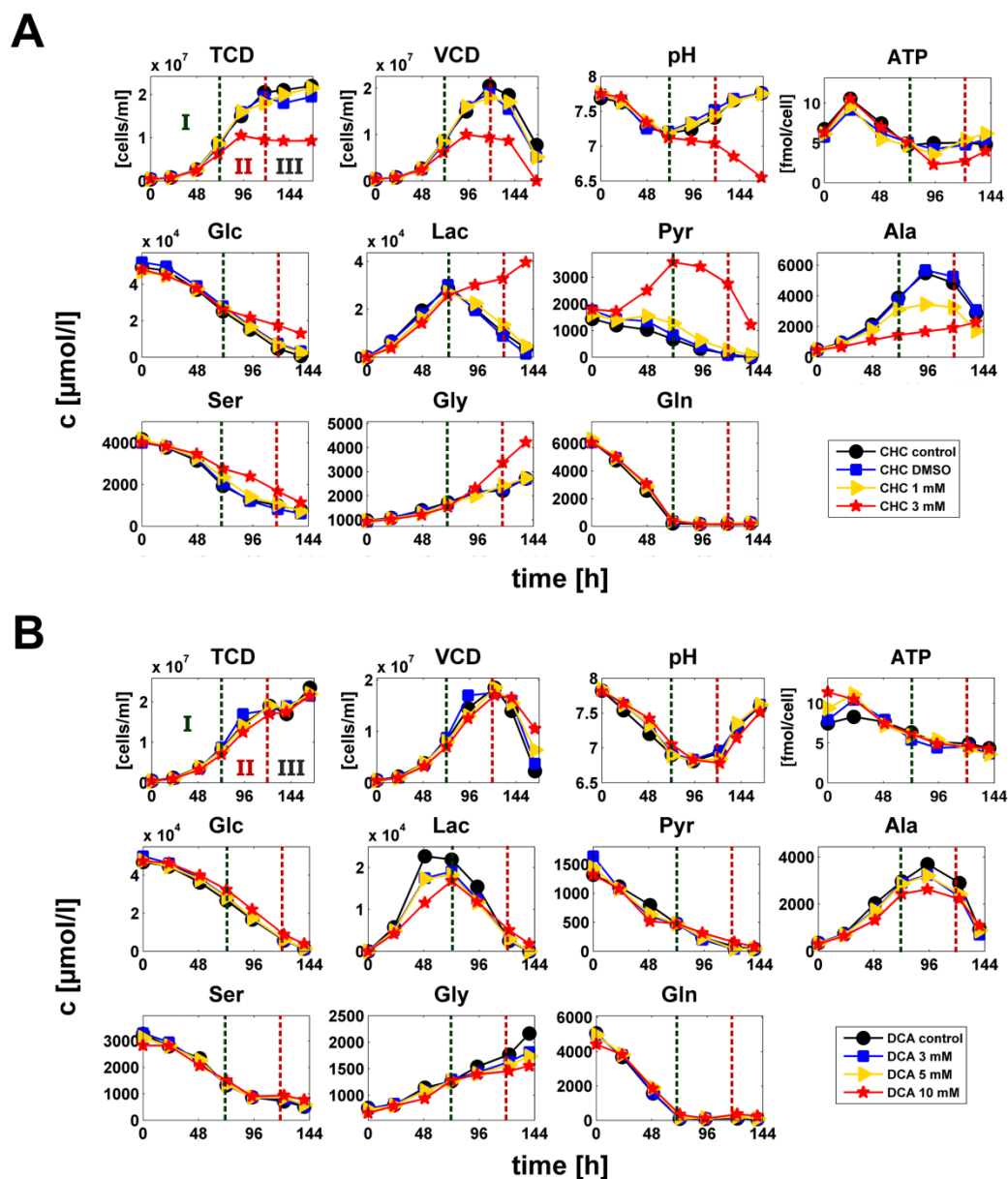


Figure 4-2. Cultivation profiles of CHO-K1 cells upon treatment with CHC and DCA. (A) Cultivation profiles upon treatment with 1 mM and 3 mM CHC compared to control cultivations with 0.5% DMSO (CHC DMSO) and without CHC and DMSO (CHC control). (B) Cultivation profiles upon treatment with 3 mM, 5 mM or 10 mM DCA compared to control cultivation without DCA (DCA control). Shown are total and viable cell densities [cells/ml], the pH profile, the cellular ATP concentration [fmol/cell] and selected extracellular metabolite concentrations [$\mu\text{mol/l}$] over time [h]. Abbreviations: CHC α -cyano-4-hydroxy cinnamic acid, DCA dichloroacetic acid, TCD total cell density, VCD viable cell density, Glc glucose, Lac lactate, Pyr pyruvate, for amino acids the standard three-letter code is used. Dashed lines indicate the different metabolic phases, phase I (0-72 h), phase II (72-120 h) and phase III (>120h).

4.4.3 Metabolic fluxes of CHO-K1 cells with CHC or DCA treatment

Metabolic fluxes were calculated for the first (Figure 4-3A) and the second metabolic phases (Figure 4-3B). A scheme of the metabolic network illustrating the lumping of metabolites is depicted in Supplementary Figure S1. The complete set of calculated and measured metabolic fluxes can be found in the Supplementary Tables S4 and S5. The results of both experiments, (a) inhibition of the MPC by CHC (CHC Experiment) and (b) stimulation of the PDH by DCA (DCA Experiment), are presented in the same flux maps for better comparison. For the two control cultivations of both experiments without any addition of effectors, mean values with standard deviations are shown to reflect the normal metabolic variability between distinct biological experiments (Figure 4-3, white bar).

The overall metabolic effects of DMSO in the applied low concentration were usually very small in both metabolic phases (Figure 4-3, black bar). In most cases, fluxes were not significantly different from control cultivations or are not expected to have a significant impact on overall metabolic flux distributions. DMSO effects did not cover effects of the CHC treatment and are therefore not further considered in the discussion. This was justified due to three reasons: (i) although relative differences might be large, the absolute differences were rather negligible, (ii) DMSO treatment changed the flux in the opposite direction as observed for CHC treatment, or (iii) the effect of CHC was substantially larger and could not be explained by DMSO treatment alone.

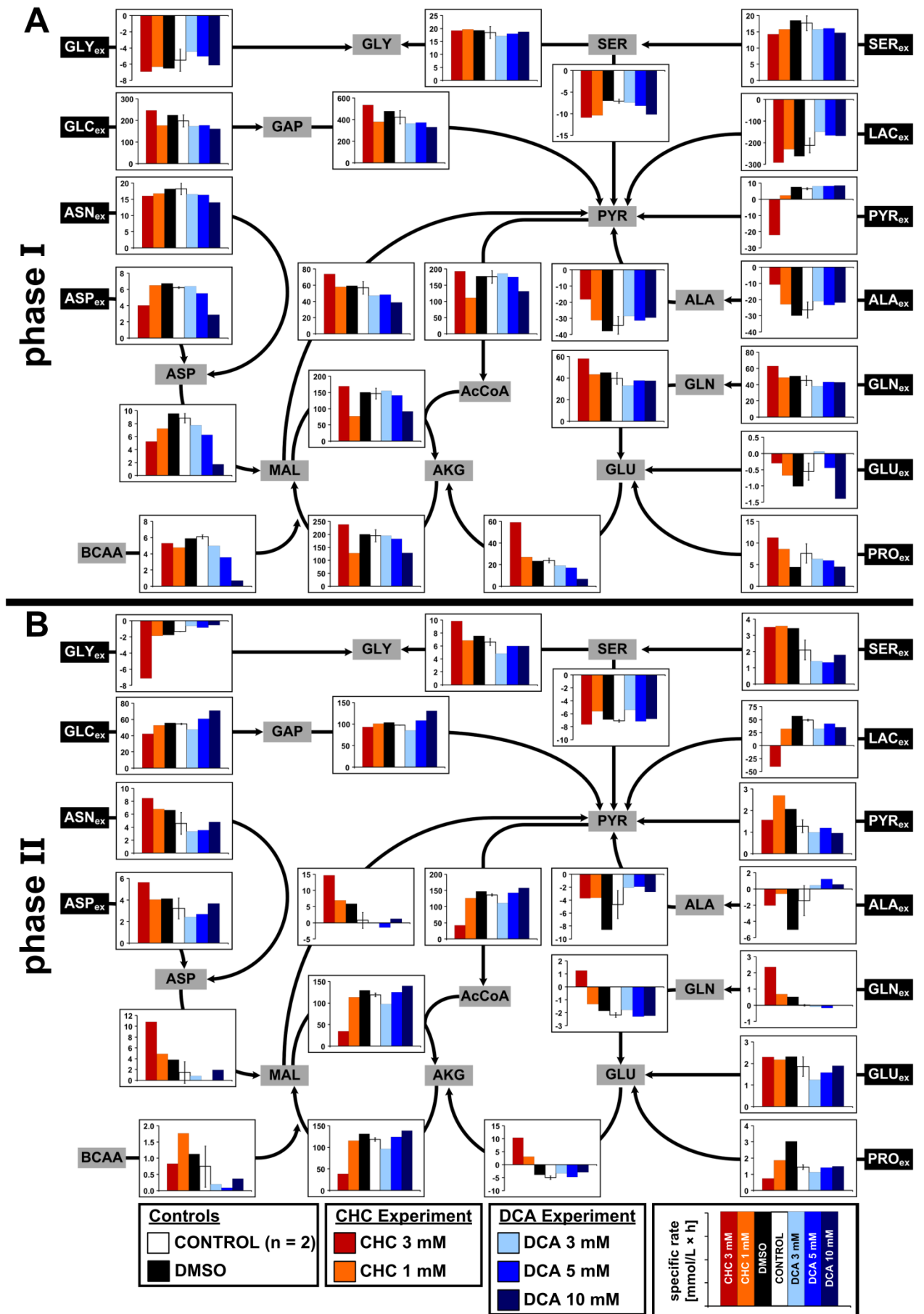
4.4.3.1 Metabolic fluxes in the glutamine consumption phase (phase I)

Glycolytic fluxes and Lac excretion were clearly reduced at DCA treatment (80-89% and 70-79%, respectively, relative to untreated control) (Figure 4-3A). Reduced glycolysis upon DCA treatment was also found in human fibroblasts (Simpson et al., 2006) and human breast cancer cell lines (Lefort et al., 2013). We determined lower glycolytic fluxes at 1 mM CHC (89%) but higher rates of Glc uptake (124%), glycolysis (127%) and Lac excretion (138%) at 3 mM CHC. Increased Glc uptake rates upon CHC treatment have been previously observed in astrocytes (McKenna et al., 2001). The Pyr uptake rate increased dose-dependently in DCA-treated cells to 122%, 124% and 128% for 3, 5 and 10 mM DCA, respectively. In contrast, Pyr uptake was significantly reduced to 36% at 1 mM CHC. Pyr was even excreted in substantial amounts at 3 mM CHC (Figure 4-3A). This points to an accumulation of cytosolic Pyr due to block of the Pyr transport into the mitochondria. PDH and TCA cycle fluxes were significantly reduced at 1 mM CHC (52-65%) and 10 mM DCA treatment (62-75%). In contrast, these fluxes increased to 109-122% of the control at 3 mM CHC (Figure 4-3A). The reflux from TCA cycle to glycolysis, represented by the cataplerotic flux connecting malate (Mal) (C4) and Pyr (C3) pools (see Supplementary Figure S1), was increased to 130% at 3 mM CHC treatment and reduced to 68-85% in DCA-treated cells.

Ser synthesis increased in a dose-dependent manner both upon DCA (105-144%) and CHC treatment (147-154%) as indicated by a negative flux from Ser to the C3 pool represented by Pyr

(see supplementary Figure S1). Increased Ser production rates were accompanied by reduced Ser uptake rates (80-91%) (Figure 4-3A). Similarly, Ala production decreased to 87% and 41% for 1 and 3 mM CHC, respectively, and by 11-20% in DCA-treated cells (Figure 4-3A). The glutamate dehydrogenase (GDH) flux to α -ketoglutarate (AKG) increased dose-dependently with increasing CHC concentrations (112% and 247% for 1 and 3 mM CHC) and decreased dose-dependently with increasing DCA concentrations (80%, 71%, and 29% for 3, 5 and 10 mM DCA, respectively) (Figure 4-3A). Gln consumption rates were accordingly higher at CHC treatment and lower at DCA treatment compared to control cultivations. The aspartate aminotransferase (ASAT) reaction feeding carbons of aspartate (Asp) and asparagine (Asn) into the TCA cycle decreased dose-dependently with increasing CHC (82% and 60% for 1 and 3 mM CHC) and also with increasing DCA concentrations (88%, 71%, and 20% for 3, 5, and 10 mM DCA). Accordingly, Asn and Asp uptake rates were largely reduced in a dose-dependent manner with increasing CHC and DCA concentrations (Figure 4-3A). Furthermore, catabolic reactions of branched chain amino acids (BCAA) were significantly reduced upon CHC and even more at DCA treatment.

Figure 4-3. Flux maps of CHO-K1 upon treatment with CHC and DCA. (A) Metabolic fluxes in the glutamine consumption phase (phase I, 0 – 72 h). (B) Metabolic fluxes in the glutamine depletion phase (phase II, 72 – 120 h). Shown are the metabolic rates related to the cell volume [mmol/(L × h)] for CHO-K1 cells upon treatment with 1 mM and 3 mM CHC and upon treatment with 3 mM, 5 mM or 10 mM DCA. For the control cultivation without any addition of effectors, mean values with standard deviations of two biological replicates are shown. Since the CHC stock solution was resolved in DMSO, a solvent-control cultivation with identical DMSO concentration but without CHC is shown for comparison (DMSO). Extracellular metabolites are highlighted in black boxes, intracellular metabolites in grey ones. Abbreviations: CHC α -cyano-4-hydroxy cinnamic acid, DCA dichloroacetic acid, GLC glucose (representing the lumped C6 metabolite pools glucose-6-phosphate, G6P, and fructose-6-phosphate, F6P), GAP glyceraldehyde-3-phosphate (representing also dihydroxyacetone phosphate, DHAP), PYR pyruvate (representing also the lumped C3 metabolite pools of 1,3-bisphosphoglycerate, 1,3-PG, 3-phosphoglycerate, 3-PG, and phosphoenolpyruvate PEP), LAC lactate, AcCoA acetyl-CoA, AKG α -ketoglutarate (representing also citrate, CIT), MAL malate (representing also the lumped C4 metabolite pools of succinate SUC, fumarate FUM, and oxaloacetate OAA), BCAA branched chain amino acids (summed up fluxes of LEU, ILE, and VAL that are degraded to TCA cycle intermediates acetyl-CoA and succinyl-CoA and consume AKG in the transamination reactions), for amino acids, the standard three-letter code is used. Negative values indicate fluxes in the opposite direction of the arrow. A negative flux from serine to pyruvate indicates serine synthesis from 3-PG. The flux from malate to pyruvate represents the lumped cataplerotic reflux from TCA cycle to glycolysis via metabolic reactions connecting C3 and C4 pools.



4.4.3.1 Metabolic fluxes in the glutamine depletion phase (phase II)

Glc uptake rates increased dose-dependently with increasing DCA concentration (87%, 111%, and 130% for 3, 5, and 10 mM DCA) and decreased dose-dependently with increasing CHC concentration (96% and 78% for 1 and 3 mM CHC) (Figure 4-3B). Lac consumption was reduced at 1 mM CHC treatment (66% of the control) and in DCA-treated cells (66-86% of the control). In contrast, Lac excretion persisted in phase II at 3 mM CHC (Figure 4-3B). In phase II, CHC treatment increased the Pyr uptake rate (123-212%) while DCA treatment reduced it (75-94%) (Figure 4-3B). Similar to the glycolytic fluxes, PDH and TCA cycle fluxes increased dose-dependently with increasing DCA concentration (82%, 105%, and 117% for 3, 5, and 10 mM DCA) and decreased dose-dependently with increasing CHC concentration (95% and 30% for 1 and 3 mM CHC). The cataplerotic flux from Mal to the Pyr pool was negligible for the control cultivations and DCA-treated cultivations. However, this flux was active at CHC treatment (Figure 4-3B).

Ser uptake and Gly production rates were elevated upon CHC treatment and significantly reduced in DCA-treated cells (Figure 4-3B). Ala production was lower at CHC and DCA treatment compared to untreated control. Gln depletion resulted in a reversed GDH flux for control cultivations and DCA-treated cells. Upon CHC treatment, GDH was still feeding into the TCA cycle. Catabolism of Asn and Asp increased with increasing CHC concentration. BCAA degradation was only significantly increased at 1 mM CHC. Anaplerotic fluxes from Asp and BCAA into the TCA cycle were very small for DCA-treated cultivations.

4.4.3.2 Specific metabolic flux ratios indicate metabolic efficiency

In phase I, the Lac/Glc ratio ($LAC_{ex} \rightarrow LAC_{in} / GLC_{ex} \rightarrow GLC_{in}$) was higher upon CHC treatment (122% and 111%, for 1 and 3 mM CHC) but lower at DCA treatment (81%, 88% and 98% for 3, 5, and 10 mM DCA), relative to the ratio of -1.07 in the control experiment (Figure 4-4A). This indicates more carbon spilling by Lac excretion in CHC-treated but less in DCA-treated cells. In phase II, the Lac/Glc ratio was negative for the 3 mM CHC cultivation due to persistent carbon spilling (Figure 4-4D). Positive ratios for all other cultivations indicate simultaneous utilization of Glc and Lac as carbon sources as observed before in this CHO-K1 cell line (Wahrheit et al., 2014b). Significantly lower values for 1 mM CHC and DCA-treated cells compared to the control (55-77%) indicate a lower significance of Lac as substrate compared to the control (Figure 4-4D).

The TCA cycle/glycolysis ratio ($OAA \rightarrow CIT / F6P \rightarrow GAP$) (Wahrheit et al., 2014b) was significantly reduced to 59% at 1 mM CHC but restored to 91% at 3 mM CHC (Figure 4-4B) in phase I. We determined higher ratios for 3 and 5 mM DCA (122% and 108%, respectively) but a lower ratio at 10 mM DCA (78%). Higher ratios indicate an enhanced connectivity between glycolysis and TCA cycle and a more efficient metabolism of glucose and other glycolytic substrates (Wahrheit et al., 2014b). In phase II, the ratio was significantly reduced upon 3 mM CHC treatment but in a similar range for all other cultivations.

The glutamate dehydrogenase/pyruvate dehydrogenase (GDH/PDH) ratio ($\text{GLU} \rightarrow \text{AKG} / \text{PYR} \rightarrow \text{AcCoA}$) describes the relative contribution of AKG and acetyl-CoA in fueling the TCA cycle. The relative contribution of AKG as TCA cycle substrate increased with increasing CHC concentrations but decreased with increasing DCA concentrations in phase I (Figure 4-4C). In phase II, the GDH/PDH ratio was still significant for 3 mM CHC, however, negligibly small for the other cultivations (Figure 4-4F).

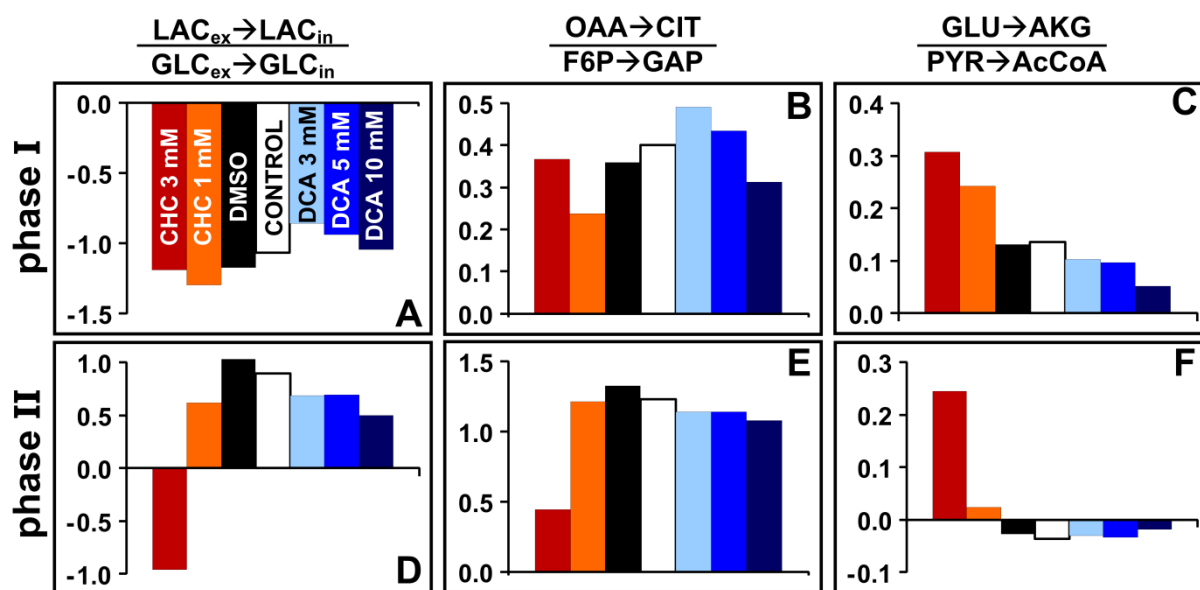


Figure 4-4. Influence of CHC and DCA on specific metabolic flux ratios. Specific metabolic flux ratios [mol/mol] are shown for phase I from 0 to 72 h (top, A-C) and phase II from 72 to 120 h (bottom, D-F). (A) and (D) The lactate/glucose ratio was calculated as the ratio between lactate uptake and glucose uptake ($\text{LAC}_{\text{ex}} \rightarrow \text{LAC}_{\text{in}} / \text{GLC}_{\text{ex}} \rightarrow \text{GLC}_{\text{in}}$). A negative ratio indicates lactate excretion. (B) and (E) The TCA cycle activity relative to the glycolytic activity was calculated as the ratio between the citrate synthase flux ($\text{OAA} \rightarrow \text{CIT}$) and the phosphofruktokinase flux ($\text{F6P} \rightarrow \text{GAP}$). (C) and (F) The relative contribution of AcCoA and AKG in fueling the TCA cycle was calculated as the ratio between the glutamate dehydrogenase flux from GLU to AKG ($\text{GLU} \rightarrow \text{AKG}$) and the pyruvate dehydrogenase flux ($\text{PYR} \rightarrow \text{AcCoA}$) (GDH/PDH ratio). A negative ratio indicates net flux from AKG to GLU.

4.4.4 Robustness and susceptibility towards perturbations of the cellular pyruvate metabolism in CHO-K1 cells

In the present study, the cellular Pyr metabolism was investigated by perturbation with two different biochemical effectors, CHC and DCA. CHC blocks the mitochondrial pyruvate carrier (MPC) (Halestrap, 1975). It should therefore result in (i) an impaired connectivity between glycolysis and TCA cycle with reduced Glc oxidation and (ii) a relative shortage of Pyr in the mitochondria. The most prominent effect of DCA is PDH stimulation by inhibition of the pyruvate dehydrogenase kinase (PDK). However, DCA is expected to show an effect only if the MPC is not the limiting step. If the MPC activity limits the mitochondrial availability of Pyr, DCA will not increase the flux into the TCA cycle. Furthermore, DCA and its potential metabolites (e.g. oxalate, glycolate, glyoxylate) exert multiple, partially even opposite, effects on the cellular metabolism (Crabb et al., 1981; Stacpoole, 1989). Nevertheless, PDH stimulation by DCA as predominant effect can theoretically result in (i) indirect stimulation of the PDH flux, (ii) higher availability of acetyl-CoA feeding the TCA cycle and eventually (iii) an improved connectivity between glycolysis and TCA cycle with a shift from Lac production to Glc oxidation.

4.4.4.1 Susceptibility to low effector concentrations of CHC and DCA

The direct effects of CHC and DCA on the cellular Pyr metabolism are best evidenced by the extracellular Pyr rates and Lac/Glc ratios. Increased Pyr uptake rates (122-128%) (Figure 4-5C and D) in combination with reduced Lac/Glc ratios (81-98%) (Figure 4-4) clearly indicate an improved metabolization of cellular Pyr at DCA treatment. Upon CHC treatment on the other hand, an impaired Pyr metabolization was obvious from a switch to reduced Pyr uptake (36%) or even Pyr excretion (Figure 4-5A and B) and from higher Lac/Glc ratios (111-122%) (Figure 4-4).

Surprisingly, further effects of CHC and DCA on the central metabolism (see above) were only evident at low effector concentrations. At 1 mM CHC, expected impaired Glc oxidation resulted in increased Lac excretion rates and reduced glycolytic fluxes (Figure 4-5B). The relative shortage of mitochondrial Pyr further led to substantially decreased PDH and TCA cycle fluxes (52-65%). An impaired connectivity between glycolysis and TCA cycle and concomitant increased overflow metabolism was also illustrated by a significantly lower TCA cycle/glycolysis ratio (59%) (Figure 4-4B) and a higher Lac/Glc ratio (122%) (Figure 4-4A). Although the energy generation from TCA cycle was severely impaired at 1 mM CHC (Figure 4-6A) this was not reflected in growth and cellular ATP levels which remained almost unaffected (Figure 4-2A and 4-6C). This indicates that the remaining TCA cycle activity was sufficient to meet the cellular energy demand. In phase II, the central metabolism had completely recovered its functionality suggesting that the MPC-inhibiting effect of CHC ceased after 72 h for 1 mM CHC (Figure 4-5F and 4-6B).

At 3 mM DCA treatment, PDH and TCA cycle fluxes were slightly increased (Figure 4-5C). The lower Lac/Glc ratio (81%) (Figure 4-4A) and higher TCA cycle/glycolysis ratio (122%) (Figure 4-4B) clearly demonstrate efficient flux redistribution from Lac production to oxidative decarboxylation of Pyr as expected at DCA treatment. A dose-dependent increase of cellular ATP levels within the first 48 h of cultivation was in agreement with the expected DCA effect in terms of PDH and TCA cycle stimulation (Figure 4-2B and 4-6C). This short-term response of elevated ATP levels is in accordance with reported fast mode of action of DCA (Simpson et al., 2006).

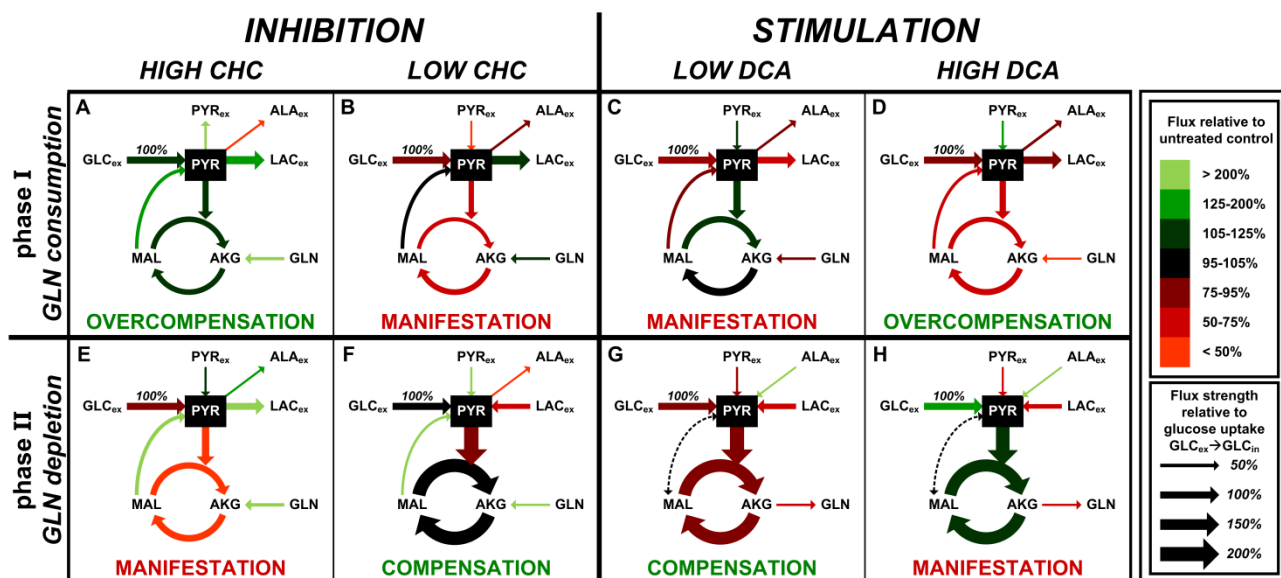


Figure 4-5. Summary of CHC and DCA effects in different metabolic phases. Specific metabolic effects of low and high concentrations of CHC (1 mM and 3 mM CHC, left) and DCA (3 mM and 10 mM DCA, right) in metabolic phases of glutamine consumption (phase I, top) and glutamine depletion (phase II, bottom). The arrow thickness is proportional to the flux strength relative to the respective glucose uptake flux (100%) as indicated in the legend. The arrow color indicates the flux strength relative to the respective untreated control cultivations (100%).

4.4.4.2 Overcompensation of CHC and DCA effects shows robustness towards elevated effector concentrations

Unexpectedly, higher CHC and DCA doses did not result in an extrapolation of the effects observed at low effector concentrations. At 3 mM CHC, PDH and TCA cycle activities were completely restored and even increased compared to the untreated control (Figure 4-5A). The Lac/Glc ratio (111%) and TCA cycle/glycolysis ratio (91%) were closer to control values at 3 mM CHC as well (Figure 4-4A and 4-4B). In phase I, cellular ATP levels were not affected (Figure 4-2A and 4-6C) and ATP production rates were even increased by 17% (Figure 4-6A) at 3 mM CHC. At higher concentration of CHC, the cells respond to a block of the MPC by initiation of a series of compensation mechanisms which all aim at increasing the TCA cycle activity and eventually the cellular energy status. This is attained by the combination of three complementing strategies: (1) Feeding of the AKG pool to fuel the TCA cycle is achieved by (i) stimulation of glutaminolysis and

a large increase of the GDH flux ($\text{Glu} \rightarrow \text{AKG}$) (Figure 4-5A and 4-5B), (ii) reduced ASAT activity ($\text{Asp} + \text{AKG} \rightarrow \text{OAA} + \text{Glu}$), and (iii) reduced catabolism of BCAA ($\text{BCAA} + \text{AKG} \rightarrow \text{acetyl-CoA/succinyl-CoA} + \text{Glu}$) (Figure 4-3A). (2) Feeding of the mitochondrial Pyr pool is accomplished by (i) reduced Ala production and (ii) an increased cataplerotic flux from Mal to Pyr pools (Figure 4-5A). (3) Well-known up-regulation of glycolytic fluxes by feedback mechanisms (e.g. via AMP and citrate levels) (Michal and Schomburg, 2012) additionally contribute significantly to maintain a high ATP production (Figure 4-5A). This requires an increased Lac production to maintain the redox balance by regenerating NAD^+ (Figure 4-5A). The combined interplay of these overcompensating flux rearrangements efficiently restores the cellular energy metabolism at 3 mM CHC (Figure 4-5A).

At DCA treatment, PDH and TCA cycle fluxes as well as the TCA cycle/glycolysis ratio decreased dose-dependently with increasing DCA levels (Figure 4-3A and 4-4B). Especially at high DCA concentrations, aforementioned potential side effects of DCA, e.g. competitive inhibition of MPC, might contribute to reduced PDH and TCA cycle fluxes (Crabb et al., 1981; Stacpoole, 1989). However, the short-term dose-dependent increase of cellular ATP levels within the first 48 h of cultivation clearly proves the fast stimulating effect of DCA (Figure 4-2B and 4-6C) (Simpson et al., 2006). On the other hand, restored cellular ATP levels after 48 h demonstrate a complete reversal of the initial DCA effects by metabolic adaptation (Figure 4-2B). The absence of significant and lasting metabolic stimulation by DCA indicates a limitation of respiratory capacity or mitochondrial pyruvate import via MPC. A dose-dependent increase of average cellular ATP levels (Figure 4-6C) was accompanied by a dose-dependent decrease in ATP production rates (Figure 4-6A). It is well established, that glycolysis and TCA cycle are very strictly regulated by the cellular redox and energy state and down-regulated at high ATP levels (Michal and Schomburg, 2012). Interestingly, we observed adaptation of the same metabolic key reactions as for compensation of CHC effects, however, in the opposite direction. Down-regulation of PDH and TCA cycle fluxes during DCA application was achieved by (1) dose-dependent decrease of the GDH flux, (2) reduced flux from Mal (C4) to Pyr (C3) pools, and (3) down-regulation of glycolysis (Figure 4-5C and 4-5D).

Simpson et al. showed that human fibroblasts maintain normal cellular ATP/ADP levels despite reduced glycolytic rates at DCA treatment. This indicates improved metabolic efficiency by promoting glucose oxidation (Simpson et al., 2006). Lefort et al. profiled the extra- and intracellular metabolome in different human breast cell lines. They found that DCA-induced changes were only observed in the exometabolome while the cells efficiently maintained their normal intracellular state (Lefort et al., 2013). Both studies demonstrate an efficient intracellular compensation of DCA effects. For some metabolic pathways, CHC and DCA treatment led to similar metabolic responses. Reduced degradation of Asp, Asn and BCAA in DCA-treated cultures most likely represents a

secondary effect of the lower TCA cycle fluxes induced by compensation as proposed previously (Lefort et al., 2013).

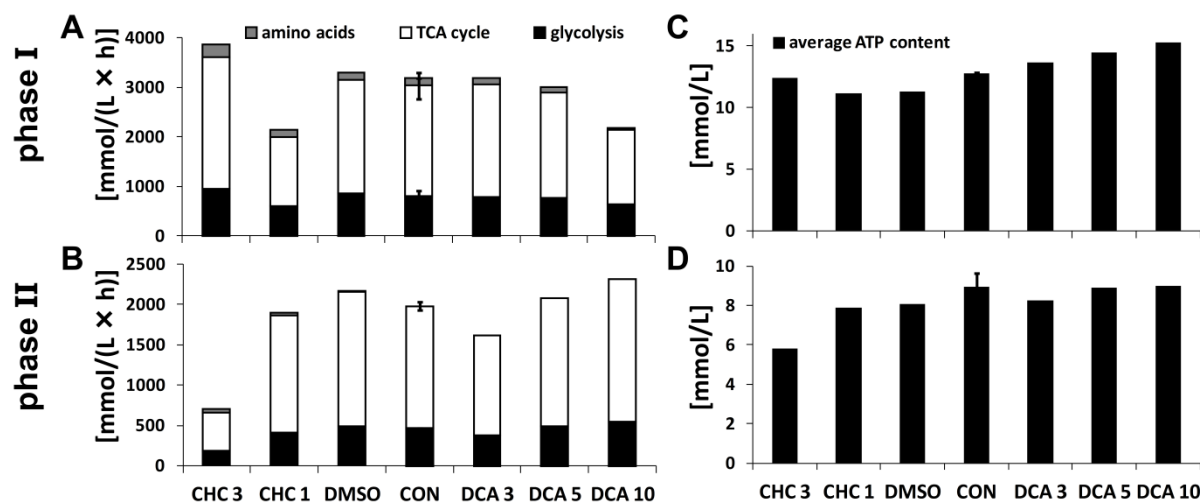


Figure 4-6. Effect of CHC and DCA on cellular ATP production and cellular ATP content. (A) and (B) ATP production rates [mmol/(L cell × h)] with relative contribution of glycolysis, TCA cycle and amino acid metabolism in growth phases I and II. ATP production rates were calculated considering P/O ratios of 2.5 for NADH and 1.5 for FADH₂. (C) and (D) Cellular ATP content [mmol/L cell] for phases I and II. Abbreviations: CON control without any effector (n = 2); DMSO control with 0.5% DMSO; CHC 1 and CHC 3 cultivation with 1 mM or 3 mM CHC; DCA 3, DCA 5 and DCA 10 cultivation with 3 mM, 5 mM or 10 mM DCA.

4.4.4.3 Emergence of CHC and DCA effects after glutamine depletion shows trade-off with resource demands

The compensation of CHC and DCA effects depended on Gln availability. In phase I, the cells were able to maintain their physiological function despite the presence of high effector concentrations imposing substantial stress. After Gln depletion in phase II, however, the anticipated metabolic effects, impaired TCA cycle activity at CHC- and promoted TCA cycle activity at DCA-treatment, reappeared (Figure 4-5E and 4-5H).

The mitochondrial Pyr availability induced an instantaneous adaptation of TCA cycle fluxes by variation of the GDH flux. This is clearly demonstrated by the GDH/PDH ratio (Figure 4-4C). The GDH/PDH ratio increased with increasing CHC concentration, i.e. increasing inhibition of Pyr import. On the other hand, it decreased with increasing DCA concentration, i.e. increasing decarboxylation of Pyr. In other words, an impaired or improved supply of carbons at the site of Pyr was offset by an increased or decreased carbon entry into the TCA cycle at the site of AKG derived

mainly from Gln. Therefore, increased glutaminolysis represented an essential adjustment to mitigate the effects of CHC and DCA.

At Gln depletion, we observed increased catabolism of Asn and Asp as well as a switch from Pyr excretion to Pyr uptake at 3 mM CHC. In addition, the cataplerotic flux from Mal to Pyr pools was significantly higher at CHC treatment. These modifications were, however, not sufficient. As a result, PDH and TCA cycle fluxes were dramatically reduced at 3 mM CHC treatment in phase II (29-31%) (Figure 4-5E). Growth and cellular ATP content were significantly impaired (Figure 4-2A and 4-6D). The cells were able to maintain viability but at a largely reduced cellular performance. Thus, the successful compensation of CHC-induced TCA cycle impairment was strictly Gln-dependent.

After Gln depletion, the TCA cycle was strongly supported by Lac-derived Pyr in control cultivations and also but to a lesser extent at 1 mM CHC. At 3 mM CHC, MPC-inhibition prevented an efficient utilization of Pyr. Due to an impaired connection between glycolysis and TCA cycle (TCA cycle/glycolysis ratio was 36% of control; Figure 4-4E), the cells relied (i) on glycolysis as major ATP source and (ii) on the regeneration of NAD⁺ by Lac formation. Consequently, Lac excretion persisted at 3 mM CHC treatment (Figure 4-5E).

Interestingly, also the compensation of DCA effects appears to be Gln-dependent (Figure 4-5H). Although glycolytic, PDH, and TCA cycle fluxes were slightly decreased at 3 mM DCA compared to the control, these fluxes increased with increasing DCA concentrations (Figure 4-3B). The two major fluxes influencing the TCA cycle carbon input, namely the cataplerotic flux from Mal to Pyr pools and the anaplerotic flux from Gln/Glu to AKG, were either not active or working in the opposite direction (Figure 4-5G and 4-5H). In a recent study, we have shown that these fluxes are directly correlated with the extracellular Gln flux (Wahrheit et al., 2014a). The manifestation of DCA effects at higher concentrations later in the cultivation (Figure 4-5H) might also be the consequence of a stabilization and resulting reduced turnover of the PDH complex (Michelakis et al., 2008; Simpson et al., 2006; Stacpoole et al., 1983; Stacpoole et al., 1978).

4.5 Conclusions and future directions

The extraordinary robustness and flexibility of CHO cells have substantially contributed to their success and popularity as working horse of industrial production and mammalian model system (Altamirano et al., 2013; Jayapal et al., 2007; Kildegaard et al., 2013). These features allow a reproducible cultivation and easy adaptation of CHO cells to changing environmental conditions. On the other hand, an extreme robustness and adaptive compensation mechanisms limit the potential of improving cellular performance. A better understanding of cellular adaptation and metabolic compensation mechanisms can help to develop new ideas and strategies for increasing productivity or identifying therapeutic targets.

We have shown that CHO-K1 cells can effectively cope with a severe perturbation of cellular Pyr metabolism. In the case of MPC inhibition by CHC, they can rapidly activate tailored compensation mechanisms that enable the successful restoration of a functional central metabolism and physiological energy state. On the other hand, a stimulation of mitochondrial metabolism by DCA is only achieved for a very short-term and quickly compensated by down-regulation of the same metabolic modules. The compensation of DCA effects most likely aims at avoiding energy spilling and preventing oxidative stress that mostly results from increased respiratory chain activity. The modules that are adjusted in order to increase or decrease the cellular energy state to physiological levels are: (1) readjustment of the GDH/PDH ratio according to Pyr availability, (2) up- or down-regulation of the fluxes connecting C4 and C3 pools ($MAL \rightarrow PYR$), and (3) feedback regulation of glycolysis.

In a recent study, we identified Pyr and Gln as the most important carbon sources fueling the TCA cycle in the used CHO-K1 cell line. We demonstrated that a tailored up- and down-regulation of aminotransferases and anaplerotic enzymes compensate an unbalanced supply of these two substrates to maintain TCA cycle activity (Nicolae et al., 2014b; Wahrheit et al., 2014b). In further studies investigating the metabolic implications of different Gln availabilities, we found that low Gln availability is compensated by increased Pyr feeding into the TCA cycle (Nicolae et al., 2014b; Wahrheit et al., 2014a). Here, we show that a decrease or increase in the PDH flux is offset by increased or decreased glutaminolytic rates feeding the AKG pools, respectively.

Feeding of the TCA cycle by Gln and Pyr working as independent, alternative modules represents a “fail-safe” mechanism in a wide range of situations (Kitano, 2004). The system behaves robust at high effector concentrations due to available parallel modules (Pyr and Gln) with their redundant function of TCA cycle feeding and due to full activation of compensation mechanisms.

However, we identified two scenarios where the robustness of the system was partially lost. The system has been shown to be highly robust towards failure of one module, either Pyr or Gln (Wahrheit et al., 2014a). However, the system collapsed at the failure of both modules, namely

CHC treatment at Gln depletion. A carbon shortage at both entry sites of the TCA cycle, Pyr and Gln, could not be compensated by the cell, thus leading to impaired culture performance, reduced energy levels, and growth arrest. Extreme susceptibility in the face of unexpected perturbations is an inherent property of highly robust systems (Kitano, 2004; Kitano, 2007; Whitacre, 2012). We conclude that a successful manipulation of an extremely robust biological system like CHO cells might be feasible if two modules that are able to compensate each other are manipulated simultaneously.

Furthermore, it has been described that a system is more vulnerable when a module behaves in an inappropriate way than when a module is completely removed (Kitano, 2004). This might explain that the central carbon metabolism showed to be susceptible to low rather than to high CHC and DCA concentrations. Gradually increasing the dose of an effector like often applied when setting a patient's medication might be a useful approach to avoid overcompensation and allow a slow adaptation to the desired phenotype.

4.6 Acknowledgements

We thank Ester Hoffmann for experimental assistance in determination of ATP concentrations. We thank Michel Fritz for his most valuable support in HPLC analysis. We thank the Institute of Cell Culture Technology (University Bielefeld, Germany) for supplying the CHO-K1 cells and the BMBF (German Federal Ministry of Education and Research) project SysCompart (project ID 031555D), part of the Systems Biology program, New Methods in Systems Biology (SysTec), for funding.

4.7 Supplementary material

Supplementary material associated with this chapter can be found in chapter 12.

Part II

**In-depth metabolic characterization of CHO cells
using labeling studies and non-stationary
¹³C metabolic flux analysis**

5 Non-stationary ^{13}C metabolic flux analysis of Chinese hamster ovary cells in batch culture using extracellular labeling highlights metabolic reversibility and compartmentation

5.1 Abstract

Background Mapping the intracellular fluxes for established mammalian cell lines becomes increasingly important for scientific and economic reasons. However, this is being hampered by the high complexity of metabolic networks, particularly concerning compartmentation.

Results Intracellular fluxes of the CHO-K1 cell line central carbon metabolism were successfully determined for a complex network using non-stationary ^{13}C metabolic flux analysis. Mass isotopomers of extracellular metabolites were determined using $[\text{U-}^{13}\text{C}_6]$ glucose as labeled substrate. Metabolic compartmentation and extracellular transport reversibility proved essential to successfully reproduce the dynamics of the labeling patterns. Alanine and pyruvate reversibility changed dynamically even if their net production fluxes remained constant. Cataplerotic fluxes of cytosolic phosphoenolpyruvate carboxykinase and mitochondrial malic enzyme and pyruvate carboxylase were successfully determined. Glycolytic pyruvate channeling to lactate was modeled by including a separate pyruvate pool. In the exponential growth phase, alanine, glycine and glutamate were excreted, and glutamine, aspartate, asparagine and serine were taken up; however, all these amino acids except asparagine were exchanged reversibly with the media. High fluxes were determined in the pentose phosphate pathway and the TCA cycle. The latter was fueled mainly by glucose but also by amino acid catabolism.

Conclusions The CHO-K1 central metabolism in controlled batch culture proves to be robust. It has the main purpose to ensure fast growth on a mixture of substrates and also to mitigate oxidative stress. It achieves this by using compartmentation to control NADPH and NADH availability and by simultaneous synthesis and catabolism of amino acids.

This chapter was published as

Nicolae A, Wahrheit J, Bahnemann J, Zeng A-P, Heinzle E. Non-stationary ^{13}C metabolic flux analysis of Chinese hamster ovary cells in batch culture using extracellular labeling highlights metabolic reversibility and compartmentation. *BMC Systems Biology*. 8, 50

5.2 Introduction

Economic importance and ease of cultivation make CHO cells a desirable candidate for metabolic studies in eukaryotic systems. Alongside with being the most important mammalian cell line for producing biopharmaceuticals (Butler and Meneses-Acosta, 2012; Kim et al., 2012; Walsh, 2010a), CHO cells are able to grow in suspension cultures using chemically defined media (Deshpande et al., 2009), use multiple carbon sources simultaneously and maintain a stable metabolism for long periods in batch cultivations. This has led to a wealth of studies aimed at exploring CHO metabolism. After the decoding of the CHO-K1 cell line genome (Brinkrolf et al., 2013; Xu et al., 2011) and transcriptome (Becker et al., 2011), we can expect such studies to increase both in number and complexity. Metabolic flux analysis (MFA) of CHO cell cultures evolved from flux balancing analysis (Altamirano et al., 2001b) to more complex metabolic or isotopomer dynamic models (Ahn and Antoniewicz, 2012). Newer studies rely on ^{13}C -MFA applied by fitting the summed fractional labeling (Ahn and Antoniewicz, 2011) or by fitting steady-state labeling data (Templeton et al., 2013) resulted from using in parallel more labeled substrates for determining the intracellular fluxes at metabolic steady state in different growth phases. However, the labeling patterns of the intracellular metabolites or of amino acids from hydrolyzed proteins that are usually needed for non-stationary ^{13}C -MFA are obtained through a tedious methodology (Zamboni, 2011; Zamboni et al., 2009) and are susceptible to errors stemming mostly from the quenching/extraction phase (Dietmair et al., 2010; Wahrheit and Heinzle, 2013). In the absence of metabolite exchange with the media, intracellular labeling would reach steady state relatively fast, in the order of minutes for glycolytic intermediates and few hours for TCA cycle metabolites, as it was determined in *Pichia pastoris* (Jorda et al., 2013). In mammalian cells, exchange with the extracellular pools (Divakaruni and Murphy, 2012) delays the intracellular isotopic steady state usually beyond the possibility to maintain metabolic steady state. Due to the large extracellular pools of amino acids, their exchange will transfer the time constant of the extracellular labeling process, which is in the order of days, to the intracellular labeling. One option is to use isotopic non-stationary metabolic flux analysis (INST- ^{13}C MFA) applied at short time scales (Nöh et al., 2007), but this approach has the drawback of requiring accurate determination of intracellular concentrations of metabolites (Nöh et al., 2006).

Metabolite and reaction compartmentation is important for a realistic representation of the mammalian cell metabolism, but determining it raises supplementary demands from the experimental and modeling procedures, as we have already reviewed in (Wahrheit et al., 2011). In the exponential growth phase, a typical culture of CHO is characterized by high uptake rates of glucose and glutamine, the Warburg effect and the exchange of non-essential amino acids with the extracellular media (Deshpande et al., 2009; Provost et al., 2006). We can expect that by feeding a ^{13}C labeled substrate, some of the extracellular metabolites will exhibit labeling patterns that can

then be detected using GC-MS. As these metabolites will be enriched in ^{13}C dynamically, non-stationary ^{13}C metabolic flux analysis (INST- ^{13}C MFA) applied to extracellular and intracellular isotopomers (Becker et al., 2011; Noack et al., 2011; Nöh et al., 2006) provides a suitable framework to determine the intracellular fluxes. Extracellular pools have a large time scale for labeling (hours) compared to the intracellular pools (seconds/minutes), thus removing the need to sample intracellular pools provided that the labeling information in the extracellular metabolites is sufficient.

We show that by using only the labeling patterns of extracellular metabolites produced by feeding $[\text{U-}^{13}\text{C}_6]\text{glucose}$ as the only labeled substrate, intracellular fluxes can be successfully determined in a complex, compartmented metabolic network of the CHO-K1 cell line. In parallel, we prove that a simplified, non-compartmented model is not sufficient for describing the metabolism. We also underline the importance of considering reversibility when dealing with non-stationary isotopomer models.

5.3 Methods

5.3.1 Cell culture and experimental set-up

The CHO-K1 cell line was kindly provided by the Institute of Cell Culture Technology (University Bielefeld, AG Noll, Germany). The cells were growing in suspension under serum and protein free conditions in the chemically defined medium TC-42 (TeutoCell AG, Bielefeld, Germany) supplemented with 4 mM L-glutamine (PAA, Germany). Precultures were cultivated in 125 mL baffled Erlenmeyer flasks (Corning Inc., Germany) at an initial cell density of 0.4×10^6 cells/mL and a working volume of 50 mL on a shaking device (225 rpm) at 37°C and 5% CO_2 in a humid atmosphere. For the main cultivation, cells were harvested during the exponential growth phase at a viability of $\geq 98\%$ and resuspended in TC-42 medium with 100% $[\text{U-}^{13}\text{C}_6]$ glucose (99%, Euriso-Top, Saarbrücken, Germany). The main cultivation was performed in a Vario1000 bioreactor (Medorex e.K., Nörten-Hardenberg, Germany) at batch mode with a starting culture volume of 200 mL. The bioreactor was inoculated at a cell density of 0.4×10^6 cells/mL. The cultivation temperature was kept constant at 37°C and the impeller (3-blade marine propeller) speed was set to 300 rpm. During the cultivation, the pH value was controlled at 7.2 by gassing with CO_2 and by using 0.5 M sodium carbonate solution. Dissolved oxygen was maintained at 30% of the saturation concentration. Samples were taken three times a day. Cell density and viability were determined by cell counting using the Trypan blue exclusion method. Supernatants were transferred into fresh tubes and stored at -20°C until further analysis. The average cell diameter was determined using an automated cell counter (Invitrogen, Darmstadt, Germany) in a separate experiment. This experiment was performed in a shaking incubator (2 inches orbit, 185 rpm, 37°C , 5% CO_2 supply) using 250 mL baffled Erlenmeyer flasks (Corning Inc., Germany), an initial cell density of

0.4×10^6 cells/mL, a working volume of 100 mL and using the same medium TC-42 medium (TeutoCell, Bielefeld, Germany) supplemented with 4 mM glutamine. Differences of cell diameters during the cultivation were maximum 5% and not taken into account. Cell volume was computed assuming the cells are spherical using a diameter of 10.6 μm . Glutamine degradation kinetics were determined experimentally in a cell-free setup identical to the one employed for cell volume estimation. The determined glutamine degradation rate constant was $kd_{\text{GLN}} = 0.0033 \text{ h}^{-1}$.

5.3.2 Quantification of metabolites

Quantification of glucose, organic acids and amino acids via HPLC was carried out as described previously by Strigun et al. (Strigun et al., 2011b).

5.3.3 Analysis of isotopomer labeling patterns

5.3.3.1 Sample preparation

For determination of labeling patterns of lactate and amino acids, 50 μl of supernatants were lyophilized, resolved in 50 μl N,N-dimethylformamide (0,1 % pyridine) and incubated at 80°C for 30 min. 50 μl N-methyl-N-t-butyltrimethylsilyl-trifluoro-acetamide (MBDSTFA) was added followed by another incubation at 80°C for 30 min for derivatization of metabolites into corresponding dimethyl-t-butylsilyl derivatives. For determination of the labeling pattern of pyruvate, lyophilized supernatants were resolved in 50 μl pyridine containing 20 mg/ml methoxyamine hydrochloride and 50 μl MSTFA (Macherey-Nagel, Düren, Deutschland) and incubated at 80°C for 30 min for derivatization into the methoxyamine-trimethylsilyl derivative. Derivatized samples were centrifuged at $13000 \times g$ for 5 min at 4 °C and supernatants transferred into fresh glass vials with micro inlets.

5.3.3.2 GC-MS measurements

Extracellular ^{13}C -labeling dynamics were analyzed by gas chromatography mass spectrometry (GC-MS). The GC-MS measurements were carried out on a GC (HP 6890, Hewlett Packard, Palo Alto, CA, USA) equipped with an HP5MS capillary column (5% phenyl-methyl-siloxane diphenylpolysiloxane, 30 m \times 0.25 mm \times 0.25 μm , Agilent Technologies, Waldbronn, Germany), electron impact ionization at 70 eV, and a quadrupole detector (Agilent Technologies). The injection volume was 1 μl (7683B Autosampler, Agilent, Waldbronn, Germany; PTV-Injektor, Gerstel, Mühlheim a. d. Ruhr, Germany). Helium was used as carrier gas at a flow rate of 1.1 ml/min for analysis of lactate and amino acids or 0.7 ml/min for pyruvate analysis. The following temperature gradient was applied for lactate and amino acid analysis: 135°C for 7 min, 10°C/min up to 162°C, 7°C/min up to 170°C, 10°C/min up to 325°C, 325°C for 2.5 min; inlet temperature: 140°C and heating with 720°C/min up to 320°C; interface temperature 320°C; quadrupole temperature 150°C. The temperature gradient for pyruvate analysis was as follows:

70°C for 1 min, 1°C/min up to 75°C, 5°C/min up to 315°C, 25°C/min up to 340°C, 340°C for 5 min; inlet temperature: 70°C and heating with 360°C/min up to 360°C; interface temperature 320°C; quadrupole temperature 280°C.

5.3.3.3 Data analysis

After identification of metabolites in the scan mode using the NIST data bank, quantification of labeling enrichment was done in SIM (single ion monitoring) mode in two technical replicates using the following unique fragments (m/z) containing the complete carbon skeleton of metabolites: pyruvate 174, lactate 261, alanine 260, glycine 246, serine 390, aspartate 418, glutamate 432, glutamine 431. Mass isotopomer distributions were corrected for naturally occurring isotopes using the method of Yang et al. (Yang et al., 2009).

5.3.4 Metabolic network models

Two metabolic networks were established based on experimental observations related to metabolite uptake and production and extracellular labeling. Both networks included: glycolysis; TCA cycle; anaplerotic reactions; synthesis of fatty acids, proteins and carbohydrates for biomass production; amino acid production and degradation. Transport from the extracellular media was reversible in both models for all metabolites with the exception of glucose, asparagine and essential amino acids. Mitochondrial transport of malate, α -ketoglutarate, alanine, and reactions of transaminase, malate and lactate dehydrogenase were also reversible. The first model shown in Figure 5-1A considers the intracellular space without compartmentation. In the second model (Figure 5-1B), the mitochondrial reactions and pools are separated from the cytosol. Both models start from the annotation of the genomes of CHO-K1 and *Mus musculus* (Hammond et al., 2012; Zhu et al., 2003) (KEGG, Kyoto encyclopedia of genes and genomes). Enzyme localization was established using information from the MGI database and data from J. Wahrheit (Wahrheit et al., 2014b) who measured compartmented enzyme activity using a method adapted from Niklas et al. (Niklas et al., 2011a). Mitochondrial transport of alanine was included to explain the existence of alanine aminotransferases in both compartments. Metabolite pools were lumped where it did not influence the simulated labeling dynamics. Pentose phosphate pathway was reduced to one reaction where one carbon atom is lost for each G6P molecule and 5/3 molecules of PG are produced. Glycolysis was lumped to three fluxes transforming G6P into PYR_{cyt} . Isocitrate and citrate were condensed into one citrate (CIT) pool. Succinate, fumarate and malate were condensed into one MAL pool. Two cytosolic pyruvate pools were used to describe metabolic channeling to lactate. Non-essential amino acids catabolism was lumped to three fluxes fueling the MAL, AcoA and GLU pool respectively. No carbon mapping was required in this case as essential amino acids are unlabeled. Glutaminase activity was mitochondrial (Xu et al., 2011) and glutamine synthetase was cytosolic (Hayward et al., 1986).

Fatty acids, protein and storage carbohydrates composition of the cell was taken from Altamirano et al. (Altamirano et al., 2001b).

In total, the compartmented model consisted of 60 fluxes and 25 metabolites and the non-compartmented model of 42 fluxes and 16 metabolites. The complete flux list for the two models, together with the carbon transfer rules, is provided in the Additional file 1.

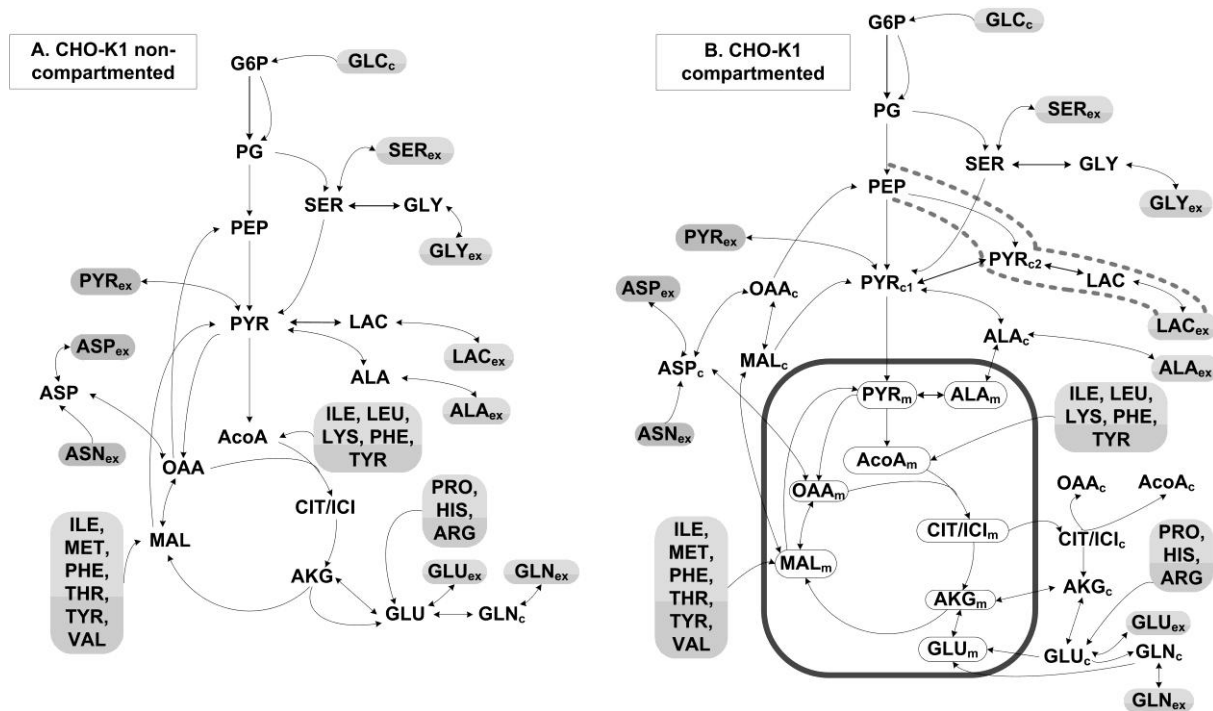


Figure 5-1. Compartmented (A) and non-compartmented (B) networks of the CHO-K1 central metabolism used for simulations. Irreversibility is indicated by simple arrows, and reversibility by double arrows. The reactions depicted in 1B are listed in detail in the Additional file 1 together with fluxes and reversibilities determined. Subscripts meaning: *ex* – extracellular; *c* – cytosolic; *m* – mitochondrial. Abbreviations: AA – amino acids; AcoA – acetyl CoA; AKG – alpha-ketoglutarate; ALA – alanine; ASN – asparagine; ASP – aspartate; CIT/ICI – citrate/isocitrate; G6P – glucose 6-phosphate; GLC – glucose; GLN – glutamine; GLU – glutamate; GLY – glycine; MAL – malate; OAA – oxaloacetate; PEP – phosphoenolpyruvate; PG – phosphoglycerate; PYR – pyruvate; SER – serine.

5.3.5 Non-stationary- ^{13}C MFA methodology

Isotopic non-stationary metabolic flux analysis (INST- ^{13}C MFA) comprises: (1) metabolic steady-state balancing of intracellular metabolites for determining extracellular rates; (2) dynamic extracellular metabolite and isotopomer balance and (3) dynamic balances of intra-compartmental isotopomers.

5.3.5.1 Metabolite balancing

Net extracellular rates v_{M_ex} were determined for each extracellular metabolite M_ex for the batch cultivation situation, under the assumption of metabolic steady state, by fitting the cell density $X(t)$ and extracellular concentrations of metabolites C_{M_ex} to an exponential growth model with specific growth rate μ (eq. 1.a,b) and constant extracellular rates. Glutamine balance included first order degradation in the culture media (eq. 1.c).

$$dX/dt = \mu \cdot X(t) \quad (1.a)$$

$$dC_{M_ex}/dt = v_{M_ex} \cdot X(t) \quad (1.b)$$

$$dC_{GLN}/dt = v_{GLN} \cdot X(t) - kd_{GLN} \cdot C_{GLN}(t) \quad (1.c)$$

At intracellular metabolic steady state, the n metabolic fluxes that connect the m metabolites are constant and satisfy the material balance:

$$\mathbf{G} \cdot \mathbf{v} = 0 \quad (2.a)$$

$$v_j = \varphi_j, j = 1..R_{meas} \quad (2.b)$$

$$\alpha_i \leq v_i \leq \beta_i, i = 1..n \quad (2.c)$$

where G is the $m \times n$ stoichiometric matrix and its null space v is the vector of net metabolic fluxes which are constrained by R_{meas} measured fluxes φ_j (2.b) and n inequalities (2.c) determined by flux direction. To reduce the number of parameters, the free fluxes were extracted from the network as described in (Yang et al., 2008) to produce a determined stoichiometric system.

5.3.5.2 Intracellular and extracellular carbon balance

The INST- ^{13}C MFA framework developed in (Becker et al., 2011; Nöh et al., 2006) was adapted to the case of batch culture cultivation. Isotopomer balances for extracellular (eq. 3) and intracellular (eq. 4) metabolites were set to be solved together with the extracellular balances (eq. 1.a,b,c).

$$\frac{dIDV_{M_ex}}{dt} = \frac{1}{C_{M_ex}} \cdot \left[X_{conc} \cdot \left(v_{M_ex}^{in} \cdot IDV_{M_cyt} - v_{M_ex}^{out} \cdot IDV_{M_ex} \right) - \frac{dC_{M_ex}}{dt} \cdot IDV_{M_ex} \right] \quad (3)$$

$$\frac{dIDV_{M_in}}{dt} = \frac{1}{C_{M_in}} \cdot \left(\sum_{j=1}^{R_M} v_j \cdot IDV_{M_in,j} - v_{M_in}^{out} \cdot IDV_{M_in} \right) \quad (4)$$

with IDV_{M_ex} , IDV_{M_cyp} , IDV_{M_in} being the isotopomer distribution vectors of the extracellular, cytosolic and intracompartamental pools of metabolite M . $IDV_{M_in,j}$ is the j^{th} reaction contribution to isotopomers of metabolite M , computed using isotopomer mapping matrices as described by Schmidt (Becker et al., 2011). X_{conc} is the cell volumetric concentration expressed in L cell / L media. C_{M_ex} is the extracellular concentration of M , $v_{M_ex}^{in}$ is the production flux of M expressed in mmol/(L cell \times h), $v_{M_ex}^{out}$ is the uptake flux, v_j is one of the R_M fluxes entering the intracompartamental pool of M , C_{M_in} and $v_{M_in}^{out}$ is the flux exiting the pool. The metabolite and isotopomer balances from equations 1,2 and 4 are then solved simultaneously to obtain the time course of the mass isotopomer distributions. Isotopomer balancing employs absolute fluxes that can be computed from the net fluxes by introducing a reversibility parameter:

$$rev_j = \frac{v_{j,reverse}}{v_j} \quad (5)$$

where v_j is the net flux and $v_{j,forward}$ and $v_{j,reverse}$ are the forward and respectively the reverse exchange fluxes, with $v_{j,forward} - v_{j,reverse} = v_j$; $v_{j,forward} \geq 0$ and $v_{j,reverse} \geq 0$.

The contribution of reaction j was computed using isotopomer mapping matrices (Becker et al., 2011) that trace carbon from the substrate to the reaction products. The initial mass distribution of all metabolites was computed considering the naturally occurring ^{13}C fraction (1.1%) and the 99% atom purity of the employed ^{13}C labeled substrate.

The simulated time course of extracellular mass isotopomer distributions (MID) is compared with the experimental values. The objective function to be minimized was expressed as the weighted sum of square differences between the experimentally determined and simulated MID s:

$$SSQD = (MID^{sim} - MID^{exp})^T \cdot \sum_{MID}^{-1} \cdot (MID^{sim} - MID^{exp}) \quad (6)$$

where $SSQD$ is the objective function, MID^{sim} is the simulated MID , MID^{exp} is the measured MID and \sum_{MID} is the measurement covariance matrix. The optimal solution was accepted if it satisfied the χ -squared test for model verification with 95% probability, and $N-p$ degrees of freedom, where N is the number of sampled points (size of MID^{exp}) and p is the number of free parameters. To reduce the bias in the objective function generated by very small standard deviations, a minimum threshold of 0.005 was imposed. Accurate confidence intervals and sensitivity analysis of fluxes were computed according to (Antoniewicz et al., 2006b). All the code was programmed and simulated in Matlab [MATLAB and Simulink Release 2013a, The MathWorks, Inc., Natick, Massachusetts, United States].

5.4 Results and discussion

5.4.1 Metabolic profiling

The cells exhibited exponential growth for 72 h (Figure 5-2) until glutamine became exhausted and a shift in metabolism was observed (data not shown). Estimated specific growth rate as fitted to eq. (1.a) was $\mu = 0.0401 \text{ h}^{-1}$. Uptake and production of most metabolites was balanced, i.e. they were proportional to growth for the main carbon sources and produced metabolites (Figure 5-2) and for other amino acids (Additional File 2). This means that metabolic steady state was maintained during the first 72 h of cultivation. Glucose constituted the main carbon source (Table 5-1), providing 65% of the total carbon entering the central carbon metabolism, with an uptake flux of 371 mmol/(L cell \times h). Note that all fluxes are related to the cell volume specified by L cell. 39% of the glucose was converted to lactate. The observed pyruvate production rate was 3.3 mmol/(L cell \times h).

The glutamine uptake flux determined by fitting eq. (1.c) to the glutamine concentration over time was 66.4 mmol/(L cell \times h), 16% smaller than that in the case when its degradation was ignored. Glutamine uptake contributed with 10% to the total carbon pool. The rest of the carbon feeding the central carbon metabolism, i.e. 25%, was obtained from amino acids catabolism.

Table 5-1 Carbon sources for the central metabolism of the CHO-K1 cell line in batch culture during the exponential growth phase

Metabolite	Target intracellular metabolite	Uptake flux [mmol/(L cell \times h)]	Uptake flux [Cmmol/(L cell \times h)]	Percentage of the total carbon-flux
Glucose	Pyruvate	371.0	2226.2	64.9
Glutamine	AKG	66.4	331.9	9.7
AA1*	AcoA	92.6	185.2	5.4
AA2*	Malate	49.6	198.4	5.8
AA3*	AKG	11.6	58.2	1.7
ASP/ASN	OAA	68.1	272.3	7.9
Serine	Pyruvate, glycine	48.3	146.4	4.3
TOTAL	-	-	3428.53	100

The contribution of AA1, AA2 and AA3 amino acid groups considers only catabolism. Abbreviations: AA1: amino acids catabolized to AcoA (isoleucine, leucine, lysine, phenylalanine, tyrosine); AA2: amino acids catabolized to four-carbon dicarboxylic acids (isoleucine, methionine, phenylalanine, threonine, tyrosine, valine); AA3: amino acids catabolized to glutamate (arginine, histidine, proline); AcoA: acetyl coenzyme A; AKG: alpha-ketoglutarate; ASN: asparagine; ASP: aspartate; OAA: oxaloacetate.

* Excluding requirements for protein synthesis

Alanine, glycine and glutamate were produced (Figure 5-3), while the other amino acids were taken up in excess of the quantity required for biomass synthesis. As a consequence of amino acids catabolism, a flux of 92.6 mmol/(L cell \times h) fueled the mitochondrial acetyl-CoA pool from the degradation of isoleucine, leucine, lysine, phenylalanine and tyrosine, while a flux of 39.1 mmol/(L cell \times h) cytosolic AcoA was directed towards fatty acids synthesis. The catabolism of excess isoleucine, methionine, phenylalanine, threonine, tyrosine and valine that remained after protein synthesis produced 49.6 mmol/(L cell \times h) succinate and fumarate (lumped into one pool of four carbon di-carboxylic acids, here represented as MAL).

Metabolite dilution by growth was neglected due to negligible influence on the total mass balance.

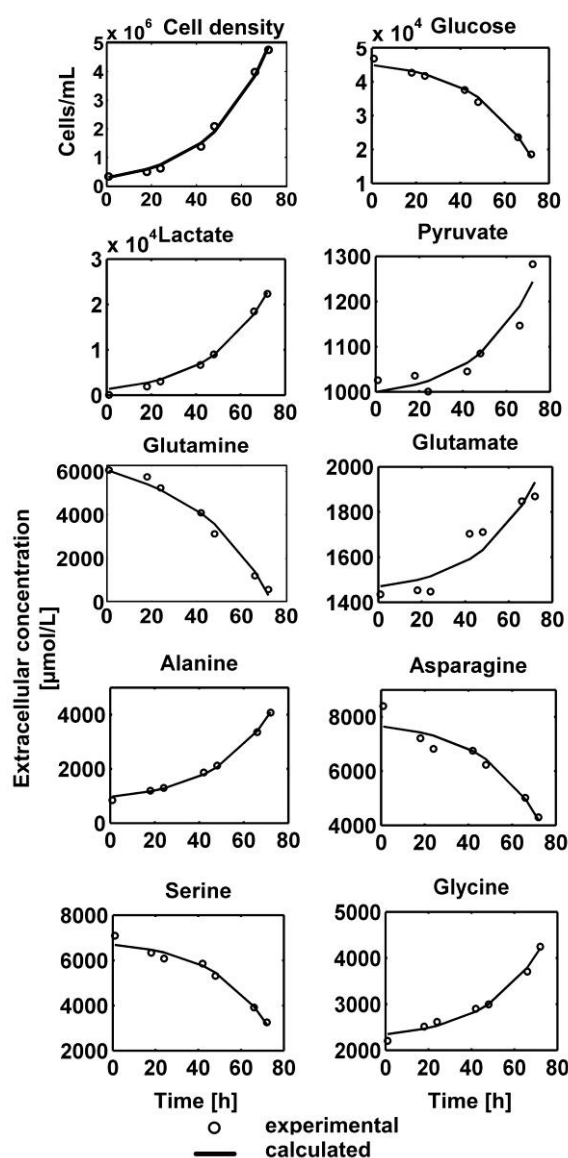


Figure 5-2. Culture profile of the CHO-K1 cells for the first 72 h during the exponential growth phase. Experimental values are shown with circles and calculated values are represented by solid lines.

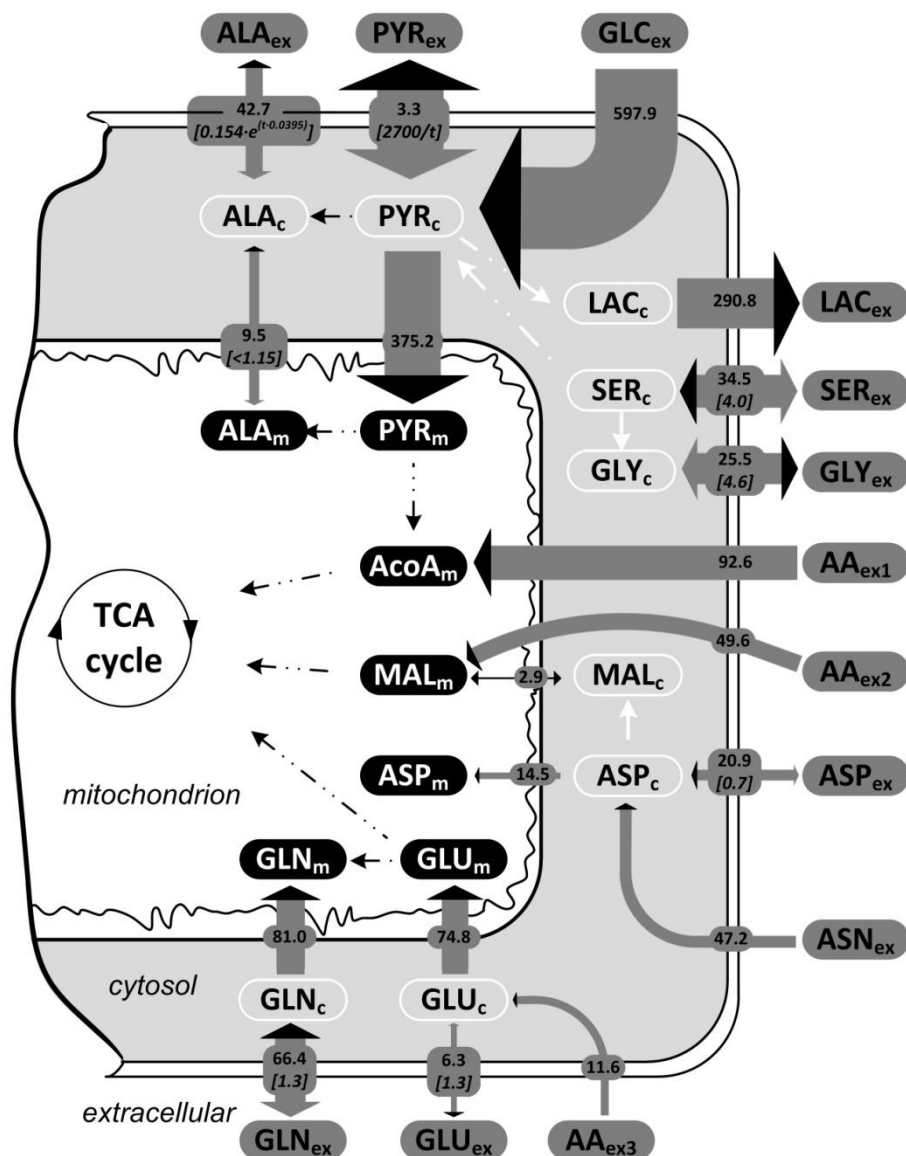


Figure 5-3. Compartmentation of the CHO-K1 metabolism and the fate of extracellular metabolites.

Net fluxes are indicated on the gray arrows in units of mmol product/ (L cell × h), and reversibility parameter defined as reverse flux/net flux is shown in the square brackets (n.d. = not determined). The thickness of the gray arrows is proportional to the forward flux (= reverse flux + net flux), and shown qualitatively for the fluxes with variable reversibility. Net flux direction is shown by the black arrow heads. Amino acids catabolism is represented as the sum of the differences between amino acid uptake flux and flux required for protein production, reported to the metabolite derived from catabolism. Subscripts meaning: ex – extracellular; c – cytosolic; m – mitochondrial. Abbreviations: AA_{ex1} – isoleucine, leucine, lysine, phenylalanine, tyrosine catabolized to acetyl-CoA; AA_{ex2} – isoleucine, methionine, phenylalanine, threonine, tyrosine, valine catabolized to fumarate and succinate; AA_{ex3} – arginine, histidine, proline catabolized to glutamate; AcoA – acetyl CoA; ALA – alanine; ASN – asparagine; ASP – aspartate; CIT/ICI – citrate/isocitrate; GLN – glutamine; GLU – glutamate; GLY – glycine; MAL – malate; PYR – pyruvate; SER – serine.

5.4.2 Non-stationary labeling experiment

The *MID* of extracellular pyruvate, lactate, alanine, glutamate, glutamine, aspartate, serine and glycine was sampled at 1, 18, 24, 42, 48, 66 and 72 h. During the exponential growth phase of 72 h none of the labeling reached steady state as shown in Figure 5-4. Lactate and pyruvate exhibited similar labeling dynamics, however with different *MID*s towards the end of the growth. This is surprising since lactate is obtained from pyruvate through the lactate dehydrogenase reaction. The predominant lactate fraction, i.e. M+3, increased to 0.85 and the pyruvate M+3 fraction stabilized at 0.81, pointing towards glycolytic channeling to lactate achieved by the localized cooperation of glycolytic enzymes as observed in rapidly proliferating cells (Mazurek et al., 2001; Vander Heiden et al., 2009). From the produced amino acids, alanine, also derived from pyruvate, had a high M+3 fraction. Glutamate and glycine M+2 fractions increased slowly, with most of the change happening in the last 24 h due to the high number of producing cells present in the media., Extracellular aspartate, glutamine and serine were found to be labeled although they exhibited a net uptake. Glutamine fractional labeling, mostly the M+2 isotopomer, increased sharply at the end of the phase, when very little glutamine remained in the media and the contribution of secreted glutamine played a large role to the labeling state.

5.4.3 Isotopomer fitting

Both the non-compartmented and compartmented isotopomer network models (Figure 5-1) were fitted to the experimental mass distributions with the goal of determining unknown fluxes and reversibilities. The 7 sampling time points of the 8 metabolites produced a total number of 252 experimental *MID*s.

Convergence to the optimal solution is difficult in isotopomer models (Srour et al., 2011) and the parameter space of the objective function is marked by a multitude of local minima (Chen et al., 2007), making gradient-based algorithms unreliable. Consequently, we applied a global optimization scheme that had the following steps: (1) generate an initial random population of ($40 \times p$) parameter sets that satisfy constraints using a simulated annealing-based algorithm, (2) submit the population to a 50-generations genetic algorithm optimization, and (3) refine the best solution using a trust region reflective algorithm. Convergence to the optimal solution was verified by repeating the optimization scheme. One simulation took about 3 s, and the optimization procedure required about 40 h on a 2.3 GHz QuadCore CPU. All the numerical integration and optimization algorithms are found in Matlab toolboxes.

We had initial difficulties in fitting pyruvate and alanine labeling dynamics. As it was shown that reversibility greatly affects labeling dynamics (Nöh and Wiechert, 2011), we assumed that the transport reversibility parameter changes in time, even if the net fluxes remain constant. The decrease with time of pyruvate transport reversibility was mechanistically expressed using a

hyperbolic function $rev_{PYR} = \frac{rev_{PYR}^0}{time + \varepsilon}$, where pyruvate transport reversibility rev_{PYR} decreases from a starting value rev_{PYR}^0 . To avoid division by zero, a negligible correction factor ε was introduced. Alanine transport into the cell intensifies as extracellular alanine becomes exponentially more abundant. Transport reversibility was expressed in this case as $rev_{ALA} = \alpha \cdot \exp(\beta \cdot time)$, where α and β are parameters to be determined.

The 24 free parameters of the non-compartmented model (Figure 5-1A) consisted of 5 fluxes, 18 reversibilities and the CO_2 pool. At convergence, the model failed to fit the data with the minimized $SSQD$ of 1572, larger than $\chi^2(0.95, 252-24) = 264.2$. Pyruvate, lactate, alanine and glutamate labeling were fit poorly even when transport reversibility was variable (Figure 5-4). In consequence, the non-compartmented model was rejected. The low labeling content of pyruvate, alanine and lactate simulated with the non-compartmented model is explained by the lumping of the cytosolic and mitochondrial pyruvate pools. As more than 30% of the carbon feeding the TCA cycle is not labeled, it is expected that the cataplerotic reactions catalyzed by phosphoenolpyruvate carboxykinase and malic enzyme will produce a large quantity of unlabeled pyruvate, which contradicts the experimental observations.

The compartmented model, consisting of 11 free fluxes and other 27 free parameters (reversibilities) depicted in Figure 5-1B, fitted the data successfully with the minimized $SSQD = 249.0$ slightly smaller than $\chi^2(0.95, 252-38) = 249.13$. The poorer fit of the 66 and 72 h time points for lactate and 72 h for alanine can be explained by the metabolic shift towards the end of the growth phase. From a parameter fitting point of view, exponential growth will add a larger contribution in the objective function to the labeling towards the end of the exponential phase compared to the beginning of the experiment because the rates of ^{13}C accumulation in the extracellular media will be much larger at high cell densities. This is best evidenced in Figure 5-4 where glutamine, aspartate, serine and glycine do not become noticeably labeled until 40 h after the introduction of the labeled substrate.

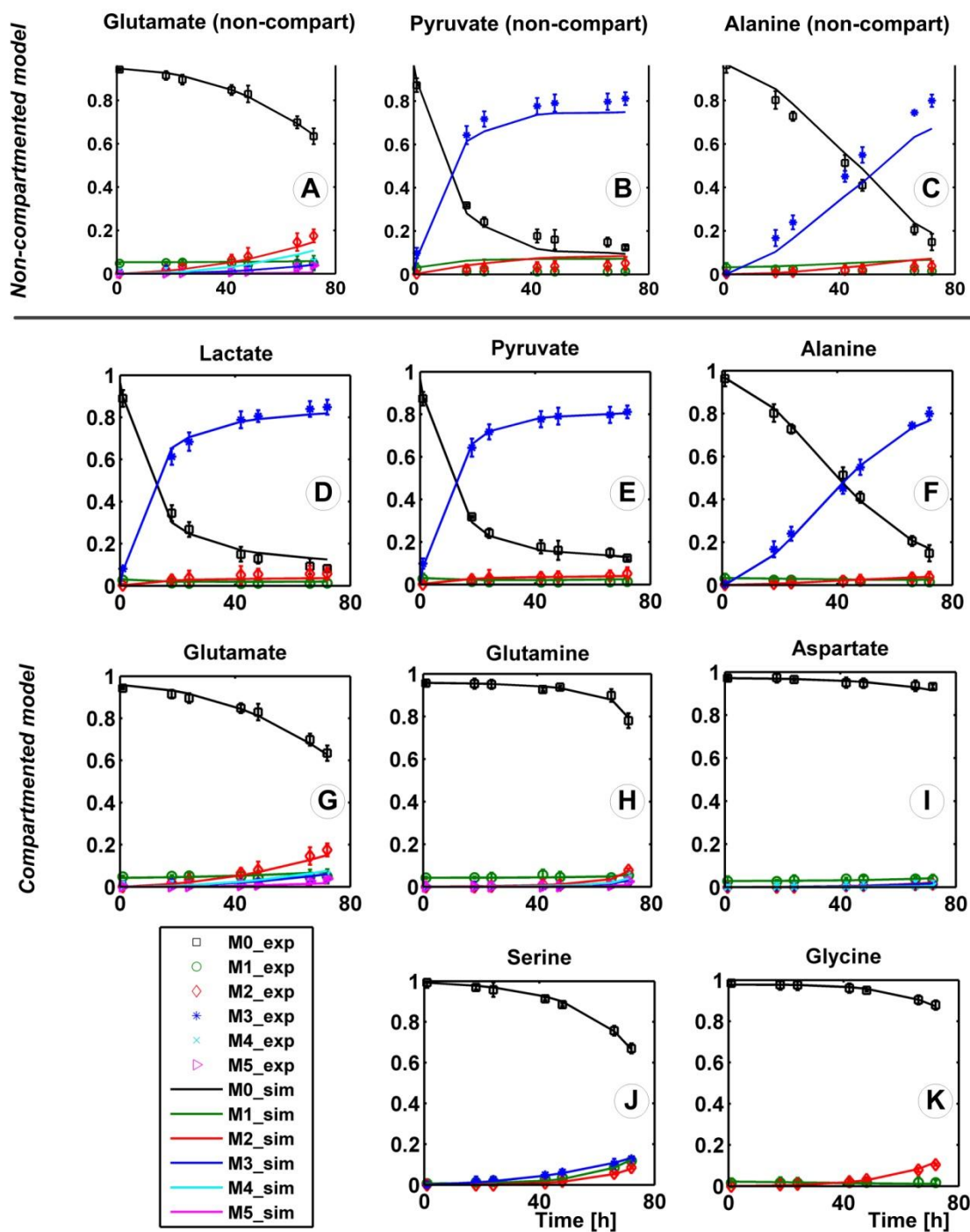


Figure 5-4. Non-stationary ^{13}C labeling experiment. Experimental mass isotopomer distributions (symbols) with their standard deviations vs. simulated (line) mass isotopomer distributions of labeled extracellular metabolites. The plots A-C represent results from using the non-compartmented metabolic network specified in Figure 5-1A. For the other eight plots (D-K), the compartmented model provided in Figure 5-1B was simulated.

5.4.4 Metabolic fluxes in the CHO-K1 cell line

Glucose was converted to PG mostly by bypassing glycolysis (Figure 5-5) through the pentose phosphate pathway (PPP). The estimated PPP flux was 80% of the total molar glucose input flux, a high activity contrasting with results obtained by Ahn and Antoniewicz for adherently growing CHO cells (Ahn and Antoniewicz, 2011) but observed for hybridoma (Bonarius et al., 1996) and cancer cells (Bensaad et al., 2006). A wide range of PPP activities, between 0-160 % of the glucose input flux, was determined for a highly-productive CHO line in fed-batch cultivation conditions at different growth phases (Templeton et al., 2013). The large quantities of cytosolic NADPH produced through PPP are used to drive fatty acids synthesis and possibly to mitigate oxidative stress by reducing reactive oxygen species (Anastasiou et al., 2011; Portner and Schafer, 1996; Sengupta et al., 2011; Tuttle et al., 2000; Vizan et al., 2009), as it has also been proposed by (Templeton et al., 2013). Overflow to lactate comprised 39% of the pyruvate produced from glycolysis. From the rest of the cytosolic pyruvate, 42.7 mmol/(L cell \times h) were converted to alanine, but most of it was transported into the mitochondria and converted to AcoA. The channeling flux from PEP to lactate was 122.7 mmol/(L cell \times h), accounting for 42% of the total lactate being produced. Low reversibility (Figure 5-5) meant no connection between the two cytosolic pyruvate pools PYR_{c1} and PYR_{c2} existed. However, lactate was produced from both cytosolic pyruvate pools, indicating that glycolytic channeling is not the only lactate source in the cell. Our possible explanation is that multi-enzyme complexes associated to membrane transporters, as characterized by Campanella et al (Campanella et al., 2005), create a micro-compartmented environment in the cytosol. Glycolytic enzymes are partly associated and partly soluble, resulting in a mixed response in the lactate labeling.

The carbon flux in the TCA cycle originated mainly from AcoA produced from glycolytic pyruvate transported into the mitochondria (Figure 5-5), with significant contributions from glutamine and essential amino acids catabolism. Such a high activity of the TCA cycle and high connectivity with the glycolysis is in contrast with some previous reports of lower activity during exponential growth phase (Ahn and Antoniewicz, 2011; Quek et al., 2009; Zamorano et al., 2010) but similar to (Goudar et al., 2010; Sengupta et al., 2011; Sheikholeslami et al., 2013b). The differences can be assigned mainly to the use of different cell lines and cultivation conditions like media composition, aeration mode, pH control and culture type e.g. suspension or immobilized, batch or fed-batch. The lower lactate/glucose molar ratio of 0.78 reported herein means more pyruvate is available for use in the TCA cycle, thus making for a more efficient metabolism.

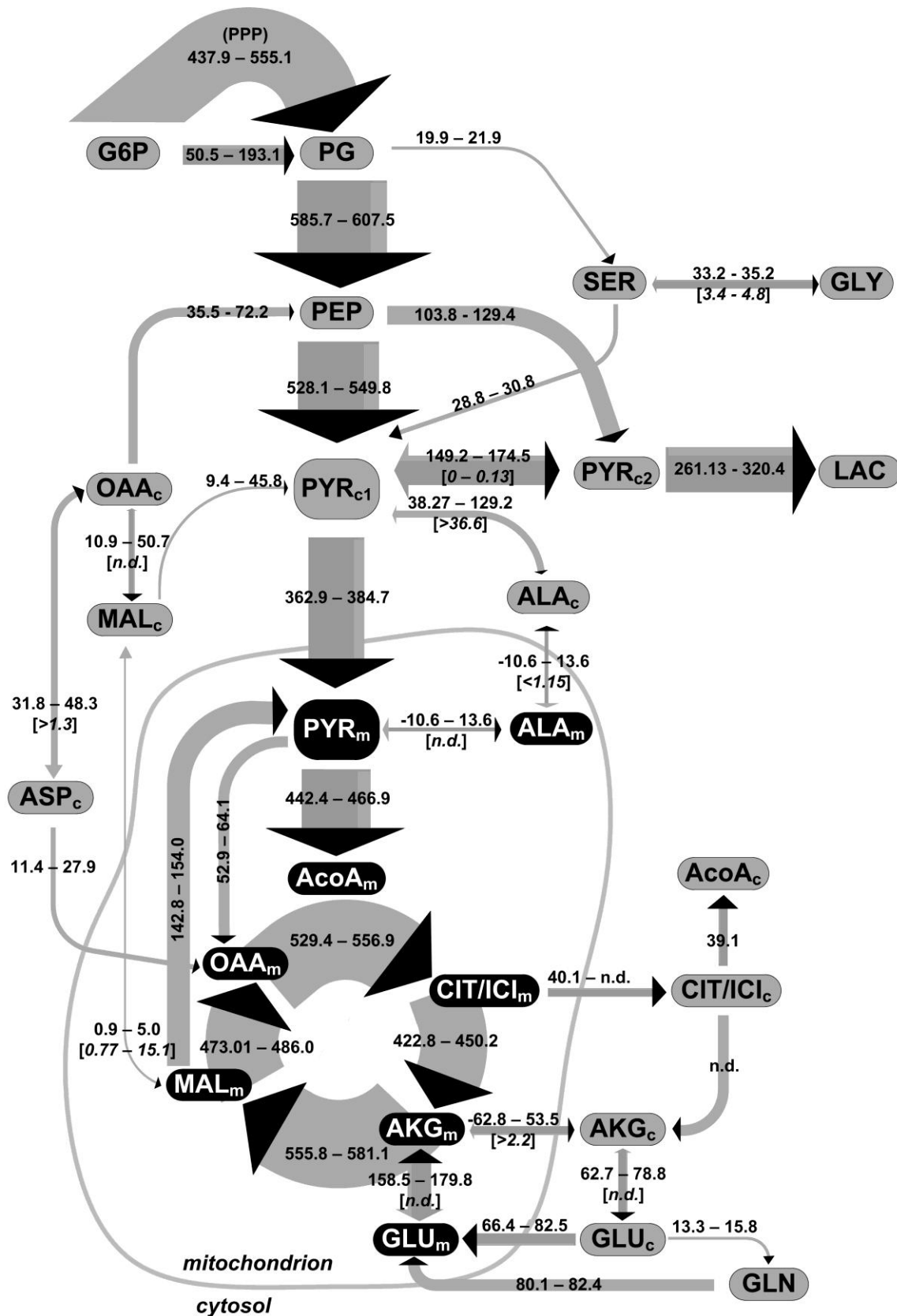


Figure 5-5. Estimated net intracellular fluxes [mmol/(L cell × h)] in the CHO-K1 central metabolism. Qualitatively shown by the arrow thickness and their 95% confidence intervals (number interval) together with reversibility confidence intervals (square brackets). n.d. – not determined.

Gluconeogenesis was active through PEP carboxykinase with 10% of the total flux entering the PEP pool, a fact explained qualitatively by the presence of M+2 lactate and pyruvate. In the absence of gluconeogenesis, only the M and M+3 mass isotopomers of these metabolites would be present after feeding fully labeled glucose. Malic enzyme activity was negligible in the cytosol, and this is in agreement with compartmented enzyme activity observed by J. Wahrheit (Wahrheit et al., 2014b). This observation reaffirms that PPP was the main source of cytosolic NADPH. Mitochondrial malic enzyme was highly active, producing one third of the total mitochondrial pyruvate. However, a part of the mitochondrial pyruvate was recycled back into the TCA cycle via pyruvate carboxylase. Mitochondrial malate net transport flux was small and reversible. This explained the lack of M+1 labeling in lactate, alanine and pyruvate that would have been otherwise linked to the M+2 malate isotopomers that are expected to be obtained in the TCA cycle. As a consequence, the M+2 labeling in these metabolites relies on mitochondrial transport of citrate and on the activity of citrate lyase producing cytosolic AcoA and OAA, which is then further converted to PEP.

About one third of the total serine was produced from PG, using cytosolic glutamate for transamination. Serine was exchanged with the media, thus explaining extracellular labeling of serine. Half of the serine was not used for protein synthesis but was reversibly converted to glycine and C1 units to sustain the high anabolic activity. Glycine was then secreted. The remaining excess of serine was converted to pyruvate. Alanine was synthesized mainly from cytosolic pyruvate in a highly reversible reaction. Connectivity between cytosolic and mitochondrial alanine pools and the direction of the mitochondrial alanine aminotransferase flux could not be determined. However, the transport flux of alanine to/from mitochondria was confined between -11.6 to 13.6 mmol/(L cell \times h), i.e. $\pm 25\%$ of the alanine production flux. The flux of 68.1 mmol/(L cell \times h) from asparagine and aspartate uptake to oxaloacetate was split through aspartate aminotransferases between cytosolic and mitochondrial oxaloacetate with a 3/1 ratio, but no other details could be inferred due to the low labeling level in extracellular aspartate.

Isocitrate dehydrogenase (IDH) activity in the cytosol could not be reliably determined due to lack of information in directly connected metabolites citrate and AKG, but also because it affects the labeling pattern in the same way as the mitochondrial isozyme. As a result, the flux in the CIT_m - CIT_c - AKG_c - AKG_m cycle could not be determined. Nevertheless, a net activity of cytosolic GDH towards producing the high glutamate flux needed for cytosolic transamination reactions implies that AKG is either produced in the cytosol by IDH or transported from the mitochondria into the cytosol. Mitochondrial glutamate pool was fed by transporting cytosolic glutamate into the mitochondria and by glutamine through GLS activity at comparable rates. In the mitochondria, glutamate was then converted to AKG and fed into the TCA cycle through mitochondrial GDH. In the cytosol, the glutamate produced from AKG in the various transaminase reactions was partially converted to glutamine, which was then exchanged with the media, leading to the presence of labeled glutamine in the media. In conclusion, simultaneous degradation and synthesis pathways for

glutamine involve glutamine uptake, transport into the mitochondria and conversion to glutamate, glutamate dehydrogenation to AKG, AKG transport to the cytosol or citrate transport and citrate conversion to AKG through cytosolic IDH activity, conversion of AKG to cytosolic glutamate, and cytosolic glutamine synthesis.

5.4.5 Transport reversibility

A very important part in modeling the extracellular labeling was considering the reversible exchange between the intracellular pools and the extracellular media, a phenomenon which affects the dynamics of the labeling process. All sampled extracellular non-essential amino acids except asparagine and proline, either produced or taken up, were exchanged with the culture media (Figure 5-3). Even if the production flux of alanine remained constant throughout the cultivation, the fitting remained poor for alanine when considering a constant reversibility factor. There, the reversibility was estimated to increase with time. The function $rev_{ALA} = 0.154 \cdot \exp(0.0359 \cdot time)$ was used to compute the forward and reverse exchange fluxes (eq. 5), with both parameters being determined with a narrow confidence interval (Additional File 1). Time is computed in hours. This successfully explained the dynamics of alanine labeling. The time constant of the reversibility function is a value close to the specific growth rate, pointing to the fact that alanine re-uptake is correlated to the extracellular concentration. Serine secretion flux, as computed with eq. 5, was up to 35 times higher than the net uptake flux. Glycine re-uptake flux was 4.6 times the net production flux. Aspartate, glutamate and glutamine exchange fluxes were in the same order with the net uptake/production flux, as expressed by the estimated reversibility parameter values of about 1. The confidence intervals for the transport reversibility parameters are larger than those for fluxes because at high reversibilities the labeling becomes less sensitive to small changes in reversibility.

Pyruvate transport reversibility is described by the function $rev_{PYR} = \frac{2700}{time + 0.01}$, where *time* is specified in hours. The hyperbolic function implies that at the beginning of the cultivation, the intense exchange of pyruvate (Cruz et al., 2001) eliminates the difference between the labeling of the intracellular and extracellular pools. Pyruvate re-uptake decreases because pyruvate concentrations changes slightly (Figure 5-1) while lactate accumulates in the media to reach high concentrations and competes with pyruvate for the monocarboxylate transporters (Halestrap and Price, 1999; Morris and Felmlee, 2008). Lactate transport reversibility parameter could not be estimated because at the beginning of the cultivation there is no lactate present in the media that could dilute the intracellular pool and affect the labeling dynamics.

5.4.6 Confidence intervals calculation and sensitivity analysis

Most of the fluxes depicted in Figure 5-5 were determined with narrow confidence intervals. Interval boundaries are not symmetrical due to the non-linear characteristics of the mathematical

model. Determining both the flux and exchange in alternative pathways was not possible in the case of high reversibility e.g. for determining the compartmentation of alanine metabolism involving reversible transaminase reactions.

The sensitivity coefficients provided quantitative information about the impact of the measured fluxes on the estimated flux values (Figure 5-6A). Sensitivity analysis also evidenced correlations between external fluxes and network pathways when $[\text{U-}^{13}\text{C}_6]$ glucose is used. In this case, the *MIDs* of metabolites will depend on the interplay between the multitude of non-labeled carbon sources and the glucose feed, as opposed to organisms that use only one carbon source (Sellick et al., 2011). The determination of anaplerotic fluxes relied on the supply of four carbon metabolites from amino acids catabolism. Changes in the glutamine uptake flux (Figure 5-6A) affected most fluxes to a large extent. Nevertheless, the high influence was mainly computational, as any increase of the flux caused depletion of glutamine at the end of the cultivation and dramatically different labeling patterns. Glucose uptake flux affected the estimation of the PPP and TCA cycle fluxes. Errors in measuring glucose concentration over time will propagate in the values of these fluxes, as the glucose uptake flux determines the fraction of ^{13}C entering the cell. G6P loses one ^{13}C through oxPPP, therefore estimating the split between glycolysis and oxPPP depends highly on determining correctly all carbon sources. This explains the high sensitivity of the glycolysis/oxPPP split to all extracellular fluxes. Unexpected correlations were observed for the glycine production flux that influenced most anaplerotic and aminotransferase fluxes. Glycine is produced at the expense of serine, which is in turn produced from 3-phosphoglycerate, also converting glutamate to alpha-ketoglutarate during transamination, and simultaneously converted to pyruvate, thus affecting the availability of both cytosolic pyruvate and glutamate.

Local sensitivity of the *SSQD* to free parameters computed as the normalized mean deviation of the objective function to variations in the estimated parameters shown in Figure 5-6B evidenced the determinable parameters and the redundant parameters. Notoriously difficult to determine anaplerotic fluxes PEP carboxykinase and mitochondrial malic enzyme induced a noticeable sensitivity in the objective function. The increased network connectivity, obtained by coupling ALA or ASP deamination to conversion of AKG to GLU, contributed to this fact. Oppositely, most intracellular reversibilities did not influence the parameter estimation results. This can be easily inferred from the fact that while reaction reversibility affects the dynamics of intracellular isotopomers, it does not mirror in the extracellular labeling apart from the reactions altering the carbon backbone. Also, in the situation where high values of the reversibilities resulted from estimation, local perturbations around these values will not influence the *MIDs*.

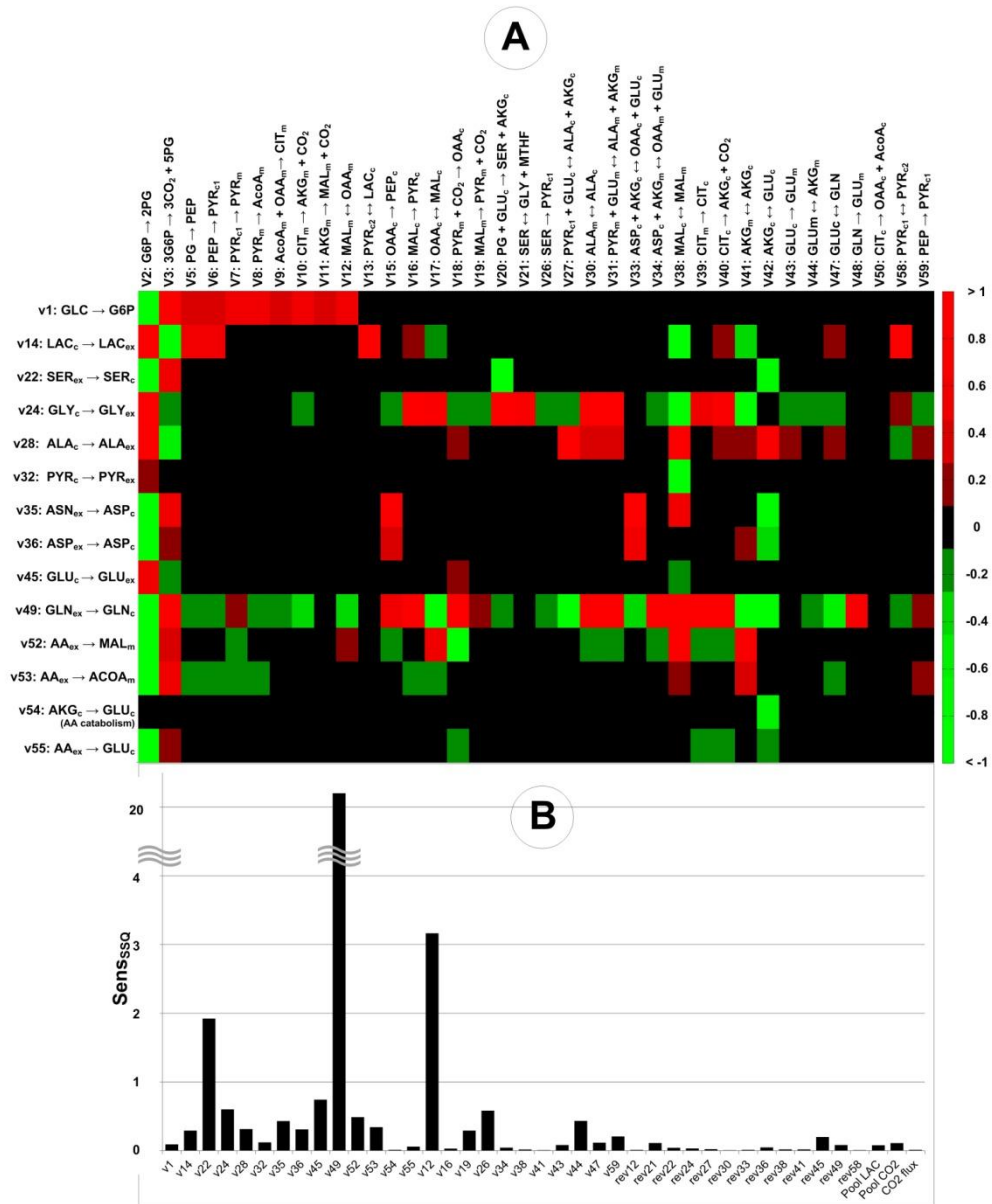


Figure 5-6. Sensitivity analysis to measured fluxes and to parameters. The sensitivity represented in the heat map (A) was computed for the compartmented network of CHO-K1 when $[U\text{-}^{13}\text{C}_6]$ glucose was used as a labeled substrate, $Sens_{v_m}^{v_e} = (dv_e/v_e^*)/(dv_m/v_m^*)$, where $Sens_{v_m}^{v_e}$ is the sensitivity of the estimated flux v_e , re-estimated using values of the measured flux v_m at the border of the confidence interval. v_m^* is the average measured flux. The bar chart below (B) shows the normalized sensitivity of the objective function (SensSSQD) to the free parameters (fluxes and rev = reversibilities). The sensitivity was obtained as a mean value of 100 perturbations of each parameter around the estimated value: $SensSSQD = (dSSQD/SSQD^*)/(dp_i/p_i^*)$, where $SSQD^*$ is the optimized value of the objective function (eq. 6), and p_i^* is the estimated value of parameter i . The rates v_i correspond to the rates in the network shown in Figure 1.A. Abbreviations: subscripts: c: cytosolic, ex: extracellular, m: mitochondrial; ALA: alanine; AcoA: acetyl coenzyme A; AKG: alpha-ketoglutarate; ASN: asparagine; ASP: aspartate; CIT: citrate; G6P: glucose 6-phosphate; GLC: glucose; GLN: glutamine; GLU: glutamate; GLY: glycine; LAC: lactate; MAL: malate; OAA: oxaloacetate; PEP: phosphoenolpyruvate; PG: phosphoglycerate; PYR: pyruvate; SER: serine.

5.5 Conclusions

We have shown that intracellular fluxes of the CHO-K1 cell line central carbon metabolism in batch culture can be determined for a complex network by making use solely of the mass isotopomers of extracellular metabolites resulted from feeding $[\text{U-}^{13}\text{C}_6]$ glucose as the only labeled substrate. To this end, non-stationary ^{13}C metabolic flux analysis proved an effective tool for unraveling important details of the CHO-K1 metabolism. Pathway compartmentation, e.g. of anaplerotic reactions and amino acid metabolism had to be considered for describing the mass isotopomer distribution. We reckon that this fact plays an essential role in controlling the availability of NADH and NADPH in mitochondria and cytosol, but also in facilitating amino acid catabolism. A cancer-like high activity of the pentose phosphate pathway produced reducing NADPH partly to counteract the oxidative stress generated by the mitochondrial respiration and partly to fuel fatty acids biosynthesis. When considering previous studies concerned with the metabolism of CHO cells, we can observe the wide range of metabolic fluxes that different cells lines and cultivation conditions are able to induce. Cytosolic pyruvate transport is reversible thousand-fold compared to the net production flux, indicating that although it is not a carbon source, pyruvate creates an extracellular environment (O'Donnell-Tormey et al., 1987) most probably by functioning as a balancing system for cytosolic NADH (Bucher et al., 1972). Considering that metabolite exchange with the media played a very important role in determining the intracellular fluxes, we expect that future ^{13}C MFA studies of mammalian cells metabolism will include this essential aspect. Compartmentation controls the simultaneous degradation and production of non-essential amino acids. Most likely, the CHO-K1 cells maintain the exponential growth phase under batch conditions by using a well-connected multi-pool system involving metabolite and reaction compartmentation, exchange with the media and inter-compartment exchange for controlling the metabolite and cofactor pools. Further studies on localizing enzyme and transporter activity together with sampling intra-compartmental concentrations would bring valuable contributions at elucidating the function of such cycling pathways. Accurate enzyme kinetics and thermodynamics (Henry et al., 2007) in mammalian cells would complement the modeling using INST- ^{13}C MFA with information about reaction direction and reversibility. The knowledge gained through INST- ^{13}C MFA depicts the CHO-K1 central metabolism as a robust, highly interconnected network that ensures fast growth and mitigates stress generated by reactive oxygen species and the accumulation of lactate in the culture media.

Due to the economic importance of CHO cells, efficient production processes leading to high product quality with minimum effort are of utmost importance. In-depth knowledge about CHO metabolism is expected to provide valuable assistance in identifying targets for metabolic engineering and guiding the design of feeding strategies leading to the development of efficient production processes. Overexpression, silencing or knockout of the specific glycolytic enzymes that

associate with channeling glucose to lactate could either be used to study the control of the Warburg effect in cancer cells or for improving glucose utilization. Because glutamine is a limiting substrate, overexpressing glutamine synthetase would enable cells to run a more efficient energy metabolism, with higher fluxes in the TCA cycle. However, as we have shown that compartmentation is important in managing metabolites, mitochondrial transporters are likely to constitute important targets for genetic modifications. Inter-compartmental transport of metabolites is a key factor in connecting the cytosol and the mitochondria energetically and we reckon that modifying the genetic expression of transporters will have significant, perhaps surprising effects on the overall metabolism.

Our proposed methodology of sampling the *MID* only in extracellular metabolites for determining intracellular fluxes using INST- ^{13}C MFA has the potential of broader applications, as it circumvents the need to extract intracellular metabolites and it is non-invasive to cells. The information contained in the extracellular mass isotopomers has a higher resolution compared to the summed fractional labeling used previously. This is sufficient for resolving a complex metabolic network when more metabolites are produced and/or exchanged with the culture media. Therefore, we foresee future applications in the study of mammalian metabolism at physiological and pathological conditions, especially related to compartmentation, as reviewed in (Gutierrez-Aguilar and Baines, 2013), and oxidative stress, e.g. in cancer, neurodegenerative disorders and ageing. Knowledge about the metabolism at the compartment level will be essential for identifying therapeutic targets and understanding disease mechanisms. Similarly, the method could be applied to other enzymatic systems or prokaryotic cells where an extended metabolite exchange with the media occurs.

5.6 Acknowledgments

We thank the Institute of Cell Culture Technology (University Bielefeld, Germany) for supplying the CHO-K1 cells and the BMBF (German Federal Ministry of Education and Research) project SysCompart (project ID 031555D), part of the Systems Biology program, New Methods in Systems Biology (SysTec), for funding.

5.7 Additional files

Additional files associated with this chapter are available online:

<http://www.biomedcentral.com/1752-0509/8/50/additional>

6 High resolution ^{13}C metabolic flux analysis in CHO cells

6.1 Abstract

The metabolism of mammalian cells is characterized by structural and functional complexity with respect to reaction compartmentation, metabolite exchange and channeling. Chinese hamster ovary cells are of high economic importance for biopharmaceutical production and an ideal model system for studying mammalian metabolism. We determined the mass isotopomer distributions from two parallel labeling experiments using $[\text{U-}^{13}\text{C}_6]$ glucose and $[\text{U-}^{13}\text{C}_5]$ glutamine as substrates in a CHO-K1 suspension culture. Using extra- and intracellular labeling dynamics we applied non-stationary ^{13}C metabolic flux analysis (INST- ^{13}C MFPA) to resolve the metabolic fluxes in a complex metabolic network that included mitochondrial transport, metabolite compartmentation and channeling. Metabolic fluxes, reversibilities and intracompartmental concentrations were determined within narrow confidence intervals. The metabolism was characterized by a high pentose phosphate pathway activity, high lactate production, low TCA cycle and cataplerotic fluxes, and simultaneous catabolism and production of non-essential amino acids. Mitochondrial glutamate was converted to α -ketoglutarate mostly by aminotransferase action while glutamate dehydrogenase flux was negligible. Malate and glutamate were cycled via several transporters between cytosol and mitochondria. Cytosolic NADH was partially transported into the mitochondria by the malate-aspartate shuttle and partially regenerated by cytosolic lactate dehydrogenase. The labeling dynamics of lactate and pyruvate indicate various metabolite channeling effects in the cytosol and the mitochondria as well as the existence of a mitochondrial lactate pool that serves most likely as intramitochondrial redox buffer. INST- ^{13}C MFPA combined with targeted parallel labeling experiments can unravel the details of mammalian metabolism.

This chapter is in preparation for submission as

Nicolae A, **Wahrheit J**, Heinzle E. High resolution ^{13}C metabolic flux analysis in CHO cells

6.2 Introduction

In the context of a fast-developing biopharmaceutical industry (Birch and Racher, 2006; Walsh, 2010a) and a continuous need to understand disease mechanisms at the molecular level, in-depth knowledge of the mammalian cell metabolism is crucial. This requires a systems biology approach that integrates “*omics*” information to determine the metabolic network structure and function by using adequate computational tools. The current challenge in metabolic flux analysis (MFA) of mammalian cells is to untangle the details related to compartmentation (Wahrheit et al., 2011). Dysfunctions in metabolite management between compartments in mammalian cells can lead to a multitude of diseases (Balaban, 2010; Calvo et al., 2006; Duchen, 2004; Nassir and Ibdah, 2014; Palmieri, 2008). In addition, metabolite channeling (Jandt et al., 2013; Malaisse et al., 2004; Zhang, 2011), association of enzymes (Campanella et al., 2005), and microcompartmentation (Holthuis and Ungermann, 2013) are phenomena contributing to the control of eukaryotic metabolism by assembly or disassembly of supramolecular structures.

Metabolic flux analysis of mammalian cells can rely only on flux balancing (Altamirano et al., 2001b; Bonarius et al., 1996; Sidorenko et al., 2008) or use also ^{13}C -labeling information to describe more complex metabolic networks (Amaral et al., 2011b; Bonarius et al., 2001; Goudar et al., 2010; Niklas et al., 2011b). Non-stationary ^{13}C metabolic flux analysis (INST- ^{13}C MFAs) is a modeling framework (Nöh et al., 2006; Nöh and Wiechert, 2006) that provides a detailed characterization of metabolic network function. By using the dynamics of mass isotopomer distributions (MIDs) it is possible to obtain detailed information about metabolic fluxes, reversibility and intracompartamental concentrations (Nöh et al., 2007; Nöh and Wiechert, 2011; Schmidt et al., 1997). However, the experimental and computational costs of this method increase substantially when compared to other MFA methods (Figure 6-1). As a tool for detailed metabolic flux analysis, INST- ^{13}C MFAs also allows the estimation of intracompartamental concentrations by using only the labeling dynamics of selected metabolites (Wiechert and Nöh, 2005). In eukaryotic cells, INST- ^{13}C MFAs was applied to study the metabolism of *Pichia pastoris* (Jorda et al., 2014), of hepatic cells (Hofmann et al., 2008; Maier et al., 2008) of cultured B-cells (Murphy et al., 2013) and of astrocytes (Amaral et al., 2011a). We previously applied INST- ^{13}C MFAs using the extracellular MIDs of metabolites from a reactor batch culture of CHO-K1 suspension cells where $[\text{U-}^{13}\text{C}_6]$ glucose was used as labeled substrate to determine the fluxes and metabolite exchange with the media in a compartmented metabolic network (Nicolae et al., 2014b).

CHO cells are the main production cell line for biopharmaceuticals (Kim et al., 2012) and considered as the “mammalian equivalent of *E. coli*” given their relevance as mammalian model system (Jayapal et al., 2007). Economic importance made CHO cells a target for various MFA studies (Ahn and Antoniewicz, 2011; Altamirano et al., 2001a; Altamirano et al., 2001b; Duarte et al., 2014; Goudar et al., 2010; Nicolae et al., 2014b; Nolan and Lee, 2011; Provost et al., 2006;

Sengupta et al., 2011; Sheikholeslami et al., 2013b; Templeton et al., 2013; Wahrheit et al., 2014a). The most detailed MFA studies used parallel labeling experiments applying $[1,2-^{13}\text{C}_2]\text{glucose}$ and $[\text{U}-^{13}\text{C}_5]\text{glutamine}$ and steady-state labeling to characterize the growth and the non-growth phases in monolayer CHO-K1 cells (Ahn and Antoniewicz, 2011). ^{13}C MFA was also applied for analyzing an inducible expression system engineered into a CHO cell line (Sheikholeslami et al., 2013b) or to characterize the metabolic shifts during antibody production in a highly-productive CHO cell line (Templeton et al., 2013). Nevertheless, all previous studies did not succeed in untangling the traffic between mitochondria and cytosol, as these models did not accurately take into consideration mitochondrial transport and metabolite compartmentation.

In the present work we studied the CHO-K1 metabolism by applying two labeled substrates, $[\text{U}-^{13}\text{C}_6]\text{glucose}$ and $[\text{U}-^{13}\text{C}_5]\text{glutamine}$, to shake flask batch cultures of CHO-K1 suspension cells. We used the dynamics of intra- and extracellular MIDs to estimate the intracellular fluxes, reversibilities and intracompartmental concentrations by applying INST- ^{13}C MFA. Such method produces a high-resolution analysis of the mammalian cell metabolism, as it allows a detailed exploration of metabolic compartmentation, mitochondrial transport and metabolic channeling. The metabolic network we have resolved offers a new perspective of the complex CHO-K1 cells metabolism in particular and more generally on the intricate system of metabolic fluxes in mammalian cells.

EXPERIMENTAL DATA	BIOMASS QUANTIFICATION <ul style="list-style-type: none"> • Proteins • DNA, RNA • Carbohydrates • Fatty acids 	Metabolic steady state	FLUX ANALYSIS METHOD	
	EXTRACELLULAR UPTAKE/ PRODUCTION <ul style="list-style-type: none"> • Organic acids • Amino acids • CO_2, O_2, NH_3 			
	^{13}C LABELING <ul style="list-style-type: none"> • Organic acids • Amino acids • Macromolecules 	Steady state		STEADY-STATE ^{13}C-MFA <ul style="list-style-type: none"> • Net fluxes • Exchange fluxes
	<ul style="list-style-type: none"> • Extracellular • Intracellular 	Transient		INST ^{13}C-MFA <ul style="list-style-type: none"> • Net fluxes • Exchange fluxes • Intracompartmental concentrations
	INTRACELLULAR CONCENTRATIONS <ul style="list-style-type: none"> • Organic acids • Amino acids 	Metabolic steady state		

Figure 6-1. Experimental requirements for metabolic flux analysis methods.

6.3 Materials and methods

6.3.1 Cell culture

The CHO-K1 cell line was kindly provided by the Institute of Cell Culture Technology of the University Bielefeld (Germany). The cells were grown in suspension culture under serum and protein free conditions in the chemically defined, protein-free TC-42 medium (TeutoCell, Bielefeld, Germany), supplemented with 6 mM L-glutamine (Sigma-Aldrich, Steinheim, Germany) from a 240 mM stock solution in dH_2O . Cultivation of the CHO-K1 cells was performed in baffled shake flasks (250 ml, Corning, New York, USA) in a shaking incubator (Innova 4230, New Brunswick Scientific, Edison, NJ, USA) at 135 rpm (2 inches orbit), 37°C and 5% CO_2 .

6.3.2 Experimental set-up of labeling experiments

The pre-culture was carried out in a 250 ml baffled shake flask (Corning Inc., Germany) at an initial cell density of 4×10^5 cells/ml and a working volume of 100 ml. For the tracer experiments, cells were harvested during the exponential growth phase and resuspended in TC-42 medium with 100% [$\text{U-}^{13}\text{C}_6$] glucose (99%, Euriso-Top, Saarbrücken, Germany) or with 100% [$\text{U-}^{13}\text{C}_3$]glutamine (99%, Cambridge Isotope Laboratories, Andover, MA, USA). Four parallel tracer experiments were performed, two replicates with fully labeled glucose and two replicates with fully labeled glutamine, respectively. The main cultures were inoculated at a start cell density of 2×10^6 cells/ml in a start volume of 120 ml medium.

Extracellular samples of 0.5 ml were taken from all four cultivations every 6 h for cell counting, determination of extracellular metabolite concentrations and extracellular labeling dynamics. 50 μl of the sample was diluted with PBS and mixed with Trypan Blue for determination of cell density, cell viability and average cell diameter using an automated cell counter (Invitrogen, Darmstadt, Germany). The sample was centrifuged ($10,000 \times g$, 5 min, Biofuge pico, Heraeus Instruments, Hanau, Germany), 300 μl of the supernatant transferred into fresh tubes and stored at -20°C for further analysis. The rest of the sample was used for pH determination (MP 220 pH Meter, Mettler-Toledo, Giessen, Germany).

Intracellular samples of 5 ml were taken alternately from the two replicates after 2 min, 10 min, 20 min, 30 min, 1 h, 2 h, 4 h, 6 h, 12 h, 18 h, 24 h, 30 h, 36 h, 42 h and 48 h. Quenching and extraction for determination of intracellular metabolites was performed as described in detail recently (Wahrheit and Heinzle, 2013; Wahrheit and Heinzle, 2014). In short, a sample of 5 ml cell suspension was quenched in 45 ml ice-cold 0.9% sodium chloride solution and centrifuged for 1 min at $2000 \times g$ in a pre-cooled centrifuge at 0°C . The supernatant was carefully decanted followed immediately by suction of residual liquid using a vacuum pump without touching the cell pellet. Washing was performed by carefully rinsing the cell pellet with 50 ml ice-cold 0.9% sodium

chloride solution without resuspending the cells. After repeating the centrifugation step and removal of the supernatant, the cell pellet was frozen in liquid nitrogen. Intracellular metabolites were extracted twice in 100% methanol and once in water by repeated freeze-thaw cycles as described previously (Wahrheit and Heinzle, 2014) and similar to (Sellick et al., 2011). Extracts were dried in a centrifugal evaporator.

6.3.3 Quantification of extracellular metabolites

Quantification of glucose, organic acids and amino acids via HPLC was carried out as described previously by Strigun et al. (Strigun et al., 2011b).

6.3.4 Analysis of isotopomer labelling patterns

6.3.4.1 Sample preparation

For determination of extracellular labeling dynamics, 50 μl of supernatants were lyophilized, resolved in 50 μl N,N-dimethylformamide (0.1 % pyridine) and incubated at 80°C for 30 min. 50 μl N-methyl-N-t-butyltrimethylsilyl-trifluoro-acetamide (MBDSTFA) was added followed by another incubation at 80°C for 30 min for derivatization of extracellular metabolites into corresponding dimethyl-t-butylsilyl derivatives. Dried cell extracts were resolved in 50 μl pyridine containing 20 mg/ml methoxylamine and 50 μl MSTFA (Macherey-Nagel, Düren, Deutschland) and incubated at 80°C for 30 min for derivatization of intracellular metabolites into corresponding methoxyamine-trimethylsilyl derivatives. Derivatized samples were centrifuged at $13000 \times g$ for 5 min at 4 °C and the supernatants transferred into fresh glass vials with micro inlets.

6.3.4.2 GC-MS measurements

Extra- and intracellular ^{13}C -labeling dynamics were analyzed by gas chromatography mass spectrometry (GC-MS). The GC-MS measurements were carried out on a GC (HP 6890, Hewlett Packard, Palo Alto, CA, USA) equipped with an HP5MS capillary column (5% phenyl-methylsiloxane diphenylpolysiloxane, 30 m \times 0.25 mm \times 0.25 μm , Agilent Technologies, Waldbronn, Germany), electron impact ionization at 70 eV, and a quadrupole detector (Agilent Technologies). The injection volume was 1 μl (7683B Autosampler, Agilent, Waldbronn, Germany; PTV-Injektor, Gerstel, Mühlheim a. d. Ruhr, Germany).

Helium was used as carrier gas at a flow rate of 1.1 ml/min for analysis of extracellular metabolites or 0.7 ml/min for analysis of intracellular metabolites. The following temperature gradient was applied for analysis of extracellular metabolites: 135°C for 7 min, 10°C/min up to 162°C, 7°C/min up to 170°C, 10°C/min up to 325°C, 325°C for 2.5 min; inlet temperature: 140°C and heating with 720°C/min up to 320°C; interface temperature 320°C; quadrupole temperature 150°C. The temperature gradient for analysis of intracellular metabolites was as follows: 70°C for 1 min, 1°C/min up to 75°C, 5°C/min up to 315°C, 25°C/min up to 340°C, 340°C for 5 min; inlet

temperature: 70°C and heating with 360°C/min up to 360°C; interface temperature 320°C; quadrupole temperature 280°C.

6.3.4.3 Data analysis

After identification of metabolites in the scan mode using the NIST data bank, quantification of labeling enrichment was done in SIM (single ion monitoring) mode in at least two technical replicates. Unique fragments (m/z) containing the whole carbon backbone were chosen for excreted extracellular metabolites and selected intracellular metabolites of the central metabolism. Following monoisotopic fragments and their corresponding mass isotopomers of extracellular metabolites (MBDSTFA derivatization) were analyzed: lactate 261, alanine 260, glycine 246, serine 390, aspartate 418, glutamate 432, glutamine 431. Identified monoisotopic fragments and corresponding mass isotopomers in cell extracts (MSTFA derivatization) were as follows: pyruvate 174, lactate 219, alanine 218, fumarate 245, malate 335, citrate 465, α -ketoglutarate 304, glycine 276, serine 278, aspartate 334, glutamate 348. Mass isotopomer distributions were corrected for naturally occurring isotopes using the method of Yang et al. (Yang et al., 2009).

6.3.5 Metabolic network

A detailed metabolic network of the CHO-K1 cell line was constructed using the annotated CHO genome database (Hammond et al., 2012), the *Mus musculus* genome (Zhu et al., 2003) and the KEGG Pathway database (Kanehisa et al., 2014). We included available data base information about enzyme compartmentation, mitochondrial transporters and metabolic channeling. The network included compartmentation of cytosolic and mitochondrial alanine and aspartate aminotransferases, cytosolic glutamine synthesis and mitochondrial glutaminase, cytosolic and mitochondrial isocitrate dehydrogenase. Concerning mitochondrial carriers, we have considered the following: irreversible pyruvate carrier (confirmed by own mitochondrial studies, unpublished data), reversible dicarboxylate carrier, irreversible citrate carrier, reversible α -ketoglutarate carrier, reversible glutamate carrier, reversible aspartate-glutamate carrier, reversible alanine transport and irreversible glutamine transport into the mitochondria.

In addition, the network was modified using enzyme activity localization determined by Wahrheit et al. (Wahrheit et al., 2014b). The pathways leading to macromolecules e.g. carbohydrates, proteins, fatty acids, nucleic acids were lumped as sink fluxes for precursor metabolites. The catabolism of amino acids was lumped into fluxes feeding target metabolite pools. The detailed reaction list and the carbon transfer rules are given in the Supplementary Table S1.

6.3.6 Non-stationary- ^{13}C CMFA

We applied metabolite and carbon balancing for both intracellular and extracellular metabolites for simulating the mass isotopomer distribution (MID) of selected metabolites over time. The

mathematical modeling procedure of non-stationary ^{13}C metabolic flux analysis (INST- ^{13}C MFPA) is the same as we have described and applied in Nicolae et al. (Nicolae et al., 2014b). In this study we have used also intracellular MIDs and consequently we could estimate intracompartmental concentrations of metabolites with sampled MIDs. The sampled intracellular MID of a metabolite is an average of the mitochondrial and cytosolic MIDs, weighed by the intracompartmental pools of that respective metabolite. For this, we considered the total mitochondrial volume to be 20% of the total cell volume (personal communication, Uwe Jandt). For all the metabolites that were included in the model but for which the MIDs were not sampled, we considered negligible intracompartmental pool values of 0.1 mmol/L cell. The accepted standard deviation of extracellular MIDs in the objective function was 0.01 and of intracellular MIDs it was 0.03.

6.4 Results and Discussion

6.4.1 Cell growth and extracellular metabolite concentrations

Growth and extracellular metabolite concentrations were determined from four biological replicates. The CHO-K1 cells maintained exponential growth for the whole cultivation period of 48 h (Supplementary Figure S1). The parallel cultivations were reproducible, as it can be seen by the low standard deviations in Supplementary Figure S1 and Supplementary Figure S2. The estimated specific growth rate was $\mu = 0.034 \text{ h}^{-1}$ (Supplementary Figure S1). Glucose, glutamine, pyruvate, serine, asparagine, aspartate and essential amino acids were taken up (Supplementary Figure S2). Lactate, alanine, glutamate and glycine were produced throughout the cultivation period. By the end of the 48 h, 60% of the glucose was converted to lactate. Although the specific growth rate was constant (Supplementary Figure S1), the specific uptake and production rates generally decreased over the 48 h, the most marked trend being observed for lactate production (Supplementary Figure S2). However, no switch from production to uptake or vice-versa was observed.

6.4.2 Labeling experiment

Extracellular MIDs were determined from two biological replicates. For determination of the time courses for intracellular labeling dynamics, MIDs were obtained alternatively from two parallel cultivations for each labeled substrate. In the experiment where $[\text{U-}^{13}\text{C}_6]$ glucose was used, the sampled metabolites became labeled gradually, and no steady state was reached after 48 h (Supplementary Figure S3A). The general trend was of increasing labeling fraction, the exception being intracellular lactate, whose M3 mass fraction decreased after 36 h. The mass isotopomer with the highest proportion for pyruvate, lactate and alanine was M3, while for metabolites related to the TCA cycle e.g. citrate, α -ketoglutarate, fumarate and malate, it was the M2. Lactate and alanine pools were labeled differently intra- and extracellularly. This evidence supports the hypothesis of metabolic compartmentation of these two metabolites. Partitioning of lactate dehydrogenase

activity, either by channeling (Jandt et al., 2013; Malaisse et al., 2004; Perez-Bercoff et al., 2011) or in cellular compartments (Baba and Sharma, 1971; Brooks et al., 1999; Gladden, 2004; Hashimoto and Brooks, 2008; Lemire et al., 2008; Philp et al., 2005; Sagrista and Bozal, 1987a) can also be inferred by comparing the intracellular labeling of pyruvate and lactate. During the first 24 h, intracellular pyruvate and lactate follow similar labeling patterns. Afterwards, a switch in the partitioning of lactate dehydrogenase around 18 h after inoculation was evident from different labeling patterns of intracellular pyruvate and lactate.

In the first 2 h, the labeling in pyruvate exhibited a sharp overshooting of the M3 fraction, that was manifested later also in lactate (Supplementary Figure S3B). A similar overshooting behavior was observed in the M4 isotopomer of malate, and it transmitted to aspartate.

When $[\text{U-}^{13}\text{C}_5]$ glutamine was used as the ^{13}C label source, no labeling was observed in serine and glycine, indicating that gluconeogenesis was not active. Pyruvate and lactate displayed a sharp overshooting in the first 2 h in all mass isotopomers (Supplementary Figure S3B). However, after 12h, the labeling of pyruvate and lactate returned close to the natural labeling state, indicating the absence of fluxes that connect glutamine to pyruvate. The M4 MID fraction in aspartate, fumarate and malate increased until 18 h, and then it decreased in favor of the non-labeled fraction. This is most likely the result of a metabolic shift occurring around 18 h after inoculation. The shift is mirrored in glutamine and glutamate labeling, where the non-labeled fraction increases steadily after 24 h. The metabolic shift consists most likely of a decrease in the ratio between glutaminolysis and glycolysis in contributing to the TCA cycle.

The specific uptake and production rates were therefore computed for the period of 0-18 h by fitting the model of exponential balanced growth in batch culture to the sampled extracellular concentrations (Supplementary Figure S2).

Aspartate, fumarate and malate had similar labeling patterns on both labeled substrates, suggesting a high degree of connection and exchange between these metabolites.

On both labeled substrates, the MID curves that exhibited overshooting returned to a smooth behavior after 2 h. We assign the overshooting to a stress response of the cells to media change at the beginning of the culture (Wellen and Thompson, 2010). The stress response is characterized by very high metabolic rates that quickly convert the fed substrates after being resuspended to replenish the depleted intracellular pools. Once these pools were replenished, the metabolism followed a steady state behavior, as it can be seen in Supplementary Figure S2. Since there is no observable difference in the cell number and extracellular concentrations in the first two hours, assessing the extracellular fluxes during this brief period and proving the existence of metabolic steady state required for metabolic flux analysis tools is not possible.

6.4.3 Fitting of MIDs and model re-adaptation

For applying INST- ^{13}C MFAs, we considered that the cells were at metabolic steady state between 2-18 h after the beginning of the labeling experiments (Deshpande et al., 2009; Nöh et al., 2006). This is a valid assumption for most metabolites, as it was shown by fitting the extracellular concentrations to an exponential growth with balanced uptake and production model (Supplementary Figure S2). We have considered the MIDs of 15 extracellular and intracellular metabolites, 5 time points for $[\text{U-}^{13}\text{C}_6]$ glucose and 4 time points for $[\text{U-}^{13}\text{C}_5]$ glutamine, totaling 675 experimental MID points (Figure 6-2). Because of the noisy data, the MIDs of intracellular alanine and α -ketoglutarate were excluded from parameter estimation. After several trials in which no successful fitting was obtained, the initial model was modified to include: (1) two pools of cytosolic pyruvate, of which one is channeled to lactate that is then directly secreted, (2) two pools of mitochondrial pyruvate, of which one is converted to acetyl-CoA via pyruvate dehydrogenase, (3) a pool of mitochondrial lactate, (4) cytosolic synthesis of glutamine and (5) serine degradation to pyruvate.

The parameter estimation was made using two strategies in parallel: one was using a genetic optimization algorithm, as we previously did in (Nicolae et al., 2014b), and the other was to (1) generate 1000 random initial points that satisfy constraints, (2) use the point that produced the smallest value of the objective function as the starting point of a gradient-based algorithm and (3) find the minimum of the trust region reflective algorithm. The second optimization strategy was repeated 30 times, and it provided the best fit of the MIDs. One simulation took about 6.5 s, and the optimization procedure required about 6 days on a 2.3 GHz QuadCore CPU. A total of 64 parameters were estimated, of which 13 were free fluxes, 29 were flux reversibilities, 20 were intracompartmental pools and 2 additional parameters that expressed the non-labeled CO_2 flux entering the cytosol and the mitochondria. This flux was needed to evaluate the labeling dynamics of CO_2 used by carboxylation reactions.

The best fit (Figure 6-2) resulted in a minimized weighted sum of square differences value of 665, which is smaller than the criteria for fitting $\chi^2(0.95, 675-64) = 670$. Most of the MIDs of metabolites were reasonably well fitted, except intracellular lactate when $[\text{U-}^{13}\text{C}_6]$ glucose was used. Because the labeling of extracellular lactate is different from the labeling of intracellular lactate (Figure 6-2), we have considered more pyruvate pools from which lactate can derive. While this assumption produced a much better approximation of lactate labeling, it is still possible that other metabolic configurations involving more sophisticated channeling and compartmentation are responsible for the observed labeling pattern in lactate.

Confidence intervals were computed accordingly to (Antoniewicz et al., 2006a) and were very narrow for most estimated parameters (Supplementary Table S1). This is a strong indication that fitting simultaneously the intracellular MIDs from two parallel labeling experiments that used two

different labeled substrates validates INST- ^{13}C CMFA is an effective methodology for untangling the details of complex metabolic networks, as it was also described by (Murphy et al., 2013).

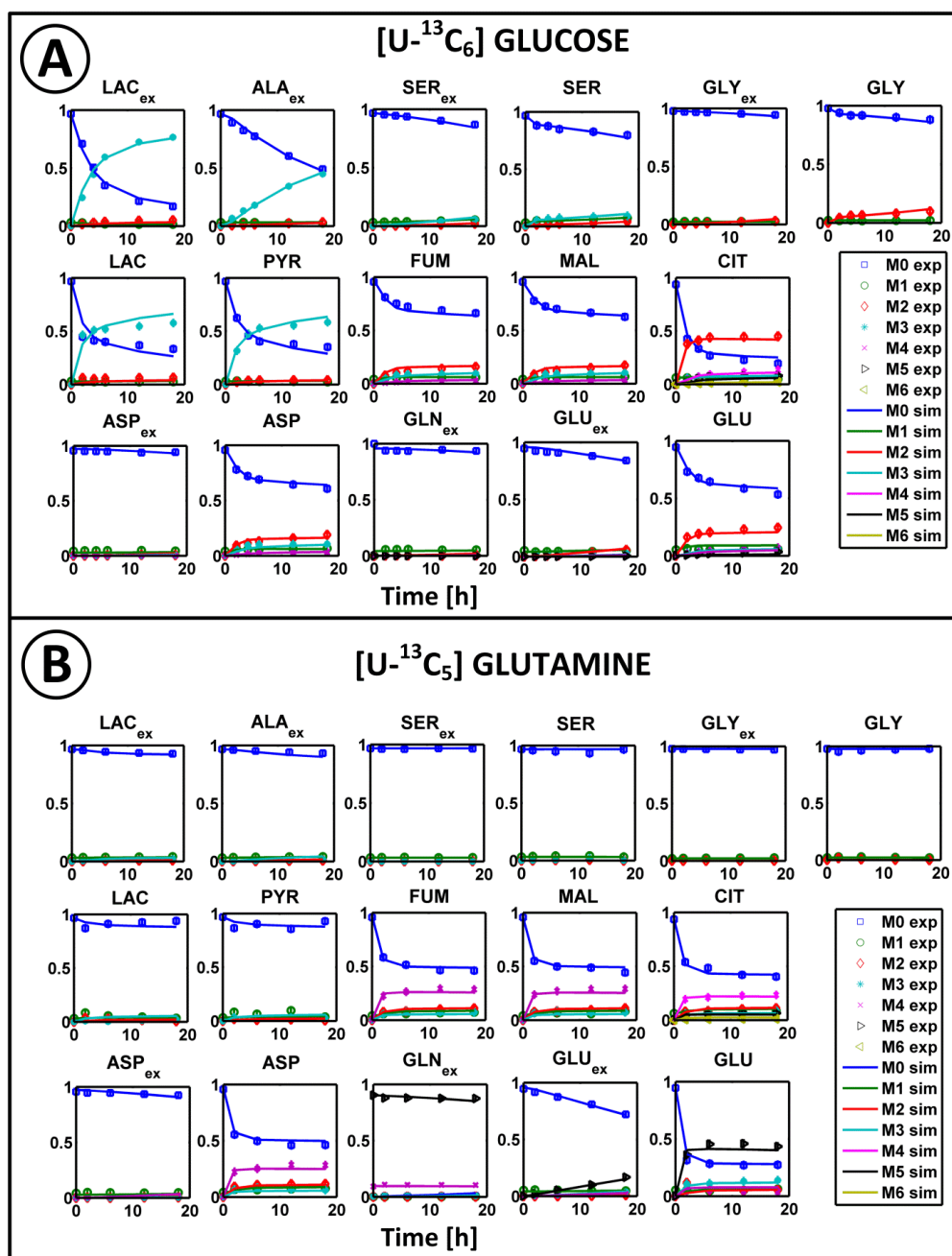


Figure 6-2. Mass isotopomer distributions (MIDs) of sampled metabolites during the first 18 h of cultivation of CHO-K1 suspension cells with (A) [U- $^{13}\text{C}_6$] glucose and (B) [U- $^{13}\text{C}_5$] glutamine. The values of the extracellular MIDs are the average of two biological replicates and the intracellular MIDs are obtained alternatively from two parallel cultivations for each labeled substrate. The continuous lines represent the best simulated fit of the MIDs. Subscripts meaning: *ex* – extracellular. Abbreviations: exp – experimental; sim – simulated; ALA – alanine; ASP – aspartate; CIT – citrate; FUM – fumarate; GLN – glutamine; GLU – glutamate; GLY – glycine; LAC – lactate; MAL – malate; PYR – pyruvate; SER – serine.

6.4.4 Metabolic fluxes, compartmentation and channeling

Glycolysis was the main carbon source of the CHO-K1 cell metabolism (Figure 6-3A). Consistently with our previous finding for the CHO-K1 cell line cultivated in a reactor batch culture (Nicolae et al., 2014b), most of the glucose-6-phosphate was metabolized by the oxidative branch of the pentose phosphate pathway (PPP) and not by the upper glycolysis. 75% of the glucose was converted to lactate that was then secreted. The remaining glucose was converted to pyruvate that was transported to the mitochondria. In previous studies of this CHO-K1 cell line, we found that partial glycolytic channeling resulted in two cytosolic pyruvate pools (Nicolae et al., 2014b; Wahrheit et al., 2014b), a phenomenon observed before in CHO cells (Ahn and Antoniewicz, 2013; Deshpande, 2008) and also in other mammalian cells (Campanella et al., 2005; Cruz et al., 2001; Peuhkurinen et al., 1983; Zwingmann et al., 2001). In the present study, the channeling effect was less pronounced, as the two cytosolic pyruvate pools were estimated to be strongly connected (Figure 6-3A). However, we found active exchange from pyruvate towards a second cytosolic dead-end lactate pool. Also, the exchange between the extracellular and intracellular lactate pool was significant. This exchange must be considered to describe the MID's dynamics of intracellular lactate and pyruvate. Furthermore, the model was expanded by a mitochondrial lactate pool and channeling of mitochondrial pyruvate to describe the difference in labeling between extracellular and intracellular lactate. Since the pyruvate dehydrogenase was found to be associated to the inner mitochondrial membrane (Simonot et al., 1997), we assumed that a part of the pyruvate entering the mitochondria is directly converted to acetyl-CoA, without mixing with the mitochondrial pyruvate pool (Figure 6-3B), as it was also modeled by Ahn et al. (Ahn and Antoniewicz, 2013). This setup explained the low ^{13}C fractional labeling of intracellular pyruvate and lactate with $[\text{U-}^{13}\text{C}_6]$ glucose feeding. The pyruvate with high ^{13}C fractional labeling produced in the glycolysis is consumed in the TCA cycle, and cataplerotic reactions replenish the second mitochondrial pyruvate pool with ^{12}C from other carbon sources. The existence of mitochondrial lactate dehydrogenase was already confirmed in various tissues, e.g. heart mitochondria (Brooks et al., 1999), breast cancer cells (Hussien and Brooks, 2011), muscle cells (Hashimoto et al., 2006), liver cells (Brooks et al., 1999; Kline et al., 1986), astrocytoma (Lemire et al., 2008) and neurons (Hashimoto et al., 2008). Mitochondrial metabolism of lactate occurs when lactate is being metabolized as a carbon source, due to its high intracellular concentration (Brooks et al., 1999). However, in our case, lactate was secreted by the cells and it constituted a dead end metabolite in the mitochondria. We therefore assume its role is to function as a buffer for mitochondrial NADH, a mediator of redox states between compartments (Gladden, 2004).

Glycolytic pyruvate and glutamine constituted the main fuels of the TCA cycle as we previously found for this cell line (Wahrheit et al., 2014a; Wahrheit et al., 2014b). The catabolism of essential amino acids was limited to a small flux feeding the acetyl-CoA pool. Otherwise, the uptake of

essential amino acids was mostly restricted to the requirements for protein synthesis also previously found for this cells line (Wahrheit et al., 2014b).

At the cytosol-mitochondria boundary, most mitochondrial transporters carried significant fluxes. The mitochondrial pyruvate carrier (Bricker et al., 2012; Herzig et al., 2012) was the only connection between glycolysis and the TCA cycle, providing most of the mitochondrial pyruvate, as the mitochondrial malic enzyme activity was estimated to be very low (Figure 6-3B), consistent with enzyme assays (Wahrheit et al., 2014b). The aspartate-malate shuttle (Figure 6-3C) exported mitochondrial aspartate via the glutamate-aspartate carrier (Cavero et al., 2003; Lane and Gardner, 2005) and imported cytosolic malate via the malate- α -ketoglutarate carrier. The cytosolic aspartate was converted to oxaloacetate by the activity of aspartate aminotransferase. Cytosolic malate dehydrogenase converted oxaloacetate to malate and consumed a part of the cytosolic NADH. Malate was also exported via the malate-citrate carrier to export citrate used for fatty acids synthesis (Gnoni et al., 2009; Zara et al., 2005), and then was re-imported in the mitochondria via the malate carrier (Fiermonte et al., 1999; Mizuarai et al., 2005) (Figure 6-3C). Phosphoenolpyruvate carboxykinase activity was modest as a starting point of gluconeogenesis. Complete gluconeogenesis did not occur; a fact that can be qualitatively seen by the lack of labeling in serine and glycine when $[\text{U-}^{13}\text{C}_5]$ glutamine was used as tracer (Figure 6-2B).

Glutamine uptake in the mitochondria was 3.6 times higher than the net glutamine uptake. This is the result of a considerable cytosolic synthesis of glutamine from glutamate (Figure 6-3D). We have observed previously for CHO-K1 cells that the glutamine synthesis pathway was active even at high glutamine consumption rates (Nicolae et al., 2014b). In the mitochondria, glutamine feeds the TCA cycle via glutamate that is converted to α -ketoglutarate not by NADH-producing glutamate dehydrogenase, but by transamination reactions. Aspartate was synthesized in the mitochondria, exported and re-converted to oxaloacetate in the cytosol. Alanine synthesis was estimated to occur mostly in the mitochondria. Glutamate transporter carried a high flux exiting the mitochondria (Figure 6-3D). Glutamate was procured in the cytosol either via transport from the mitochondria or transamination of α -ketoglutarate. Cytosolic glutamate was used to fuel glutamine synthesis and as an antiport partner to the aspartate-glutamate transporter. Despite the high activity detected *in vitro* for cytosolic isocitrate dehydrogenase (Wahrheit et al., 2014b), this did not reflect in the labeling patterns, regardless of the reaction direction that was considered. Even setting the labeling of the CO_2 pool as a free parameter did not result in the estimation of a significant activity. The role of such a high activity of cytosolic isocitrate dehydrogenase could be to control variations of the cytosolic NADPH content and stress response (Lee et al., 2002).

In what concerns NADH and NADPH metabolism compartmentation, the excess of cytosolic NADH produced in the glycolysis is consumed by lactate dehydrogenase and the malate shuttle. Cytosolic NADPH is provided only by PPP, as the activity of cytosolic malic enzyme was found to

be virtually absent, and also not found in enzyme assays (Wahrheit et al., 2014b). The very low activity of mitochondrial malic enzyme means little mitochondrial NADPH was produced via this route. The need for NADPH in the mitochondria must be supplied by other reactions, most likely the transhydrogenase or NADP-dependent isocitrate dehydrogenase (Ceccarelli et al., 2002; Hatefi and Galante, 1977). It was shown by previous enzyme assays that around 90% of mitochondrial IDH activity is NADP-dependent (Wahrheit et al., 2014b).

All aminotransferase reactions and also many of the transport reactions were determined to be highly reversible (Supplementary Table S1). This determination relies on the shape of the MID curves, as it is significantly influenced by reversibility (Nöh and Wiechert, 2011). Transport reversibility explained the reduced summed fractional labeling when $[\text{U-}^{13}\text{C}_6]$ glucose was used as a substrate, as the intracellular labeling was diluted by the large extracellular pool of non-labeled metabolites, consistent with our previous observations (Nicolae et al., 2014b).

Using intracellular labeling and two labeling experiments improved considerably the resolution and quality of estimated fluxes (Supplementary Table S1) compared to our previous study, where we have used the same cell line but only extracellular labeling and one labeling experiment in a batch reactor cultivation (Nicolae et al., 2014b). We were able to establish the compartmentation of alanine synthesis and to solve the cytosolic and mitochondrial isocitrate – α -ketoglutarate – glutamate cycling. In terms of the extracellular fluxes values, we reiterate our conclusion that they are highly dependent on the cultivation conditions. The major differences of this shake flask cultivation compared to the reactor cultivation performed in our previous study (Nicolae et al., 2014b) are: (1) reduced glucose uptake (~80% of the previous), (2) higher lactate production from glucose (75% compared to 39%) , (3) smaller TCA cycle flux, (4) reduced catabolism of essential amino acids, (5) low mitochondrial malic enzyme activity and (6) reduced uptake of asparagine. We also mark the consistencies in the CHO-K1 metabolism: (1) almost complete diversion of glucose-6-phosphate through the PPP, (2) absence of cytosolic malic enzyme activity, (3) similar phosphoenolpyruvate-carboxykinase activities, (4) simultaneous uptake and production of glutamine, (5) simultaneous uptake and production of serine and (6) excessive exchange of metabolites with the extracellular media.

The metabolic flux map we have determined is the most complex to date for mammalian cells with respect to metabolic compartmentation, mainly because we have considered mitochondrial transport of metabolites based on known mitochondrial transporters. The results of studies that use ^{13}C CMFA to unravel the eukaryotic cell metabolism are highly dependent on the network structure. Any new added reaction can lead to completely different estimated fluxes due to parameter interdependency and non-linearity characteristics of carbon balances. It is therefore difficult to compare our results with previous ^{13}C CMFA studies of CHO cells. We have estimated a high activity of the PPP in the early exponential growth phase in a previous study that applied INST- ^{13}C CMFA of CHO cells

(Nicolae et al., 2014b). A high PPP was found to be a characteristic of the late non-growth phase (Ahn and Antoniewicz, 2011; Sengupta et al., 2011) or late-exponential (Templeton et al., 2013). A high production of NADPH is required to counteract the oxidative stress induced by reactive oxygen species generated by mitochondrial respiration (Schafer et al., 2009; Vizan et al., 2009).

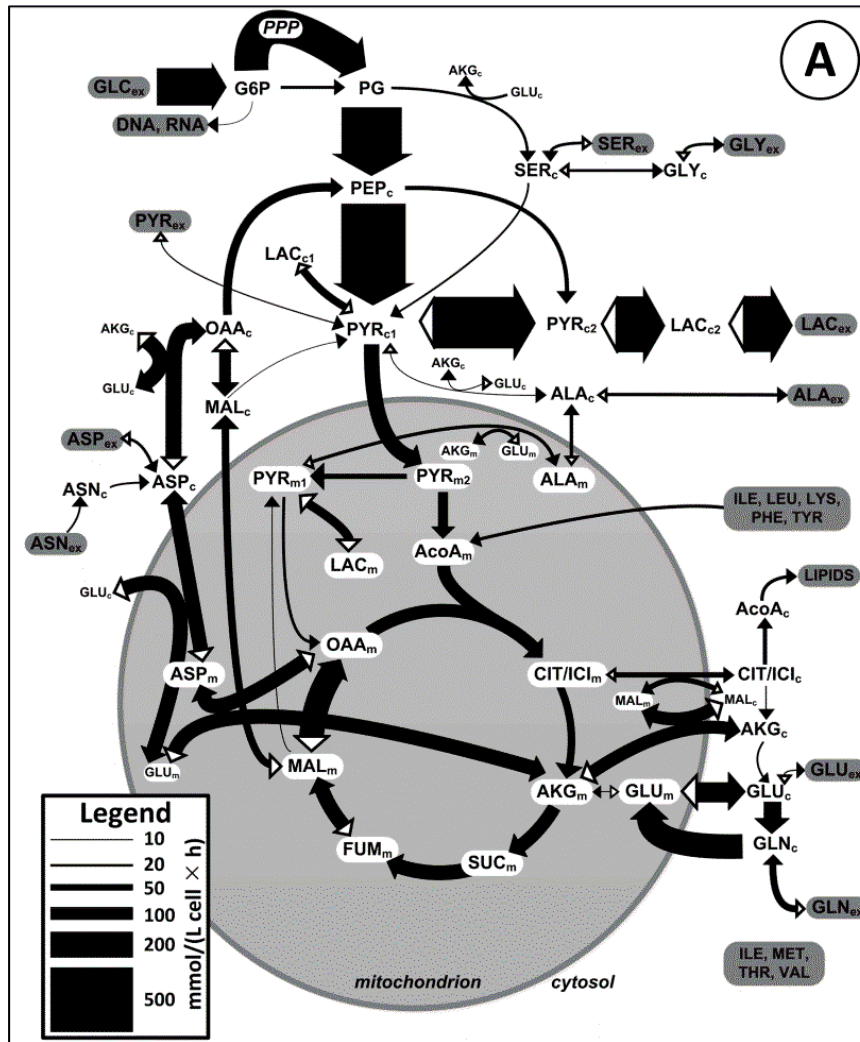


Figure 6-3. (A) Metabolic fluxes of the central carbon metabolism of CHO-K1 cells in the 2 – 18 h period of cultivation estimated using non-stationary ^{13}C metabolic flux analysis. The thickness of the lines is proportional to the net flux values. The full arrows indicate the direction of the net flux, and the empty arrows indicate a reversible flux. Subscripts meaning: c – cytosolic; ex – extracellular; m – mitochondrial; Abbreviations: AcoA – acetyl-CoA; AKG – α -ketoglutarate; ALA – alanine; ASN – asparagine; ASP – aspartate; CIT – citrate; FUM – fumarate; GLC – glucose; G6P – glucose-6-phosphate; PG – phosphoglycerate; PEP – phosphoenolpyruvate; GLN – glutamine; GLU – glutamate; GLY – glycine; ICI – isocitrate; ILE – isoleucine; LAC – lactate; LEU – leucine; LYS – lysine; MAL – malate; MET – methionine; OAA – oxaloacetate; PHE – phenylalanine; PYR – pyruvate; SER – serine; SUC – succinate; THR – threonine; TYR – tyrosine; VAL – valine.

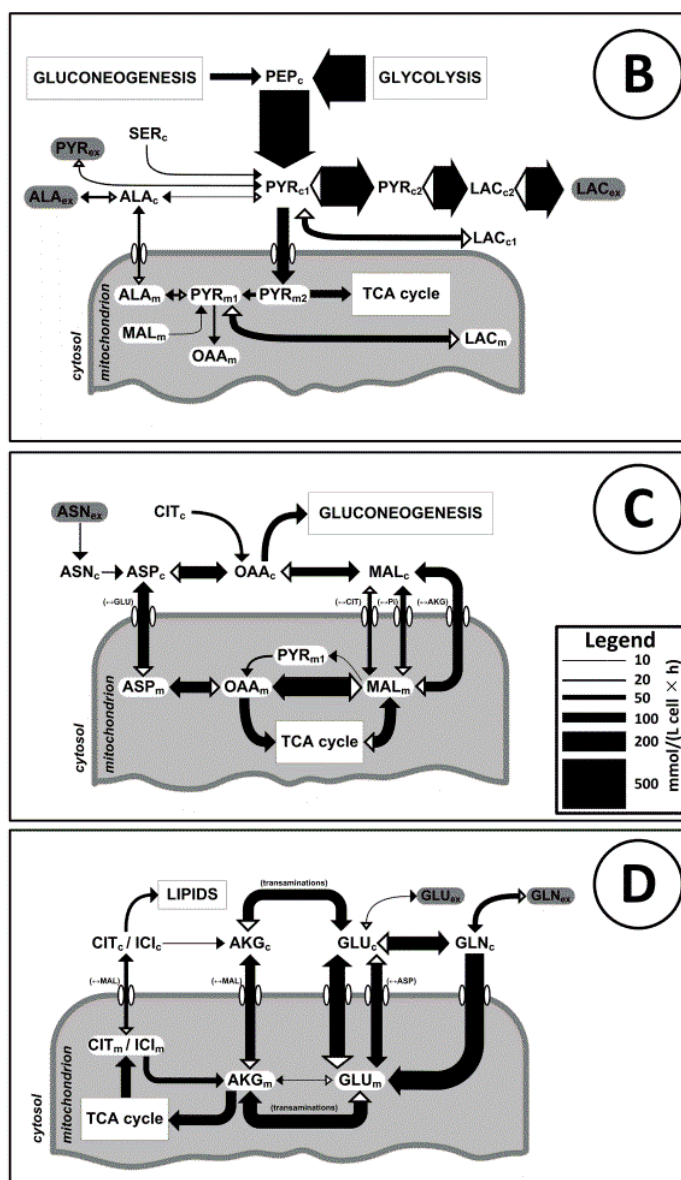


Figure 6-3. (B) Glycolysis and pyruvate metabolism compartmentation in CHO-K1 cells. (C) Metabolism of oxaloacetate (OAA), aspartate (ASP) and malate (MAL) in CHO-K1 cells. (D) Metabolism of glutamine (GLN), glutamate (GLU), α -ketoglutarate (AKG) and citrate (CIT) in CHO-K1 cells. The thickness of the lines is proportional to the net flux values. The full arrows indicate the direction of the net flux, and the empty arrows indicate a reversible flux. Subscripts meaning: c – cytosolic; ex – extracellular; m – mitochondrial; Abbreviations: AcoA – acetyl-CoA; AKG – α -ketoglutarate; ALA – alanine; ASN – asparagine; ASP – aspartate; CIT – citrate; FUM – fumarate; GLC – glucose; G6P – glucose-6-phosphate; PG – phosphoglycerate; PEP – phosphoenolpyruvate; GLN – glutamine; GLU – glutamate; GLY – glycine; ICI – isocitrate; ILE – isoleucine; LAC – lactate; LEU – leucine; LYS – lysine; MAL – malate; MET – methionine; OAA – oxaloacetate; PHE – phenylalanine; PYR – pyruvate; SER – serine; SUC – succinate; THR – threonine; TYR – tyrosine; VAL – valine.

6.4.5 Estimated intracompartamental pools

The use of INST- ^{13}C MFAs and the MIDs of intracellular metabolites required the simultaneous estimation of fluxes, reversibilities and intracompartamental concentrations of certain metabolites. Using the available sampled intracellular MIDs (Figure 6-2), we estimated the intracompartamental concentrations of 7 metabolites (Figure 6-4) and the intracellular concentration of two more, i.e. serine and glycine (Figure 6-4A). Interestingly, pyruvate and lactate cytosolic concentrations were very low (Figure 6-4A) and considerably high in the mitochondria. Lactate and pyruvate concentration distributions and the considered channeling effects explained the difference between extracellular and intracellular labeling in lactate when $[\text{U-}^{13}\text{C}_6]$ glucose was used (Figure 6-2A). Malate and fumarate had almost identical MID dynamics (Figure 6-2). This makes simultaneous determination of intracompartamental concentrations impossible. We set fumarate intramitochondrial concentration to a low value (0.1 mmol/L cell). The estimated malate intracompartamental concentration had an upper value of 5.2 mmol/L cell in the mitochondria and 3.9 mmol/L cell in the cytosol, and lower values of 2.1 mmol/L cell and 0.8 mmol/L cell respectively. Considering that high exchange between compartments equilibrates the labeling between compartments, the exact values of malate concentration for each compartment cannot be determined. The α -ketoglutarate concentration was high in the cytosol, and citrate was concentrated in the mitochondria. The high cytosolic α -ketoglutarate concentration might provide another reason why there was no estimated activity of cytosolic isocitrate dehydrogenase towards α -ketoglutarate synthesis. Alanine had comparable concentrations in both compartments. Aspartate was concentrated in the mitochondria, but only the upper threshold of the cytosolic concentration could be estimated. We also determined a relatively high cytosolic concentration of serine and glycine. The most concentrated metabolite was glutamate, with a mitochondrial concentration reaching almost 50 mmol/L cell, which might explain why glutamate is transported from the mitochondria. However, the cytosolic concentration of glutamate could not be estimated.

All metabolites except α -ketoglutarate were more concentrated in the mitochondria than in the cytosol. Also, the estimated concentrations of amino acids are higher than reported intracellular concentrations for CHO cells (Hansen and Emborg, 1994a; Lu et al., 2005). By applying INST- ^{13}C MFA, the average intracompartamental concentrations might be overestimated as an effect of assigning negligible values to concentrations that are not estimated. However, since the dynamics of the MIDs depends on the pool size / flux ratio, the intracompartamental concentrations cannot be higher than their estimated upper boundary. Parameter estimation using INST- ^{13}C MFA instead of experimental determination has the advantage that the concentrations are estimated *in vivo*, without the risk of metabolite leakage during quenching and extraction (Dietmair et al., 2010; Sellick et al., 2009; Wahrheit and Heinzle, 2013; Wahrheit and Heinzle, 2014). In addition, INST- ^{13}C MFA provided a method to estimate intracompartamental concentrations of key metabolites of the central carbon metabolism, which was not yet achieved experimentally.

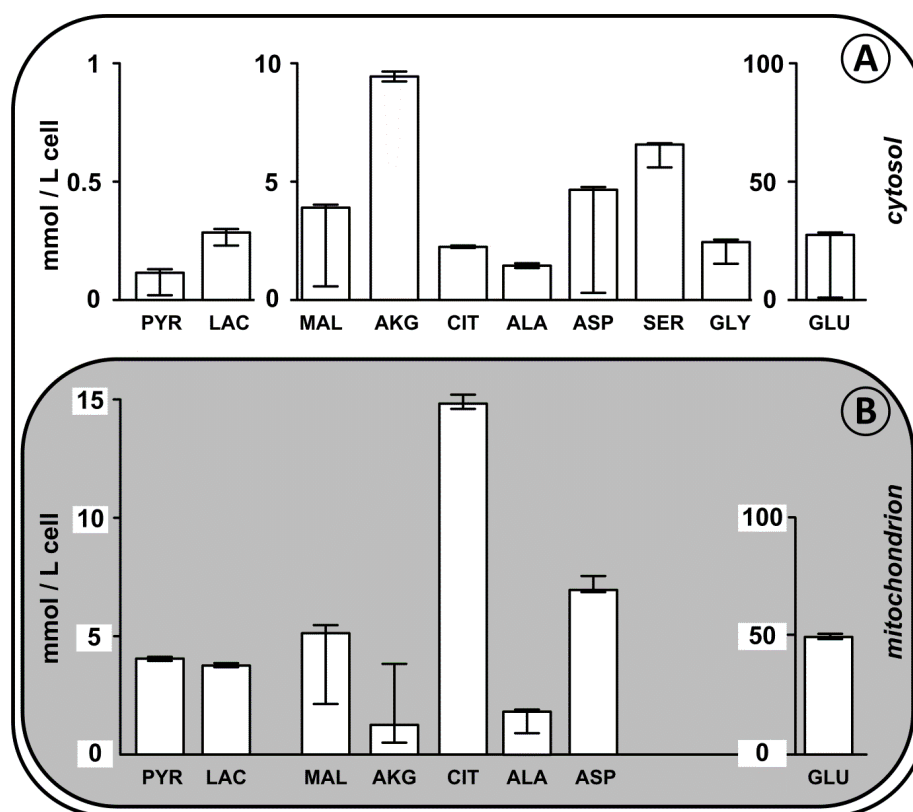


Figure 6-4. Cytosolic and mitochondrial concentrations of metabolites estimated using non-stationary ^{13}C metabolic flux analysis. The error bar represents the 95% confidence interval evaluated by refitting the model until the minimized objective function took the value of χ^2 ($0.95, n_r \text{ experimental points} - n_r \text{ parameters}$). Abbreviations: AKG – α -ketoglutarate; ALA – alanine; ASP – aspartate; CIT – citrate; GLU – glutamate; GLY – glycine; LAC – lactate; MAL – malate; PYR – pyruvate; SER – serine.

6.5 Conclusions

We estimated the fluxes and reversibility for the most complex metabolic network to date by applying INST- ^{13}C CMFA and using the intracellular and extracellular MID dynamics of metabolites obtained from two parallel labeling experiments with $[\text{U-}^{13}\text{C}_6]$ glucose and $[\text{U-}^{13}\text{C}_3]$ glutamine as labeled substrates. We used the labeling of MIDs during the exponential growth phase in the 2 – 18 h interval when the cells were at metabolic steady state. In the first 2 h of the labeling experiment, the MIDs of intracellular metabolites indicated a stress response to the cultivation condition. After 18 h, the metabolic state of the cells changed, visible by a shift in the MIDs of the metabolites. Most of the parameters were determined with narrow confidence intervals. They included: (1) metabolic fluxes in cycles and alternative pathways, (2) flux reversibility and (3) intracompartmental concentrations. This confirms that INST- ^{13}C CMFA is a powerful method that can resolve the metabolic fluxes in a network that included multiple mitochondrial transporters, reaction reversibility, metabolite exchange with the media and metabolite channeling. The activity at the mitochondria – cytosol boundary is complex, involving intense metabolite trafficking and cycling.

Malate and glutamate are both imported and exported via various mitochondrial carriers with the purpose of managing NADH in the two compartments and providing antiport partners for other metabolites. The anaplerotic and cataplerotic fluxes were negligible with phosphoenolpyruvate-carboxykinase being the highest cataplerotic flux. The aspartate-malate shuttle consumed cytosolic NADH and produced mitochondrial NADH. Aspartate and alanine were synthesized in the mitochondria, and then transported to the cytosol. However, this is only a single metabolic state of the CHO-K1 cells. We have evidenced that there are significant differences between the metabolic fluxes in CHO-K1 cells in different cultivation setups (shake flask vs. reactor), even if the two cultivations used the same cell line and the same media and the sampling was done during the exponential growth phase.

A most interesting finding was related to the different labeling patterns in intracellular and extracellular lactate, which could not be explained by cytosol-mitochondria compartmentation. We included four pyruvate pools, two dead-end lactate pools and lactate production channeling for modeling the observed difference in labeling. Our results show that a large mitochondrial lactate pool is maintained, most likely to control the mitochondrial NADH content. Also, due to channeling of lactate production, the cytosolic lactate concentration is very small. Because the fitting of intracellular lactate left room for improvement, it is possible that the network configuration around the pyruvate nodes consists of more complex microcompartmented structures (al-Habori, 1995). Such complexity is both a hindrance and an opportunity for INST- ^{13}C MFPA to characterize metabolic networks. We therefore believe that a systems biology approach that combines biological knowledge from experiments that unravel the spatial structure of the mammalian cell metabolism with realistic mathematical models is the strategy to follow when studying metabolic networks. Ideally, such strategy accepts feedback for guiding future experiments and creating new modeling paradigms that include the spatial organization of the metabolism.

6.6 Acknowledgements

We thank the Institute of Cell Culture Technology (University Bielefeld, Germany) for supplying the CHO-K1 cells. We thank the BMBF (German Federal Ministry of Education and Research) projects SysCompart [project ID 031555D] and OxiSys [project ID 031 5891 B] for funding.

6.7 Supplementary material

Supplementary material associated with this chapter can be found in chapter 12.

Part III

**Detailed studies of mitochondrial metabolism
using selectively permeabilized CHO cells**

7 High-throughput respiration screening of single mitochondrial substrates using permeabilized CHO cells

7.1 Abstract

We present a high-throughput respiration screening for functional in situ mitochondrial studies in permeabilized CHO cells. We verified transporter-mediated uptake and metabolization of single mitochondrial substrates and substrate combinations. The determination of oxygen uptake rates allowed a quantitative comparison between different conditions and a distinction of substrates into three groups providing an insight into TCA cycle regulation. Metabolic regulation was different for reactions (i) in the first half, (ii) in the second half and (iii) at the initiation of the TCA cycle. The mitochondrial metabolization of citrate, isocitrate, glutamine and glutamate was highly controlled by the energy state. In contrast, the metabolization of α -ketoglutarate, succinate, fumarate and malate was less controlled. Metabolization of pyruvate was very strictly regulated by several independent mechanisms. Furthermore, it was restricted by the availability of oxaloacetate required for the citrate synthase reaction. A moderate stimulation of pyruvate metabolization could be accomplished by feeding both pyruvate and aspartate simultaneously. The presented high-throughput respiration screening for functional mitochondrial studies allows differentiated and comprehensive conclusions about mitochondrial metabolic activities including TCA cycle regulation. Our novel approach provides a profound basis for the investigation of biological, biotechnological, medical, and pharmacological questions with mitochondrial background on a larger scale.

This chapter was submitted for publication as

Wahrheit J, Nonnenmacher Y, Sperber S, Heinzle E. High-throughput respiration screening of single mitochondrial substrates using permeabilized CHO cells

7.2 Introduction

The physiological function of mitochondria is essential for cellular energy metabolism and apoptosis, controlling life and death of a cell. Therefore, the assessment of mitochondrial function is of great importance for the biotechnological application of eukaryotic organisms. Even more, mitochondrial dysfunction has become central in the study and diagnosis of a variety of diseases. Essential metabolic pathways of mitochondria include oxidative phosphorylation, TCA cycle, initiation of gluconeogenesis, anaplerosis, β -oxidation of fatty acids, amino acid metabolism, C1-metabolism, and the urea cycle (Michal and Schomburg, 2012; Wahrheit et al., 2011). Mitochondria are also the primary site for generation and detoxification of reactive oxygen species (ROS) and are thus the major cause for oxidative stress (Adam-Vizi and Tretter, 2013).

The maintenance of an efficient energy metabolism as well as the prevention of apoptosis and oxidative stress are particularly critical factors in the energy-intensive production of therapeutic proteins using mammalian cell factories (Kim et al., 2012). A profound understanding of the CHO mitochondrial metabolism will assist in a more targeted and rational development of efficient bioprocesses for the manufacture of biopharmaceuticals. Mitochondrial dysfunction is associated with ageing and a wide range of severe diseases including neurodegenerative disorders (Albers and Beal, 2000; Chaturvedi and Flint Beal, 2013; Coskun et al., 2012; Saks et al., 1998), cancer (Fogg et al., 2012; Martin-Requero et al., 1986; Modica-Napolitano and Singh, 2004; Wallace, 2012), diabetes (Newsholme et al., 2012), metabolic syndrome and cardiovascular diseases (James et al., 2012). In particular an impaired energy metabolism and/or an increased production of ROS are thought to be responsible for the onset of pathological conditions (Lenaz, 2001).

In this study, we present a high-throughput method using permeabilized cells and respiration analysis for investigation of the mitochondrial metabolism. The application of selectively permeabilized cells and tissues is well established for *in situ* mitochondrial studies (Kuznetsov et al., 2008). Although the assessment of mitochondrial function *in vivo* has the highest physiological relevance, the investigation of intact cells is often not possible due to impermeability to many mitochondrial substrates and effectors. The *in situ* investigation of mitochondria is a useful and valuable trade-off between the use of intact cells and isolated mitochondria. Mitochondria within selectively permeabilized cells are directly accessible by effectors, thus allowing a comparable experimental control as for isolated mitochondria. Many cellular structures and interactions, e.g. with the cytoskeleton, are preserved after permeabilization, representing a situation that is closer to the actual *in vivo* situation. Selective permeabilization is faster, easier and requires less cell material than the isolation of mitochondria. Furthermore, artifacts due to the isolation procedure itself, e.g. mitochondrial damage, biased loss of mitochondrial subpopulations, are avoided. Therefore, selectively permeabilized cells represent a convincing model system for mitochondrial studies. It

provides a balance between ease of manipulation, precise experimental control and physiological relevance (Kuznetsov et al., 2008).

Respiration analysis as a general measure for mitochondrial function and dysfunction goes primarily back to the studies of Chance and Williams in the 1950s (Gosalvez et al., 1974). Since then, it has become well-established in the study of physiological and pathophysiological conditions related to mitochondrial metabolism. In classical studies, respiration is measured in an oxygraph involving a closed, stirred reaction vessel and a Clark electrode. Mitochondrial function is usually assessed by testing the functionality of different respiratory chain complexes using a substrate-titration approach (Frezza et al., 2007; Kuznetsov et al., 2008). Such closed systems provide the highest precision and sensitivity, yet require substantial experimental effort. Also open systems can be used for the determination of respiration rates when the volumetric mass (oxygen) transfer coefficient ($k_L a$) is known for the applied system (John et al., 2003). Microtiter plate-based assays for monitoring dissolved oxygen concentrations have proven to be a valuable tool for the assessment of cell viability and mitochondrial function (John et al., 2003), e.g. in toxicity screenings (Beckers et al., 2009; Noor et al., 2009; Strigun et al., 2012) and medium optimization studies (Deshpande et al., 2004). It has been used in high-throughput studies of mitochondrial toxicity, although the oxygen consumption has not been quantified in absolute terms (Porceddu et al., 2012).

Here, we apply high-throughput quantification of mitochondrial oxygen consumption using microtiter plates with optical oxygen sensors for an in-depth investigation of mitochondrial metabolism. In classical mitochondrial studies, the effects of different single substrates are not considered. We provide a more differentiated analysis turning the focus towards TCA cycle activities, feeding reactions and metabolic reactions not directly involved in the formation of NADH or FADH₂. A range of metabolites feeding the TCA cycle were selected according to known mitochondrial transport mechanisms described in literature (Arco and Satrustegui, 2005; Michal and Schomburg, 2012; Palmieri, 1994; Palmieri et al., 1993) and evidence of enzyme activity based on previous metabolic flux analysis studies, e.g. active reactions of pyruvate carboxylase and malic enzyme in CHO-K1 cells (Nicolae et al., 2014b; Wahrheit et al., 2014b). Selected metabolites were tested regarding their ability to stimulate respiration in permeabilized CHO suspension cells. The resulting oxygen uptake rates are a function of their transporter-mediated uptake and metabolization. The presented high-throughput set-up allows the parallel screening of a wide range of different substrates, combinations of substrates, and experimental conditions and most importantly a quantitative comparison between them. This represents a particular advancement since it facilitates a distinguished and comprehensive study of various mitochondrial activities. This provides a profound basis for the investigation of a wide range of biological, biotechnological, medical, and pharmacological questions. It allows differentiated conclusions about activities of mitochondrial transporters and enzymes and reflects the regulation of TCA cycle reactions. Such

detailed investigations will be very useful in complementing classical mitochondrial studies in future applications.

7.3 Materials and methods

7.3.1 Cell culture

CHO-K1 cells were cultivated in baffled shake flasks (250 ml, Corning, New York, USA) in a shaking incubator (Innova 4230, New Brunswick Scientific, Edison, NJ, USA) at 135 rpm (2 inches orbit), 37°C and 5% CO₂. The medium used was chemically defined, serum-free TC-42 medium (TeutoCell, Bielefeld, Germany), supplemented with 6 mM L-glutamine from a 240 mM stock solution in dH₂O. The cells were passaged at the latest 72 h after inoculation and seeded with a cell density of 4 - 5 × 10⁵ cells/ml.

7.3.2 Preparation of mitochondrial medium

The mitochondrial medium used in this study was derived from different media used for the assessment of respiration in isolated mitochondria (Madeira, 2012) and optimized with respect to osmolarity and ionic strength. The composition of the mitochondrial medium was as follows: 9.6 mM K₂HPO₄, 2.4 mM KH₂PO₄, 80 mM KCl, 75 mM sorbitol, 2 mM MgCl₂ and 100 μM EGTA. pH was set to 7.4 with 5 N KOH.

7.3.3 Microscopic characterization of permeabilized CHO cells

For microscopic investigation of permeabilized CHO cells a IX70 microscope (Olympus, Hamburg, Germany) linked with a digital CC12 camera (Olympus, Hamburg, Germany) was used. The duration of the permeabilization process was monitored with two different staining methods. For recording of the entry of Trypan blue into the cells, the cell suspension (10 × 10⁶ cells/ml) was mixed simultaneously with 0.01% (w/v) digitonin and Trypan blue dye. For recording the release of Calcein (Invitrogen, Darmstadt, Germany) from the cells, CHO-K1 cells were stained with 4 μg/ml Calcein-AM in TC-42 medium prepared from a stock solution of 1 mg/ml in DMSO for 20 min at 37°C and washed twice with PBS. The diffusion of the blue dye into the cells and the dilution of the fluorescent dye (excitation/emission: 495 nm/515 nm) visualize the membrane permeabilization of the cells. In both cases, 3 μl of cell suspension was inserted into a Countess[®] Cell Counting Chamber Slide (Invitrogen, Darmstadt, Germany) for recording of videos. The intactness of the mitochondrial membrane potential was verified by staining with Rhodamine 123 (excitation/emission: 535 nm/585 nm). A working solution of 1 mM Rhodamine 123 in mitochondrial medium was prepared from a 25 mM stock solution in DMSO. 5 × 10⁶ cells/ml were stained with 20 μM Rhodamine 123 by incubation at 37°C (protected from light) and washed in mitochondrial medium (centrifugation for 5 min at 380 × g). Cells were either first permeabilized

and then stained or pre-stained followed by permeabilization. For counterstaining of nuclei with DAPI (100 nM) (excitation/emission: 358 nm/461 nm) permeabilized cells were washed twice in mitochondrial medium. The stability of permeabilized cells and mitochondrial functionality in mitochondrial medium was investigated by checking the morphology of Trypan Blue and Rhodamine 123 stained cells 2 h and 3 h after permeabilization. Between sampling, the permeabilized cell suspension was maintained in a shaking incubator to avoid sedimentation of cells.

7.3.4 Experimental set-up of respiration measurements

CHO-K1 cells were harvested from a culture in the early exponential growth phase (48 - 50 h after inoculation) by centrifugation (5 min, $125 \times g$, Labofuge 400R, Function Line, Heraeus Instruments, Hanau, Germany) and resuspended in mitochondrial medium. The cell number was determined using an automated cell counter (*Countess[®] Automated Cell Counter*, Invitrogen, Karlsruhe, Germany) and set to 4×10^6 cells/ml. Selective permeabilization was performed by adding 0.005 % (w/v) digitonin from a 0.5 % stock solution in dH₂O and verified under the microscope using the Trypan blue exclusion method. 100 μ l of the permeabilized cell solution were transferred per well into a 96-well round-bottom *OxoPlate* (PreSens, Regensburg, Germany) containing 100 μ l of the respective substrate solutions (2-fold concentrated in mitochondrial medium). The respiration on each substrate (or combination of substrates) was assessed in triplicates, all solutions were pre-warmed to 37°C prior to use. The final cell concentration was 2×10^6 cells/ml. Final concentrations of tested substrates were 4 mM carbon substrate and 2 mM ADP if not stated otherwise.

Dissolved oxygen concentration was measured every 208 s in a fluorescence-reader (FLUOstar, BMG Labtechnologies, Offenburg, Germany) with an integrated shaker-unit and temperature control at 37°C, placed in an airtight box with 5 % CO₂. Before each measurement, the plate was shaken for 30 s (140 rpm, 4 mm orbit) in order to prevent sedimentation of the cells. Calibration and calculation of dissolved oxygen levels at each time point was performed as described in the literature (John et al. 2003).

7.3.5 Determination of the oxygen transfer coefficient $k_{L,a}$

Estimation of the oxygen transfer coefficient $k_{L,a}$ was performed using a sodium dithionite method (John et al. 2003). An oxygen-free solution was prepared by addition of 10 μ l 2% (w/w) sodium dithionite to 190 μ l dH₂O in a 96-well *OxoPlate*. Oxygen measurements in the fluorescence reader for $k_{L,a}$ determination were carried out in exactly the same way as respiration measurements. The dynamics of the re-saturation process were recorded by dissolved oxygen measurement using exactly the same set-up and protocol as described for the *OUR* estimation. This was performed in

triplicates for wells at different positions of the microtiter plate to prevent deviations caused by evaporation. The following equation (1) was computed in Berkeley Madonna:

$$\frac{dC_L}{dt} = k_L a (C_L^* - C_L) \quad (1)$$

C_L : oxygen concentration in the liquid phase

C_L^* : saturation concentration of oxygen in the liquid phase

The oxygen transfer coefficient was determined by fitting this model to the experimental data using the curve fit tool of Berkeley Madonna with $k_L a$ as the only variable.

Calculation of oxygen uptake rates (OUR)

A liquid phase oxygen balance was set up as follows:

$$\frac{dC_L}{dt} = k_L a (C_L^* - C_L) - OUR \cdot X \quad (2)$$

OUR : maximum specific oxygen uptake rate

X : cell concentration

Maximum specific OUR was determined by fitting the model to the experimental data (Figure 7-2). Prior to the fitting process, all values were converted from percent oxygen saturation to the respective molar concentration based on a maximum solubility for oxygen in water of 0.209 mmol/l (at 37°C). For the fitting process, C_L^* was set to 0.209 mmol/l. The maximum OUR was determined using a moving window technique. The following criteria were used for parameter estimation: (i) use at least 5 consecutive data points, (ii) integrate Equation (2) over respective time period, (iii) vary OUR and initial concentration of dissolved oxygen until obtaining a least square fit. During this procedure, the time window was varied to span the experimental space of each experiment. The maximal value of OUR was then used for further evaluations. MATLAB was used for these calculations. The initial delay in the decrease of the dissolved oxygen signal is most likely caused by small temperature deviations originating from pipetting procedures that had to be carried out at room temperature. As stated above, all component solutions were kept at 37 °C in the incubator prior to their use.

7.4 Results and Discussion

7.4.1 Microscopic characterization of permeabilized CHO cells

Selective plasma membrane permeabilization using digitonin generates functioning mitochondria enclosed in a cell ghost (Bahnmann et al., 2014; Kuznetsov et al., 2008). Since CHO cells have not commonly been used as biological system in mitochondrial studies, we performed different stainings to characterize the permeabilization of CHO suspension cells as quality control for the

preparation of intact, functional mitochondria. The duration of the permeabilization process was monitored by recording (1) the entry of Trypan Blue (MW 872.88 g/mol) into and (2) the release of Calcein (MW 622.55 g/mol) out of the permeabilized cells. Representative video snapshots are shown in Figure 7-1A and B. The staining of the permeabilized cells with Trypan Blue (Figure 7-1A) as well as the dilution of the fluorescent label Calcein (Figure 7-1B) was completed within 16 seconds. Calcein-stained cells without digitonin treatment were recorded as control to verify that the decrease in fluorescence intensity is due to dilution into the medium and not caused by a bleaching of the dye. Rhodamine 123 is a dye that specifically labels mitochondria depending on the electrochemical gradient across the inner mitochondrial membrane (Chen, 1988). We verified the mitochondrial integrity and intactness of the mitochondrial membrane potential in permeabilized cells by Rhodamine 123 staining (Figure 7-1C-E). Rhodamine 123 specifically labeled the mitochondria surrounding the nucleus as demonstrated by a counterstaining of the cellular nucleus using DAPI (Figure 7-1C). It made no difference if the cells were stained before or after permeabilization (Figure 7-1D). Furthermore, we verified the stability of the ghost cells while incubating in mitochondrial medium in a shaking incubator (Figure 7-1E). The ghost cell suspension remained mostly homogenous. After 3 h a little more aggregates of cells were observed. The permeabilized cells have a characteristic morphology that was maintained over at least 3 h. They are enlarged and swollen compared to non-permeabilized cells and have a knaggy, uneven surface (Figure 7-1E, magnification pictures). As shown in the little inserts (overlay of bright field and fluorescence pictures of Rhodamine 123 staining) in Figure 7-1E, the mitochondrial membrane potential remained intact during the investigated time period. In contrast, the mitochondria lost their metabolic activity when centrifuged after permeabilization most likely due to increased susceptibility to shear stress.

Following conclusions can be drawn from the microscopic characterization of permeabilized CHO cells: (1) Selective permeabilization of CHO suspension cells with digitonin is a very fast process within the range of seconds. A longer incubation period is not necessary to complete the permeabilization. (2) Molecules can freely diffuse in and out of the cell ghost as demonstrated by Trypan blue entry and Calcein release. This indicates that soluble components in the extracellular medium and the cytosol are quickly equilibrated with each other. (3) Intactness of the mitochondrial membrane potential was verified by Rhodamine 123 staining indicating mitochondrial integrity and functionality. (4) The cell ghosts maintain a stable cellular morphology containing functional mitochondria for at least 3 h during incubation in mitochondrial medium in a shaking incubator.

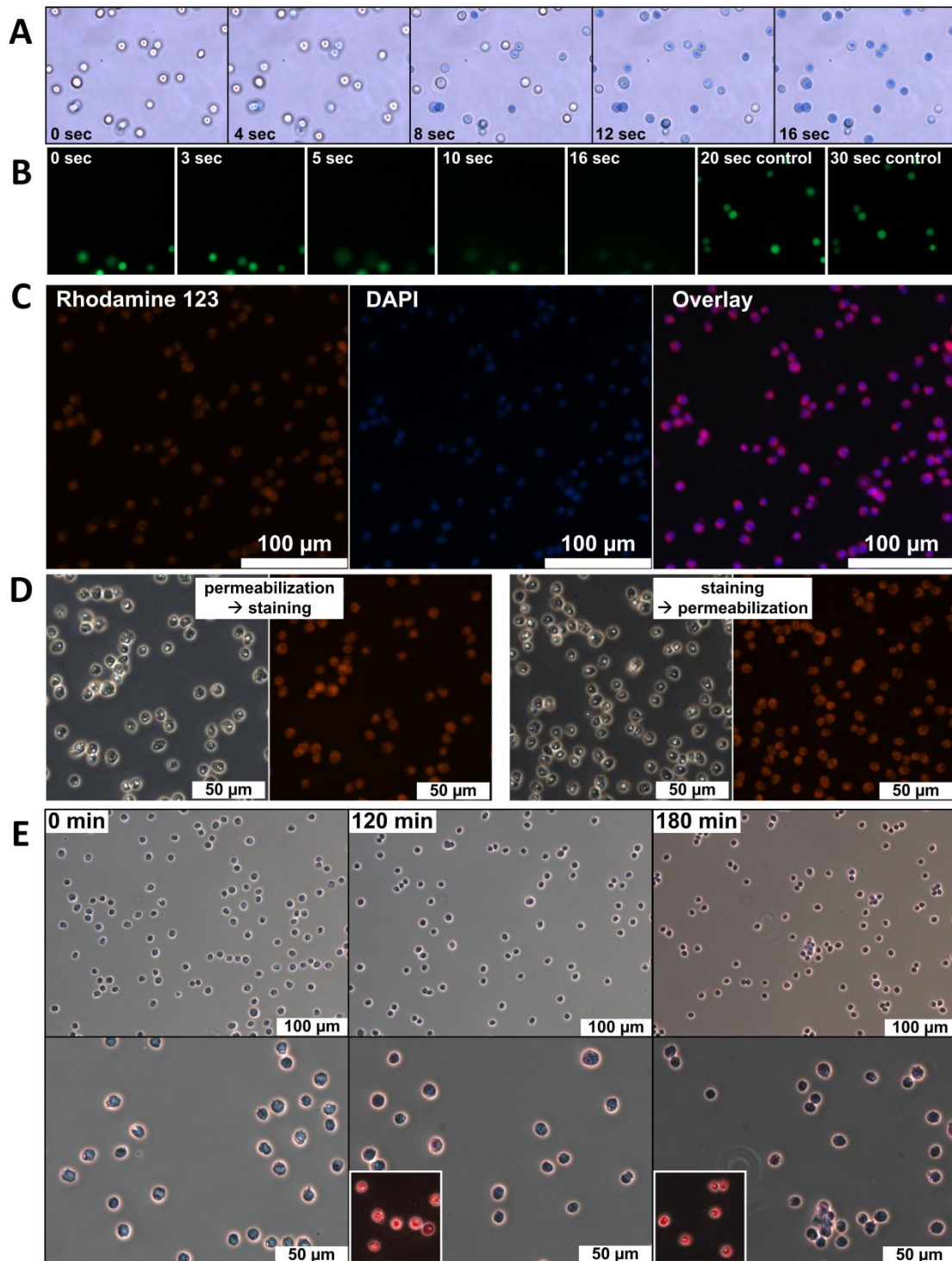


Figure 7-1 Microscopic characterization of selectively permeabilized CHO suspension cells. (A) Monitoring of the permeabilization process by Trypan blue entry into permeabilized cells. (B) Monitoring of the permeabilization process by Calcein release from pre-stained permeabilized cells. (C) Rhodamine 123 staining of mitochondria with an intact membrane potential and DAPI staining of cellular nuclei. (D) Rhodamine 123 staining of functional mitochondria before and after permeabilization. (E) Morphology of Trypan blue stained CHO cell ghosts 0, 120 min, and 180 min after permeabilization. In the small inserts, Rhodamine 123 stained permeabilized cells (overlay of bright field and fluorescence pictures) at the respective time points are depicted.

7.4.2 Screening of mitochondrial substrates with and without ADP stimulation

We tested different TCA cycle intermediates and selected metabolites feeding into the TCA cycle for their ability to stimulate mitochondrial respiration in permeabilized cells. Since it was not possible to centrifuge and wash the permeabilized cells without loss of metabolic activity, two additional controls were included in order to test the experimental set-up: (1) permeabilized cells in mitochondrial medium without substrate and (2) permeabilized cells in mitochondrial medium containing only 2 mM ADP but no carbon substrate (Figure 7-2 A, NO SUBSTRATE). No oxygen consumption was determined for both negative controls. As reckoned by the microscopic characterization of permeabilized cells, the free cytosolic components are quickly equilibrated with the surrounding medium after plasma membrane permeabilization. In the applied experimental set-up, the cytosolic components are approximately diluted by a factor 1000 (volume of 4×10^5 cells $\sim 2.3 \times 10^{-7}$ L; reaction volume in well = 2×10^{-4} L). Since we observed no respiration in the controls, we demonstrated that residual metabolites present in the crude ghost cell suspension are sufficiently diluted to not affect mitochondrial respiration studies.

Mitochondrial respiration was measured on all tested TCA cycle intermediates, citrate (CIT), isocitrate (ISO), α -ketoglutarate (AKG), succinate (SUC), fumarate (FUM) and malate (MAL), as well as on pyruvate (PYR), glutamate (GLU) and glutamine (GLN) feeding into the TCA cycle (Figure 7-2A, w/o ADP). Furthermore, for these substrates, a substantial stimulation of respiration was achieved by adding 2 mM ADP (Figure 7-2A, w/ ADP). Respiration on PYR with and without ADP-stimulation was much lower than for all other substrates. On aspartate (ASP) as substrate, respiration was found neither with nor without addition of ADP.

ISO, AKG, MAL, PYR, GLU can be classified as complex I substrates feeding NADH generating reactions, while the complex II substrate SUC directly feeds FADH_2 into the respiratory chain. The other tested substrates (CIT, FUM, GLN, ASP) do not directly stimulate NADH or FADH_2 generating reactions. They may, however, be converted into complex I or complex II substrates, resulting in an indirect stimulation of respiration. Respiration on specific substrates proves their transporter-mediated uptake into the mitochondria and indicates activity of the metabolic reactions required to metabolize these substrates. A significant increase in the respiration rates upon ADP stimulation indicates coupling of electron transport and oxidative phosphorylation. It provides evidence for the functionality of the mitochondria within the permeabilized cells (Brand and Nicholls, 2011).

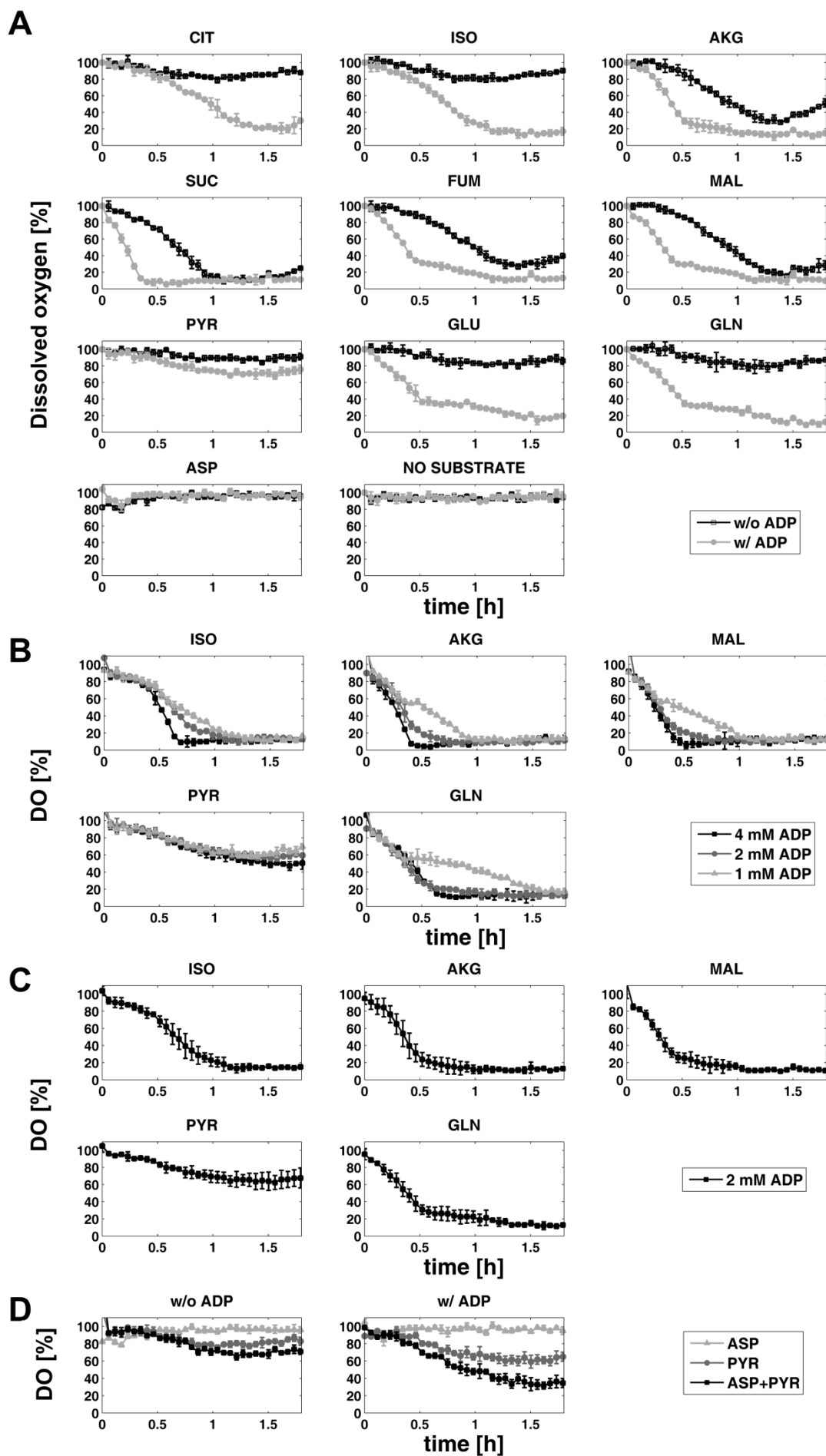
Interestingly, for AKG, FUM, MAL, GLU and GLN, two distinct phases could be distinguished upon ADP stimulation. A first phase of strong respiration that was even increasing was followed by a second phase characterized by a nearly stabilized respiration as seen by almost constant but low dissolved oxygen concentration. The second phase represents a state of ADP depletion as was confirmed by a rough estimation of ADP consumption based on OUR and a P/O quotient of 2.5.

Due to ATP hydrolyzing reactions, ADP will not be completely exhausted, however, but is limiting as ATP synthase substrate.

The impact of different ADP concentrations was investigated for selected substrates that had shown a response in the first respiration screening (Figure 7-2B). We observed an increase in respiration with increasing ADP concentrations for ISO, AKG, MAL, and GLN. For PYR, however, respiration was not significantly different upon stimulation with different ADP concentrations. In addition, we compared the respiration profiles of the first screening with the results of the 2 mM ADP profile of the second screening to validate the reproducibility of the experimental set-up (Figure 7-2C). We obtained highly reproducible respiration profiles with low standard deviations for separate biological experiments.

Since the application of ASP alone did not stimulate respiration, we hypothesized that we might get a response if we add a suitable reaction partner. ASP can enter the mitochondria via the aspartate/glutamate antiporter. Inside the mitochondria, it can be converted into oxaloacetate (OAA) which is an essential reaction partner for acetyl-CoA in the condensation to CIT via the citrate synthase (CS) reaction. No mammalian transporter for OAA has been described (Arco and Satrustegui, 2005; Michal and Schomburg, 2012). Thus, we tested the combination of the substrates PYR and ASP. The combination of 2 mM PYR with 2 mM ASP resulted in stronger respiration than 2 mM PYR alone (Figure 7-2D).

Figure 7-2 Mitochondrial respiration in permeabilized CHO cells upon stimulation with different substrates. (A) Respiration on single metabolites (4 mM) without ADP stimulation (w/o ADP) and upon stimulation with 2 mM ADP (w/ ADP). (B) Respiration on selected metabolites (4 mM) upon stimulation with 1 mM, 2 mM or 4 mM ADP. (C) Reproducibility of respiration profiles between separate experiments ($n = 2$). Respiration on selected metabolites (4 mM) upon stimulation with 2 mM ADP. (D) Respiration on 2 mM aspartate, 2 mM pyruvate, and the combination of 2 mM pyruvate with 2 mM aspartate without ADP (w/o ADP) and upon stimulation with 2 mM ADP (w/ ADP). In A, B and D mean values of dissolved oxygen (DO) [%] with standard deviations of three replicates using the same cell material are shown. In C mean values of DO [%] with standard deviations of two biological replicates from experiments with separate preparation of permeabilized CHO cells are shown.



7.4.3 Comparison of oxygen uptake rates (OUR) between different mitochondrial substrates and substrate combinations

Knowledge on the oxygen transfer coefficient $k_L a$ for the applied experimental system facilitates the calculation of specific oxygen uptake rates (OUR) (see material and methods section) and a quantitative comparison between different substrates and conditions. The different tested substrates covered a wide range of OUR (Figure 7-3). The highest OUR were measured for the substrate SUC (w/o ADP 3.59 ± 0.35 fmol/(cell \times min); w/ ADP 6.65 ± 0.58 fmol/(cell \times min)), the lowest for PYR (w/o ADP 0.48 ± 0.05 fmol/(cell \times min); w/ ADP 1.50 to 1.76 fmol/(cell \times min)). This accounts for a difference of 4 to 7 times stronger respiration on SUC compared to PYR. The combination of 2 mM PYR and 2 mM ASP resulted in a 1.4 to 2.4 times increase of OUR compared to 4 mM PYR alone. Most substrates used could be classified into two groups of metabolites characterized by a similar response. OUR on CIT, ISO, GLU and GLN were in a similarly low range between 0.70 and 0.84 fmol/(cell \times min) corresponding to only 20% of the respiration on SUC (Figure 7-3). In contrast, the substrates AKG, FUM and MAL were characterized by similarly high OUR in a range between 2.71 and 2.77 fmol/(cell \times min), which was only 25% lower than the respiration on SUC. In accordance with the proposed grouping, stimulation of respiration by ADP was modest for AKG, FUM and MAL and while a substantial increase of OUR upon ADP stimulation was determined for CIT, ISO, GLU and GLN. OUR increased with increasing ADP concentrations approaching a saturation effect. However, on PYR as substrate the stimulation effect of different ADP levels was negligible.

The OUR and stimulating effects of ADP determined in our study were in a similar range with literature data presented for permeabilized CHO cells (Kim et al., 2006) and other mammalian cells (Clerc and Polster, 2012; Duicu et al., 2013; Manko et al., 2013; Picard et al., 2012) or isolated mitochondria from different tissues (Gottlieb et al., 2002; Yao et al., 2003). However, an absolute comparison between different studies is difficult since the respiration rates are specific for substrates or substrate combinations, tissue, species and cell line and also dependent on experimental conditions and history of cells, e.g. the training state and fitness level of cells (Brand and Nicholls, 2011; Gnaiger, 2009; Gnaiger, 2012). Furthermore, it has been shown, that the mitochondrial affinity to ADP is substantially lower *in situ* in permeabilized cells and closer to the *in vivo* situation compared to isolated mitochondria. In addition, the apparent K_M values for ADP were shown to be strongly tissue-dependent (Kuznetsov et al., 1996; Kuznetsov et al., 2008; Saks et al., 1993; Saks et al., 1998).

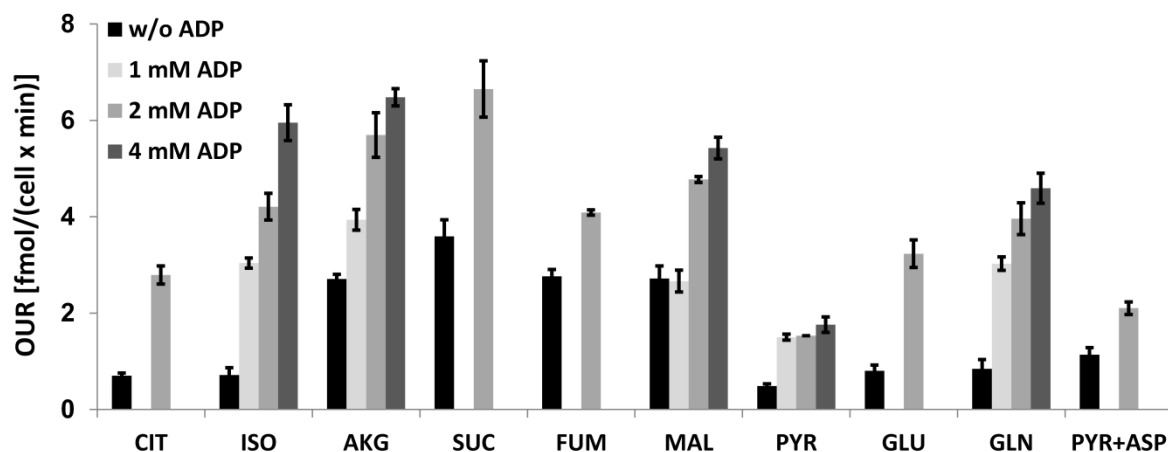


Figure 7-3 Oxygen uptake rates on different mitochondrial substrates. Oxygen uptake rates (OUR) [fmol/(cell × min)] in permeabilized CHO cells on different carbon substrates (4 mM) (w/o ADP) and upon stimulation with 1 mM, 2 mM or 4 mM ADP. Shown are mean values and standard deviations of three technical replicates.

7.4.4 Partial reconstitution of the mitochondrial metabolism

In the following section, we illustrate what information can be derived from such straightforward investigations. In contrast to the vast majority of previous mitochondrial studies, the aim of this study was neither testing the functionality of different respiratory chain complexes nor evaluating maximum capacities of oxidative phosphorylation nor a detailed study of mitochondrial transport. We focused on investigating the effects of single mitochondrial substrates and a partial reconstitution of the mitochondrial metabolism, i.e. mainly the TCA cycle, feeding reactions and mitochondrial transport. The application of substrate combinations, with redundant effects, e.g. PYR, MAL and GLU directly yielding NADH for stimulating complex I, as usually applied in former studies (Gnaiger, 2012) of mitochondrial bioenergetics, does not allow a distinction of single substrate effects. Differences between tested substrates can be explained as a function of enzyme activities, transport capacity, as well as specific regulatory events.

7.4.5 Distinction of low control and high control substrates

The comparison of OUR between different single substrates enabled a classification into different groups. We determined high OUR and relatively low stimulation by ADP for the substrates AKG, SUC, FUM and MAL. In contrast, CIT, ISO, GLU and GLN were characterized by low OUR and a large stimulation of respiration by ADP addition. This clustering corresponds to a group of highly controlled substrates and a group of substrates with lower control (Figure 7-4). PYR and the combination of PYR and ASP were characterized by both low OUR and a modest ADP stimulation and are therefore discussed separately.

The four major regulatory enzymes known to control the TCA cycle are (1) the pyruvate dehydrogenase (PDH), (2) the citrate synthase (CS), (3) the isocitrate dehydrogenase (IDH), and (4) the α -ketoglutarate dehydrogenase (AKGDH). These enzymes are strictly regulated by product inhibition and by the cellular energy status, i.e. stimulation by ADP and inhibition by high concentrations of ATP and NADH (Michal and Schomburg, 2012). The TCA cycle can be separated in a highly controlled first half of the cycle, beginning with the reactions of PDH and CS, and a second half of much lower control starting after the AKGDH reaction (Figure 7-5A).

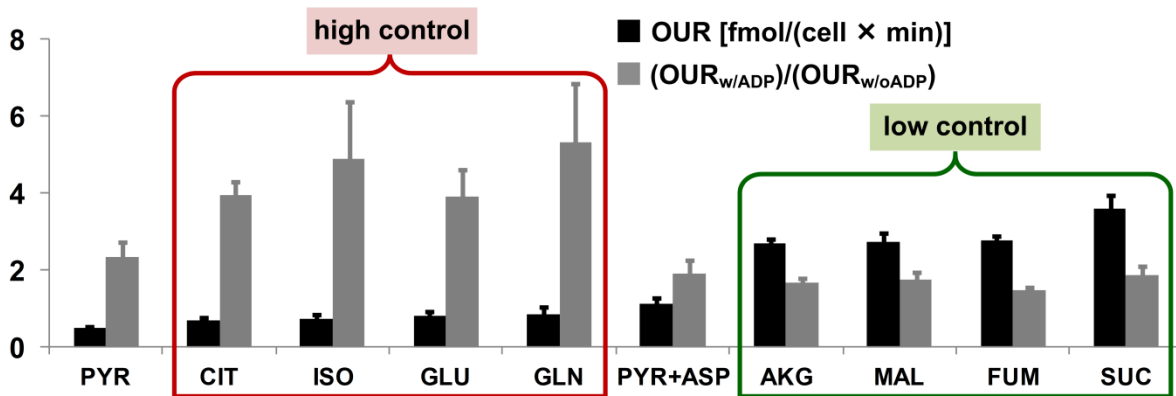


Figure 7-4 Distinction of low control and high control substrates by comparison of oxygen uptake rates (OUR) with and without ADP stimulation. The tested substrates are sorted in ascending order of OUR [fmol/(cell × min)] values of respiration without ADP stimulation (black bars). The fold-change of respiration upon ADP stimulation was calculated as the ratio between the OUR with 2 mM ADP stimulation and the OUR without ADP stimulation (grey bars). For OUR, mean and standard deviations of three replicates are shown (black bars). Mean and standard deviations of OUR ratios (grey bars) were determined by Monte Carlo simulation ($n = 100$) using the standard deviation of the OUR estimations.

7.4.5.1 Mitochondrial metabolism of α -ketoglutarate, succinate, fumarate and malate is little controlled

MAL, FUM and SUC are transported by the mitochondrial dicarboxylate carrier in exchange for phosphate (Berg et al., 2012). MAL is a complex I substrate directly generating NADH by malate dehydrogenase (MDH). FUM indirectly stimulates complex I respiration after conversion into MAL via fumarase. The complex II substrate SUC is converted to FUM by the succinate dehydrogenase (SUCDH) reducing FAD to FADH₂. The SUCDH participates in both the TCA cycle and the respiratory chain, thus allowing for a more direct and probably faster electron transfer than complex I substrates. In classical mitochondrial studies, SUC is used in combination with the complex I inhibitor rotenone. In our study, however, complex I activity is not excluded. The dehydrogenation of SUC fuels fumarase and MDH, the following reactions in the TCA cycle. NADH generation by MDH will additionally stimulate complex I respiration. SUC, FUM and MAL enter the TCA cycle

in the less regulated second part of the cycle and directly fuel the cycle between malic enzyme (ME) and pyruvate carboxylase (PCx) (Figure 7-5A). The existence and activity of this cycle has been proven in recent metabolic flux analysis studies of this CHO cell line (Nicolae et al., 2014b). The ME-PCx cycle results in the hydrolysis of ATP, thus removing its inhibiting effect and stimulating respiration. The dynamics of the dissolved oxygen measurements with a sigmoidal increase of OUR that is seen in the sigmoidal decrease of dissolved oxygen tension further indicate an autocatalytic effect in stimulating this cycle and respiration (Figure 7-1). The direct feeding of electrons into the respiratory chain in combination with a simultaneous stimulation of complexes I and II and a strong stimulation of the ATP-hydrolyzing cycle explain that SUC caused the highest respiration rates of all tested substrates. The ME-PCx cycle is responsible for the high respiration rates on MAL, FUM and SUC when ADP is not supplied and has to be regenerated by this cycle. Addition of ADP and the mitochondrial energy status have only a low effect in this little controlled part of the TCA cycle. Consequently, we observed relatively high respiration rates with and without ADP stimulation.

AKG is transported by the α -ketoglutarate-malate carrier in exchange with MAL or other dicarboxylates. As substrate of the feedback inhibited enzyme AKGDH, AKG theoretically belongs to the first part of the TCA cycle (Figure 7-5A). However, concerning OUR and ADP stimulation its behavior is similar to the little controlled substrates (Figure 7-4). This indicates that the downstream reactions of the TCA cycle, namely succinyl-CoA synthetase, SUCDH, fumarase and MDH, are fast enough that the feedback inhibition (e.g. by succinyl-CoA) does not come into effect. Since AKG enters the mitochondria in exchange with a dicarboxylate removed from the mitochondria, the equilibrium is shifted towards forward reactions additionally promoting a fast metabolization of AKG. Fueling of these reactions also feeds the ATP-hydrolyzing ME-PCx cycle. Therefore, the high respiration rates on AKG can be explained by the proximity to the SUCDH facilitating a direct electron transfer, very fast and little controlled downstream reactions and additionally a stimulation of the ME-PCx cycle.

7.4.5.2 Mitochondrial metabolization of citrate, isocitrate, glutamine and glutamate is highly controlled

ISO and CIT enter the mitochondria through the tricarboxylate transporter in exchange with MAL or other dicarboxylates. For GLU (Palmieri, 1994) and GLN (Palmieri et al., 1993), different transport systems are described. The substrates ISO and GLU represent complex I substrates stimulating respiration by NADH generation via IDH and glutamate dehydrogenase (GDH). CIT and GLN stimulate respiration indirectly by supplying ISO and GLU via reactions of aconitase and glutaminase, respectively. All four substrates enter the TCA cycle in its highly controlled first part and converge into the mitochondrial AKG pool (Figure 7-5A). CIT, ISO, GLN and GLU can potentially also fuel the following reactions of the TCA cycle. The low respiration on these

substrates can be explained by an efficient feedback inhibition at the sites of the IDH and AKGDH reactions. However, the high respiration rates on AKG suggest a minor regulatory role for the AKGDH. The addition of ADP results in substantial stimulation of respiration (Figure 7-4). Since we observed significantly lower OUR on GLU and GLN than on AKG this further points to a regulation of GLU and GLN transport.

7.4.5.3 Initiation of the TCA cycle – the interplay of pyruvate and aspartate

The application of PYR resulted in the lowest respiration rates of all tested substrates. Although, we observed a significant yet moderate stimulation of respiration upon ADP addition, there was no concentration dependent effect of ADP. Considering the fact that PYR besides GLN can be regarded as the major substrate feeding the mitochondrial metabolism in CHO cells (Wahrheit et al., 2014a; Wahrheit et al., 2014b), this finding was surprising. The low respiration on PYR might indicate a bottleneck in metabolism, either at the site of the pyruvate carrier (PyC) or at the site of pyruvate oxidation via the strictly regulated PDH.

The PDH requires free CoA as a co-substrate that is only available at limited amounts in mitochondria. Regeneration is only possible via the reaction catalyzed by CS (Figure 7-5A). The PDH uses a reaction mechanism that is equivalent to the AKGDH. High respiration rates found on AKG indicate that it is efficiently further metabolized to SUC by succinyl-CoA-synthetase. However, different to the succinyl-CoA-synthetase reaction, the CS reaction requires the second substrate OAA to proceed in the cycle. The mitochondrial PCx reaction has been shown to be active in CHO cells (Goudar et al., 2010; Nicolae et al., 2014b; Templeton et al., 2013). Thus, OAA can be supplied via active PCx. The PCx reaction, however, is strictly regulated. It requires acetyl-CoA as an essential allosteric activator and ATP as energy source (Michal and Schomburg, 2012). In contrast to the AKGDH and to the other regulated enzymes of the TCA cycle, the PDH is additionally controlled by reversible phosphorylation through pyruvate dehydrogenase kinase (PDK) (Modak et al., 2002; Zeng et al., 2002) (Figure 7-5B).

The low OUR is explained by a direct competitive inhibition of PDH by its products acetyl-CoA and NADH. In addition, acetyl-CoA and NADH allosterically stimulate PDK. ADP competitively inhibits PDK, resulting in a partial activation of PDH and a stimulation of NADH generation and respiration. However, the missing concentration-dependent effect of ADP stimulation indicates a moderate effect of ADP. This finding suggests that the unavailability of free CoA and inhibiting effects of acetyl-CoA and NADH are predominating and cannot completely be antagonized by ADP stimulation.

We tested the hypothesis that an additional supply of OAA could stimulate the TCA cycle. In contrast to yeast cells, there has been no evidence of a mitochondrial transporter for OAA in mammalian cells (Arco and Satrustegui, 2005; Michal and Schomburg, 2012). Therefore, OAA

itself could not be used in the set-up using intact mitochondria. MAL is directly converted to OAA via MDH and could be used to supply OAA. However, since MAL itself is a complex I substrate and stimulates respiration with high OUR, it is not a desirable reaction partner in this question. Therefore, we decided to test the combination of PYR and ASP.

We found a significant stimulation of respiration on PYR by addition of ASP, although no respiration on ASP alone was detectable. ASP enters the mitochondria via exchange with GLU (aspartate/glutamate carrier). The mitochondrial aspartate aminotransferase (ASAT) converts ASP and AKG into OAA and GLU. Thus, catalytic amounts of AKG have to be available to initiate the transaminase reaction. Subsequently, AKG can also be regenerated in the process of the TCA cycle (Figure 7-5B).

When the substrates PYR and ASP were combined, the conversion of ASP to OAA via active ASAT provides a reaction partner for acetyl-CoA fueling the CS reaction. The condensation of acetyl-CoA and OAA via the CS reaction has several consequences. First, the removal of acetyl-CoA as predominant inhibitor results in a stimulation of PDH. Second, due to the release of CoA, its limitation is unmade further stimulating PDH. Third, the production of CIT and following ISO fuels the IDH reaction. This leads to an increase in NADH production and a stimulation of respiration. However, increased ATP production due to stimulated respiration supports the phosphorylation of PDH by the inhibiting PDK, resulting in an efficient feedback inhibition of PDH and of following reactions in the TCA cycle and overall moderate respiration rates (Figure 7-5B).

We conclude that PYR and ASP are both transported into the mitochondria and metabolized. The mitochondrial metabolization of PYR is, however, very strictly regulated. A lack of the reaction partner OAA for the PDH product acetyl-CoA results in stagnation of the TCA cycle. An increased supply of OAA (e.g. by addition of ASP) stimulates PYR metabolization moderately. This bottleneck of mitochondrial metabolism might be involved in an impaired coupling between glycolysis and TCA cycle. An unbalanced supply of acetyl-CoA and OAA, which are both necessary to initiate the TCA cycle, might contribute to the phenomenon of overflow metabolism with high lactate excretion as commonly observed in CHO cells (Wahrheit et al., 2014a; Wahrheit et al., 2014b).

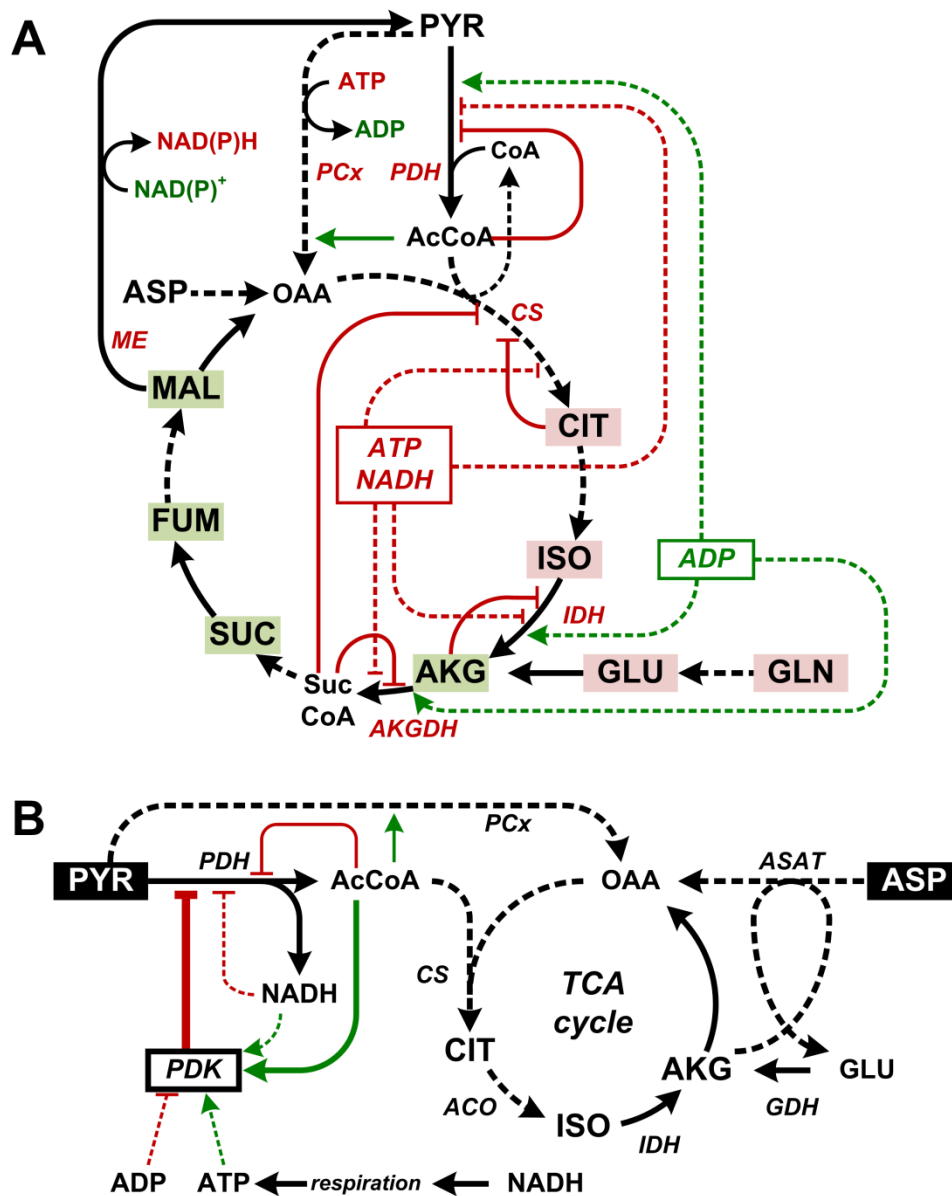


Figure 7-5 Regulation of the TCA cycle and the pyruvate dehydrogenase reaction. (A) High control substrates CIT, ISO, GLU, and GLN (Figure 7-4) are highlighted in red. Low control substrates AKG, SUC, FUM, and MAL (Figure 7-4) are highlighted in green. (B) Interplay of pyruvate and aspartate in fueling the TCA cycle and stimulating mitochondrial respiration. The activity of PDH, CS, IDH, AKGDH, PCx and ME, all printed in red, controls the TCA cycle activity (A). NADH or FADH₂ generating reactions are indicated by solid arrows, reactions feeding these NADH or FADH₂ generating reactions are indicated by dotted arrows. Inhibition and stimulation by competitive or allosteric effects is indicated by red and green arrows where dashed lines are used for ATP, ADP and NADH and solid lines for metabolites. The thick solid line in B indicates the inactivation of PDH by phosphorylation. Abbreviations: PDH pyruvate dehydrogenase, PDK pyruvate dehydrogenase kinase, CS citrate synthase, ACO aconitase, IDH isocitrate dehydrogenase, AKGDH α -ketoglutarate dehydrogenase, GDH glutamate dehydrogenase, ASAT aspartate aminotransferase, PDK pyruvate dehydrogenase kinase, PCx pyruvate carboxylase, ME malic enzyme.

7.5 Concluding remarks

We present a high-throughput method for a quantitative investigation of the mitochondrial metabolism. The experimental set-up was validated by a microscopic characterization of permeabilized cells and by showing the specificity and reproducibility of respiration on tested substrates. As an example, we tested the effect of ADP stimulation on respiration and we were able to obtain valuable information about regulation of mitochondrial metabolism. We demonstrated that the feedback inhibition of succinyl-CoA is abrogated by the fast action of downstream reactions in the TCA cycle. We further showed the superior effect of CoA limitation and acetyl-CoA product inhibition and a lower effect of the regulation by ADP on PDH activity.

7.6 Acknowledgements

We thank Vasileios Delis and Christian Weyler for fruitful discussions. We thank the Institute of Cell Culture Technology (University Bielefeld, Germany) for supplying the CHO-K1 cells and the BMBF (German Federal Ministry of Education and Research) projects SysCompart (project ID 031555D), OxiSys (project ID 031 5891 B) and Virtual Liver Network (project ID 0315738) for funding.

8 Elementary mode analysis of the mitochondrial metabolism in selectively permeabilized CHO cells

8.1 Abstract

Metabolic compartmentation is a key feature of mammalian cells. Mitochondria are the powerhouse of the cell, responsible for respiration and the TCA cycle. Mitochondrial dysfunctions are related to diseases and the aging process. It is therefore important to understand the mitochondrial metabolism when searching for eventual targets for treatments. We accessed the mitochondrial metabolism of the economically important CHO cells using selective permeabilization. We tested several substrates without and with addition of ADP. Based on quantified uptake and production rates, we could determine the contribution of different elementary flux modes to the metabolism of a substrate or substrate combination. ADP stimulated the uptake of most metabolites, directly by serving as substrate for the respiratory chain, thus removing the inhibitory effect of NADH, or as allosteric effector. Addition of ADP favored substrate metabolization to CO₂ and did not enhance the production of other metabolites. The controlling effect of ADP was more pronounced when we supplied metabolites to the first part of the TCA cycle: pyruvate, citrate, α -ketoglutarate and glutamine. In the second part of the TCA cycle, the rates were primarily controlled by the concentrations of C4-dicarboxylates. Without ADP addition, the activity of the pyruvate carboxylase – malate dehydrogenase – malic enzyme cycle used the ATP produced by oxidative phosphorylation. Aspartate was taken up only in combination with pyruvate, whose uptake also increased, a fact explained by complex regulatory effects. Isocitrate dehydrogenase and α -ketoglutarate dehydrogenase were identified as the key regulators of the TCA cycle. We have shown that selectively permeabilized cells are a suitable system for studying the mitochondrial metabolism and regulation.

This chapter is in preparation for submission as

Nicolae A, **Wahrheit J**, Nonnenmacher Y, Weyler C, Heinzle E. Elementary mode analysis of the mitochondrial metabolism in selectively permeabilized CHO cells

8.2 Introduction

Eukaryotic cells are able to tune their complex metabolism through compartmentation. This involves confining reactions to designated compartments and controlling the access of metabolites through specific transporters. Mitochondria play an important part in the organization of the eukaryotic cell metabolism (Wahrheit et al., 2011). They work as the powerhouse of the cell, being responsible for the TCA cycle, oxidative phosphorylation and other essential reactions in the central carbon metabolism. Furthermore, mitochondria play a key role in the signaling processes leading to apoptosis (Kroemer et al., 2007). Mitochondrial dysfunctions are associated with the aging process and with a wide range of human diseases (Calvo et al., 2006; Duchen, 2004; Lemasters, 2007; Moreno-Sanchez et al., 2014; Nassir and Ibdah, 2014; Raimundo et al., 2011; Thiele et al., 2005). Metabolite traffic between cytosol and mitochondria is mediated by carriers. These carriers, excellently reviewed by Palmieri (Palmieri, 2013), have important roles in physiological and pathological processes (Gutierrez-Aguilar and Baines, 2013). Studies related to mitochondrial function and metabolism have been so far focused on isolated features, like respiration and the respiratory chain (Frezza et al., 2007; Kuznetsov et al., 2008) or on the function of single mitochondrial transporters. Even after the advent of the systems biology era, the studies focused on the mitochondrial metabolic network as a whole remain scarce (Balaban, 2006). So far, the most complex studies related to mitochondrial metabolism used enzyme kinetics, but their results are limited by insufficient knowledge about regulation and parameter values (Smith and Robinson, 2011; Wu et al., 2007). Studying the mitochondrial metabolism in whole cells is complicated by the overlapping with other cellular reactions and by the limited accessibility of the mitochondria. Selective permeabilization using digitonin (Kuznetsov et al., 2008) is a simple and efficient way to access mitochondria while maintaining their functionality (Bahnemann et al., 2014).

Because mitochondria are capable of taking up several metabolites, either alone or in combination, process them through their metabolic network and secrete resulting metabolites, new methods are required for analyzing the data obtained from studies of the mitochondrial metabolism. Elementary Mode Analysis (EMA) (Papin et al., 2004; Schuster et al., 2000) operates with network stoichiometry to generate all minimal subsets of reactions that can function as standalone metabolic units. Each flux distribution can be written as a linear combination of elementary modes. Therefore, the relevance of a reaction can be assessed by its participation and its flux values in the elementary modes. EMA has been used to study metabolic networks (Kaleta et al., 2009; Schwartz and Kanehisa, 2006), discover targets for metabolic engineering and drug development (Beuster et al., 2011) and to identify high-yield mutants of producer strains (Carlson et al., 2002; Neuner and Heinzle, 2011). The main application of EMA remains the microbial metabolism because available genome annotations and the relatively small network size allow genome-scale analyses.

Stoichiometric analysis is recently gaining an increasingly important role at studying mammalian cells (Orman et al., 2010; Orman et al., 2011; Zamorano et al., 2013).

CHO cells are the mammalian workhorse in the biotechnology industry, responsible for the biggest share of biopharmaceuticals production (Jayapal et al., 2007; Walsh, 2010a). The wealth of studies using CHO cells as model system has led to them being nicknamed the “mammalian equivalent of *E. coli*” (Puck, 1985). They are characterized by the ability to grow in suspension cultures using chemically defined media, can reach high cell densities and high product titers of recombinant proteins. The availability of recently published CHO genome and other omics data (Becker et al., 2011; Brinkrolf et al., 2013; Hackl et al., 2011; Xu et al., 2011) facilitates network studies.

We think that the application of mitochondria-wide metabolic networks adds a new dimension to the analysis of mitochondrial metabolism. It permits access for studying interactions of several processes, e.g. transport, metabolite conversion, respiration as well as their control. This can be done in a most directed way by using intact mitochondria made accessible by selective permeabilization of the cell membrane. We used EMA to study the metabolism of CHO-K1 mitochondria made accessible through selective permeabilization. Key substrates were screened for their ability to be metabolized by the permeabilized cells, both alone or with addition of ADP. We then quantified the uptake and production of metabolites. The observations were used to compute the contribution of mitochondrial elementary modes to the metabolic flux distribution in each tested case. Therefore, this analysis reaches beyond mere metabolic flux analysis by providing additional information, e.g. on the coupling of processes or on the control of metabolic pathways. Furthermore, we quantified the effect of ADP stimulation and we evidenced metabolic bottlenecks. Overall, we demonstrate the great opportunities that arise by applying this methodical methodology to study the mitochondrial metabolism. For future studies it can easily be combined with other well-established methods, e.g. respiration analysis.

8.3 Materials and methods

8.3.1 Cell culture

Cultivation of the CHO-K1 cells was performed in baffled shake flasks (250 ml, Corning, New York, USA) in a shaking incubator (Innova 4230, New Brunswick Scientific, Edison, NJ, USA) at 135 rpm (2 inches orbit), 37°C and 5% CO₂. The cells were cultivated in chemically defined, protein-free TC-42 medium (TeutoCell, Bielefeld, Germany), supplemented with 6 mM L-glutamine (Sigma-Aldrich, Steinheim, Germany) from a 240 mM stock solution in dH₂O. The cells were passaged at the latest 72 h after inoculation and seeded with a cell density of $4 - 5 \times 10^5$ cells/mL.

8.3.2 Preparation of mitochondrial medium

The mitochondrial medium used in this study was derived from different media used for the assessment of respiration in isolated mitochondria (Madeira, 2012) and optimized with respect to osmolarity and ionic strength. The composition of the mitochondrial medium was as follows: 9.6 mM K_2HPO_4 , 2.4 mM KH_2PO_4 , 80 mM KCl, 75 mM sorbitol, 2 mM $MgCl_2$ and 100 μ M EGTA. The pH was set to 7.4 with 5 N KOH. The individual components have been chosen to minimize interactions with the downstream analytics (MALDI-ToF, HPLC).

8.3.3 Mitochondrial Transport Experiments

The experimental set-up is schematically depicted in Figure 8-1 and the different tested substrates and substrate combinations are listed in Table 1. CHO-K1 cells were harvested from a culture in the early exponential growth phase (48 - 50 h after inoculation) by centrifugation (5 min, $125 \times g$, Labofuge 400R, Function Line, Heraeus Instruments, Hanau, Germany). The supernatant was discarded quantitatively and the cells were resuspended in mitochondrial medium. Afterwards, the cell number was determined using an automated cell counter (*Countess[®] Automated Cell Counter*, Invitrogen, Karlsruhe, Germany) and set to 10^7 cells/mL by adding mitochondrial medium. Selective permeabilization of the cytosolic membrane was performed by adding 0.01 % (w/v) digitonin from a 1 % stock solution in dH_2O and verified under the microscope using the Trypan blue exclusion method. 5 mL of permeabilized cell suspension were transferred into a 50 mL filter-tube bioreactor (TPP, Trasadingen, Switzerland) containing 5 mL of the respective substrate solution (2-fold concentrated in respiration medium). The final cell concentration was 5×10^6 cells/mL, the final concentration of tested substrates was 4 mM. Afterwards, incubation was performed for 150 min in a shaking incubator (Innova 4230, New Brunswick Scientific, Edison, NJ, USA) at 135 rpm (2 inches orbit), 37°C and 5 % CO_2 .

For experiments without ADP-stimulation, 400 μ l samples were taken every 30 min. The samples were centrifuged (5 min, $6000 \times g$, Biofuge pico, Heraeus Instruments, Hanau, Germany) and the supernatants were frozen for subsequent analysis. For experiments with ADP-stimulation, 100 μ L of 100 mM ADP (resolved in respiration medium) were added every 30 min. 350 μ L samples were taken before and after each addition of ADP. The samples were centrifuged (5 min, $6000 \times g$, Biofuge pico, Heraeus Instruments, Hanau, Germany) and the supernatants were frozen at -20°C for subsequent analysis. Metabolites in these samples were identified using MALDI-ToF and quantified using HPLC.

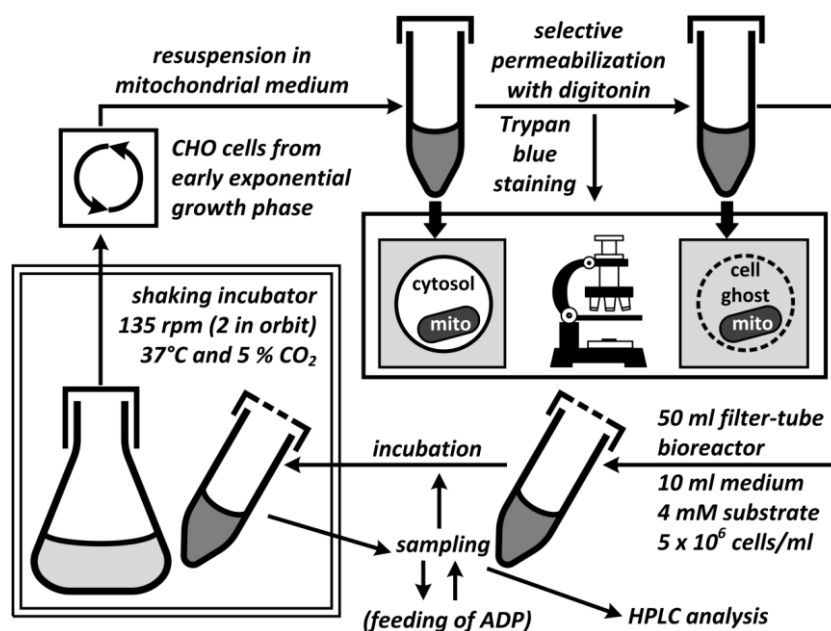


Figure 8-1. Experimental set-up for mitochondrial transport studies. CHO cells from the early exponential growth phase were harvested and resuspended in mitochondrial medium. Selective plasma membrane permeabilization with 0.01% (w/v) digitonin was microscopically verified using Trypan blue staining. Permeabilized cells were transferred into filter-tube bioreactors, mixed with a mitochondrial substrate and incubated in a shaking reactor for mitochondrial transport studies. Sampling (and ADP feeding) was performed every 30 min.

Table 8-1. Substrates and substrate combinations used for metabolization by selectively permeabilized CHO-K1 cells. Abbreviations: AKG – α -ketoglutarate; ASN – asparagine; ASP – aspartate; CIT – citrate; FUM – fumarate; GLN – glutamine; GLU – glutamate; MAL – malate; PYR – pyruvate; SER – serine.

without ADP stimulation		with ADP stimulation	
No.	Substrate(s)	No.	Substrate(s)
1a	PYR	1b	PYR, ADP
2a	PYR, ASP	2b	PYR, ASP, ADP
3a	CIT	3b	CIT, ADP
4a	AKG	4b	AKG, ADP
5a	SUC	5b	SUC, ADP
6a	FUM	6b	FUM, ADP
7a	MAL	7b	MAL, ADP
8a	GLN	8b	GLN, ADP
9a	GLU	9b	GLU, ADP
10a	ASP	-	-
11a	ASN	-	-
12a	SER	-	-

8.3.4 Analytical determination of organic acids and amino acids

Quantification of tested substrates and resulting products was performed by different established HPLC methods as described previously (Strigun et al., 2011b). In the presence of ADP, citrate could not be quantified at low concentrations because of an unresolvable overlay of metabolite peaks in the chromatogram. Identification of organic acids was confirmed by MALDI-TOF MS (matrix-assisted laser desorption/ionization time-of-flight mass-spectrometry) analysis. Since the analytes were negatively charged, the mass spectrometer (ABI 4800, Applied Biosystems, Foster City, USA) was operated in negative ion mode. The used laser is a Nd:YAG solid-state laser (neodymium-doped yttrium aluminum garnet) emitting UV radiation with a wavelength of 355 nm by third harmonic generation. The laser intensity was set to 3700 and the number of shots per spot was 1250. The flight distance of the ions was doubled by using the reflector-mode, thus achieving an improved mass accuracy. Prior to MALDI-TOF MS measurements, the samples were diluted 1:10 with dH₂O. This was necessary due to the high content of phosphate in the buffer (12 mM), which might disturb the measurement by signal suppression. 30 μ L of diluted sample were mixed with 30 μ L of matrix (9 mg/mL 9-aminoacridine in methanol) and 0.5 μ L of this mixture were spotted on a 384-spot MALDI target (Applied Biosystems, Foster City, USA).

8.3.5 Mitochondrial network

The model of the mitochondrial reactions network of the CHO-K1 cells (Figure 8-2) was reconstructed using genome annotation (Hammond et al., 2012). The connection with the extramitochondrial medium is made through carrier-mediated transport for large molecules (e.g. amino acids, organic acids, ATP/ADP) and free diffusion for small molecules i.e. O₂, CO₂ and NH₃. The model was then limited to the observed uptake and production of metabolites and included information about enzyme activity determined by Wahrheit (Wahrheit et al., 2014b) for the same cell line. Accordingly, mitochondrial NADP⁺-dependent malic enzyme (ME) was active and mitochondrial PEP carboxykinase was not active. Carriers that transport C4-dicarboxylates did not discriminate between fumarate, succinate or malate. With the exception of α -ketoglutarate, glutamine, oxygen and pyruvate, all other metabolites are transported reversibly. NAD(P)⁺ transhydrogenase was added to account for transferring electrons from NADPH to NADH. The stoichiometry of oxidative phosphorylation was 2.5 moles of ATP per mole of NADH and 1.5 moles of ATP per mole of FADH₂ (Hinkle, 2005).

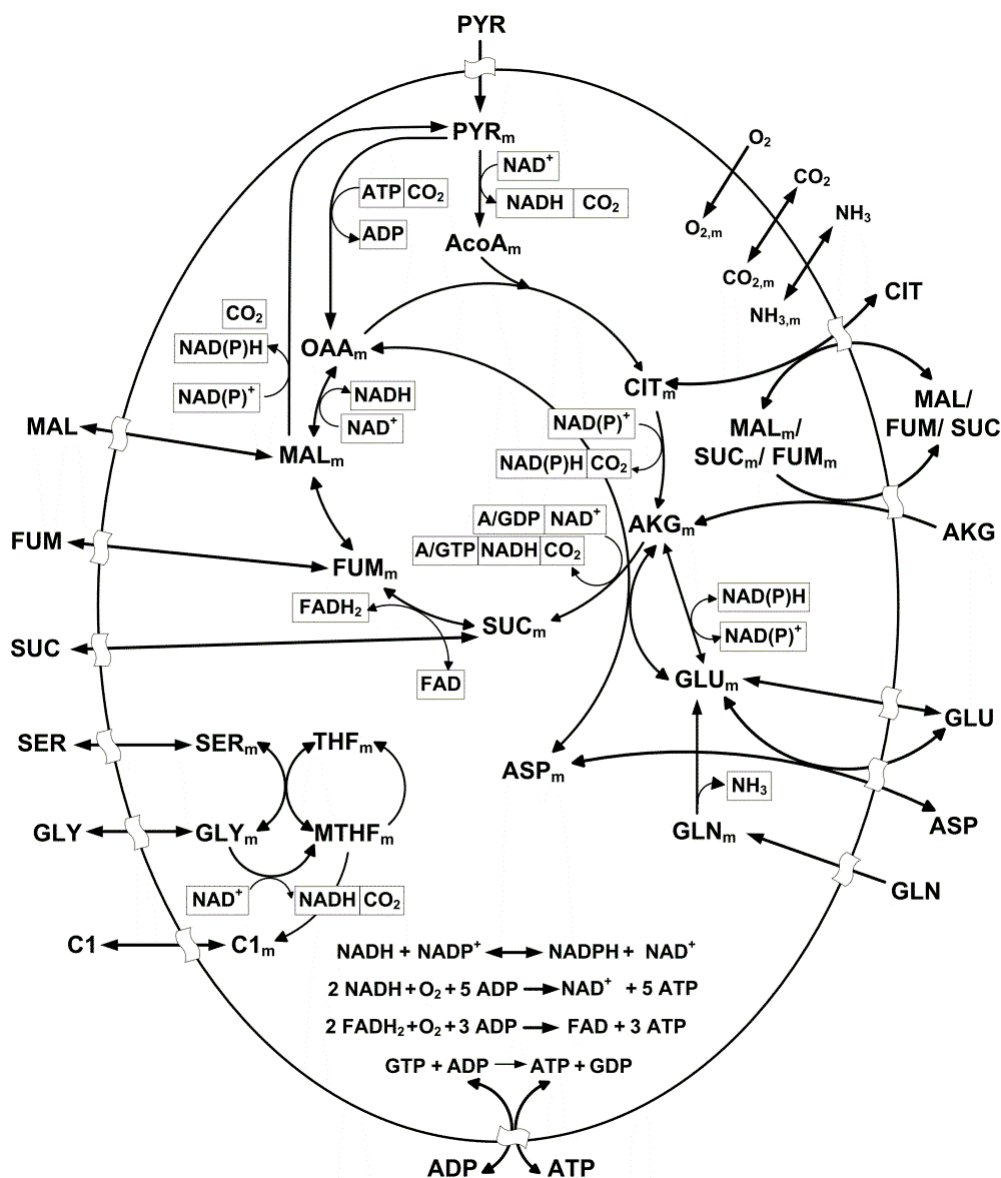


Figure 8-2. Metabolic network of the CHO-K1 mitochondria build based on genome annotation.  - Mitochondrial carrier. Subscripts: *m* – mitochondrial. Abbreviations: AcoA – acetyl-CoA; AKG – α -ketoglutarate; ASP – aspartate; C1 – one-carbon units; CIT – citrate; FUM – fumarate; GLN – glutamine; GLU – glutamate; GLY – glycine; MAL – malate; OAA – oxaloacetate; PYR – pyruvate; SER – serine; SUC – succinate.

8.3.6 Elementary mode analysis

The elementary modes of the mitochondrial network were computed using the *EFMtool* software (Terzer and Stelling, 2008). In our model, succinyl-CoA ligase used only ADP, and isocitrate dehydrogenase (IDH) isoenzymes and glutamate dehydrogenase (GDH) used only NAD^+ . An algorithm was then used to identify from the totality of elementary modes the pathways that contribute to the metabolite conversion for each tested substrate or substrate combinations. We included all possible modes involving CO_2 , though CO_2 itself was not measured. An observed flux set v can be expressed as a linear combination of elementary modes

$$v = \sum_{j=1}^M \alpha_j \cdot EM_j \quad (\text{eq. 1})$$

where M is the total number of elementary modes described by the vectors EM containing the mode stoichiometry. The weight coefficients α_j are usually not unique, as the number of elementary modes can exceed the dimension of the flux cone. The mode flux representing the contribution of each mode to the measured fluxes was computed for the situations where the system from eq. 1 was invertible.

8.4 Results and Discussion

8.4.1 Mitochondrial uptake and production of metabolites

In a previous study, we applied a high-throughput respiration screening method to verify the uptake and metabolization of a range of potential mitochondrial substrates (chapter 7). The outcome of this screening served as starting point to design further in-depth mitochondrial studies.

Here, we used an extended experimental set-up (Figure 8-1) to investigate the mitochondrial metabolism of CHO cells. We stimulated mitochondrial metabolism in selectively permeabilized cells by addition of selected substrates or combinations of substrates and quantified mitochondrial uptake and production of metabolites (Table 8-2) by fitting the extracellular concentrations over time (Supplementary Figure S1).

Metabolite uptake and production rates remained constant over time (Supplementary Figure S1). This proves that the mitochondria remained intact and functioned at metabolic steady state throughout the sampling period. No mitochondrial uptake of aspartate or asparagine alone was observed. However, aspartate was taken up when fed in combination with pyruvate. Uptake rates increased in the order of glutamate, serine, pyruvate, citrate, α -ketoglutarate, malate, glutamine, and succinate, with the uptake rate for succinate being 7.3 times (C-mole/C-mole) higher than that of glutamate (Table 8-2). Addition of ADP stimulated the uptake and excretion of metabolites by the mitochondria. With feeding of ADP, uptake rates increased in the order of aspartate, pyruvate, malate, succinate, citrate, α -ketoglutarate, and glutamine (Table 8-2). In this case, the uptake rate of glutamine was 4.6 times higher than the uptake of aspartate (C-mole/C-mole). We observed the highest impact of ADP on stimulating the uptake of citrate and α -ketoglutarate. ADP addition doubled the uptake of aspartate, from 6.1 to 12.2 fmol / (cell \times min), but not of pyruvate, that increased only by 3.7 fmol / (cell \times min) when both substrates were fed in combination.

Table 8-2. Uptake and production rates of metabolites by the selectively permeabilized CHO-K1 cells [$\mu\text{mole} / (10^9 \text{ cells} \times \text{min})$] and the computed 95% confidence intervals (C.I.) given in square brackets. n.m. – not measured. Abbreviations: AKG – α -ketoglutarate; ASP – aspartate; CIT – citrate; FUM – fumarate; GLN – glutamine; GLU – glutamate; GLY – glycine; MAL – malate; PYR – pyruvate; SER – serine; SUC – succinate.

No.	Substrate	Uptake rate [95% C.I.]	Product	Production rate [95% C.I.]
1a	PYR	4.6 [3.4, 5.7]	CO ₂	n.m.
1b	PYR	14.2 [12.6, 15.9]	CO ₂	n.m.
	ADP	n.m.	ATP	n.m.
2a	PYR	11.9 [10.2, 13.5]	GLU	3.0 [2.5, 3.6]
	ASP	6.1 [4.0, 8.2]	CO ₂	n.m.
2b	PYR	15.6 [13.8, 17.3]	GLU	6.7 [5.4, 8.0]
	ASP	12.2 [6.9, 17.6]	CO ₂	n.m.
	ADP	n.m.	ATP	n.m.
3a	CIT	5.6 [3.7, 7.5]	CO ₂	n.m.
3b	CIT	38.0 [25.4, 50.6]	CO ₂	n.m.
	ADP	n.m.	ATP	n.m.
4a	AKG	12.7 [8.1, 17.3]	FUM	0.48 [0.46, 0.50]
			CO ₂	n.m.
4b	AKG	40.2 [30.8, 49.6]	FUM	2.5 [2.2, 2.7]
	ADP	-	CO ₂	n.m.
			ATP	n.m.
5a	SUC	24.5 [19.1, 29.9]	FUM	2.2 [1.7, 2.8]
			MAL	14.5 [11, 17.9]
			CIT	1.9 [0.9, 2.8]
			CO ₂	n.m.
5b	SUC	30.5 [27.1, 33.9]	FUM	2.1 [1.5, 2.8]
	ADP	-	MAL	14.6 [10.7, 18.5]
			CIT	n.m.
			CO ₂	n.m.
			ATP	n.m.
6a/7a	MAL	14.6 [10.2, 19]	CIT	4.9 [3.7, 6.0]
	FUM	1.9 [0.9, 2.9]	CO ₂	n.m.
6b/7b	MAL	19.7 [14.6, 24.8]	CIT	n.m.
	FUM	1.7 [0.9, 2.5]	CO ₂	n.m.
	ADP	n.m.	ATP	n.m.
8a	GLN	20.0 [17.9, 22.1]	GLU	14.4 [11.4, 17.4]
			ASP	3.3 [2.4, 4.2]
			CO ₂	n.m.
8b	GLN	44.7 [35.7, 53.7]	GLU	19.0 [15.4, 22.6]
	ADP	n.m.	ASP	11.4 [9.98, 12.9]
			CO ₂	n.m.
			ATP	n.m.
9a	GLU	2.69 [1.22, 4.16]	ASP	3.38 [2.61, 4.15]
			CO ₂	n.m.
9b	GLU	3.99 [-14.2, 22.2]	ASP	15.5 [13.0, 18.0]
	ADP	n.m.	CO ₂	n.m.
			ATP	n.m.
12a	SER	4.5 [2.3, 6.7]	GLY	2.6 [2.0, 3.2]

Although an absolute comparison with previous respiration studies is not possible due to different experimental setups, similar trends were observed: (1) stimulation of mitochondrial metabolism by addition of ADP, (2) without addition of ADP the highest respiration and uptake was observed on succinate, (3) relatively minor impact of ADP on stimulating the uptake of malate, fumarate, succinate, (4) relatively higher impact of ADP stimulation on the uptake of citrate and glutamine. This is in accordance with previous mitochondrial studies using respiration analysis (chapter 7).

8.4.2 Connection of tested substrates and observed products using elementary mode analysis

We selected the mitochondrial elementary modes that connect tested substrates and observed products. Based on the stoichiometry of these modes, we determined the partitioning of a certain substrate metabolism into different pathways (Figure 8-3). The production rate of a metabolite from a substrate or a combination of substrates is a linear combination of all modes that achieve the conversion. The case presented in Figure 8-3 allows to compute the mode fluxes through A, B and C if the uptake of Substrate 1 and Substrate 2, as well as the production of Product 1 and Product 2 are measured. However, there were situations when the linear system that relates mode fluxes to external fluxes was not invertible. For our model, we were able to determine the contribution of each mode to the metabolism of all substrates except when pyruvate and aspartate were used together. While in almost all cases a full metabolization to CO₂ was possible, many substrates led to partial TCA cycle activity that ended with the secretion of corresponding metabolites.

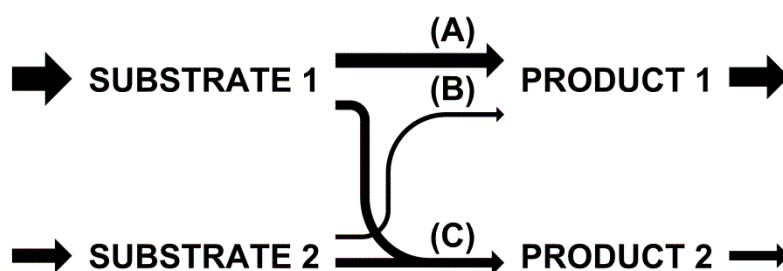


Figure 8-3. Example of establishing the partitioning of Substrate 1 and Substrate 2 into the elementary modes (A), (B) and (C) for yielding Product 1 and Product 2. The thickness of the arrows indicates the theoretical flux through each elementary mode.

8.4.2.1 General characteristics

All experiments where ADP was supplied exhibited higher uptake rates for all tested metabolites. This happens mainly because (1) ADP increases the availability of NAD⁺ via the respiratory chain and (2) ADP stimulates pyruvate dehydrogenase, isocitrate dehydrogenase and α -ketoglutarate dehydrogenase (AKGDH), three key enzymes responsible for controlling the TCA cycle (Michal

and Schomburg, 2012; Strumilo, 2005). In the modes where ADP is not supplied, the pyruvate carboxylase (PCX) – malate dehydrogenase (MDH) – malic enzyme (ME) cycle needs to be highly active to consume the excess of ATP produced by oxidative phosphorylation. The activity of this cycle has been shown in previous MFA studies of CHO cells (Ahn and Antoniewicz, 2011; Ahn and Antoniewicz, 2013; Goudar et al., 2010; Nicolae et al., 2014b). In addition, we have shown earlier that ME is active in the mitochondria of the used CHO-K1 cell line (Wahrheit et al., 2014b). This cycle is the rate-limiting element in metabolizing substrates in the absence of ADP, as accumulated ATP and NADH inhibit most enzymes involved in the TCA cycle (Michal and Schomburg, 2012). If pyruvate was not provided, ME was responsible for replenishing it from malate to produce the acetyl-CoA required for initiating the citrate synthase reaction.

In the mitochondria, glutamate dehydrogenase and isoenzymes of IDH can use both NAD^+ and NADP^+ as cofactors. When NADPH is produced in excess, the transhydrogenase enzyme can oxidize it to produce NADH. The conversion of NADPH is coupled with pumping H^+ out of the mitochondria thereby contributing to building up the proton gradient across the inner mitochondrial membrane. Another option for transferring reducing factors from NADPH to NADH is by the reverse functioning (towards isocitrate) of NADP^+ -dependent IDH (Sazanov and Jackson, 1994). Also, ATP synthesis can become partially uncoupled from respiration through the presence of uncoupling proteins (Boss et al., 2000; Moreno-Sanchez et al., 2014). This can change the stoichiometry of using reducing equivalents to produce ATP, hence of the computed activity of the PCX-MDH-ME cycle when ADP is not provided. However, uncoupling proteins were not found to be expressed in wild-type CHO cells (Pecqueur et al., 2008) and were shown to play a role in thermogenesis, protection against oxidative stress, export of fatty acids or mediation of insulin secretion (Rousset et al., 2004). We can therefore assume that the effect of uncoupling is negligible for balancing ADP/ATP.

8.4.2.2 Pyruvate and aspartate

Pyruvate fed alone sustained a complete TCA cycle. Upon stimulation with ADP, the pyruvate uptake flux increased 3.1 times (Table 8-2). In the modes we computed, this requires an active mitochondrial pyruvate carrier and all mitochondrial enzymes that metabolize pyruvate to CO_2 (Figure 8-4.A1, 8-4.B1).

When pyruvate and aspartate were fed together, the two metabolites had a reciprocal stimulating effect. In a separate experiment, aspartate alone was not taken up. The uptake of pyruvate in the presence of aspartate increased 2.6 times compared to the uptake of pyruvate alone. A double amount of aspartate was taken up per amount of glutamate produced (Table 8-2). The activity of four possible elementary modes can combine to explain the observations: (1) uptake of pyruvate to produce CO_2 , (2) co-uptake of pyruvate and aspartate to produce CO_2 and one mole of glutamate per mole of aspartate, (3) uptake of aspartate to produce CO_2 and one mole of glutamate per two moles

of aspartate and (4) uptake of aspartate to produce only CO₂. Aspartate uptake through the glutamate-aspartate carrier occurs with equimolar secretion of glutamate. Glutamate must be partially re-transported into the mitochondria through a different carrier (Fiermonte et al., 2002) to account for the aspartate uptake/glutamate secretion rate ratio of 2.03. Surprisingly, the stoichiometry of the mode with co-uptake of pyruvate and aspartate (mode (2)), where aspartate provides one mole of oxaloacetate and pyruvate provides one mole of acetyl-CoA to fuel the TCA cycle, does not match the observed rates and does not occur. Therefore, aspartate (Figure 8-4.A3, B3) and pyruvate (Figure 8-4.A2, B2) must be metabolized individually. Although aspartate is only taken up in combination with pyruvate, its metabolization happens only via modes that don't include pyruvate. This is possible by mutual activation of modes, i.e. activation of rate controlling enzymes. The first regulatory step in the conversion of aspartate is aspartate aminotransferase, which is controlled by its products and substrates in a complex manner (Cascante and Cortes, 1988). This enzyme converts aspartate to oxaloacetate simultaneously with converting α -ketoglutarate into glutamate. Glutamate is exchanged when aspartate enters the mitochondria, as shown in Figure 8-2. Production of α -ketoglutarate in the TCA cycle is needed to sustain the outflow of glutamate, as shown in Figure 8-4.A3. Aspartate accumulation was observed in retina cells treated with an inhibitor of the mitochondrial pyruvate carrier (Du et al., 2013), which suggests that aspartate needs pyruvate for metabolization. Although oxaloacetate could exert product inhibition on PCX (Barden et al., 1972), it is consumed by MDH to produce malate, while the acetyl-CoA synthesized from pyruvate activates PCX (Jitrapakdee and Wallace, 1999), thus favoring the PCX-MDH-ME cycle towards hydrolyzing the ATP produced from intramitochondrial pool of ADP in the respiratory chain. ME activity could be another bottleneck in the conversion of pyruvate and aspartate in the absence of ADP. It was shown that AKG inhibits mitochondrial ME and MDH in brain cells (McKenna et al., 1995). Therefore, ME activity depends on the efficiency of AKG removal from the mitochondria as glutamate.

Addition of ADP to the pyruvate-aspartate mixture did not change the pyruvate uptake flux, compared to when pyruvate and ADP were used. Under ADP stimulation, the PCX-MDH-ME cycle is not needed for pyruvate catabolism. The most probable limitation in this case is pyruvate transport into the mitochondria, which was shown to influence the respiration capacity in yeast (Timon-Gomez et al., 2013) and is suspected to regulate pyruvate metabolism in cancer cells (Schell and Rutter, 2013). Aspartate uptake flux increased although the aspartate/glutamate ratio remained close to 2 (Table 8-2), comparable to the case without ADP. This result strengthens the assumption that the mode which uses aspartate to produce glutamate and CO₂ is responsible for aspartate metabolism by the mitochondria.

Pyruvate metabolization to CO₂ is limited to approx. 15 fmol/ (cell \times min) in all the three cases where other substrates were used together with pyruvate (i.e. ADP, aspartate, aspartate and ADP).

This suggests the existence of a tightly controlled upper threshold in the mitochondrial pyruvate metabolism achieved using the pyruvate transporter and/or allosteric control by the PDH complex.

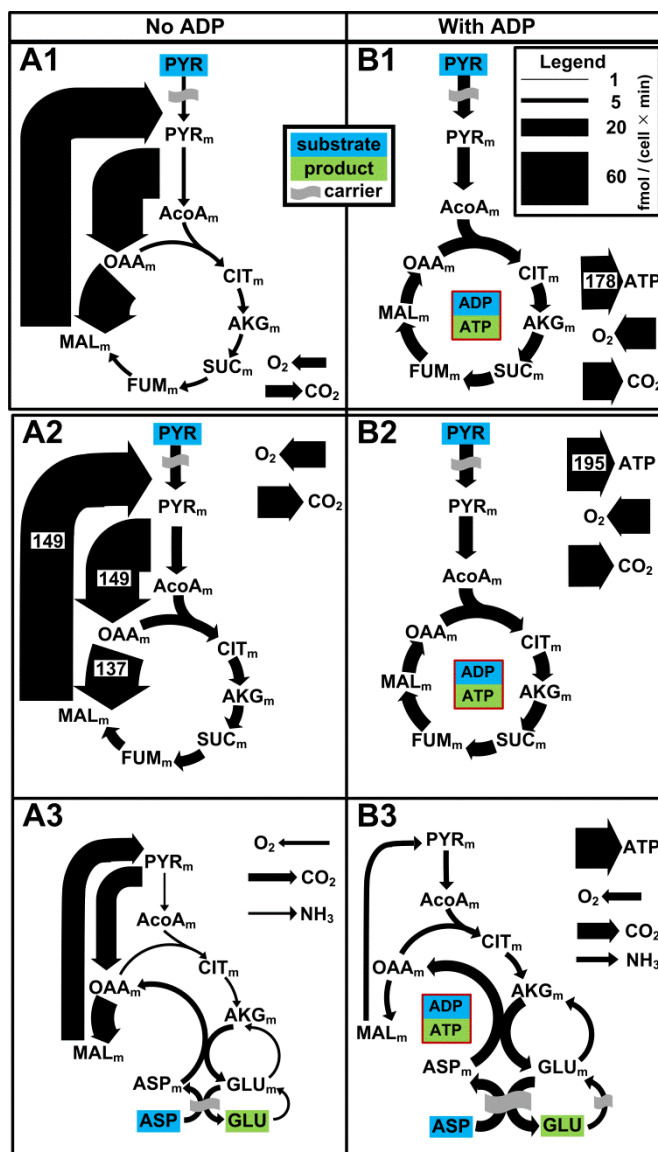


Figure 8-4. Fluxes of the mitochondrial elementary modes determined after feeding the permeabilized cells pyruvate (A1, B1) and a combination of pyruvate and aspartate (A2, A3, B2, B3). Modes from lines 1 and 2 metabolize pyruvate to CO₂. Modes from line 3 metabolize aspartate to glutamate and CO₂. The modes in the A-column do not use supplied ADP, and the modes in the B-column contained ADP as substrate. The fluxes higher than 60 fmol/ (cell × min) are indicated by numbers on the corresponding arrow. Subscripts: m – mitochondrial. Abbreviations: AcoA – acetyl-CoA; AKG – α-ketoglutarate; ASP – aspartate; CIT – citrate; FUM – fumarate; GLU – glutamate; MAL – malate; OAA – oxaloacetate; PYR – pyruvate; SUC – succinate.

8.4.2.3 Citrate

We observed no metabolite production when citrate was used as substrate, also when ADP was added. Because citrate is taken up by antiport with C4-carboxylates, these are taken up again via the dicarboxylate carrier (Figure 8-5.A, B) thus explaining their absence in the extramitochondrial medium. For this, we can assume more mechanisms: (1) the dicarboxylate carrier can take up dicarboxylates at very low extramitochondrial concentrations, (2) reuptake of C4-carboxylates occurs via a mechanism that bypasses their dilution into the media by maintaining a high concentration in the inter-membrane space, (3) there is a mitochondrial carrier that takes up citrate alone, (4) there is collaboration between the citrate carrier (Gnoni et al., 2009) and the dicarboxylic one. When ADP was added, there was a significant stimulation of citrate metabolization of 6.8 fold increase (Figure 8-5. B), citrate being the metabolite taken up with the highest carbon flux.

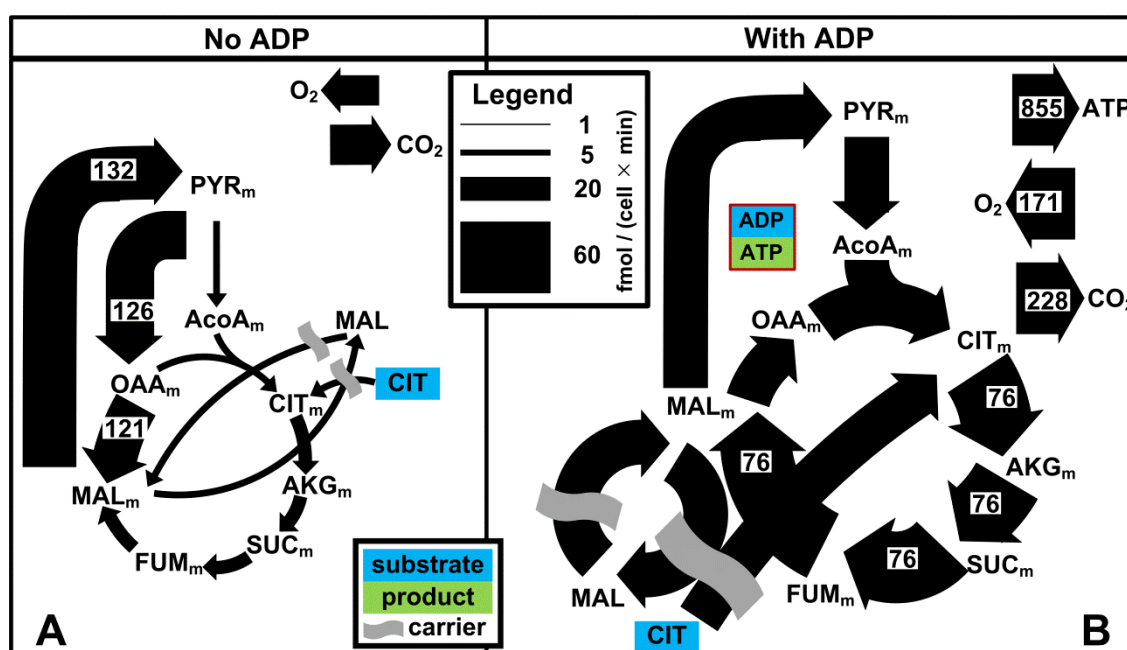


Figure 8-5. Fluxes of the mitochondrial elementary modes that completely oxidize citrate to CO_2 . Mode A does not contain added ADP, and mode B uses ADP as substrate. The fluxes higher than $60 \mu\text{mol}/(\text{cell} \times \text{min})$ are indicated by numbers on the corresponding arrow. Subscripts: m – mitochondrial. Abbreviations: AcoA – acetyl-CoA; AKG – α -ketoglutarate; CIT – citrate; FUM – fumarate; MAL – malate; OAA – oxaloacetate; PYR – pyruvate; SUC – succinate.

ADP and citrate have a joint activating effect on IDH, which is a limiting step of the TCA cycle as previously found for this cell line by Wahrheit et al. (Wahrheit et al., 2014b). The effect of citrate feeding is also in qualitative accordance with respiration studies performed on selectively permeabilized CHO-K1 cells (chapter 7), where a high stimulation of respiration was observed when citrate was used together with ADP. Citrate is known to inhibit citrate synthase (Williamson

and Cooper, 1980), which would in this case be a bottleneck in the TCA cycle, but the high metabolization rate suggests that citrate is consumed quickly by enzymes downstream the TCA cycle e.g. IDH and AKGH leading to low citrate and isocitrate concentrations and a release of its inhibiting effect. Citrate and isocitrate uptake by the mitochondria is not a typical physiological event described for the metabolism of mammalian cells. In contrast, citrate is usually transported out of the mitochondria to supply the fatty acid synthesis in the cytosol. However, given the high cytosolic IDH activity (Wahrheit et al., 2014b), it is possible that in a physiological state the excess of NADPH generated by the pentose phosphate pathway (Nicolae et al., 2014b) drives the reaction towards consuming AKG. A reversed functioning of the IDH (Metallo et al., 2012) has been described before for mammalian metabolism. Isocitrate and citrate are then produced from cytosolic AKG and then taken up by the mitochondria to be used in the TCA cycle.

8.4.2.4 α -ketoglutarate

Similarly to citrate, α -ketoglutarate could sustain the TCA cycle alone (Figure 8-6.A). α -ketoglutarate was taken up with the highest flux from all metabolites without ADP stimulation (Table 8-2). Also, as in the case of citrate, α -ketoglutarate enters the mitochondria using C4-dicarboxylate antiporter (Figure 8-6.A, B1, B2). Though it was shown for astrocytes that α -ketoglutarate inhibits ME (McKenna et al., 1995), this effect was not manifested in our experiments considering the high metabolization rate in the absence of ADP and hence the high ME flux (Figure 8-6). With addition of ADP, the activation of IDH and AKGDH results in a 3-fold increase in α -ketoglutarate uptake rate.

8.4.2.5 C4 carboxylates

Succinate and malate were metabolized by the mitochondria with relatively high rate, both with and without addition of ADP. They were transported through the dicarboxylate carrier, which requires mitochondrial phosphate antiport (Fiermonte et al., 1998). Phosphate is then replenished through another transport system e.g. via the phosphate carrier (Hamel et al., 2004). Extracellular fumarate was converted before being taken up to malate in a fast equilibrium reaction, probably by extramitochondrial fumarase activity (Supplementary Figure S1). The equilibrium explains the presence of fumarate in the media when malate is produced from succinate (Figure 8-7.A4, B4).

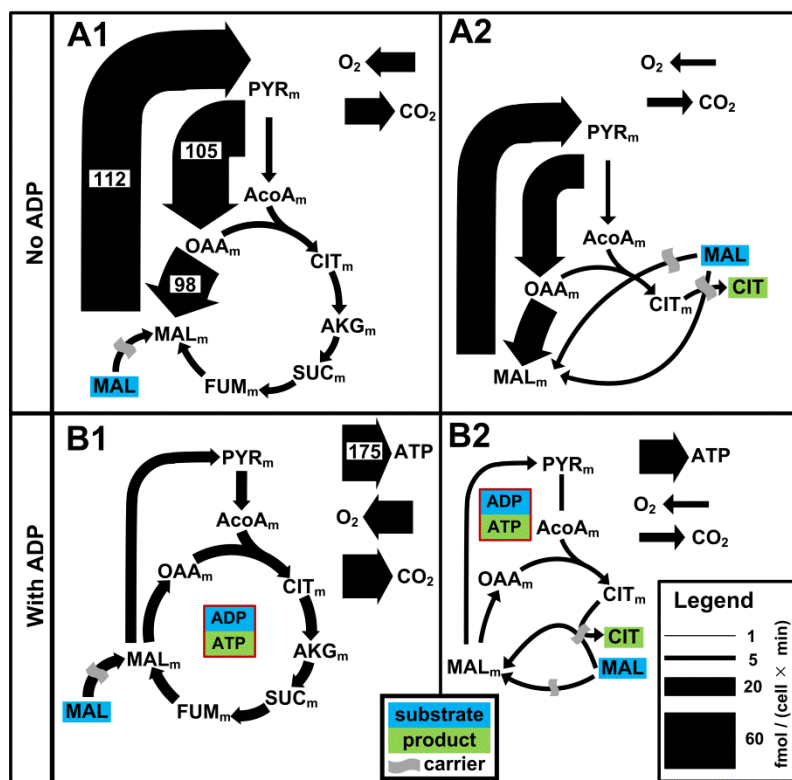


Figure 8-8. Metabolic fluxes of the mitochondrial elementary modes that metabolize malate to CO₂ (A1, B1) and malate to citrate and CO₂ (A2, B2). The modes in the A-column do not use supplied ADP, and the modes in the B-column contained ADP as substrate. The fluxes higher than 60 fmol/ (cell × min) are indicated by numbers on the corresponding arrow. Subscripts: m – mitochondrial. Abbreviations: AcoA – acetyl-CoA; AKG – α -ketoglutarate; CIT – citrate; FUM – fumarate; MAL – malate; OAA – oxaloacetate; PYR – pyruvate; SUC – succinate.

Addition of ADP increased the metabolization rate of succinate to CO₂ 2.5 times (Figure 8-7.A1, B1) and of malate by 1.7 times (Figure 8-8.A1, B1). ADP had no effect on the production of citrate from succinate or malate, as shown in Figure 8-7.A3, B3 and Figure 8-8.A2, B2. Succinate was converted to malate with the same rate in both non-stimulated (Figure 8-7.A2) and stimulated (Figure 8-7.B2) cases. It can be inferred that fast pathway kinetics between succinate and malate and reduced activity in disposing of malate in the TCA cycle leads to accumulation that favors malate secretion instead of full metabolization. Compared to the high metabolization rates observed for CIT and AKG, the supply of C4-dicarboxylates resulted in a lower activity of the TCA cycle. This implies that the second part of the TCA cycle, involving C4-dicarboxylates, is mainly controlled by the concentrations of C4-dicarboxylates and less by the availability of cofactors. The metabolic steady state and therefore the intramitochondrial C4-dicarboxylates concentrations are maintained by removing the excess from the mitochondria via the dicarboxylate carrier. Complete catabolism to CO₂ in the absence of ADP was 17% for succinate and 48% for malate, and with ADP it was increased to 33% and 60% respectively. Citrate production from either succinate (Figure 8-

7.B3) or malate (Figure 8-8.B2) suggests that high cytosolic concentrations of dicarboxylates induce *de novo* fatty acids synthesis by providing citrate to the cytosol, as it was shown on mouse models (Mizuarai et al., 2005).

Analytical determination of citrate was difficult in the presence of ADP due to an overlay of metabolite peaks in the chromatogram. Although the uptake fluxes of C4 carboxylates increased, we computed the modes under the assumption that the citrate secretion rate does not increase. We based our assumption on the fact that ADP enhances significantly the metabolization of citrate, as we have shown above. Also, the situation when citrate is produced from C4 and then taken up again for metabolization to CO₂ is equivalent to a mode that metabolizes C4 to CO₂. It is therefore unlikely that citrate will accumulate in the media when ADP is added.

8.4.2.6 Glutamine and glutamate

The permeabilized cells took up glutamine via the glutamine carrier (Hassanein et al., 2013; Indiveri et al., 1998) and used it to produce mostly glutamate, with a conversion of 72% in the absence of ADP (Figure 8-9.A3). By adding ADP, the conversion to glutamate decreased to 42% (Figure 8-9.B3) although the net production rate increased by 32%. This shows that it is possible for glutamate to leave the mitochondria through a different transport system than the aspartate-glutamate carrier, most likely the glutamate carrier (Fiermonte et al., 2002). The glutamate carrier has been shown to operate in the reverse direction, hence by facilitating glutamate to exit the mitochondria when it is produced in excess. The supply of cytosolic glutamate could then be used *in vivo* for transamination, e.g. the production of alanine, and also for producing glutamine, as we have shown previously (Nicolae et al., 2014b). Because GDH is activated by ADP (Fang et al., 2002), glutamine catabolism to CO₂ by a full TCA cycle increased significantly in the presence of ADP (Figure 8-9.A1, B1), indicating that this enzyme is the first step in controlling glutamine metabolism. The presence of extramitochondrial glutamate also activated the secretion of aspartate (Figure 8-9.A2, B2). Most likely, under the experimental conditions the aspartate-glutamate carrier is controlled by the intracompartmental concentrations of these two amino acids and is not subjected to allosteric control by other metabolites.

Glutamate was taken up in modest amounts in the absence of ADP, and aspartate was produced in nearly equimolar amounts, considering the confidence intervals of the rates computed for glutamate uptake and aspartate production (Table 8-2). Glutamate concentration could not be determined reliably when using ADP (Supplementary Figure S1). Nevertheless, an increased production of aspartate was observed, which indicates that glutamate uptake increased considerably by adding ADP. This means that the preferred uptake system for glutamate is the glutamate-aspartate carrier and not the glutamate carrier (Fiermonte et al., 2002).

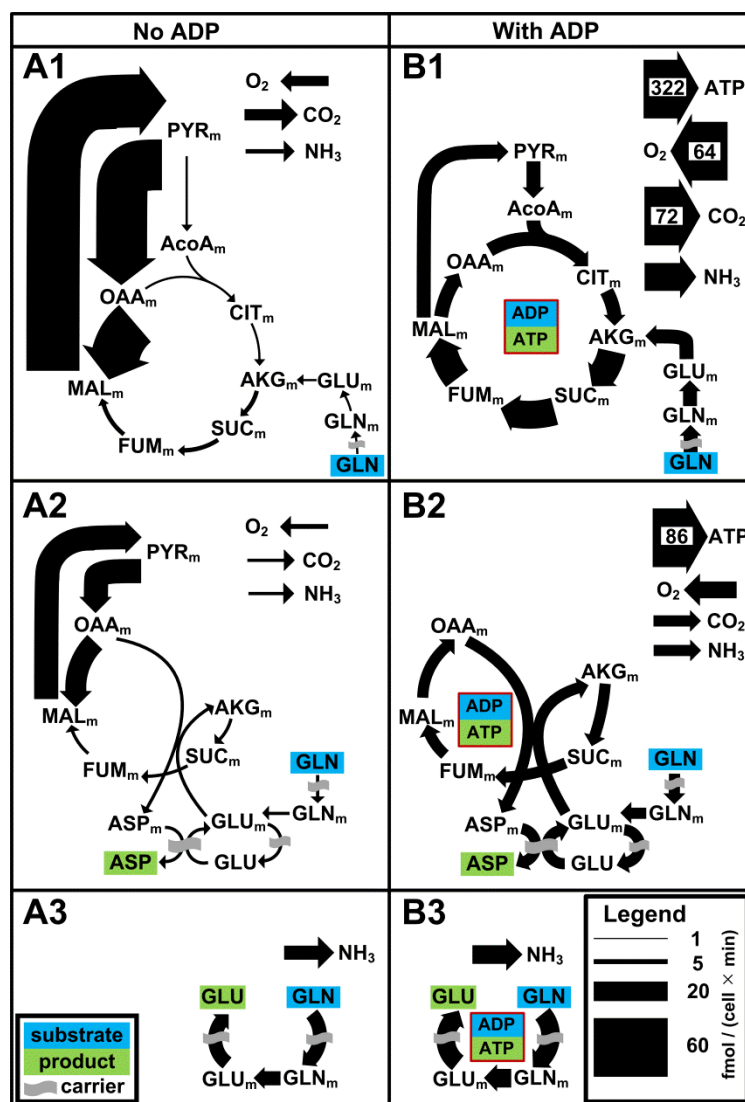


Figure 8-9. Metabolic fluxes of the mitochondrial elementary modes that metabolize glutamine to CO₂ (A1, B1), glutamine to aspartate and CO₂ (A2, B2) and glutamine to glutamate (A3, B3). The modes in the A-column do not use supplied ADP, and the modes in the B-column contained ADP as substrate. The fluxes higher than 60 fmol/ (cell × min) are indicated by numbers on the corresponding arrow. Subscripts: *m* – mitochondrial. Abbreviations: AcoA – acetyl-CoA; AKG – α-ketoglutarate; ASP – aspartate; CIT – citrate; FUM – fumarate; GLN – glutamine; GLU – glutamate; MAL – malate; OAA – oxaloacetate; PYR – pyruvate; SUC – succinate.

8.4.2.7 Serine

Serine was taken up by the permeabilized cells in moderate amounts (Table 8-2). Consistent with previous studies (Appling, 1991; Barlowe and Appling, 1988; Narkewicz et al., 1996), serine is converted by mitochondrial serine hydroxymethyltransferase to produce glycine and C1 units, that can subsequently be converted to and secreted as formate (not measured) (Figure 8-2). Only 59% of the glycine that could be potentially produced was secreted, the rest being probably converted by

the glycine cleavage system into C1 units and CO₂. The produced NADH is then consumed by the PCX-MDH-ME cycle to maintain the metabolic steady state in the mitochondria.

8.4.3 Conclusions

Selectively permeabilized CHO-K1 cells proved to be a useful system for detailed studies of the mitochondrial metabolism. The permeabilized cells retain functional mitochondria that are able to process at metabolic steady state various single or combinations of carbon sources. By using EMA we have evidenced that the mitochondrial reactions involved in the TCA cycle, anaplerotic and cataplerotic reactions, reactions involved in amino acid metabolism, as well as the oxidative phosphorylation and mitochondrial transport are active. Beyond demonstrating the functionality of mitochondrial metabolic pathways, we used EMA to confirm the observations from earlier screening experiments (chapter 7). Additionally, we could quantify the contributions of separate pathways at processing a certain substrate or combination of substrates.

In the absence of ADP, substrate uptake was limited in most cases. Full metabolization to CO₂ has been observed for pyruvate, citrate, α -ketoglutarate, C4 dicarboxylic acids and glutamate. This requires an active PCX-MDH-ME cycle that disposes of the ATP generated by oxidative phosphorylation. The PCX-MDH-ME cycle is the limiting step in processing substrates, as the accumulation of ATP and NADH inhibits key enzymes involved in the TCA cycle. Uncoupling ATP synthesis from respiration could provide another way disposing of the excess of reducing factors, but this hypothesis would need further exploration, also by including ADP/ATP and O₂ measurements.

Stimulation by ADP enhanced respiration and the metabolization to CO₂ of most substrates, as shown in chapter 7, with considerable differences for α -ketoglutarate and citrate and less for C4 dicarboxylic acids. The differences are explained by the way in which the enzymes of the TCA cycle are controlled. In the first part of the TCA cycle, IDH and AKGDH are positively modulated by substrate and cofactor availability. The second part of the TCA cycle, involving the interconversion of C4-dicarboxylates, is subjected to limiting control by the concentration of C4-dicarboxylates. The high concentrations of C4-dicarboxylates could inhibit enzymes that do not process them directly. This effect may lead indirectly to a reduced TCA cycle. Glutamine metabolism is controlled by GDH and by removing glutamate from the mitochondria via the glutamate carrier. We summarized our conclusions, organized by the feeding experiments that support them, in Supplementary Table S4.

A question mark that is left after analyzing our results is related to the regulatory role played by the mitochondrial carriers. Little is known about their function to control metabolite concentrations for achieving a specific metabolic state in the mitochondria. We consider that knowledge about regulation of mitochondrial transporters would improve the understanding of the mitochondrial

metabolic system. Complex regulatory effects that span over more reactions are difficult to establish without further information about transporter properties. Our findings indicate a limiting role of the pyruvate carrier, a high sensitivity of the aspartate-glutamate antiporter for balancing the content of these amino acids in the mitochondria, and a potential cooperation between the citrate and the dicarboxylate carrier. Also, determining intracompartmental concentrations under selected feeding conditions would be of great value at establishing the control checkpoints in the mitochondrial metabolism. Off-gas analysis of O_2 and CO_2 would add extra constraints to the linear system used to calculate the mode fluxes, making possible the resolution of more complex modes, where e.g. more substrates are taken up together. Sampling ADP and ATP concentrations would enable the quantification of uncoupling effects.

Using selectively permeabilized cells and flux analysis methods provides a great system for metabolic studies that aim at understanding diseases related to mitochondrial dysfunctions or at debottlenecking the metabolic connection between mitochondria and cytosol. By removing the background noise of cytosolic reactions, it becomes possible to study the effect of transport or enzyme inhibitors and of genetic modifications of the mitochondrial enzymes on the mitochondrial metabolism.

8.5 Acknowledgements

We thank the Institute of Cell Culture Technology (University Bielefeld, Germany) for supplying the CHO-K1 cells. We thank the BMBF (German Federal Ministry of Education and Research) projects SysCompart [project ID 031555D] and OxiSys [project ID 031 5891 B] for funding.

9 Conclusion

9.1 Summary statement

Metabolism controls life and death, function and dysfunction of any living cell and organism. Increasing our basic understanding of metabolism has an equally considerable impact on significant questions in biotechnology and biomedicine. The presented thesis provides an in-depth quantitative characterization of the central metabolism and its control in Chinese hamster ovary (CHO) cells (Figure 9-1). Focusing on metabolic dynamics and compartmentation, the work tackles a very challenging issue. Different innovative experimental strategies and advanced computational methods have been developed and implemented breaking fresh ground for detailed metabolic studies in higher eukaryotic organisms in the future. The work substantially enhances our knowledge about the complex metabolism of industrially highly relevant CHO cells in particular and of mammalian cells in general. These fascinating novel findings significantly contribute to improved biopharmaceutical production and design of successful therapies for the treatment of severe diseases in the future.

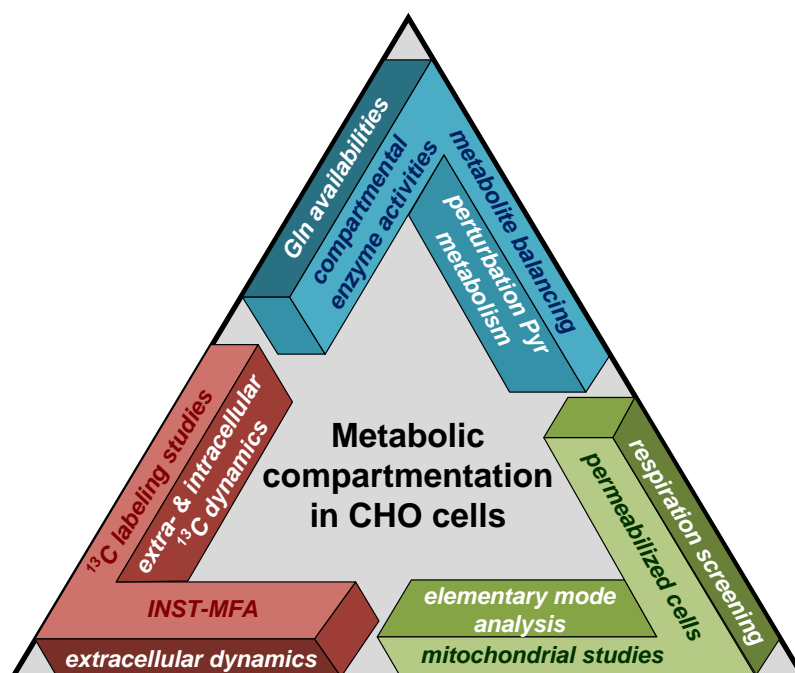


Figure 9-1. Three building stones contribute to the bigger picture and an increased understanding of metabolic compartmentation in CHO cell metabolism: (1) Metabolite balancing used in three different case studies: (i) DMFA in combination with compartmental enzyme activities, (ii) DMFA to describe different glutamine availabilities, and (iii) MFA to characterize a perturbed pyruvate metabolism. (2) ^{13}C labeling studies for INST-MFA: (i) based on one tracer and extracellular labeling dynamics of readout metabolites and (ii) based on two parallel tracers and extra- and intracellular labeling dynamics. (3) Mitochondrial studies using selectively permeabilized cells: (i) used in a high throughput respiration screening and (ii) used for mitochondrial pathway investigation applying elementary mode analysis.

9.2 Future applications of the established methods and concepts

The variety of novel experimental, analytical, and computational methods and strategies applied in this thesis represent a significant technological and conceptual advancement. They provide a solid base for in-depth metabolic studies in various contexts. On the one hand, these methods offer new possibilities for addressing specific scientific questions that are difficult to access and have therefore been neglected in the past. On the other hand, the presented methods and concepts provide guidance on how to improve data analysis and increase the information that can be drawn from experimental data. In the next paragraphs, particular advantages of the applied methods are summarized and future fields of application in industrial and biomedical research are illustrated.

Mammalian cell cultures are usually characterized by changing environmental conditions and adapting cellular responses. **Dynamic metabolic flux analysis (DMFA)** as applied in the chapters 2 and 3 is a very elegant and easy to implement tool that allows exploring biological systems at non steady state conditions. A time-resolved analysis is particularly useful for studying metabolic dynamics and monitoring metabolic shifts (Niklas et al., 2011c). The applicability of DMFA to industrially relevant, non stationary process modes like fed-batch cultivations has been demonstrated in chapter 3. Understanding the dynamics of a producer strain's physiology can assist in speeding up process development, e.g. by rationally optimizing media and feeding profiles. Another example where metabolic steady state is usually not (fully) achieved is adherent cell cultivation which is the most common cultivation method in toxicological or medical studies. DMFA may be applied to monitor the dynamic cellular response to perturbations, e.g. after application of drugs, toxic compounds or other effectors.

In the past, detailed MFA studies, e.g. using non-stationary ^{13}C metabolic flux analysis (INST-MFA) methods, were hampered by the lack of reliable methods for **intracellular metabolite analysis** in mammalian suspension cells (Wahrheit et al., 2011). Therefore, a strategy for measuring intracellular metabolites in CHO suspension cells including sampling/quenching, metabolite extraction, and GC/MS analytics has been developed and implemented as an essential building block for the success of this thesis. In this context, different critical steps in the sampling and quenching procedure were identified (Wahrheit and Heinzle, 2013; Wahrheit and Heinzle, 2014). The method was successfully applied in the experiments presented in chapter 6. In this study, extra- and intracellular labeling dynamics were analyzed for the first time in CHO suspension cells to be used for INST-MFA (Nicolae et al., 2014a; Wahrheit et al., 2013). The established and validated protocol makes a substantial contribution to the challenging and tedious efforts of method development for intracellular metabolite analysis in mammalian cells (Wahrheit and Heinzle, 2014). Increasing the accessibility of intracellular metabolite data is crucial for in-depth metabolic studies in higher organisms and a prerequisite for the application of advanced MFA methods (Wahrheit et al., 2011).

The enormous potential and particular advantages of **non-stationary ^{13}C metabolic flux analysis (INST-MFA)** over classical stationary MFA approaches have been illustrated in the introduction (chapter 1.4.3) and in recent reviews (Wiechert and Nöh, 2013). Although demanding experimental and computational methods are required, the high information content of INST-MFA makes it an indispensable tool when challenging questions in metabolism are to be addressed. Therefore, its application is expected to increase tremendously in the future when the required technologies become more and more available. The studies presented in chapters 5 and 6 are the first examples describing the application of INST-MFA in mammalian suspension cells. In chapter 5, a useful modification of INST-MFA using only the information of extracellular labeling dynamics is proposed for the first time. This represents a remarkable technological advancement since it eliminates the necessity of sampling intracellular metabolites. The study presented in chapter 6 is the first example demonstrating the use of parallel tracers for INST-MFA in CHO cells. Integrating the labeling dynamics of 32 readout metabolites derived from two different tracer substrates, this study represents at the same time the most comprehensive investigation of CHO cell metabolism available at present. INST-MFA is the method of choice when isotopic steady state is not achieved in biological systems. Moreover, INST-MFA was demonstrated as a valuable tool in exploring complex metabolic networks unraveling details of (i) metabolic compartmentation and micro-compartmentation, (ii) reactions around the highly redundant and intertwined C3-C4 node, (iii) exchange fluxes and reversibilities, (iv) synthesis and degradation pathways occurring simultaneously, and (v) intracellular as well as intracompartmental metabolite concentrations. Providing the highest resolution of all MFA methods available to date, this methodology provides unique opportunities to tackle challenging questions in biology, biomedicine and biotechnology related to metabolism.

Selective permeabilization of the plasma membrane is a well-known and established method to generate intact mitochondria enclosed in cell ghosts (Kuznetsov et al., 2008). This technique has been employed in several contexts in this thesis. In chapter 2, selective permeabilization of the plasma membrane using digitonin and complete cell lysis using Triton X-100 were applied to discriminate between cytosolic and mitochondrial enzyme activities. The determination of **compartment-specific *in situ* enzyme activities** first described by Niklas et al. is a powerful enhancement of classical enzyme assays (Niklas et al., 2011a). It is a valuable method in all scientific questions where the localization or compartmentation of metabolic enzymes is of importance. It can support the set-up of relevant metabolic network models when the activity and location of enzymes are uncertain. It helps identifying metabolic bottlenecks by assessing maximum capacities of enzymes in the respective compartments, as demonstrated for the examples of IDH and aminotransferases in chapter 2. This information can be used to design targeted metabolic engineering strategies and overall assist in a rational optimization of industrial producer cells. The subcellular distribution of metabolic enzymes has been mostly neglected in the past. Including this

additional information will lead to significantly improved metabolic studies yielding much richer information about a cell's physiology.

In the last part of this thesis, **selectively permeabilized cells** were successfully applied for **mitochondrial studies**. Illustrating the permeabilized cell's stability, integrity and, most importantly, their function at metabolic steady state, their potential as experimental system for in-depth studies of mitochondrial metabolism was clearly demonstrated. Permeabilized cells are easier to handle and have a higher physiological relevance than isolated mitochondria. Bahnemann et al. showed that the mitochondria are kept inside the permeabilized CHO cells, thus maintaining their functional connections with cellular structures (Figure 9-2). They also confirmed the superior integrity of outer and inner mitochondrial membranes in digitonin-permeabilized CHO-K1 suspension cells compared to other cell disruption techniques (Dounce homogenization, sonication, electroporation). The mitochondrial integrity was efficiently preserved even at digitonin concentrations up to 100 or 200 times higher than applied in our studies (Bahnemann et al., 2014).

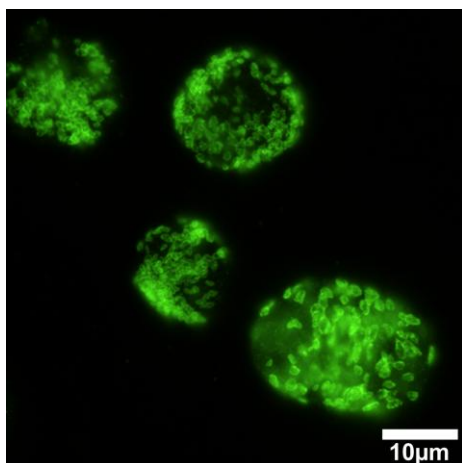


Figure 9-2. Mitochondria within digitonin-permeabilized CHO-K1 cells. Mitochondria were labeled with specific anti-Tom20 antibody and a secondary green fluorescent antibody (AlexaFluor 488, Goat-Anti-Rabbit-IgG) and visualized using confocal laser-scanning microscopy. CHO-K1 suspension cells were permeabilized with 0.01% (w/v) digitonin. Picture by courtesy of J. Bahnemann (group of Prof. Zeng, TUHH, Hamburg, Germany).

Two original strategies for investigating the mitochondrial metabolism in permeabilized CHO cells are presented in this thesis. First, permeabilized CHO cells were used in a **high-throughput quantitative respiration screening** (chapter 7). Microtiter plates with optical oxygen sensors are an easy to handle system suitable for high-throughput studies and requiring little experimental effort as shown in numerous previous applications (Beckers et al., 2009; Deshpande and Heinzle, 2004; Deshpande et al., 2004; Niklas et al., 2009; Noor et al., 2009; Strigun et al., 2011b; Zitova et al., 2009). Even more importantly, the presented methodology involves the corresponding $k_L a$ determination and thus allows a quantification of mitochondrial oxygen consumption without establishing an experimentally more complex oxygraph set-up. The outcome of the respiration screening was used to design even more **in-depth studies of mitochondrial metabolism using elementary mode analysis (EMA)** (chapter 8). The combination of selective cell permeabilization with the concept of EMA allows exploring details of the mitochondrial network. This innovative methodology facilitates the investigation of capacities, limitations, significance, and control of

mitochondrial pathways isolated from their cytosolic environment. Considering the involvement of the mitochondrial metabolism in ageing and various pathological conditions, a wide range of future applications can be imagined for both approaches quantitative high-throughput respiration analysis and mitochondrial EMA.

Chapters 3 and 4 aimed at investigating the metabolism of pyruvate and glutamine as major carbon sources for the mitochondrial TCA cycle in more detail. As shown in chapter 3, the cellular glutamine metabolism was directly connected to the extracellular glutamine supply in CHO cells. In contrast, varying the extracellular pyruvate concentration in the medium was found to have only little impact on the intracellular pyruvate metabolism (data not shown). However, this was not surprising, since the intracellular pyruvate is mainly derived from other sources in CHO cells, mostly from glucose and lactate. Therefore, a different strategy was tested. The application of **biochemical effectors in combination with MFA** was shown as a useful approach to investigate flux rearrangements as a result of increased or reduced pyruvate flux into the TCA cycle. Such experimental set-ups can be used to investigate metabolic flexibility, adaptability and limitations of biological systems and may be applied to assess the potential of producer strains or of therapeutic strategies. In addition to the combination with classical MFA as described in chapter 3, another interesting application is the use of biochemical effectors in combination with permeabilized cells and EMA using the set-up described in chapter 8. The feasibility of such an experimental system has already been demonstrated (Figure 9-3), e.g. to study mitochondrial transport in more detail. However, the corresponding data was not presented in this thesis.

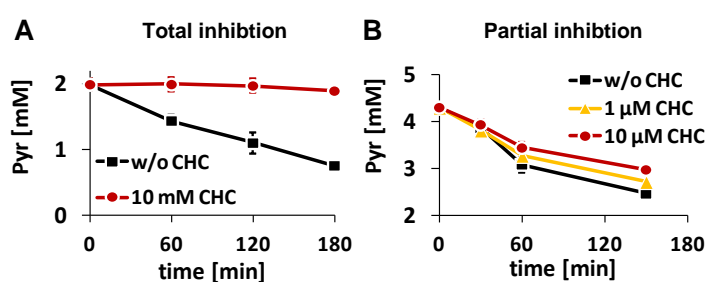


Figure 9-3. (A) Total and (B) partial inhibition of mitochondrial pyruvate uptake in permeabilized CHO cells by α -cyano-4-hydroxy cinnamic acid (CHC) compared to mitochondrial pyruvate uptake without (w/o) CHC addition.

The determination of **metabolic ratios** as useful parameters to characterize different physiological conditions was stressed at several points within this work, especially in the first part of this thesis (chapter 2, 3 and 4). The lactate/glucose ratio is commonly used to describe metabolic efficiency of cell cultures. In the presented thesis, the use of metabolic ratios was expanded by introducing several novelties. In chapter 2, a time-resolved analysis of metabolic ratios was proposed as means to monitor very sensitively metabolic shifts and stable states. New metabolic ratios were suggested in order to better explore specific questions. The TCA cycle/glycolysis ratio was demonstrated as a useful additional indicator to assess metabolic efficiency (chapters 2 and 4). The relation of all metabolic fluxes to the varied parameter, in this case the extracellular glutamine rate, was a

successful strategy to identify metabolic links (chapter 3). The relative importance of anaplerotic reactions was evaluated by comparing pyruvate dehydrogenase/glutamate dehydrogenase ratios between different conditions (chapter 4). The concept of metabolic ratios can be extended to other scientific questions. It allows for a more functional and network-oriented characterization of biological systems than looking at isolated metabolic rates. Metabolic ratios are usually also more sensitive when monitoring changing conditions. In addition, the calculation of ratios represents a specific normalization of data. Therefore, the comparison of data derived in various contexts (e.g. data from different patients) or when absolute metabolic rates are very different between conditions might be more reliable and meaningful for normalized metabolic ratios than for specific single fluxes.

In chapter 2, the **combination of different complementary methods** was illustrated as a solid strategy to significantly enrich data analysis in a rational way. In the age of systems biology, the collection of various huge (omics) data sets becomes more and more popular. The possibility to produce and store enormous amounts of data offers new prospects and bears certain risks. Collecting big data must not be mistaken for generating knowledge. The initial idea and the final goal of systems biology is to obtain a meaningful, multidimensional and holistic picture of the functioning of a biological system. In this study, it is emphasized that the experimental design should rather focus on generating selected data sets with complementary information than on collecting as much data as possible. The question on how to integrate these different and well chosen data sets has to be put at the beginning. In the presented study in chapter 2, the correlation of information from three different, complementary dimensions, (1) time, corresponding to the metabolic state, (2) space, i.e. localization of activity, and (3) function within the cellular hierarchy, i.e. maximum capacity (*in vitro* activity) vs. actual flux (*in vivo* activity) made it possible to derive detailed conclusions about the central metabolism and its control in CHO cells. The proposed systems-oriented approach can be understood as a general methodology. It demonstrates how an integrative interpretation of different selected information can be used to transfer data into knowledge.

9.3 Novel findings and potential implications

9.3.1 Glycolytic regulation

The HK reaction was confirmed as the rate-limiting step in glycolysis in CHO cells (chapter 2). Most importantly, the involvement of glycolytic channeling as a key aspect of glycolytic regulation in CHO cells was identified and its dynamic behavior described for the first time (chapter 2). It was found that the glycolytic enzymes exist partially in a soluble form and partially attached to cellular structures or associated with each other. This was especially evident for the two key enzymes of glycolytic control, HK and PFK. Binding of the HK to the outer mitochondrial membrane facilitates preferential access to mitochondrially generated ATP, stimulates glycolytic flux and was shown to inhibit apoptosis (Kim and Dang, 2005; Vyssokikh and Brdiczka, 2003). A fine-tuning of glycolytic fluxes matching the metabolic state is most likely achieved by a dynamic shift in the equilibrium between bound and soluble glycolytic enzymes. It was concluded that glycolysis in CHO cells occurs as a mixed response of partly glycolytic channeling and partly free diffusion. This finding was additionally verified by the results of the INST-MFA (chapters 5 and 6). Comparing the results of these two in-depth INST-MFA studies, we found that glucose uptake as well as glycolytic channeling to either lactate excretion or mitochondrial TCA cycle was significantly affected by the cultivation conditions. These findings further support our hypothesis established in chapter 2 that the dynamics of glycolytic channeling affect the availability of pyruvate to the mitochondria and thus the connection between glycolysis and TCA cycle. On the other hand, it was demonstrated that a perturbation of the cellular pyruvate metabolism by CHC and DCA resulted in feedback regulation of glycolysis (chapter 4). A decreased or increased pyruvate flux into the TCA cycle was partially compensated by up- and downregulation of glycolytic fluxes, respectively.

9.3.2 TCA cycle control

The higher glucose uptake and efficient channeling of pyruvate into the mitochondria in the reactor cultivation resulted in five times higher TCA cycle fluxes compared to the shake flask cultivations which were characterized by significant overflow metabolism. The most important findings regarding glycolytic and TCA cycle control are summarized in Figure 9-4.

The results of the mitochondrial studies indicate a separation of the TCA cycle into an effector-controlled first half and a concentration-controlled second half of the TCA cycle (chapter 7 and 8). The first part of the TCA cycle is tightly controlled by the availability and allosteric effects of substrates and cofactors. Activities of the PDH, the IDH and the AKGDH are strongly stimulated by ADP and most reactions are inhibited by high levels of ATP and NADH. In addition, the IDH activity was identified as rate-limiting reaction in the TCA cycle by determining its maximum capacity in the mitochondria (chapter 2). The respective intramitochondrial concentrations estimated by INST-MFA (chapter 6), high for citrate and low for α -ketoglutarate, additionally point to a

limiting function of the mitochondrial IDH reaction. Significantly higher TCA cycle activity and higher rates of full metabolization to CO_2 could be obtained when supplying intermediates entering the first half of the cycle (e.g. citrate, α -ketoglutarate, glutamine) compared to supply of C4-dicarboxylates (succinate, malate, fumarate) entering the second half of the cycle (chapter 8). The second half of the TCA cycle is controlled by a relatively constant mitochondrial pool of C4-dicarboxylates. Identical intracellular labeling dynamics determined for fumarate, malate and aspartate also point to a rapid equilibrium between C4 metabolites (chapter 6). An excess of C4 carbon is removed from the TCA cycle by cataplerotic reactions (chapters 2, 3, and 4) and from the mitochondria by the dicarboxylate carrier (chapter 8). High concentrations of C4-dicarboxylates potentially inhibit other enzymes involved in the TCA cycle (chapter 8).

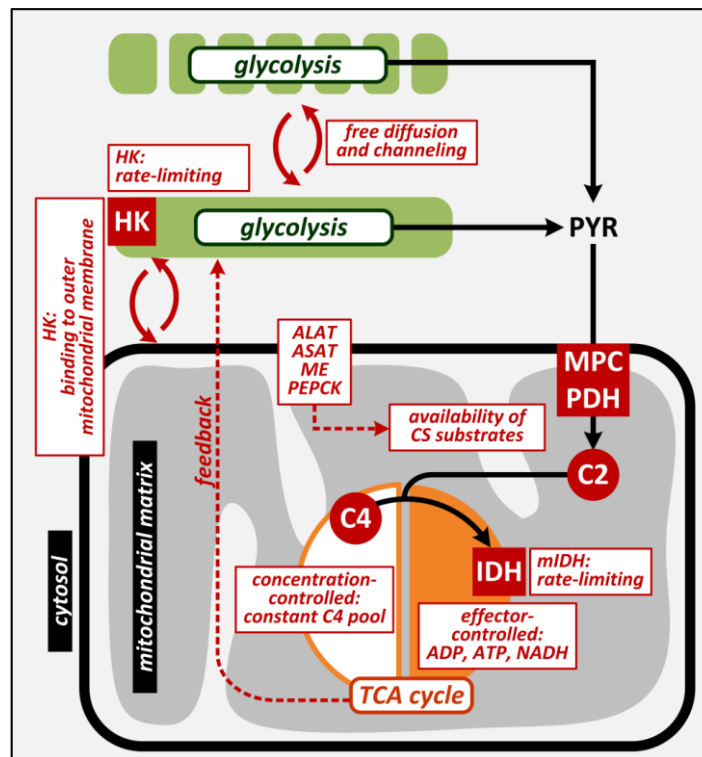


Figure 9-4. Metabolic control of glycolysis and TCA cycle in CHO-K1 cells. HK – hexokinase, mIDH – mitochondrial isocitrate dehydrogenase, MPC – mitochondrial pyruvate carrier, PDH – pyruvate dehydrogenase, PYR – pyruvate, C2 – acetyl-CoA (two carbon substrate), C4 – oxaloacetate (four carbon substrate). Important regulatory events are highlighted in red.

In addition, the TCA cycle flux is strictly regulated by availability of C2 (acetyl-CoA) and C4 substrates (oxaloacetate) to initiate the CS reaction. Pyruvate and glutamine were determined as most significant carbon sources to supply C2- and C4-units to the TCA cycle in CHO cells (chapter 2). Integrating the findings of the chapters 2, 3 and 4, it was concluded that the carbon input into the TCA cycle at the sites of pyruvate and glutamine can partially work as complementary, redundant

modules. It was shown that glutamine limitation was compensated by increased pyruvate consumption (chapter 3). On the other hand, an increased or decreased pyruvate flux into the TCA cycle upon metabolic perturbation by DCA or CHC, respectively, was offset by an adjustment of glutamine fluxes into the TCA cycle (chapter 4). Furthermore, it was found that a tailored adaptation of aminotransferases (ALAT and ASAT) and anaplerotic enzymes (ME and PEPCK) control a balanced carbon supply into the TCA cycle at varying pyruvate and glutamine availabilities in different growth phases of CHO cell batch cultivation (chapter 2). It is noteworthy that the highly efficient reactor cultivation was characterized by a significantly higher mitochondrial ME activity than the shake flask cultivations (chapter 5 and 6).

9.3.3 Amino acid metabolism

CHO cells are able to adapt to a wide range of glutamine availabilities (chapter 3). Flux rearrangements in the amino acid metabolism (mainly alanine, glutamate, serine, glycine, asparagine and aspartate) effectively mitigate ammonia stress as a result of glutamine excess and facilitate the utilization of alternative carbon sources to compensate glutamine limitation. The glutamine metabolism affects the growth behavior and partially the waste product excretion in CHO cells. A controlled feeding of glutamine avoids both glutamine limitation and glutamine excess which eventually reduces ammonia stress and increases culture longevity (chapter 3).

In particular the alanine production was directly coupled to glutamine consumption. In chapter 2, we observed that the mitochondrial ALAT (mALAT) was active at glutamine consumption in the first growth phase. After glutamine depletion, however, only cytosolic ALAT was found in the second growth phase. At high glutamine consumption rates, ammonia is mostly released in the mitochondria suggesting that mALAT is needed as a mitochondrial nitrogen sink. In chapter 2, we hypothesized that mitochondrial alanine is a potential source of mitochondrial pyruvate, although the contrary might also be true. It is possible that mALAT is consuming mitochondrial pyruvate, thereby contributing to the lack of C2 units in the exponential growth phase. The results of the INST-MFA favor the second hypothesis demonstrating that alanine is produced intramitochondrially and transported out in the cytosol (chapters 5 and 6). However, the high reversibilities determined for both ALAT isoenzymes indicate that back and forward reactions, pyruvate consumption and pyruvate production, are highly active. Both hypotheses might be partially valid and take effect situation-dependently.

Extracellular concentrations of alanine, glycine and glutamate increased in the exponential growth phase and decreased in later growth phases of CHO cell batch culture (chapters 2, 3 and 4). For all other amino acids net consumption was observed throughout the cultivation. However, even if net uptake was observed, degradation and synthesis of non-essential amino acids (NEAA) (e.g. serine, glutamine, aspartate) occurred simultaneously. Even at glutamine excess, glutamine synthesis was active (chapters 5 and 6). In addition, an excessive reversible exchange with the extracellular

medium, often significantly exceeding their net fluxes, was determined for NEAA (chapters 5 and 6).

The consideration of simultaneous synthesis and degradation pathways and exchange with the medium as well as the accurate representation of metabolic compartmentation in the metabolic model is essential to obtain a realistic picture of the cellular amino acid metabolism. This is especially critical to describe the cellular glutamate metabolism which is affected by e.g. glutaminase, glutamine synthetase, glutamate dehydrogenase, serine synthesis, alanine and aspartate aminotransferases, isocitrate dehydrogenases, and the mitochondrial aspartate-glutamate carrier. Integrating the results from two parallel tracer experiments in one parameter estimation of INST-MFA, it was possible for the first time to resolve a detailed metabolic network including all these aspects (chapter 6). Interestingly, mitochondrial glutamate was mostly metabolized by mitochondrial ALAT and ASAT and not by glutamate dehydrogenase. The high mitochondrial glutamate concentration estimated by INST-MFA favors its efflux into the cytosol. Cytosolic glutamate fuels the glutamine synthesis and serves as antiport partner for the aspartate-glutamate carrier.

9.3.4 The cytosol-mitochondria interface

For a detailed investigation of the cytosol-mitochondria interface a novel approach for in-depth quantitative studies of mitochondrial activities was designed and established. The strategy included experimental access of CHO cell mitochondria by selective permeabilization as well as a quantitative assessment of mitochondrial uptake and production rates integrated by EMA in order to resolve a mitochondrial network model. C4 dicarboxylates (e.g. malate and succinate) were transported in and out of the mitochondria at high rates. This demonstrates a high capacity of the dicarboxylate carrier that is mainly driven by extra- and intramitochondrial concentrations. This is additionally supported by the high reversibilities determined for the malate carrier in the two INST-MFA studies (chapters 5 and 6).

Citrate and α -ketoglutarate are both transported in antiport with a dicarboxylate. From all tested mitochondrial substrates, α -ketoglutarate and citrate sustained the highest complete TCA cycle activity. The findings of the mitochondrial studies suggest a potential cooperation between the dicarboxylate carrier and the citrate carrier or the α -ketoglutarate carrier, respectively, that prevents a dilution of malate into the extramitochondrial space and facilitates its direct reuptake (Figure 9-5) (chapter 8). This might result in an autocatalytic effect on the uptake of citrate and α -ketoglutarate explaining their high metabolization rates. Citrate and isocitrate uptake by the mitochondria is not described in a typical physiological context. Usually, citrate is transported out of the mitochondria to supply acetyl-CoA for the fatty acid synthesis. In addition, cytosolic citrate affects glycolytic activity by inhibiting PFK (Michal and Schomburg, 2012). The removal of citrate from the cytosol might be essential in some physiological situations to prevent an inhibition of glycolysis.

Considering the high cytosolic IDH activity with yet uncertain biological significance another role can be imagined. In a state of (cytosolic) NADPH excess (e.g. by a high PPP activity as shown in chapters 5 and 6), the reversed functioning of cytosolic IDH as described previously (Fendt et al., 2014; Metallo et al., 2012; Wise et al., 2011; Yoo et al., 2008) might result in cytosolic isocitrate and citrate production followed by their uptake into the mitochondria and utilization in the TCA cycle. Interestingly, intracompartmental concentrations of citrate and α -ketoglutarate as estimated by INST-MFA were reversed in cytosol and mitochondria. The high cytosolic and low mitochondrial α -ketoglutarate concentrations might even hint at a functioning of cytosolic and mitochondrial IDH in opposite directions.

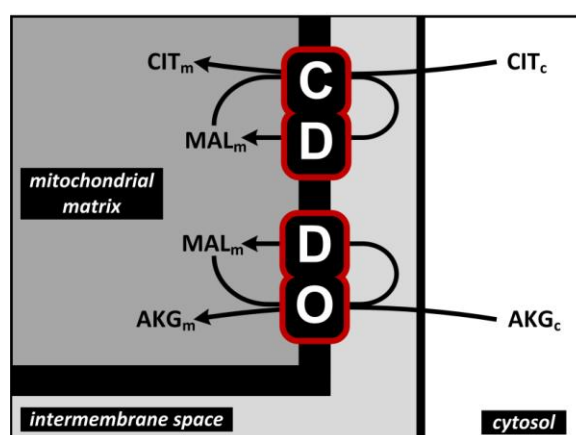


Figure 9-5. Cooperation between mitochondrial transporters obviates the dilution of intermediates. CIT – citrate, MAL – malate, AKG – α -ketoglutarate, C – citrate carrier, D – dicarboxylate carrier, O – α -ketoglutarate carrier.

In contrast to the reversible action of dicarboxylate carrier, citrate carrier and α -ketoglutarate carrier, our results indicate that pyruvate enters the mitochondria via irreversible action of the MPC. Although previous MFA studies of CHO cells considered a reversible mechanism of MPC in their network model (Ahn and Antoniewicz, 2011; Sheikholeslami et al., 2013b), there was no indication that pyruvate can be transported out of the mitochondria. Mitochondrial pyruvate metabolism was limited in mitochondrial studies when stimulated with ADP, aspartate, and both ADP and aspartate (chapters 7 and 8), but also *in vivo* when stimulated with DCA (chapter 4). These findings point to an upper limit of mitochondrial pyruvate transport by MPC. This suggests that the mitochondrial pyruvate supply cannot be adapted by increasing its transport. Alternatively, it can be controlled by ME facilitating intramitochondrial pyruvate generation. As illustrated above, an equimolar supply of C2 and C4 units is required to initiate the CS reaction and an important aspect of TCA cycle control. Instead of increasing the carbon input from the cytosol by increasing pyruvate uptake, pyruvate is rather produced from mitochondrial malate resulting in a redistribution of carbon from

C4 to C2 units and in an overall moderated carbon input into the TCA cycle. However, ME activity varied significantly at different cultivations conditions and in different growth phases (chapters 2, 5 and 6).

Interestingly, mitochondrial aspartate uptake required the presence of pyruvate. This indicates that pyruvate activates aspartate transport via the aspartate-glutamate carrier and its metabolization via ASAT by a yet unknown regulatory mechanism. Nevertheless, pyruvate and aspartate are metabolized individually by separate elementary modes (chapter 8). The aspartate-glutamate antiporter exchanges these amino acids across the mitochondrial membrane. Therefore, aspartate uptake stimulates glutamate excretion and glutamate uptake induces aspartate production by the mitochondria. In addition, glutamate can be transferred by a glutamate carrier in cotransport with H^+ . This was also the preferred system to export glutamate at conditions of excess glutamine consumption to prevent mitochondrial glutamate accumulation as shown by the mitochondrial studies (chapter 8) and the INST-MFA (chapter 6).

9.3.5 Metabolic compartmentation controlling the cellular redox balance

The cellular redox state is crucial in controlling metabolism. A huge number of different metabolic processes contribute to it. The NADH produced in glycolysis, TCA cycle and various redox reactions is used in the respiratory chain for energy generation. NADPH on the other hand is an important electron donor in biosynthesis reactions. In addition, NADPH has an essential role in scavenging ROS originating mainly from the respiratory chain as a byproduct.

Since reducing equivalents cannot pass the mitochondrial membrane, the cytosolic and mitochondrial redox balances are also controlled by metabolic compartmentation. In contrast to metabolites such as organic acids, amino acids, and ATP, where specific mitochondrial carriers are available, the transfer of electrons across the mitochondrial membrane requires the activity of mitochondrial shuttle systems. The malate-aspartate-shuttle and to a minor importance the glycerol phosphate shuttle usually transfer the electrons of NADH from the cytosol into the mitochondria where they contribute to energy generation by oxidative phosphorylation. Interestingly, the lack of mitochondrial ASAT activity determined in the exponential growth phase in chapter 2 indicates a dysfunctional malate-aspartate-shuttle at certain conditions. Therefore, the high lactate production in the first growth phase was responsible for NAD^+ regeneration (NADH oxidation) in the cytosol. Lactate consumption, on the other hand, was accompanied by an activation of mitochondrial ASAT indicating a fully functional malate-aspartate-shuttle in the second growth phase of CHO cell batch cultivation (chapter 2). Previous studies reported a connection between a functional malate-aspartate shuttle and the lactate shift in CHO cells (Zagari et al., 2013b). The malate-aspartate shuttle was found to be active in both INST-MFA studies (chapters 5 and 6). However, the mitochondrial studies revealed a complex regulation of mitochondrial aspartate metabolism that needs to be further elucidated (chapters 7 and 8).

In contrast, so far there has been no shuttle system described for the transfer of electrons of NADPH into the mitochondria. Since the mitochondria represent the major site of ROS generation and accumulation, the mitochondrial NADPH content is critical for counteracting oxidative stress. However, for the conditions studied in the presented thesis, cellular NADPH was mainly produced by PPP in the cytosol as consistently found for both INST-MFA studies (chapters 5 and 6). A potential source of mitochondrial NADPH is the malic enzyme reaction which has been shown to be active in the mitochondria (chapters 2, 5, 6, 7, and 8). In addition, mitochondrial NADPH can be generated by the NAD(P)^+ -transhydrogenase (NNT) that is located in the inner mitochondrial membrane (Michal and Schomburg, 2012). Using the mitochondrial proton gradient, NNT enables an intramitochondrial reduction of NADP^+ using NADH. Yet another possibility is the generation of NADPH by glutamate dehydrogenase (GDH) and isocitrate dehydrogenase (IDH). Besides the finding, that the IDH was identified as the rate-limiting step in the TCA cycle (chapter 2, 7, 8), some remarkable observations were made. Unexpectedly, the major part of the cellular IDH activity was found to be NADP^+ -dependent and less than 5% NAD^+ -dependent. Another interesting finding was that only 30% of IDH activity was mitochondrial while the major part of cellular activity was localized in the cytosol. Both cytosolic and mitochondrial NADP^+ -dependent IDH (IDH_{NADP}) isoenzymes have been associated with resistance to oxidative stress. Reduced IDH_{NADP} expression in either compartment was shown to induce DNA fragmentation, increased levels of peroxides and oxidized glutathione (GSSG) and reduced cellular ATP and NADPH levels in fibroblast cell cultures (Jo et al., 2001; Lee et al., 2002). Considering the protective role of IDH_{NADP} , its high proportion of more than 95% of cellular IDH activity indicates a successful adaptation of CHO K1 metabolism to cope with oxidative stress.

However, in particular the biological importance of the high cytosolic IDH activity remains an unanswered question in this respect. Considering the excess cytosolic NADPH production by PPP activity and the significant mitochondrial NADPH demand for ROS scavenging, a functioning of IDH in opposite directions in different compartments can be imagined. Reductive carboxylation of AKG by reverse flux through IDH has been described in various studies of mammalian cells, especially in the context of cancer metabolism, high proliferation rates, hypoxia and impaired mitochondrial function (Fan et al., 2013; Fendt et al., 2014; Leonardi et al., 2012; Metallo et al., 2012; Mullen et al., 2014; Mullen et al., 2012; Wise et al., 2011; Yoo et al., 2008).

Similar to the malate-aspartate shuttle responsible for the transfer of cytosolic NADH to be used in the mitochondrial respiratory chain, a shuttle system for cytosolic NADPH to be used for mitochondrial defense against oxidative stress can be hypothesized. The proposed shuttle system is schematically depicted in Figure 9-6. It involves a reverse cytosolic IDH consuming NADPH, import of citrate by the mitochondrial citrate carrier (as demonstrated in chapter 8), release of mitochondrial NADPH by forward mitochondrial IDH, and export of α -ketoglutarate via the α -ketoglutarate carrier to close the cycle. Malate can cycle between the two antiporters. The shuttle

9.3.6 Cellular robustness and its limitations

Robustness is a fundamental property of complex biological systems that allows maintaining functionality in the face of internal and external perturbations. CHO cells are famous for their extraordinary robustness and flexibility. Very different metabolic phenotypes have been observed at various different cultivation conditions. In the presented thesis, some key players of this robustness have been revealed.

An important aspect in terms of their flexibility is their ability to utilize a variety of different substrates. Different metabolites, e.g. lactate, glutamate and alanine, are first excreted as waste products but can be consumed as important carbon sources later in the cultivation (chapters 2, 3 and 4). We demonstrated that the reversible exchange of metabolites with the extracellular medium is in the order of their net fluxes or even substantially higher (chapters 5 and 6). Using this strategy the cells are able to perceive their environment very sensitively and rapidly shift from net excretion to net consumption depending on extra- and intracellular metabolite concentrations and kinetic properties of the respective plasma membrane transporters. That indicates that the utilization of alternative carbon sources is not a newly occurring event in the course of a cultivation process. Available carbon sources are always utilized, only their contribution to overall carbon intake can increase tremendously when the availability of other carbon sources decreases.

In chapter 2, it was observed that the cells maintained their viability and a functional TCA cycle over three metabolic phases characterized by (a) initial nutrient excess, (b) depletion of the major substrate glutamine and (c) nutrient scarcity towards the end of the cultivation. It was demonstrated which key enzymes are dynamically adjusted in different growth phases with respect to their activities and their subcellular localization in order to match the metabolism to changing substrate availabilities. The enzymes HK, PFK, IDH, ME, PEPCK, ALAT, and ASAT were shown to be of crucial importance in controlling the central metabolism in CHO cells.

The extreme metabolic robustness of CHO cells was further demonstrated in chapters 3 and 4. It was shown that CHO cells are able to grow at a wide range of different glutamine availabilities and also without glutamine supplementation. Interestingly, it was found that the glutamine synthesis pathway is active even at glutamine excess (chapters 5 and 6). In general, the simultaneous synthesis and catabolic degradation of NEAA enables an extraordinary flexibility in response to changing conditions. It allows a fast adaptation to varying anabolic and catabolic demands in the whole culture and in separate cellular compartments. Furthermore, additional carbon sources, mainly pyruvate, serine, asparagine, aspartate and glutamate, compensated a shortage of the preferred substrate glutamine. On the other hand, CHO cells also tolerate high glutamine abundance resulting in substantial ammonia accumulation. Cellular stress due to elevated ammonia levels was successfully extenuated by increasing cellular ammonia fixation (e.g. by alanine and serine synthesis) and reducing ammonia release from certain amino acids by decreasing their degradation

(e.g. asparagine and serine) (chapter 3). In addition, the energy metabolism of CHO cells proved to be robust upon perturbation of the cellular pyruvate metabolism with the biochemical effectors CHC and DCA (chapter 4). An impaired energy metabolism but also increased ATP levels were counterbalanced by effective rearrangements of anaplerotic fluxes (e.g. the glutamate dehydrogenase flux) and feedback regulation of the glycolysis. The interplay of pyruvate and glutamine input exemplifies this modular system of anaplerosis and cataplerosis that maintains TCA cycle activity at various internal and external perturbations (chapters 2, 3, 4).

Another aspect is the adaptation of the CHO cell redox metabolism towards high resistance to oxidative stress. This is facilitated by (i) the high PPP activity, (ii) cytosolic and mitochondrial lactate/pyruvate redox buffers, (iii) the substantial proportion of cellular NADP-dependent IDH, and (iv) potentially by the hypothesized NADPH shuttle system (Figure 9-6).

Although robustness is a valuable achievement, there are potential trade-offs with several cellular functions. Robustness is achieved at the cost of (i) resource demands, e.g. glutamine dependence upon a perturbed pyruvate metabolism (chapter 4), (ii) overall performance, e.g. reduced specific growth rate at glutamine free conditions (chapter 2 and 3), (iii) increased susceptibility towards unexpected perturbations, e.g. growth arrest and reduced energy levels when glutamine depletion and CHC treatment were combined (chapter 4), (iv) metabolic efficiency, e.g. putative substrate cycles by simultaneous amino acid catabolism and anabolism. Such compromising characteristics are inherent properties of robust systems (Kitano, 2004).

Understanding the means of cellular robustness is crucial to understand the dynamic nature of metabolism. In particular contexts, it is even desirable to avoid cellular robustness. Diseases can be regarded as a manifestation of robustness, e.g. the specific metabolic features of cancer cells. The development of high-yielding producer strains is often limited by cellular robustness, e.g. when genetic modifications do not manifest as intended. It was shown that the CHO cell metabolism was susceptible to low CHC and DCA concentrations due to insufficient activation of compensation mechanisms (chapter 4). Similarly, culture performance could be improved at mild glutamine limiting conditions by avoiding waste production and cataplerotic carbon output from the TCA cycle (chapter 3). Mild intervention seems to be a successful way to achieve the desired effect and necessary to avoid overcompensation of metabolism. On the other hand, the cellular performance could not be maintained or restored by compensation mechanisms when both major carbon sources of the TCA cycle, pyruvate and glutamine, failed. Knowing these weak points of the cell's metabolism is desirable either to avoid those conditions or to lead a cell into a vulnerable state on purpose to induce its collapse. The targeting of multiple enzymes or pathways that can potentially compensate each other (e.g. glycolysis and glutaminolysis) is a promising strategy to increase the efficacy of therapeutic treatments.

9.3.7 Implications for improving biotechnological production in CHO cells

Understanding the control of metabolism is crucial for leading cells into a desirable metabolic phenotype, and thus for achieving progress in bioprocesses. The results of the presented thesis provide novel and detailed insights into the central metabolism of CHO cells. In particular, we stress the importance of conducting comprehensive and in-depth studies and emphasize the dynamic nature of cellular metabolism. Oversimplifications of metabolism lead to misinterpretations and ultimately result in misguided measures and a waste of resources.

Many strategies for improving cellular performance involve reducing overflow metabolism by reducing substrate load (e.g. by low glucose and glutamine feeding) (Altamirano et al., 2004; Wong et al., 2005; Xie and Wang, 1994) or genetic engineering strategies (e.g. knockdown of LDH) (Chen et al., 2001; Jeong et al., 2001; Kim and Lee, 2007) with the aim of increasing the pyruvate carbon flux into the TCA cycle. However, especially genetic modifications do often not lead to the desired effect (Ha et al., 2013; Kim and Lee, 2009). Although remarkable improvements have been achieved in the past by simple genetic manipulations and screening for favorable cultivation conditions, more sophisticated strategies might be necessary in the future to continue progress and obtain significant further advancements. Our findings indicate that the wealth of regulatory measures, most importantly the universal feedback by the cellular redox and energy state, can in many cases not be suspended by targeting a single enzyme (usually only a single isoenzyme) or a single pathway.

In the presented thesis, key control elements in glycolysis, in TCA cycle, and for the first time also at the cytosol-mitochondria interface have been unraveled and highlighted as targets for metabolic engineering. Influencing glycolytic channeling (the distribution of bound and soluble glycolytic enzymes), e.g. by genetic or biochemical manipulation of specific isoenzymes of HK and PFK, might be an interesting approach to control glycolytic flux and apoptosis in industrial applications. Our findings revealed that the pyruvate flux into the TCA cycle is also affected by channeling effects in cytosol and mitochondria. These channeling events are, however, hardly understood, highly dynamic and with the current state of knowledge impossible to control by interventions. The mitochondrial pyruvate metabolism is strictly controlled by PDH. Activation of PDH by DCA was partially counterbalanced by flux rearrangements (e.g. down regulation of malic enzyme and glycolysis). However, the mitochondrial studies indicate that also the MPC is a limiting element in cellular pyruvate metabolism and thus a potential engineering target. An alternative strategy to increase intramitochondrial pyruvate supply is the overexpression of mitochondrial malic enzyme. This seems particularly promising because a higher ME activity was associated with a very efficient metabolism found for the reactor cultivation (chapter 5). Although glutamine was an important carbon source for the TCA cycle, it was found that it is not efficiently utilized in the mitochondria due to following efflux of glutamate out of the mitochondria. The efficient uptake and

metabolization of citrate by CHO cell mitochondria, however, stimulates ideas for testing citrate as an additional carbon source in CHO cell culture media. Nevertheless, all attempts to increase the carbon flux into TCA cycle might be effectless if its capacity or the capacity of oxidative phosphorylation is limited. Our findings indicate that the TCA cycle flux is very strictly controlled. An excess of carbon entering the TCA cycle is directly counterbalanced by cataplerotic reactions. Generally, increasing the rate-limiting mitochondrial activity of IDH seems to be a prerequisite for realizing higher TCA cycle activities. However, an elimination of feedback inhibition by NADH and ATP is most likely additionally required to achieve a higher TCA cycle flux.

10 Outlook and future prospects

The single studies presented in this thesis and most importantly their collective integration and interpretation provide deep insights into the functioning of the complex compartmented metabolism in CHO cells. However, we end up with more unanswered questions than we posed at the beginning. Further steps towards understanding the mammalian metabolism with respect to compartmentation should focus on following issues. While there is a wealth of data about enzyme properties in general, knowledge about kinetic and regulatory parameters of distinct isoenzymes located in different compartments is scarce (Rakhmanova and Popova, 2006). The determination of compartment-specific enzyme activities made a first small step towards increasing the awareness of the importance of such data. Similarly, information about existence, specificity and regulation of mitochondrial transporters is insufficient or uncertain. These data will provide a substantial contribution to refining compartmented metabolic models. We have shown that an evaluation of intracellular and even intracompartmental metabolite concentrations can be done by means of parameter estimation. Nevertheless, a reliable experimental determination of absolute intracellular concentrations in CHO suspension cells would significantly enrich MFA studies. Improving quenching and extraction methods, potentially implementing microfluidic lab-on-a-chip approaches (Rajabi et al., 2012; Wiendahl et al., 2007; Wurm et al., 2010), could eventually succeed in obtaining valid intracellular concentrations, yet are unlikely to resolve intracompartmental concentrations. FRET-sensors have been successfully applied to monitor the concentration of single metabolites in specific compartments (De Michele et al., 2014). For a more broad coverage of subcellular metabolite concentrations adaptations of non-aqueous fractionation methods might be a promising starting point (Gerhardt and Heldt, 1984; Krueger et al., 2011; Soboll et al., 1979). The main focus of this work was the determination of metabolic activities using MFA, EMA, enzyme assays and respiration rates. We have demonstrated what rich knowledge can be derived from integrating data sets of different hierarchical levels. The availability of CHO genome data paves the way for comprehensive systems biology studies. The integration of different omics data is expected to achieve a systems understanding of mammalian metabolism. This includes also the correlation between metabolism and other cellular processes, e.g. signalling (Goncalves et al., 2013; Ryll et al., 2014). The range of distinct metabolic phenotypes described in this thesis for different cultivation conditions, different metabolic phases in the course of cultivation, and different perturbations, illustrate the metabolic heterogeneity of CHO cell metabolism. Future studies should bring into focus this dynamic nature of metabolism. A practical implication of metabolic dynamics is that static interventions are not optimal to control metabolism. Flexible and adjustable methods for manipulating cell physiology and metabolism, e.g. by genetic switches (Kramer et al., 2004; Mazur et al., 1999), are needed to come up to dynamic metabolic control mechanisms.

11 References

- KEGG. <http://www.genome.jp/kegg/>. Kyoto encyclopedia of genes and genomes.
- Adam-Vizi, V., Tretter, L., 2013. The role of mitochondrial dehydrogenases in the generation of oxidative stress. *Neurochem Int.* 62, 757-63.
- Aggarwal, R. S., 2014. What's fueling the biotech engine-2012 to 2013. *Nat Biotechnol.* 32, 32-9.
- Ahn, W. S., Antoniewicz, M. R., 2011. Metabolic flux analysis of CHO cells at growth and non-growth phases using isotopic tracers and mass spectrometry. *Metab Eng.* 13, 598-609.
- Ahn, W. S., Antoniewicz, M. R., 2012. Towards dynamic metabolic flux analysis in CHO cell cultures. *Biotechnol J.* 7, 61-74.
- Ahn, W. S., Antoniewicz, M. R., 2013. Parallel labeling experiments with [1,2-(13)C]glucose and [U-(13)C]glutamine provide new insights into CHO cell metabolism. *Metab Eng.* 15, 34-47.
- al-Habori, M., 1995. Microcompartmentation, metabolic channelling and carbohydrate metabolism. *Int J Biochem Cell Biol.* 27, 123-32.
- Albers, D. S., Beal, M. F., 2000. Mitochondrial dysfunction and oxidative stress in aging and neurodegenerative disease. *J Neural Transm Suppl.* 59, 133-54.
- Allen, D. K., Libourel, I. G., Shachar-Hill, Y., 2009. Metabolic flux analysis in plants: coping with complexity. *Plant Cell Environ.* 32, 1241-57.
- Altamirano, C., Berrios, J., Vergara, M., Becerra, S., 2013. Advances in improving mammalian cells metabolism for recombinant protein production. *Electronic Journal of Biotechnology.* 16, 10-10.
- Altamirano, C., Cairo, J. J., Godia, F., 2001a. Decoupling cell growth and product formation in Chinese hamster ovary cells through metabolic control. *Biotechnol Bioeng.* 76, 351-60.
- Altamirano, C., Illanes, A., Becerra, S., Cairo, J. J., Godia, F., 2006. Considerations on the lactate consumption by CHO cells in the presence of galactose. *J Biotechnol.* 125, 547-56.
- Altamirano, C., Illanes, A., Casablanco, A., Gamez, X., Cairo, J. J., Godia, C., 2001b. Analysis of CHO cells metabolic redistribution in a glutamate-based defined medium in continuous culture. *Biotechnol Prog.* 17, 1032-41.
- Altamirano, C., Paredes, C., Cairo, J. J., Godia, F., 2000. Improvement of CHO cell culture medium formulation: simultaneous substitution of glucose and glutamine. *Biotechnol Prog.* 16, 69-75.
- Altamirano, C., Paredes, C., Illanes, A., Cairo, J. J., Godia, F., 2004. Strategies for fed-batch cultivation of t-PA producing CHO cells: substitution of glucose and glutamine and rational design of culture medium. *J Biotechnol.* 110, 171-9.
- Amaral, A. I., Teixeira, A. P., Hakonsen, B. I., Sonnewald, U., Alves, P. M., 2011a. A comprehensive metabolic profile of cultured astrocytes using isotopic transient metabolic flux analysis and C-labeled glucose. *Front Neuroenergetics.* 3, 5.

- Amaral, A. I., Teixeira, A. P., Sonnewald, U., Alves, P. M., 2011b. Estimation of intracellular fluxes in cerebellar neurons after hypoglycemia: Importance of the pyruvate recycling pathway and glutamine oxidation. *J Neurosci Res.* 89, 700-10.
- Anastasiou, D., Poulogiannis, G., Asara, J. M., Boxer, M. B., Jiang, J. K., Shen, M., Bellinger, G., Sasaki, A. T., Locasale, J. W., Auld, D. S., Thomas, C. J., Vander Heiden, M. G., Cantley, L. C., 2011. Inhibition of pyruvate kinase M2 by reactive oxygen species contributes to cellular antioxidant responses. *Science.* 334, 1278 - 1283.
- Antoniewicz, M. R., 2013a. ¹³C metabolic flux analysis: optimal design of isotopic labeling experiments. *Curr Opin Biotechnol.* 24, 1116-21.
- Antoniewicz, M. R., 2013b. Dynamic metabolic flux analysis--tools for probing transient states of metabolic networks. *Curr Opin Biotechnol.* 24, 973-8.
- Antoniewicz, M. R., Kelleher, J. K., Stephanopoulos, G., 2006a. Determination of confidence intervals of metabolic fluxes estimated from stable isotope measurements. *Metab Eng.* 8, 324-37.
- Antoniewicz, M. R., Stephanopoulos, G., Kelleher, J. K., 2006b. Evaluation of regression models in metabolic physiology: predicting fluxes from isotopic data without knowledge of the pathway. *Metabolomics.* 2, 41-52.
- Appling, D. R., 1991. Compartmentation of folate-mediated one-carbon metabolism in eukaryotes. *FASEB J.* 5, 2645-51.
- Arco, A. D., Satrustegui, J., 2005. New mitochondrial carriers: an overview. *Cell Mol Life Sci.* 62, 2204-27.
- Baba, N., Sharma, H. M., 1971. Histochemistry of lactic dehydrogenase in heart and pectoralis muscles of rat. *J Cell Biol.* 51, 621-35.
- Baeza, D., Gerdtzen, Z. P., Salgado, C. J., 2011. Design and simulation of a controller system for metabolic shift regulation in mammalian cells. *BMC Proc.* 5 Suppl 8, P11.
- Bahnemann, J., Kayo, S., Wahrheit, J., Heinzle, E., Pörtner, R., Zeng, A.-P., 2014. In search of an effective cell disruption method to isolate intact mitochondria from Chinese hamster ovary cells. *Engineering in Life Sciences.* 14, 161-169.
- Balaban, R. S., 2006. Modeling mitochondrial function. *Am J Physiol Cell Physiol.* 291, C1107-13.
- Balaban, R. S., 2010. The mitochondrial proteome: a dynamic functional program in tissues and disease states. *Environ Mol Mutagen.* 51, 352-9.
- Barden, R. E., Fung, C. H., Utter, M. F., Scrutton, M. C., 1972. Pyruvate carboxylase from chicken liver. Steady state kinetic studies indicate a "two-site" ping-pong mechanism. *J Biol Chem.* 247, 1323-33.
- Barlowe, C. K., Appling, D. R., 1988. In vitro evidence for the involvement of mitochondrial folate metabolism in the supply of cytoplasmic one-carbon units. *Biofactors.* 1, 171-6.
- Batke, J., 1989. Channeling of glycolytic intermediates by temporary, stationary bi-enzyme complexes is probable in vivo. *Trends Biochem Sci.* 14, 481-2.
- Baycin-Hizal, D., Tabb, D. L., Chaerkady, R., Chen, L., Lewis, N. E., Nagarajan, H., Sarkaria, V., Kumar, A., Wolozny, D., Colao, J., Jacobson, E., Tian, Y., O'Meally, R. N., Krag,

- S. S., Cole, R. N., Palsson, B. O., Zhang, H., Betenbaugh, M., 2012. Proteomic analysis of Chinese hamster ovary cells. *J Proteome Res.* 11, 5265-76.
- Bebbington, C. R., Renner, G., Thomson, S., King, D., Abrams, D., Yarranton, G. T., 1992. High-level expression of a recombinant antibody from myeloma cells using a glutamine synthetase gene as an amplifiable selectable marker. *Biotechnology (N Y)*. 10, 169-75.
- Becker, J., Hackl, M., Rupp, O., Jakobi, T., Schneider, J., Szczepanowski, R., Bekel, T., Borth, N., Goesmann, A., Grillari, J., Kaltschmidt, C., Noll, T., Puhler, A., Tauch, A., Brinkrolf, K., 2011. Unraveling the Chinese hamster ovary cell line transcriptome by next-generation sequencing. *J Biotechnol.* 156, 227-35.
- Beckers, S., Noor, F., Muller-Vieira, U., Mayer, M., Strigun, A., Heinzle, E., 2009. High throughput, non-invasive and dynamic toxicity screening on adherent cells using respiratory measurements. *Toxicol In Vitro*.
- Bensaad, K., Tsuruta, A., Selak, M. A., Vidal, M. N., Nakano, K., Bartrons, R., Gottlieb, E., Vousden, K. H., 2006. TIGAR, a p53-inducible regulator of glycolysis and apoptosis. *Cell.* 126, 107-20.
- Berg, J. M., Tymoczko, J. L., Stryer, L., 2012. *Biochemistry*. W.H. Freeman, Basingstoke.
- Berthiaume, F., Maguire, T. J., Yarmush, M. L., 2011. Tissue engineering and regenerative medicine: history, progress, and challenges. *Annu Rev Chem Biomol Eng.* 2, 403-30.
- Beuster, G., Zarse, K., Kaleta, C., Thierbach, R., Kiehntopf, M., Steinberg, P., Schuster, S., Ristow, M., 2011. Inhibition of alanine aminotransferase in silico and in vivo promotes mitochondrial metabolism to impair malignant growth. *J Biol Chem.* 286, 22323-30.
- Beutner, G., Ruck, A., Riede, B., Brdiczka, D., 1998. Complexes between porin, hexokinase, mitochondrial creatine kinase and adenylate translocator display properties of the permeability transition pore. Implication for regulation of permeability transition by the kinases. *Biochim Biophys Acta.* 1368, 7-18.
- Beutner, G., Ruck, A., Riede, B., Welte, W., Brdiczka, D., 1996. Complexes between kinases, mitochondrial porin and adenylate translocator in rat brain resemble the permeability transition pore. *FEBS Lett.* 396, 189-95.
- Birch, J. R., Racher, A. J., 2006. Antibody production. *Adv Drug Deliv Rev.* 58, 671-85.
- Bonarius, H. P., Hatzimanikatis, V., Meesters, K. P., de Gooijer, C. D., Schmid, G., Tramper, J., 1996. Metabolic flux analysis of hybridoma cells in different culture media using mass balances. *Biotechnol Bioeng.* 50, 299-318.
- Bonarius, H. P., Ozemre, A., Timmerarends, B., Skrabal, P., Tramper, J., Schmid, G., Heinzle, E., 2001. Metabolic-flux analysis of continuously cultured hybridoma cells using $(^{13}\text{C})\text{CO}_2$ mass spectrometry in combination with (^{13}C) -lactate nuclear magnetic resonance spectroscopy and metabolite balancing. *Biotechnol Bioeng.* 74, 528-38.
- Boss, O., Hagen, T., Lowell, B. B., 2000. Uncoupling proteins 2 and 3: potential regulators of mitochondrial energy metabolism. *Diabetes.* 49, 143-56.
- Brand, M. D., Nicholls, D. G., 2011. Assessing mitochondrial dysfunction in cells. *Biochem J.* 435, 297-312.
- Bricker, D. K., Taylor, E. B., Schell, J. C., Orsak, T., Boutron, A., Chen, Y. C., Cox, J. E., Cardon, C. M., Van Vranken, J. G., Dephoure, N., Redin, C., Boudina, S., Gygi, S. P.,

- Brivet, M., Thummel, C. S., Rutter, J., 2012. A mitochondrial pyruvate carrier required for pyruvate uptake in yeast, *Drosophila*, and humans. *Science*. 337, 96-100.
- Brinkrolf, K., Rupp, O., Laux, H., Kollin, F., Ernst, W., Linke, B., Kofler, R., Romand, S., Hesse, F., Budach, W. E., Galosy, S., Muller, D., Noll, T., Wienberg, J., Jostock, T., Leonard, M., Grillari, J., Tauch, A., Goesmann, A., Helk, B., Mott, J. E., Puhler, A., Borth, N., 2013. Chinese hamster genome sequenced from sorted chromosomes. *Nat Biotechnol*. 31, 694-5.
- Brooks, G. A., Dubouchaud, H., Brown, M., Sicurello, J. P., Butz, C. E., 1999. Role of mitochondrial lactate dehydrogenase and lactate oxidation in the intracellular lactate shuttle. *Proc Natl Acad Sci U S A*. 96, 1129-34.
- Bucher, T., Brauser, B., Conze, A., Klein, F., Langguth, O., Sies, H., 1972. State of oxidation-reduction and state of binding in the cytosolic NADH-system as disclosed by equilibration with extracellular lactate-pyruvate in hemoglobin-free perfused rat liver. *Eur J Biochem*. 27, 301 - 317.
- Buhler, S., Michels, J., Wendt, S., Ruck, A., Brdiczka, D., Welte, W., Przybylski, M., 1998. Mass spectrometric mapping of ion channel proteins (porins) and identification of their supramolecular membrane assembly. *Proteins. Suppl 2*, 63-73.
- Burleigh, S. C., van de Laar, T., Stroop, C. J., van Grunsven, W. M., O'Donoghue, N., Rudd, P. M., Davey, G. P., 2011. Synergizing metabolic flux analysis and nucleotide sugar metabolism to understand the control of glycosylation of recombinant protein in CHO cells. *BMC Biotechnol*. 11, 95.
- Butler, M., Meneses-Acosta, A., 2012. Recent advances in technology supporting biopharmaceutical production from mammalian cells. *Appl Microbiol Biotechnol*. 96, 885-94.
- Calvo, S., Jain, M., Xie, X., Sheth, S. A., Chang, B., Goldberger, O. A., Spinazzola, A., Zeviani, M., Carr, S. A., Mootha, V. K., 2006. Systematic identification of human mitochondrial disease genes through integrative genomics. *Nat Genet*. 38, 576-82.
- Campanella, M. E., Chu, H., Low, P. S., 2005. Assembly and regulation of a glycolytic enzyme complex on the human erythrocyte membrane. *Proc Natl Acad Sci U S A*. 102, 2402-7.
- Campanella, M. E., Chu, H., Wandersee, N. J., Peters, L. L., Mohandas, N., Gilligan, D. M., Low, P. S., 2008. Characterization of glycolytic enzyme interactions with murine erythrocyte membranes in wild-type and membrane protein knockout mice. *Blood*. 112, 3900-6.
- Carinhas, N., Duarte, T. M., Barreiro, L. C., Carrondo, M. J., Alves, P. M., Teixeira, A. P., 2013. Metabolic signatures of GS-CHO cell clones associated with butyrate treatment and culture phase transition. *Biotechnol Bioeng*. 110, 3244-57.
- Carlson, R., Fell, D., Srienc, F., 2002. Metabolic pathway analysis of a recombinant yeast for rational strain development. *Biotechnol Bioeng*. 79, 121-34.
- Cascante, M., Cortes, A., 1988. Kinetic studies of chicken and turkey liver mitochondrial aspartate aminotransferase. *Biochem J*. 250, 805-12.
- Cavero, S., Voza, A., del Arco, A., Palmieri, L., Villa, A., Blanco, E., Runswick, M. J., Walker, J. E., Cerdan, S., Palmieri, F., Satrustegui, J., 2003. Identification and

- metabolic role of the mitochondrial aspartate-glutamate transporter in *Saccharomyces cerevisiae*. *Mol Microbiol.* 50, 1257-69.
- Ceccarelli, C., Grodsky, N. B., Ariyaratne, N., Colman, R. F., Bahnson, B. J., 2002. Crystal structure of porcine mitochondrial NADP⁺-dependent isocitrate dehydrogenase complexed with Mn²⁺ and isocitrate. Insights into the enzyme mechanism. *J Biol Chem.* 277, 43454-62.
- Chaturvedi, R. K., Flint Beal, M., 2013. Mitochondrial diseases of the brain. *Free Radic Biol Med.* 63, 1-29.
- Chen, J., Zheng, H., Liu, H., Niu, J., Liu, J., Shen, T., Rui, B., Shi, Y., 2007. Improving metabolic flux estimation via evolutionary optimization for convex solution space. *Bioinformatics.* 23, 1115 - 1123.
- Chen, K., Liu, Q., Xie, L., Sharp, P. A., Wang, D. I., 2001. Engineering of a mammalian cell line for reduction of lactate formation and high monoclonal antibody production. *Biotechnol Bioeng.* 72, 55-61.
- Chen, L. B., 1988. Mitochondrial membrane potential in living cells. *Annu Rev Cell Biol.* 4, 155-81.
- Chen, N., Koumpouras, G. C., Polizzi, K. M., Kontoravdi, C., 2012. Genome-based kinetic modeling of cytosolic glucose metabolism in industrially relevant cell lines: *Saccharomyces cerevisiae* and Chinese hamster ovary cells. *Bioprocess Biosyst Eng.* 35, 1023-33.
- Chen, P., Harcum, S. W., 2006. Effects of elevated ammonium on glycosylation gene expression in CHO cells. *Metab Eng.* 8, 123-32.
- Chong, W. P., Thng, S. H., Hiu, A. P., Lee, D. Y., Chan, E. C., Ho, Y. S., 2012. LC-MS-based metabolic characterization of high monoclonal antibody-producing Chinese hamster ovary cells. *Biotechnol Bioeng.* 109, 3103-11.
- Chong, W. P., Yusufi, F. N., Lee, D. Y., Reddy, S. G., Wong, N. S., Heng, C. K., Yap, M. G., Ho, Y. S., 2011. Metabolomics-based identification of apoptosis-inducing metabolites in recombinant fed-batch CHO culture media. *J Biotechnol.* 151, 218-24.
- Clark, S., Francis, P. S., Conlan, X. A., Barnett, N. W., 2007. Determination of urea using high-performance liquid chromatography with fluorescence detection after automated derivatisation with xanthidol. *J Chromatogr A.* 1161, 207-13.
- Clegg, J. S., Jackson, S. A., 1990. Glucose metabolism and the channeling of glycolytic intermediates in permeabilized L-929 cells. *Arch Biochem Biophys.* 278, 452-60.
- Clerc, P., Polster, B. M., 2012. Investigation of mitochondrial dysfunction by sequential microplate-based respiration measurements from intact and permeabilized neurons. *PLoS One.* 7, e34465.
- Coskun, P., Wyrembak, J., Schriener, S. E., Chen, H. W., Marciniack, C., Laferla, F., Wallace, D. C., 2012. A mitochondrial etiology of Alzheimer and Parkinson disease. *Biochim Biophys Acta.* 1820, 553-64.
- Crabb, D. W., Yount, E. A., Harris, R. A., 1981. The metabolic effects of dichloroacetate. *Metabolism.* 30, 1024-39.
- Cruz, F., Villalba, M., Garcia-Espinosa, M. A., Ballesteros, P., Bogonez, E., Satrustegui, J., Cerdan, S., 2001. Intracellular compartmentation of pyruvate in primary cultures of cortical neurons as detected by (13)C NMR spectroscopy with multiple (13)C labels. *J Neurosci Res.* 66, 771-81.

- Dang, L., White, D. W., Gross, S., Bennett, B. D., Bittinger, M. A., Driggers, E. M., Fantin, V. R., Jang, H. G., Jin, S., Keenan, M. C., Marks, K. M., Prins, R. M., Ward, P. S., Yen, K. E., Liao, L. M., Rabinowitz, J. D., Cantley, L. C., Thompson, C. B., Vander Heiden, M. G., Su, S. M., 2009. Cancer-associated IDH1 mutations produce 2-hydroxyglutarate. *Nature*. 462, 739-44.
- Datta, P., Linhardt, R. J., Sharfstein, S. T., 2013. An 'omics approach towards CHO cell engineering. *Biotechnol Bioeng*. 110, 1255-71.
- De Michele, R., Carimi, F., Frommer, W. B., 2014. Mitochondrial biosensors. *Int J Biochem Cell Biol*. 48, 39-44.
- Dean, J., Reddy, P., 2013. Metabolic analysis of antibody producing CHO cells in fed-batch production. *Biotechnol Bioeng*. 110, 1735-47.
- Deshpande, R. R., 2007. Mammalian cell culture: High throughput applications of oxygen sensor plates and cellular physiological studies. Dissertation, Universität des Saarlandes.
- Deshpande, R. R., Mammalian Cell Culture: High Throughput Applications of Oxygen Sensor Plates and Cellular Physiological Studies Using ¹³C-Labeling Universität des Saarlandes, Saarbrücken, 2008.
- Deshpande, R. R., Heinzle, E., 2004. On-line oxygen uptake rate and culture viability measurement of animal cell culture using microplates with integrated oxygen sensors. *Biotechnol Lett*. 26, 763-7.
- Deshpande, R. R., Wittmann, C., Heinzle, E., 2004. Microplates with integrated oxygen sensing for medium optimization in animal cell culture. *Cytotechnology*. 46, 1-8.
- Deshpande, R. R., Yang, T. H., Heinzle, E., 2009. Towards a metabolic and isotopic steady state in CHO batch cultures for reliable isotope-based metabolic profiling. *Biotechnol J*. 4, 247-63.
- Dietmair, S., Nielsen, L. K., Timmins, N. E., 2011. Engineering a mammalian super producer. *Journal of Chemical Technology & Biotechnology*. 86, 905-914.
- Dietmair, S., Timmins, N. E., Gray, P. P., Nielsen, L. K., Kromer, J. O., 2010. Towards quantitative metabolomics of mammalian cells: Development of a metabolite extraction protocol. *Anal Biochem*. 404, 155-164.
- Divakaruni, A. S., Murphy, A. N., 2012. Cell biology. A mitochondrial mystery, solved. *Science*. 337, 41-3.
- Doverskog, M., Ljunggren, J., Ohman, L., Häggström, L., 1997. Physiology of cultured animal cells. *J Biotechnol*. 59, 103-15.
- Du, J., Cleghorn, W. M., Contreras, L., Lindsay, K., Rountree, A. M., Chertov, A. O., Turner, S. J., Sahaboglu, A., Linton, J., Sadilek, M., Satrustegui, J., Sweet, I. R., Paquet-Durand, F., Hurley, J. B., 2013. Inhibition of mitochondrial pyruvate transport by zaprinast causes massive accumulation of aspartate at the expense of glutamate in the retina. *J Biol Chem*. 288, 36129-40.
- Duarte, T. M., Carinhas, N., Barreiro, L. C., Carrondo, M. J., Alves, P. M., Teixeira, A. P., 2014. Metabolic responses of CHO cells to limitation of key amino acids. *Biotechnol Bioeng*. 111, 2095-106.
- Duchen, M. R., 2004. Roles of mitochondria in health and disease. *Diabetes*. 53 Suppl 1, S96-102.

- Duicu, O., Jusca, C., Falnita, L., Mirica, S., Maximov, D., Fira-Mladinescu, O., Muntean, D., 2013. Substrate-specific impairment of mitochondrial respiration in permeabilized fibers from patients with coronary heart disease versus valvular disease. *Mol Cell Biochem.* 379, 229-34.
- Eagle, H., 1955. Nutrition needs of mammalian cells in tissue culture. *Science.* 122, 501-14.
- Elustondo, P. A., White, A. E., Hughes, M. E., Brebner, K., Pavlov, E., Kane, D. A., 2013. Physical and functional association of lactate dehydrogenase (LDH) with skeletal muscle mitochondria. *J Biol Chem.* 288, 25309-17.
- Fan, J., Kamphorst, J. J., Rabinowitz, J. D., Shlomi, T., 2013. Fatty acid labeling from glutamine in hypoxia can be explained by isotope exchange without net reductive isocitrate dehydrogenase (IDH) flux. *J Biol Chem.* 288, 31363-9.
- Fang, J., Hsu, B. Y., MacMullen, C. M., Poncz, M., Smith, T. J., Stanley, C. A., 2002. Expression, purification and characterization of human glutamate dehydrogenase (GDH) allosteric regulatory mutations. *Biochem J.* 363, 81-7.
- Fendt, S. M., Bell, E. L., Keibler, M. A., Olenchock, B. A., Mayers, J. R., Wasylenko, T. M., Vokes, N. I., Guarente, L., Vander Heiden, M. G., Stephanopoulos, G., 2014. Reductive glutamine metabolism is a function of the alpha-ketoglutarate to citrate ratio in cells. *Nat Commun.* 4, 2236.
- Fernyhough, P., Roy Chowdhury, S. K., Schmidt, R. E., 2010. Mitochondrial stress and the pathogenesis of diabetic neuropathy. *Expert Rev Endocrinol Metab.* 5, 39-49.
- Fiermonte, G., Dolce, V., Arrigoni, R., Runswick, M. J., Walker, J. E., Palmieri, F., 1999. Organization and sequence of the gene for the human mitochondrial dicarboxylate carrier: evolution of the carrier family. *Biochem J.* 344 Pt 3, 953-60.
- Fiermonte, G., Palmieri, L., Dolce, V., Lasorsa, F. M., Palmieri, F., Runswick, M. J., Walker, J. E., 1998. The sequence, bacterial expression, and functional reconstitution of the rat mitochondrial dicarboxylate transporter cloned via distant homologs in yeast and *Caenorhabditis elegans*. *J Biol Chem.* 273, 24754-9.
- Fiermonte, G., Palmieri, L., Todisco, S., Agrimi, G., Palmieri, F., Walker, J. E., 2002. Identification of the mitochondrial glutamate transporter. Bacterial expression, reconstitution, functional characterization, and tissue distribution of two human isoforms. *J Biol Chem.* 277, 19289-94.
- Fischbach, M. A., Bluestone, J. A., Lim, W. A., 2013. Cell-based therapeutics: the next pillar of medicine. *Sci Transl Med.* 5, 179ps7.
- Fisher, M. B., Mauck, R. L., 2013. Tissue engineering and regenerative medicine: recent innovations and the transition to translation. *Tissue Eng Part B Rev.* 19, 1-13.
- Fogg, V. C., Lanning, N. J., Mackeigan, J. P., 2012. Mitochondria in cancer: at the crossroads of life and death. *Chin J Cancer.* 30, 526-39.
- Freshney, R. I., 2010. Introduction. *Culture of Animal Cells.* John Wiley & Sons, Inc., pp. 1-10.
- Frezza, C., Cipolat, S., Scorrano, L., 2007. Organelle isolation: functional mitochondria from mouse liver, muscle and cultured fibroblasts. *Nat Protoc.* 2, 287-95.
- Genzel, Y., Reichl, U., 2009. Continuous cell lines as a production system for influenza vaccines. *Expert Review of Vaccines.* 8, 1681-1692.

- Genzel, Y., Ritter, J. B., Konig, S., Alt, R., Reichl, U., 2005. Substitution of glutamine by pyruvate to reduce ammonia formation and growth inhibition of mammalian cells. *Biotechnol Prog.* 21, 58-69.
- Gerhardt, R., Heldt, H. W., 1984. Measurement of subcellular metabolite levels in leaves by fractionation of freeze-stopped material in nonaqueous media. *Plant Physiol.* 75, 542-7.
- Glacken, M. W., 1988. Catabolic Control of Mammalian Cell Culture. *Nature Biotechnology.* 6, 1041-1050.
- Gladden, L. B., 2004. Lactate metabolism: a new paradigm for the third millennium. *J Physiol.* 558, 5-30.
- Gnaiger, E., 2009. Capacity of oxidative phosphorylation in human skeletal muscle: new perspectives of mitochondrial physiology. *Int J Biochem Cell Biol.* 41, 1837-45.
- Gnaiger, E., 2012. Mitochondrial Pathways and Respiratory Control. An Introduction to OXPHOS Analysis. OROBOROS MiPNet Publications, Innsbruck.
- Gnoni, G. V., Priore, P., Geelen, M. J., Siculella, L., 2009. The mitochondrial citrate carrier: metabolic role and regulation of its activity and expression. *IUBMB Life.* 61, 987-94.
- Goncalves, E., Bucher, J., Ryll, A., Niklas, J., Mauch, K., Klamt, S., Rocha, M., Saez-Rodriguez, J., 2013. Bridging the layers: towards integration of signal transduction, regulation and metabolism into mathematical models. *Mol Biosyst.* 9, 1576-83.
- Gosalvez, M., Blanco, M., Hunter, J., Miko, M., Chance, B., 1974. Effects of anticancer agents on the respiration of isolated mitochondria and tumor cells. *Eur J Cancer.* 10, 567-74.
- Gottlieb, E., Armour, S. M., Thompson, C. B., 2002. Mitochondrial respiratory control is lost during growth factor deprivation. *Proc Natl Acad Sci U S A.* 99, 12801-6.
- Goudar, C., Biener, R., Boisart, C., Heidemann, R., Piret, J., de Graaf, A., Konstantinov, K., 2010. Metabolic flux analysis of CHO cells in perfusion culture by metabolite balancing and 2D [¹³C, ¹H] COSY NMR spectroscopy. *Metab Eng.* 12, 138-49.
- Goudar, C., Biener, R., Zhang, C., Michaels, J., Piret, J., Konstantinov, K., 2006. Towards industrial application of quasi real-time metabolic flux analysis for mammalian cell culture. *Adv Biochem Eng Biotechnol.* 101, 99-118.
- Goudar, C. T., Biener, R. K., Piret, J. M., Konstantinov, K. B., 2014. Metabolic flux estimation in mammalian cell cultures. *Methods Mol Biol.* 1104, 193-209.
- Graham, J. W., Williams, T. C., Morgan, M., Fernie, A. R., Ratcliffe, R. G., Sweetlove, L. J., 2007. Glycolytic enzymes associate dynamically with mitochondria in response to respiratory demand and support substrate channeling. *Plant Cell.* 19, 3723-38.
- Gray, L. R., Tompkins, S. C., Taylor, E. B., 2013. Regulation of pyruvate metabolism and human disease. *Cell Mol Life Sci.*
- Gunness, P., Mueller, D., Shevchenko, V., Heinzle, E., Ingelman-Sundberg, M., Noor, F., 2013. 3D organotypic cultures of human HepaRG cells: a tool for in vitro toxicity studies. *Toxicol Sci.* 133, 67-78.
- Gutfreund, H., Chock, P. B., 1991. Substrate channeling among glycolytic enzymes: fact or fiction. *J Theor Biol.* 152, 117-21.

- Gutierrez-Aguilar, M., Baines, C. P., 2013. Physiological and pathological roles of mitochondrial SLC25 carriers. *Biochem J.* 454, 371-86.
- Ha, T. K., Jeon, M. K., Yu da, Y., Lee, G. M., 2013. Effect of Bcl-x(L) overexpression on lactate metabolism in chinese hamster ovary cells producing antibody. *Biotechnol Prog.* 29, 1594-8.
- Haas, R. H., 2010. Autism and mitochondrial disease. *Dev Disabil Res Rev.* 16, 144-53.
- Hackl, M., Jakobi, T., Blom, J., Doppmeier, D., Brinkrolf, K., Szczepanowski, R., Bernhart, S. H., Honer Zu Siederdisen, C., Bort, J. A., Wieser, M., Kunert, R., Jeffs, S., Hofacker, I. L., Goesmann, A., Puhler, A., Borth, N., Grillari, J., 2011. Next-generation sequencing of the Chinese hamster ovary microRNA transcriptome: Identification, annotation and profiling of microRNAs as targets for cellular engineering. *J Biotechnol.* 153, 62-75.
- Halestrap, A. P., 1975. The mitochondrial pyruvate carrier. Kinetics and specificity for substrates and inhibitors. *Biochem J.* 148, 85-96.
- Halestrap, A. P., Price, N. T., 1999. The proton-linked monocarboxylate transporter (MCT) family: structure, function and regulation. *Biochem J.* 343, 281 - 299.
- Hamel, P., Saint-Georges, Y., de Pinto, B., Lachacinski, N., Altamura, N., Dujardin, G., 2004. Redundancy in the function of mitochondrial phosphate transport in *Saccharomyces cerevisiae* and *Arabidopsis thaliana*. *Mol Microbiol.* 51, 307-17.
- Hammond, S., Kaplarevic, M., Borth, N., Betenbaugh, M. J., Lee, K. H., 2012. Chinese hamster genome database: an online resource for the CHO community at www.CHOgenome.org. *Biotechnol Bioeng.* 109, 1353-6.
- Hanahan, D., Weinberg, R. A., 2011. Hallmarks of Cancer: The Next Generation. *Cell.* 144, 646-674.
- Hansen, H. A., Emborg, C., 1994a. Extra- and intracellular amino acid concentrations in continuous Chinese hamster ovary cell culture. *Appl Microbiol Biotechnol.* 41, 560-4.
- Hansen, H. A., Emborg, C., 1994b. Influence of ammonium on growth, metabolism, and productivity of a continuous suspension Chinese hamster ovary cell culture. *Biotechnol Prog.* 10, 121-4.
- Hardin, C. D., Finder, D. R., 1998. Glycolytic flux in permeabilized freshly isolated vascular smooth muscle cells. *Am J Physiol.* 274, C88-96.
- Hashimoto, M., Wilson, J. E., 2000. Membrane potential-dependent conformational changes in mitochondrially bound hexokinase of brain. *Arch Biochem Biophys.* 384, 163-73.
- Hashimoto, T., Brooks, G. A., 2008. Mitochondrial lactate oxidation complex and an adaptive role for lactate production. *Med Sci Sports Exerc.* 40, 486-94.
- Hashimoto, T., Hussien, R., Brooks, G. A., 2006. Colocalization of MCT1, CD147, and LDH in mitochondrial inner membrane of L6 muscle cells: evidence of a mitochondrial lactate oxidation complex. *Am J Physiol Endocrinol Metab.* 290, E1237-44.
- Hashimoto, T., Hussien, R., Cho, H. S., Kaufer, D., Brooks, G. A., 2008. Evidence for the mitochondrial lactate oxidation complex in rat neurons: demonstration of an essential component of brain lactate shuttles. *PLoS One.* 3, e2915.
- Hassanein, M., Hoeksema, M. D., Shiota, M., Qian, J., Harris, B. K., Chen, H., Clark, J. E., Alborn, W. E., Eisenberg, R., Massion, P. P., 2013. SLC1A5 mediates glutamine

- transport required for lung cancer cell growth and survival. *Clin Cancer Res.* 19, 560-70.
- Hassell, T., Gleave, S., Butler, M., 1991. Growth inhibition in animal cell culture. The effect of lactate and ammonia. *Appl Biochem Biotechnol.* 30, 29-41.
- Hatefi, Y., Galante, Y. M., 1977. Dehydrogenase and transhydrogenase properties of the soluble NADH dehydrogenase of bovine heart mitochondria. *Proc Natl Acad Sci U S A.* 74, 846-50.
- Hayward, B. E., Hussain, A., Wilson, R. H., Lyons, A., Woodcock, V., McIntosh, B., Harris, T. J., 1986. The cloning and nucleotide sequence of cDNA for an amplified glutamine synthetase gene from the Chinese hamster. *Nucleic Acids Res.* 14, 999 - 1008.
- Henderson, N. S., 1965. Isozymes of Isocitrate Dehydrogenase: Subunit Structure and Intracellular Location. *J Exp Zool.* 158, 263-73.
- Henry, C. S., Broadbelt, L. J., Hatzimanikatis, V., 2007. Thermodynamics-based metabolic flux analysis. *Biophys J.* 92, 1792 - 1805.
- Herzig, S., Raemy, E., Montessuit, S., Veuthey, J. L., Zamboni, N., Westermann, B., Kunji, E. R., Martinou, J. C., 2012. Identification and functional expression of the mitochondrial pyruvate carrier. *Science.* 337, 93-6.
- Hinkle, P. C., 2005. P/O ratios of mitochondrial oxidative phosphorylation. *Biochim Biophys Acta.* 1706, 1-11.
- Hofmann, U., Maier, K., Niebel, A., Vacun, G., Reuss, M., Mauch, K., 2008. Identification of metabolic fluxes in hepatic cells from transient ¹³C-labeling experiments: Part I. Experimental observations. *Biotechnol Bioeng.* 100, 344-54.
- Holthuis, J. C., Ungermann, C., 2013. Cellular microcompartments constitute general suborganelle functional units in cells. *Biol Chem.* 394, 151-61.
- Hussien, R., Brooks, G. A., 2011. Mitochondrial and plasma membrane lactate transporter and lactate dehydrogenase isoform expression in breast cancer cell lines. *Physiological Genomics.* 43, 255-64.
- Indiveri, C., Abruzzo, G., Stipani, I., Palmieri, F., 1998. Identification and purification of the reconstitutively active glutamine carrier from rat kidney mitochondria. *Biochem J.* 333 (Pt 2), 285-90.
- Jackson, S. A., Thomson, M. J., Clegg, J. S., 1990. Glycolysis compared in intact, permeabilized and sonicated L-929 cells. *FEBS Lett.* 262, 212-4.
- Jain, M., Nilsson, R., Sharma, S., Madhusudhan, N., Kitami, T., Souza, A. L., Kafri, R., Kirschner, M. W., Clish, C. B., Mootha, V. K., 2012. Metabolite profiling identifies a key role for glycine in rapid cancer cell proliferation. *Science.* 336, 1040-4.
- James, A. M., Collins, Y., Logan, A., Murphy, M. P., 2012. Mitochondrial oxidative stress and the metabolic syndrome. *Trends Endocrinol Metab.* 23, 429-34.
- Jandt, U., You, C., Zhang, Y. H., Zeng, A. P., 2013. Compartmentalization and metabolic channeling for multienzymatic biosynthesis: practical strategies and modeling approaches. *Adv Biochem Eng Biotechnol.* 137, 41-65.
- Jayapal, K. P., Wlaschin, K. F., Hu, W.-S., Yap, M. G. S., 2007. Recombinant Protein Therapeutics from CHO Cells - 20 Years and Counting. *Chemical Engineering Progress.* 103, 40-47

- Jeong, D., Kim, T. S., Lee, J. W., Kim, K. T., Kim, H. J., Kim, I. H., Kim, I. Y., 2001. Blocking of acidosis-mediated apoptosis by a reduction of lactate dehydrogenase activity through antisense mRNA expression. *Biochem Biophys Res Commun.* 289, 1141-9.
- Jitrapakdee, S., Wallace, J. C., 1999. Structure, function and regulation of pyruvate carboxylase. *Biochem J.* 340 (Pt 1), 1-16.
- Jo, S. H., Son, M. K., Koh, H. J., Lee, S. M., Song, I. H., Kim, Y. O., Lee, Y. S., Jeong, K. S., Kim, W. B., Park, J. W., Song, B. J., Huh, T. L., 2001. Control of mitochondrial redox balance and cellular defense against oxidative damage by mitochondrial NADP⁺-dependent isocitrate dehydrogenase. *J Biol Chem.* 276, 16168-76.
- John, G. T., Klimant, I., Wittmann, C., Heinzle, E., 2003. Integrated optical sensing of dissolved oxygen in microtiter plates: a novel tool for microbial cultivation. *Biotechnol Bioeng.* 81, 829-36.
- Jorda, J., Rojas, H. C., Carnicer, M., Wahl, A., Ferrer, P., Albiol, J., 2014. Quantitative Metabolomics and Instationary ¹³C-Metabolic Flux Analysis Reveals Impact of Recombinant Protein Production on Trehalose and Energy Metabolism in *Pichia pastoris*. *Metabolites.* 4, 281-99.
- Jorda, J., Suarez, C., Carnicer, M., ten Pierick, A., Heijnen, J. J., van Gulik, W., Ferrer, P., Albiol, J., Wahl, A., 2013. Glucose-methanol co-utilization in *Pichia pastoris* studied by metabolomics and instationary (1)(3)C flux analysis. *BMC Syst Biol.* 7, 17.
- Kahn, S. E., Hull, R. L., Utzschneider, K. M., 2006. Mechanisms linking obesity to insulin resistance and type 2 diabetes. *Nature.* 444, 840-6.
- Kaleta, C., de Figueiredo, L. F., Schuster, S., 2009. Can the whole be less than the sum of its parts? Pathway analysis in genome-scale metabolic networks using elementary flux patterns. *Genome Res.* 19, 1872-83.
- Kanehisa, M., Goto, S., Sato, Y., Kawashima, M., Furumichi, M., Tanabe, M., 2014. Data, information, knowledge and principle: back to metabolism in KEGG. *Nucleic Acids Res.* 42, D199-205.
- Kaufman, R. J., Wasley, L. C., Spiliotes, A. J., Gossels, S. D., Latt, S. A., Larsen, G. R., Kay, R. M., 1985. Coamplification and coexpression of human tissue-type plasminogen activator and murine dihydrofolate reductase sequences in Chinese hamster ovary cells. *Mol Cell Biol.* 5, 1750-9.
- Kelner, K. L., Morita, K., Rossen, J. S., Pollard, H. B., 1986. Restricted diffusion of tyrosine hydroxylase and phenylethanolamine N-methyltransferase from digitonin-permeabilized adrenal chromaffin cells. *Proc Natl Acad Sci U S A.* 83, 2998-3002.
- Kildegaard, H. F., Baycin-Hizal, D., Lewis, N. E., Betenbaugh, M. J., 2013. The emerging CHO systems biology era: harnessing the 'omics revolution for biotechnology. *Curr Opin Biotechnol.* 24, 1102-7.
- Kim, G. J., Fiskum, G. M., Morgan, W. F., 2006. A role for mitochondrial dysfunction in perpetuating radiation-induced genomic instability. *Cancer Res.* 66, 10377-83.
- Kim, J. W., Dang, C. V., 2005. Multifaceted roles of glycolytic enzymes. *Trends Biochem Sci.* 30, 142-50.
- Kim, J. Y., Kim, Y. G., Lee, G. M., 2012. CHO cells in biotechnology for production of recombinant proteins: current state and further potential. *Appl Microbiol Biotechnol.* 93, 917-30.

- Kim, S. H., Lee, G. M., 2007. Down-regulation of lactate dehydrogenase-A by siRNAs for reduced lactic acid formation of Chinese hamster ovary cells producing thrombopoietin. *Appl Microbiol Biotechnol.* 74, 152-9.
- Kim, Y. G., Lee, G. M., 2009. Bcl-xL overexpression does not enhance specific erythropoietin productivity of recombinant CHO cells grown at 33 degrees C and 37 degrees C. *Biotechnol Prog.* 25, 252-6.
- Kitano, H., 2004. Biological robustness. *Nat Rev Genet.* 5, 826-37.
- Kitano, H., 2007. Towards a theory of biological robustness. *Mol Syst Biol.* 3, 137.
- Klein, S., Mueller, D., Schevchenko, V., Noor, F., 2014a. Long-term maintenance of HepaRG cells in serum-free conditions and application in a repeated dose study. *J Appl Toxicol.* 34, 1078-86.
- Klein, T., Lange, S., Wilhelm, N., Bureik, M., Yang, T. H., Heinzle, E., Schneider, K., 2014b. Overcoming the metabolic burden of protein secretion in *Schizosaccharomyces pombe*--a quantitative approach using ¹³C-based metabolic flux analysis. *Metab Eng.* 21, 34-45.
- Kline, E. S., Brandt, R. B., Laux, J. E., Spainhour, S. E., Higgins, E. S., Rogers, K. S., Tinsley, S. B., Waters, M. G., 1986. Localization of L-lactate dehydrogenase in mitochondria. *Arch Biochem Biophys.* 246, 673-80.
- Kramer, B. P., Viretta, A. U., Daoud-El-Baba, M., Aubel, D., Weber, W., Fussenegger, M., 2004. An engineered epigenetic transgene switch in mammalian cells. *Nat Biotechnol.* 22, 867-70.
- Kroemer, G., Galluzzi, L., Brenner, C., 2007. Mitochondrial membrane permeabilization in cell death. *Physiol Rev.* 87, 99-163.
- Krueger, S., Giavalisco, P., Krall, L., Steinhauser, M. C., Bussis, D., Usadel, B., Flugge, U. I., Fernie, A. R., Willmitzer, L., Steinhauser, D., 2011. A topological map of the compartmentalized *Arabidopsis thaliana* leaf metabolome. *PLoS One.* 6, e17806.
- Kumar, A., Kant, S., Singh, S. M., 2013. alpha-Cyano-4-hydroxycinnamate induces apoptosis in Dalton's lymphoma cells: role of altered cell survival-regulatory mechanisms. *Anticancer Drugs.* 24, 158-71.
- Kurano, N., Leist, C., Messi, F., Kurano, S., Fiechter, A., 1990. Growth behavior of Chinese hamster ovary cells in a compact loop bioreactor. 2. Effects of medium components and waste products. *J Biotechnol.* 15, 113-28.
- Kurokawa, H., Park, Y. S., Iijima, S., Kobayashi, T., 1994. Growth characteristics in fed-batch culture of hybridoma cells with control of glucose and glutamine concentrations. *Biotechnol Bioeng.* 44, 95-103.
- Kuznetsov, A. V., Tiivel, T., Sikk, P., Kaambre, T., Kay, L., Daneshrad, Z., Rossi, A., Kadaja, L., Peet, N., Seppet, E., Saks, V. A., 1996. Striking differences between the kinetics of regulation of respiration by ADP in slow-twitch and fast-twitch muscles in vivo. *Eur J Biochem.* 241, 909-15.
- Kuznetsov, A. V., Veksler, V., Gellerich, F. N., Saks, V., Margreiter, R., Kunz, W. S., 2008. Analysis of mitochondrial function in situ in permeabilized muscle fibers, tissues and cells. *Nat Protoc.* 3, 965-76.
- Lane, M., Gardner, D. K., 2005. Mitochondrial malate-aspartate shuttle regulates mouse embryo nutrient consumption. *J Biol Chem.* 280, 18361-7.

- Lao, M. S., Toth, D., 1997. Effects of ammonium and lactate on growth and metabolism of a recombinant Chinese hamster ovary cell culture. *Biotechnol Prog.* 13, 688-91.
- Lee, S. M., Koh, H. J., Park, D. C., Song, B. J., Huh, T. L., Park, J. W., 2002. Cytosolic NADP(+)-dependent isocitrate dehydrogenase status modulates oxidative damage to cells. *Free Radic Biol Med.* 32, 1185-96.
- Lefort, N., Brown, A., Lloyd, V., Ouellette, R., Touaibia, M., Culf, A. S., Cuperlovic-Culf, M., 2013. H NMR metabolomics analysis of the effect of dichloroacetate and allopurinol on breast cancers. *J Pharm Biomed Anal.*
- Leighty, R. W., Antoniewicz, M. R., 2011. Dynamic metabolic flux analysis (DMFA): a framework for determining fluxes at metabolic non-steady state. *Metab Eng.* 13, 745-55.
- Leite, T. C., Coelho, R. G., Da Silva, D., Coelho, W. S., Marinho-Carvalho, M. M., Sola-Penna, M., 2011. Lactate downregulates the glycolytic enzymes hexokinase and phosphofructokinase in diverse tissues from mice. *FEBS Lett.* 585, 92-8.
- Lemasters, J. J., 2007. Modulation of mitochondrial membrane permeability in pathogenesis, autophagy and control of metabolism. *J Gastroenterol Hepatol.* 22 Suppl 1, S31-7.
- Lemire, J., Mailloux, R. J., Appanna, V. D., 2008. Mitochondrial lactate dehydrogenase is involved in oxidative-energy metabolism in human astrocytoma cells (CCF-STTG1). *PLoS One.* 3, e1550.
- Lenaz, G., 2001. The mitochondrial production of reactive oxygen species: mechanisms and implications in human pathology. *IUBMB Life.* 52, 159-64.
- Leonardi, R., Subramanian, C., Jackowski, S., Rock, C. O., 2012. Cancer-associated isocitrate dehydrogenase mutations inactivate NADPH-dependent reductive carboxylation. *J Biol Chem.* 287, 14615-20.
- Lewis, N. E., Liu, X., Li, Y., Nagarajan, H., Yerganian, G., O'Brien, E., Bordbar, A., Roth, A. M., Rosenbloom, J., Bian, C., Xie, M., Chen, W., Li, N., Baycin-Hizal, D., Latif, H., Forster, J., Betenbaugh, M. J., Famili, I., Xu, X., Wang, J., Palsson, B. O., 2013. Genomic landscapes of Chinese hamster ovary cell lines as revealed by the *Cricetulus griseus* draft genome. *Nat Biotechnol.* 31, 759-65.
- Li, J., Wong, C. L., Vijayasankaran, N., Hudson, T., Amanullah, A., 2012. Feeding lactate for CHO cell culture processes: impact on culture metabolism and performance. *Biotechnol Bioeng.* 109, 1173-86.
- Ljunggren, J., Haggstrom, L., 1992. Glutamine limited fed-batch culture reduces the overflow metabolism of amino acids in myeloma cells. *Cytotechnology.* 8, 45-56.
- Ljunggren, J., Haggstrom, L., 1994. Catabolic control of hybridoma cells by glucose and glutamine limited fed batch cultures. *Biotechnol Bioeng.* 44, 808-18.
- Llaneras, F., Pico, J., 2007a. An interval approach for dealing with flux distributions and elementary modes activity patterns. *J Theor Biol.* 246, 290-308.
- Llaneras, F., Pico, J., 2007b. A procedure for the estimation over time of metabolic fluxes in scenarios where measurements are uncertain and/or insufficient. *BMC Bioinformatics.* 8, 421.
- Lu, S., Sun, X., Zhang, Y., 2005. Insight into metabolism of CHO cells at low glucose concentration on the basis of the determination of intracellular metabolites. *Process Biochemistry.* 40, 1917-1921.

- Luo, J., Vijayasankaran, N., Autsen, J., Santuray, R., Hudson, T., Amanullah, A., Li, F., 2012. Comparative metabolite analysis to understand lactate metabolism shift in Chinese hamster ovary cell culture process. *Biotechnol Bioeng.* 109, 146-56.
- MacGregor, J. S., Singh, V. N., Davoust, S., Melloni, E., Pontremoli, S., Horecker, B. L., 1980. Evidence for formation of a rabbit liver aldolase--rabbit liver fructose-1,6-bisphosphatase complex. *Proc Natl Acad Sci U S A.* 77, 3889-92.
- Madeira, V. M., 2012. Overview of mitochondrial bioenergetics. *Methods Mol Biol.* 810, 1-6.
- Maier, K., Hofmann, U., Reuss, M., Mauch, K., 2008. Identification of metabolic fluxes in hepatic cells from transient ¹³C-labeling experiments: Part II. Flux estimation. *Biotechnol Bioeng.* 100, 355-70.
- Malaisse, W. J., Zhang, Y., Sener, A., 2004. Enzyme-to-enzyme channeling in the early steps of glycolysis in rat pancreatic islets. *Endocrine.* 24, 105-9.
- Manko, B. O., Klevets, M. Y., Manko, V. V., 2013. An implication of novel methodology to study pancreatic acinar mitochondria under in situ conditions. *Cell Biochem Funct.* 31, 115-21.
- Maranga, L., Goochee, C. F., 2006. Metabolism of PER.C6 cells cultivated under fed-batch conditions at low glucose and glutamine levels. *Biotechnol Bioeng.* 94, 139-50.
- Martin-Requero, A., Ayuso, M. S., Parrilla, R., 1986. Rate-limiting steps for hepatic gluconeogenesis. Mechanism of oxamate inhibition of mitochondrial pyruvate metabolism. *J Biol Chem.* 261, 13973-8.
- Martinez, V. S., Dietmair, S., Quek, L. E., Hodson, M. P., Gray, P., Nielsen, L. K., 2013. Flux balance analysis of CHO cells before and after a metabolic switch from lactate production to consumption. *Biotechnol Bioeng.* 110, 660-6.
- Mazur, X., Eppenberger, H. M., Bailey, J. E., Fussenegger, M., 1999. A novel autoregulated proliferation-controlled production process using recombinant CHO cells. *Biotechnol Bioeng.* 65, 144-50.
- Mazurek, S., Zwerschke, W., Jansen-Durr, P., Eigenbrodt, E., 2001. Metabolic cooperation between different oncogenes during cell transformation: interaction between activated ras and HPV-16 E7. *Oncogene.* 20, 6891 - 6898.
- McKenna, M. C., Hopkins, I. B., Carey, A., 2001. Alpha-cyano-4-hydroxycinnamate decreases both glucose and lactate metabolism in neurons and astrocytes: implications for lactate as an energy substrate for neurons. *J Neurosci Res.* 66, 747-54.
- McKenna, M. C., Tildon, J. T., Stevenson, J. H., Huang, X., Kingwell, K. G., 1995. Regulation of mitochondrial and cytosolic malic enzymes from cultured rat brain astrocytes. *Neurochem Res.* 20, 1491-501.
- Mercille, S., Massie, B., 1994. Induction of apoptosis in nutrient-deprived cultures of hybridoma and myeloma cells. *Biotechnol Bioeng.* 44, 1140-54.
- Metallo, C. M., Gameiro, P. A., Bell, E. L., Mattaini, K. R., Yang, J., Hiller, K., Jewell, C. M., Johnson, Z. R., Irvine, D. J., Guarente, L., Kelleher, J. K., Vander Heiden, M. G., Iliopoulos, O., Stephanopoulos, G., 2012. Reductive glutamine metabolism by IDH1 mediates lipogenesis under hypoxia. *Nature.* 481, 380-4.
- Metallo, C. M., Walther, J. L., Stephanopoulos, G., 2009. Evaluation of ¹³C isotopic tracers for metabolic flux analysis in mammalian cells. *J Biotechnol.* 144, 167-74.

- Michal, G., Schomburg, D., 2012. *Biochemical Pathways: An Atlas of Biochemistry and Molecular Biology*. John Wiley & Sons, Ltd., West Sussex, United Kingdom.
- Michelakis, E. D., Webster, L., Mackey, J. R., 2008. Dichloroacetate (DCA) as a potential metabolic-targeting therapy for cancer. *Br J Cancer*. 99, 989-94.
- Miller, W. M., Wilke, C. R., Blanch, H. W., 1989. Transient responses of hybridoma cells to nutrient additions in continuous culture: I. Glucose pulse and step changes. *Biotechnol Bioeng*. 33, 477-86.
- Mirabet, M., Navarro, A., Lopez, A., Canela, E. I., Mallol, J., Lluís, C., Franco, R., 1997. Ammonium toxicity in different cell lines. *Biotechnol Bioeng*. 56, 530-7.
- Miranda-Goncalves, V., Honavar, M., Pinheiro, C., Martinho, O., Pires, M. M., Pinheiro, C., Cordeiro, M., Bebiano, G., Costa, P., Palmeirim, I., Reis, R. M., Baltazar, F., 2013. Monocarboxylate transporters (MCTs) in gliomas: expression and exploitation as therapeutic targets. *Neuro-Oncology*. 15, 172-188.
- Mizuarai, S., Miki, S., Araki, H., Takahashi, K., Kotani, H., 2005. Identification of dicarboxylate carrier Slc25a10 as malate transporter in de novo fatty acid synthesis. *J Biol Chem*. 280, 32434-41.
- Modak, J., Deckwer, W. D., Zeng, A. P., 2002. Metabolic control analysis of eucaryotic pyruvate dehydrogenase multienzyme complex. *Biotechnol Prog*. 18, 1157-69.
- Modica-Napolitano, J. S., Singh, K. K., 2004. Mitochondrial dysfunction in cancer. *Mitochondrion*. 4, 755-62.
- Moreno-Sanchez, R., Marin-Hernandez, A., Saavedra, E., Pardo, J. P., Ralph, S. J., Rodriguez-Enriquez, S., 2014. Who controls the ATP supply in cancer cells? Biochemistry lessons to understand cancer energy metabolism. *Int J Biochem Cell Biol*. 50, 10-23.
- Morris, M. E., Felmler, M. A., 2008. Overview of the proton-coupled MCT (SLC16A) family of transporters: characterization, function and role in the transport of the drug of abuse gamma-hydroxybutyric acid. *AAPS J*. 10, 311 - 321.
- Mowbray, J., Moses, V., 1976. The tentative identification in *Escherichia coli* of a multienzyme complex with glycolytic activity. *Eur J Biochem*. 66, 25-36.
- Mracek, T., Drahota, Z., Houstek, J., 2013. The function and the role of the mitochondrial glycerol-3-phosphate dehydrogenase in mammalian tissues. *Biochim Biophys Acta*. 1827, 401-10.
- Mueller, D., Heinzele, E., Noor, F., 2013. 3D Hepatic In Vitro Models as Tools for Toxicity Studies. *Current Tissue Engineering*. 2, 78-89.
- Mueller, D., Kramer, L., Hoffmann, E., Klein, S., Noor, F., 2014. 3D organotypic HepaRG cultures as in vitro model for acute and repeated dose toxicity studies. *Toxicol In Vitro*. 28, 104-12.
- Mullen, A. R., Hu, Z., Shi, X., Jiang, L., Boroughs, L. K., Kovacs, Z., Boriack, R., Rakheja, D., Sullivan, L. B., Linehan, W. M., Chandel, N. S., DeBerardinis, R. J., 2014. Oxidation of alpha-ketoglutarate is required for reductive carboxylation in cancer cells with mitochondrial defects. *Cell Rep*. 7, 1679-90.
- Mullen, A. R., Wheaton, W. W., Jin, E. S., Chen, P. H., Sullivan, L. B., Cheng, T., Yang, Y., Linehan, W. M., Chandel, N. S., DeBerardinis, R. J., 2012. Reductive carboxylation supports growth in tumour cells with defective mitochondria. *Nature*. 481, 385-8.

- Murphy, T. A., Dang, C. V., Young, J. D., 2013. Isotopically nonstationary ¹³C flux analysis of Myc-induced metabolic reprogramming in B-cells. *Metab Eng.* 15, 206-17.
- Nadeau, I., Sabatie, J., Koehl, M., Perrier, M., Kamen, A., 2000. Human 293 cell metabolism in low glutamine-supplied culture: interpretation of metabolic changes through metabolic flux analysis. *Metab Eng.* 2, 277-92.
- Narkewicz, M. R., Sauls, S. D., Tjoa, S. S., Teng, C., Fennessey, P. V., 1996. Evidence for intracellular partitioning of serine and glycine metabolism in Chinese hamster ovary cells. *Biochem J.* 313 (Pt 3), 991-6.
- Nassir, F., Ibdah, J. A., 2014. Role of mitochondria in alcoholic liver disease. *World J Gastroenterol.* 20, 2136-42.
- Neermann, J., Wagner, R., 1996. Comparative analysis of glucose and glutamine metabolism in transformed mammalian cell lines, insect and primary liver cells. *J Cell Physiol.* 166, 152-69.
- Neuner, A., Heinzle, E., 2011. Mixed glucose and lactate uptake by *Corynebacterium glutamicum* through metabolic engineering. *Biotechnol J.* 6, 318-29.
- Newsholme, P., Gaudel, C., Krause, M., 2012. Mitochondria and diabetes. An intriguing pathogenetic role. *Adv Exp Med Biol.* 942, 235-47.
- Newsholme, P., Lima, M. M., Procopio, J., Pithon-Curi, T. C., Doi, S. Q., Bazotte, R. B., Curi, R., 2003a. Glutamine and glutamate as vital metabolites. *Braz J Med Biol Res.* 36, 153-63.
- Newsholme, P., Procopio, J., Lima, M. M., Pithon-Curi, T. C., Curi, R., 2003b. Glutamine and glutamate--their central role in cell metabolism and function. *Cell Biochem Funct.* 21, 1-9.
- Nicolae, A., Wahrheit, J., Bahnemann, J., Zeng, A.-P., Heinzle, E., 2014a. Non-stationary ¹³C metabolic flux analysis of Chinese hamster ovary cells in batch culture using extracellular labeling highlights metabolic reversibility and compartmentation. *BMC Systems Biology.* 8, 50.
- Nicolae, A., Wahrheit, J., Bahnemann, J., Zeng, A. P., Heinzle, E., 2014b. Non-stationary ¹³C metabolic flux analysis of Chinese hamster ovary cells in batch culture using extracellular labeling highlights metabolic reversibility and compartmentation. *BMC Syst Biol.* 8, 50.
- Niklas, J., Heinzle, E., 2012. Metabolic Flux Analysis in Systems Biology of Mammalian Cells. *Adv Biochem Eng Biotechnol.* 127, 109-32.
- Niklas, J., Melnyk, A., Yuan, Y., Heinzle, E., 2011a. Selective permeabilization for the high-throughput measurement of compartmented enzyme activities in mammalian cells. *Anal Biochem.* 416, 218-27.
- Niklas, J., Nonnenmacher, Y., Rose, T., Sandig, V., Heinzle, E., 2012a. Quercetin treatment changes fluxes in the primary metabolism and increases culture longevity and recombinant alpha(1)-antitrypsin production in human AGE1.HN cells. *Appl Microbiol Biotechnol.* 94, 57-67.
- Niklas, J., Noor, F., Heinzle, E., 2009. Effects of drugs in subtoxic concentrations on the metabolic fluxes in human hepatoma cell line Hep G2. *Toxicol Appl Pharmacol.* 240, 327-36.
- Niklas, J., Priesnitz, C., Rose, T., Sandig, V., Heinzle, E., 2012b. Primary metabolism in the new human cell line AGE1.HN at various substrate levels: increased metabolic

- efficiency and alpha1-antitrypsin production at reduced pyruvate load. *Appl Microbiol Biotechnol.* 93, 1637-50.
- Niklas, J., Priesnitz, C., Rose, T., Sandig, V., Heinzle, E., 2013. Metabolism and metabolic burden by alpha1-antitrypsin production in human AGE1.HN cells. *Metab Eng.* 16, 103-14.
- Niklas, J., Sandig, V., Heinzle, E., 2011b. Metabolite channeling and compartmentation in the human cell line AGE1.HN determined by ¹³C labeling experiments and ¹³C metabolic flux analysis. *J Biosci Bioeng.* 112, 616-23.
- Niklas, J., Schneider, K., Heinzle, E., 2010. Metabolic flux analysis in eukaryotes. *Curr Opin Biotechnol.* 21, 63-9.
- Niklas, J., Schrader, E., Sandig, V., Noll, T., Heinzle, E., 2011c. Quantitative characterization of metabolism and metabolic shifts during growth of the new human cell line AGE1.HN using time resolved metabolic flux analysis. *Bioprocess Biosyst Eng.* 34, 533-45.
- Noack, S., Noh, K., Moch, M., Oldiges, M., Wiechert, W., 2011. Stationary versus non-stationary (¹³C)-MFA: a comparison using a consistent dataset. *J Biotechnol.* 154, 179 - 190.
- Nöh, K., Gronke, K., Luo, B., Takors, R., Oldiges, M., Wiechert, W., 2007. Metabolic flux analysis at ultra short time scale: isotopically non-stationary ¹³C labeling experiments. *J Biotechnol.* 129, 249-67.
- Nöh, K., Wahl, A., Wiechert, W., 2006. Computational tools for isotopically instationary ¹³C labeling experiments under metabolic steady state conditions. *Metab Eng.* 8, 554-77.
- Nöh, K., Wiechert, W., 2006. Experimental design principles for isotopically instationary ¹³C labeling experiments. *Biotechnol Bioeng.* 94, 234-51.
- Nöh, K., Wiechert, W., 2011. The benefits of being transient: isotope-based metabolic flux analysis at the short time scale. *Appl Microbiol Biotechnol.* 91, 1247-65.
- Nolan, R. P., Lee, K., 2011. Dynamic model of CHO cell metabolism. *Metab Eng.* 13, 108-24.
- Noor, F., Niklas, J., Muller-Vieira, U., Heinzle, E., 2009. An integrated approach to improved toxicity prediction for the safety assessment during preclinical drug development using Hep G2 cells. *Toxicol Appl Pharmacol.* 237, 221-31.
- North, S. J., Huang, H. H., Sundaram, S., Jang-Lee, J., Etienne, A. T., Trollope, A., Chalabi, S., Dell, A., Stanley, P., Haslam, S. M., 2010. Glycomics profiling of Chinese hamster ovary cell glycosylation mutants reveals N-glycans of a novel size and complexity. *J Biol Chem.* 285, 5759-75.
- Nyberg, G. B., Balcarcel, R. R., Follstad, B. D., Stephanopoulos, G., Wang, D. I., 1999a. Metabolic effects on recombinant interferon-gamma glycosylation in continuous culture of Chinese hamster ovary cells. *Biotechnol Bioeng.* 62, 336-47.
- Nyberg, G. B., Balcarcel, R. R., Follstad, B. D., Stephanopoulos, G., Wang, D. I., 1999b. Metabolism of peptide amino acids by Chinese hamster ovary cells grown in a complex medium. *Biotechnol Bioeng.* 62, 324-35.
- O'Donnell-Tormey, J., Nathan, C. F., Lanks, K., DeBoer, C. J., de la Harpe, J., 1987. Secretion of pyruvate: an antioxidant defense of mammalian cells. *J Exp Med.* 165, 500 - 514.

- Orman, M. A., Arai, K., Yarmush, M. L., Androulakis, I. P., Berthiaume, F., Ierapetritou, M. G., 2010. Metabolic flux determination in perfused livers by mass balance analysis: effect of fasting. *Biotechnol Bioeng.* 107, 825-35.
- Orman, M. A., Berthiaume, F., Androulakis, I. P., Ierapetritou, M. G., 2011. Advanced stoichiometric analysis of metabolic networks of mammalian systems. *Crit Rev Biomed Eng.* 39, 511-34.
- Orth, J. D., Thiele, I., Palsson, B. O., 2010. What is flux balance analysis? *Nat Biotech.* 28, 245-248.
- Ovadi, J., 1991. Physiological significance of metabolic channelling. *J Theor Biol.* 152, 1-22.
- Ovadi, J., Aragon, J. J., Sols, A., 1986. Phosphofructokinase and fructosebisphosphatase from muscle can interact at physiological concentrations with mutual effects on their kinetic behavior. *Biochem Biophys Res Commun.* 135, 852-6.
- Ovadi, J., Saks, V., 2004. On the origin of intracellular compartmentation and organized metabolic systems. *Mol Cell Biochem.* 256-257, 5-12.
- Ozturk, S. S., Riley, M. R., Palsson, B. O., 1992. Effects of ammonia and lactate on hybridoma growth, metabolism, and antibody production. *Biotechnol Bioeng.* 39, 418-31.
- Palmieri, F., 1994. Mitochondrial carrier proteins. *FEBS Lett.* 346, 48-54.
- Palmieri, F., 2008. Diseases caused by defects of mitochondrial carriers: a review. *Biochim Biophys Acta.* 1777, 564-78.
- Palmieri, F., 2013. The mitochondrial transporter family SLC25: identification, properties and physiopathology. *Mol Aspects Med.* 34, 465-84.
- Palmieri, F., Indiveri, C., Bisaccia, F., Kramer, R., 1993. Functional properties of purified and reconstituted mitochondrial metabolite carriers. *J Bioenerg Biomembr.* 25, 525-35.
- Papin, J. A., Stelling, J., Price, N. D., Klamt, S., Schuster, S., Palsson, B. O., 2004. Comparison of network-based pathway analysis methods. *Trends Biotechnol.* 22, 400-5.
- Pecqueur, C., Bui, T., Gelly, C., Hauchard, J., Barbot, C., Bouillaud, F., Ricquier, D., Miroux, B., Thompson, C. B., 2008. Uncoupling protein-2 controls proliferation by promoting fatty acid oxidation and limiting glycolysis-derived pyruvate utilization. *Faseb J.* 22, 9-18.
- Perez-Bercoff, A., McLysaght, A., Conant, G. C., 2011. Patterns of indirect protein interactions suggest a spatial organization to metabolism. *Mol Biosyst.* 7, 3056-64.
- Peuhkurinen, K. J., Hiltunen, J. K., Hassinen, I. E., 1983. Metabolic compartmentation of pyruvate in the isolated perfused rat heart. *Biochem J.* 210, 193-8.
- Philp, A., Macdonald, A. L., Watt, P. W., 2005. Lactate--a signal coordinating cell and systemic function. *J Exp Biol.* 208, 4561-75.
- Picard, M., Wright, K. J., Ritchie, D., Thomas, M. M., Hepple, R. T., 2012. Mitochondrial function in permeabilized cardiomyocytes is largely preserved in the senescent rat myocardium. *PLoS One.* 7, e43003.

- Porceddu, M., Buron, N., Roussel, C., Labbe, G., Fromenty, B., Borgne-Sanchez, A., 2012. Prediction of Liver Injury Induced by Chemicals in Human with a Multiparametric Assay on Isolated Mouse Liver Mitochondria. *Toxicol Sci.*
- Portner, R., Schafer, T., 1996. Modelling hybridoma cell growth and metabolism--a comparison of selected models and data. *J Biotechnol.* 49, 119-35.
- Priesnitz, C., Niklas, J., Rose, T., Sandig, V., Heinzle, E., 2012. Metabolic flux rearrangement in the amino acid metabolism reduces ammonia stress in the alpha1-antitrypsin producing human AGE1.HN cell line. *Metab Eng.* 14, 128-37.
- Provost, A., Bastin, G., Agathos, S. N., Schneider, Y. J., 2006. Metabolic design of macroscopic bioreaction models: application to Chinese hamster ovary cells. *Bioprocess Biosyst Eng.* 29, 349-66.
- Puck, T. T., 1985. Development of the chinese hamster ovary (CHO) cell for use in somatic cell genetics, ed. Gottesman MM, John Wiley & Sons, 37-64. In: Gottesman, M. M., (Ed.), *Molecular Cell Genetics*. John Wiley & Sons, New York, pp. 37-64.
- Puck, T. T., Cieciura, S. J., Robinson, A., 1958. Genetics of somatic mammalian cells. III. Long-term cultivation of euploid cells from human and animal subjects. *J Exp Med.* 108, 945-56.
- Quek, L. E., Dietmair, S., Kromer, J. O., Nielsen, L. K., 2009. Metabolic flux analysis in mammalian cell culture. *Metab Eng.* 12, 161 - 171.
- Rabuazzo, A. M., Patane, G., Anello, M., Piro, S., Vigneri, R., Purrello, F., 1997. Hexokinase shift to mitochondria is associated with an increased sensitivity to glucose in rat pancreatic islets. *Diabetes.* 46, 1148-52.
- Raimundo, N., Baysal, B. E., Shadel, G. S., 2011. Revisiting the TCA cycle: signaling to tumor formation. *Trends Mol Med.* 17, 641-9.
- Rajabi, N., Bahnemann, J., Wahrheit, J., Heinzle, E., Zeng, A.-P., Müller, J., 2012. Inertia-based media exchange and quenching of cells for the continuous preparation of cells in a lab-on-a-chip. *Proceedings of the 3rd European Conference on Microfluidics, Heidelberg, Germany, December 4-5.*
- Rajendra, Y., Kiseljak, D., Baldi, L., Hacker, D. L., Wurm, F. M., 2012. Reduced glutamine concentration improves protein production in growth-arrested CHO-DG44 and HEK-293E cells. *Biotechnol Lett.* 34, 619-26.
- Rakhmanova, T. I., Popova, T. N., 2006. Regulation of 2-oxoglutarate metabolism in rat liver by NADP-isocitrate dehydrogenase and aspartate aminotransferase. *Biochemistry (Mosc).* 71, 211-7.
- Roberts, S. J., Lowery, M. S., Somero, G. N., 1988. Regulation of binding of phosphofructokinase to myofibrils in the red and white muscle of the barred sand bass, *Paralabrax nebulifer* (Serranidae). *J Exp Biol.* 137, 13-27.
- Ronnebaum, S. M., Ilkayeva, O., Burgess, S. C., Joseph, J. W., Lu, D., Stevens, R. D., Becker, T. C., Sherry, A. D., Newgard, C. B., Jensen, M. V., 2006. A pyruvate cycling pathway involving cytosolic NADP-dependent isocitrate dehydrogenase regulates glucose-stimulated insulin secretion. *J Biol Chem.* 281, 30593-602.
- Rosenstock, T. R., Duarte, A. I., Rego, A. C., 2010. Mitochondrial-associated metabolic changes and neurodegeneration in Huntington's disease - from clinical features to the bench. *Curr Drug Targets.* 11, 1218-36.

- Rousset, S., Alves-Guerra, M. C., Mozo, J., Miroux, B., Cassard-Doulcier, A. M., Bouillaud, F., Ricquier, D., 2004. The biology of mitochondrial uncoupling proteins. *Diabetes*. 53 Suppl 1, S130-5.
- Russell, J. B., 2007. The energy spilling reactions of bacteria and other organisms. *J Mol Microbiol Biotechnol*. 13, 1-11.
- Ryll, A., Bucher, J., Bonin, A., Bongard, S., Goncalves, E., Saez-Rodriguez, J., Niklas, J., Klamt, S., 2014. A model integration approach linking signalling and gene-regulatory logic with kinetic metabolic models. *Biosystems*. 124C, 26-38.
- Sagrsta, M. L., Bozal, J., 1987a. Lactate and malate dehydrogenase binding to the microsomal fraction from chicken liver. *Biochimie*. 69, 1207-15.
- Sagrsta, M. L., Bozal, J., 1987b. Lactate dehydrogenase activity in the mitochondrial fraction of chicken liver: enzyme binding and kinetic behavior of soluble and bound enzyme. *Biochimie*. 69, 205-14.
- Saks, V. A., Vasil'eva, E., Belikova Yu, O., Kuznetsov, A. V., Lyapina, S., Petrova, L., Perov, N. A., 1993. Retarded diffusion of ADP in cardiomyocytes: possible role of mitochondrial outer membrane and creatine kinase in cellular regulation of oxidative phosphorylation. *Biochim Biophys Acta*. 1144, 134-48.
- Saks, V. A., Veksler, V. I., Kuznetsov, A. V., Kay, L., Sikk, P., Tiivel, T., Tranqui, L., Olivares, J., Winkler, K., Wiedemann, F., Kunz, W. S., 1998. Permeabilized cell and skinned fiber techniques in studies of mitochondrial function in vivo. *Mol Cell Biochem*. 184, 81-100.
- Sanfeliu, A., Stephanopoulos, G., 1999. Effect of glutamine limitation on the death of attached Chinese hamster ovary cells. *Biotechnol Bioeng*. 64, 46-53.
- Sauer, U., 2004. High-throughput phenomics: experimental methods for mapping fluxomes. *Curr Opin Biotechnol*. 15, 58-63.
- Sauer, U., 2006. Metabolic networks in motion: ¹³C-based flux analysis. *Mol Syst Biol*. 2, 62.
- Sazanov, L. A., Jackson, J. B., 1994. Proton-translocating transhydrogenase and NAD- and NADP-linked isocitrate dehydrogenases operate in a substrate cycle which contributes to fine regulation of the tricarboxylic acid cycle activity in mitochondria. *FEBS Lett*. 344, 109-16.
- Schadewaldt, P., Munch, U., Staib, W., 1983. Evidence for the compartmentation of pyruvate metabolism in perfused rat skeletal muscle. *Biochem J*. 216, 761-4.
- Schafer, Z. T., Grassian, A. R., Song, L., Jiang, Z., Gerhart-Hines, Z., Irie, H. Y., Gao, S., Puigserver, P., Brugge, J. S., 2009. Antioxidant and oncogene rescue of metabolic defects caused by loss of matrix attachment. *Nature*. 461, 109-13.
- Schaub, J., Clemens, C., Kaufmann, H., Schulz, T. W., 2012. Advancing biopharmaceutical process development by system-level data analysis and integration of omics data. *Adv Biochem Eng Biotechnol*. 127, 133-63.
- Schell, J. C., Rutter, J., 2013. The long and winding road to the mitochondrial pyruvate carrier. *Cancer Metab*. 1, 6.
- Schmidt, K., Carlsen, M., Nielsen, J., Villadsen, J., 1997. Modeling isotopomer distributions in biochemical networks using isotopomer mapping matrices. *Biotechnol Bioeng*. 55, 831-40.

- Schneider, M., Marison, I. W., von Stockar, U., 1996. The importance of ammonia in mammalian cell culture. *J Biotechnol.* 46, 161-85.
- Schrauwen, P., Hesselink, M. K., 2008. Reduced tricarboxylic acid cycle flux in type 2 diabetes mellitus? *Diabetologia.* 51, 1694-7.
- Schuster, S., Fell, D. A., Dandekar, T., 2000. A general definition of metabolic pathways useful for systematic organization and analysis of complex metabolic networks. *Nat Biotechnol.* 18, 326-32.
- Schwartz, J. M., Kanehisa, M., 2006. Quantitative elementary mode analysis of metabolic pathways: the example of yeast glycolysis. *BMC Bioinformatics.* 7, 186.
- Sellick, C. A., Hansen, R., Maqsood, A. R., Dunn, W. B., Stephens, G. M., Goodacre, R., Dickson, A. J., 2009. Effective quenching processes for physiologically valid metabolite profiling of suspension cultured Mammalian cells. *Anal Chem.* 81, 174-83.
- Sellick, C. A., Hansen, R., Stephens, G. M., Goodacre, R., Dickson, A. J., 2011. Metabolite extraction from suspension-cultured mammalian cells for global metabolite profiling. *Nat. Protocols.* 6, 1241-1249.
- Selvarasu, S., Ho, Y. S., Chong, W. P., Wong, N. S., Yusufi, F. N., Lee, Y. Y., Yap, M. G., Lee, D. Y., 2012. Combined in silico modeling and metabolomics analysis to characterize fed-batch CHO cell culture. *Biotechnol Bioeng.* 109, 1415-29.
- Sengupta, N., Rose, S. T., Morgan, J. A., 2011. Metabolic flux analysis of CHO cell metabolism in the late non-growth phase. *Biotechnol Bioeng.* 108, 82-92.
- Sheikholeslami, Z., Jolicoeur, M., Henry, O., 2013a. The impact of the timing of induction on the metabolism and productivity of CHO cells in culture. *Biochemical Engineering Journal.* 79, 162-171.
- Sheikholeslami, Z., Jolicoeur, M., Henry, O., 2013b. Probing the metabolism of an inducible mammalian expression system using extracellular isotopomer analysis. *J Biotechnol.* 164, 469-78.
- Sheikholeslami, Z., Jolicoeur, M., Henry, O., 2014. Elucidating the effects of postinduction glutamine feeding on the growth and productivity of CHO cells. *Biotechnology Progress.* 30, 535-546.
- Sickmann, H. M., Schousboe, A., Fosgerau, K., Waagepetersen, H. S., 2005. Compartmentation of lactate originating from glycogen and glucose in cultured astrocytes. *Neurochem Res.* 30, 1295-304.
- Sidorenko, Y., Wahl, A., Dauner, M., Genzel, Y., Reichl, U., 2008. Comparison of metabolic flux distributions for MDCK cell growth in glutamine- and pyruvate-containing media. *Biotechnol Prog.* 24, 311-20.
- Simonot, C., Lerme, F., Louisot, P., Gateau-Roesch, O., 1997. Sub-mitochondrial localization of the catalytic subunit of pyruvate dehydrogenase phosphatase. *FEBS Lett.* 401, 158-62.
- Simpson, N. E., Han, Z., Berendzen, K. M., Sweeney, C. A., Oca-Cossio, J. A., Constantinidis, I., Stacpoole, P. W., 2006. Magnetic resonance spectroscopic investigation of mitochondrial fuel metabolism and energetics in cultured human fibroblasts: effects of pyruvate dehydrogenase complex deficiency and dichloroacetate. *Mol Genet Metab.* 89, 97-105.
- Smith, A. C., Robinson, A. J., 2011. A metabolic model of the mitochondrion and its use in modelling diseases of the tricarboxylic acid cycle. *BMC Syst Biol.* 5, 102.

- Soboll, S., Elbers, R., Heldt, H. W., 1979. Metabolite measurements in mitochondria and in the extramitochondrial compartment by fractionation of freeze-stopped liver tissue in nonaqueous media. *Methods Enzymol.* 56, 201-6.
- Spivey, H. O., Ovadi, J., 1999. Substrate channeling. *Methods.* 19, 306-21.
- Srour, O., Young, J. D., Eldar, Y. C., 2011. Fluxomers: a new approach for ¹³C metabolic flux analysis. *BMC Syst Biol.* 5, 129.
- Stacpoole, P. W., 1989. The pharmacology of dichloroacetate. *Metabolism.* 38, 1124-44.
- Stacpoole, P. W., 2012. The pyruvate dehydrogenase complex as a therapeutic target for age-related diseases. *Aging Cell.* 11, 371-7.
- Stacpoole, P. W., Harman, E. M., Curry, S. H., Baumgartner, T. G., Misbin, R. I., 1983. Treatment of lactic acidosis with dichloroacetate. *N Engl J Med.* 309, 390-6.
- Stacpoole, P. W., Moore, G. W., Kornhauser, D. M., 1978. Metabolic effects of dichloroacetate in patients with diabetes mellitus and hyperlipoproteinemia. *N Engl J Med.* 298, 526-30.
- Street, J. C., Delort, A. M., Braddock, P. S., Brindle, K. M., 1993. A ¹H/¹⁵N n.m.r. study of nitrogen metabolism in cultured mammalian cells. *Biochem J.* 291 (Pt 2), 485-92.
- Strigun, A., Noor, F., Pironti, A., Niklas, J., Yang, T. H., Heinzle, E., 2011a. Metabolic flux analysis gives an insight on verapamil induced changes in central metabolism of HL-1 cells. *J Biotechnol.* 155, 299-307.
- Strigun, A., Wahrheit, J., Beckers, S., Heinzle, E., Noor, F., 2011b. Metabolic profiling using HPLC allows classification of drugs according to their mechanisms of action in HL-1 cardiomyocytes. *Toxicol Appl Pharmacol.* 252, 183-91.
- Strigun, A., Wahrheit, J., Niklas, J., Heinzle, E., Noor, F., 2012. Doxorubicin increases oxidative metabolism in HL-1 cardiomyocytes as shown by ¹³C metabolic flux analysis. *Toxicol Sci.* 125, 595-606.
- Strumilo, S., 2005. Short-term regulation of the alpha-ketoglutarate dehydrogenase complex by energy-linked and some other effectors. *Biochemistry (Mosc).* 70, 726-9.
- Sutendra, G., Michelakis, E. D., 2013. Pyruvate dehydrogenase kinase as a novel therapeutic target in oncology. *Front Oncol.* 3, 38.
- Teixeira, A. P., Santos, S. S., Carinhas, N., Oliveira, R., Alves, P. M., 2008. Combining metabolic flux analysis tools and ¹³C NMR to estimate intracellular fluxes of cultured astrocytes. *Neurochem Int.* 52, 478-86.
- Templeton, N., Dean, J., Reddy, P., Young, J. D., 2013. Peak antibody production is associated with increased oxidative metabolism in an industrially relevant fed-batch CHO cell culture. *Biotechnol Bioeng.*
- Terzer, M., Stelling, J., 2008. Large-scale computation of elementary flux modes with bit pattern trees. *Bioinformatics.* 24, 2229-35.
- Thiele, I., Price, N. D., Vo, T. D., Palsson, B. O., 2005. Candidate metabolic network states in human mitochondria. Impact of diabetes, ischemia, and diet. *J Biol Chem.* 280, 11683-95.
- Timon-Gomez, A., Proft, M., Pascual-Ahuir, A., 2013. Differential regulation of mitochondrial pyruvate carrier genes modulates respiratory capacity and stress tolerance in yeast. *PLoS One.* 8, e79405.

- Tompa, P., Bar, J., Batke, J., 1986. Interaction of enzymes involved in triosephosphate metabolism. Comparison of yeast and rabbit muscle cytoplasmic systems. *Eur J Biochem.* 159, 117-24.
- Trinh, C. T., Wlaschin, A., Srienc, F., 2009. Elementary mode analysis: a useful metabolic pathway analysis tool for characterizing cellular metabolism. *Appl Microbiol Biotechnol.* 81, 813-26.
- Tritsch, G. L., Moore, G. E., 1962. Spontaneous decomposition of glutamine in cell culture media. *Exp Cell Res.* 28, 360-4.
- Trummer, E., Fauland, K., Seidinger, S., Schriebl, K., Lattenmayer, C., Kunert, R., Vorauer-Uhl, K., Weik, R., Borth, N., Katinger, H., Muller, D., 2006. Process parameter shifting: Part I. Effect of DOT, pH, and temperature on the performance of Epo-Fc expressing CHO cells cultivated in controlled batch bioreactors. *Biotechnol Bioeng.* 94, 1033-44.
- Turcan, S., Rohle, D., Goenka, A., Walsh, L. A., Fang, F., Yilmaz, E., Campos, C., Fabius, A. W., Lu, C., Ward, P. S., Thompson, C. B., Kaufman, A., Guryanova, O., Levine, R., Heguy, A., Viale, A., Morris, L. G., Huse, J. T., Mellinghoff, I. K., Chan, T. A., 2012. IDH1 mutation is sufficient to establish the glioma hypermethylator phenotype. *Nature.* 483, 479-83.
- Tuttle, S., Stamato, T., Perez, M. L., Biaglow, J., 2000. Glucose-6-phosphate dehydrogenase and the oxidative pentose phosphate cycle protect cells against apoptosis induced by low doses of ionizing radiation. *Radiat Res.* 153, 781-7.
- van Winden, W. A., Wittmann, C., Heinzle, E., Heijnen, J. J., 2002. Correcting mass isotopomer distributions for naturally occurring isotopes. *Biotechnol Bioeng.* 80, 477-9.
- Vander Heiden, M. G., Cantley, L. C., Thompson, C. B., 2009. Understanding the Warburg effect: the metabolic requirements of cell proliferation. *Science.* 324, 1029-33.
- Villadsen, J., Nielsen, J., Lidén, G., 2011. *Bioreaction Engineering Principles.* Springer, Heidelberg.
- Vizan, P., Alcarraz-Vizan, G., Diaz-Moralli, S., Solovjeva, O. N., Frederiks, W. M., Cascante, M., 2009. Modulation of pentose phosphate pathway during cell cycle progression in human colon adenocarcinoma cell line HT29. *Int J Cancer.* 124, 2789 - 2796.
- Vriezen, N., van Dijken, J. P., 1998a. Fluxes and enzyme activities in central metabolism of myeloma cells grown in chemostat culture. *Biotechnol Bioeng.* 59, 28-39.
- Vriezen, N., van Dijken, J. P., 1998b. Subcellular localization of enzyme activities in chemostat-grown murine myeloma cells. *J Biotechnol.* 61, 43-56.
- Vyssokikh, M. Y., Brdiczka, D., 2003. The function of complexes between the outer mitochondrial membrane pore (VDAC) and the adenine nucleotide translocase in regulation of energy metabolism and apoptosis. *Acta Biochim Pol.* 50, 389-404.
- Wahl, S. A., Noh, K., Wiechert, W., 2008. ¹³C labeling experiments at metabolic nonstationary conditions: an exploratory study. *BMC Bioinformatics.* 9, 152.
- Wahrheit, J., Heinzle, E., 2013. Sampling and quenching of CHO suspension cells for the analysis of intracellular metabolites. *BMC Proc.* 7, 42.
- Wahrheit, J., Heinzle, E., 2014. Quenching Methods for the Analysis of Intracellular Metabolites. In: Pörtner, R., (Ed.), *Animal Cell Biotechnology.* vol. 1104. Humana Press, pp. 211-221.

- Wahrheit, J., Nicolae, A., Heinzle, E., 2011. Eukaryotic metabolism: measuring compartment fluxes. *Biotechnol J.* 6, 1071-85.
- Wahrheit, J., Nicolae, A., Heinzle, E., 2013. ¹³C labeling dynamics of intra- and extracellular metabolites in CHO suspension cells. *BMC Proceedings C7 - P43.* 7, 1-2.
- Wahrheit, J., Nicolae, A., Heinzle, E., 2014a. Dynamics of growth and metabolism controlled by glutamine availability in Chinese hamster ovary cells. *Applied Microbiology and Biotechnology.* 98, 1771-1783.
- Wahrheit, J., Niklas, J., Heinzle, E., 2014b. Metabolic control at the cytosol-mitochondria interface in different growth phases of CHO cells. *Metabolic Engineering.* 23, 9-21.
- Wallace, D. C., 2012. Mitochondria and cancer. *Nat Rev Cancer.* 12, 685-98.
- Walsh, G., 2010a. Biopharmaceutical benchmarks 2010. *Nat Biotechnol.* 28, 917-24.
- Walsh, G., 2010b. Post-translational modifications of protein biopharmaceuticals. *Drug Discov Today.* 15, 773-80.
- Walsh, G., Jefferis, R., 2006. Post-translational modifications in the context of therapeutic proteins. *Nat Biotechnol.* 24, 1241-52.
- Warburg, O., 1956. On the origin of cancer cells. *Science.* 123, 309-14.
- Wellen, K. E., Thompson, C. B., 2010. Cellular metabolic stress: considering how cells respond to nutrient excess. *Mol Cell.* 40, 323-32.
- Westrin, H., Backman, L., 1983. Association of rabbit muscle glycolytic enzymes with filamentous actin. A counter-current distribution study at high ionic strength. *Eur J Biochem.* 136, 407-11.
- Whitacre, J. M., 2012. Biological robustness: paradigms, mechanisms, and systems principles. *Front Genet.* 3, 67.
- Wiback, S. J., Famili, I., Greenberg, H. J., Palsson, B. O., 2004. Monte Carlo sampling can be used to determine the size and shape of the steady-state flux space. *J Theor Biol.* 228, 437-47.
- Wiechert, W., 2001. ¹³C metabolic flux analysis. *Metab Eng.* 3, 195-206.
- Wiechert, W., Nöh, K., 2005. From stationary to instationary metabolic flux analysis. *Adv Biochem Eng Biotechnol.* 92, 145-72.
- Wiechert, W., Nöh, K., 2013. Isotopically non-stationary metabolic flux analysis: complex yet highly informative. *Curr Opin Biotechnol.* 24, 979-86.
- Wiendahl, C., Brandner, J. J., Küppers, C., Luo, B., Schygulla, U., Noll, T., Oldiges, M., 2007. A Microstructure Heat Exchanger for Quenching the Metabolism of Mammalian Cells. *Chemical Engineering & Technology.* 30, 322-328.
- Williamson, J. R., Cooper, R. H., 1980. Regulation of the citric acid cycle in mammalian systems. *FEBS Lett.* 117 Suppl, K73-85.
- Wilson, J. E., 1982. "Ambiquitous" behavior of brain hexokinase: rapid and reversible interaction of hexokinase with the outer mitochondrial membrane. *Biophys J.* 37, 18-9.
- Wilson, J. E., 2003. Isozymes of mammalian hexokinase: structure, subcellular localization and metabolic function. *J Exp Biol.* 206, 2049-57.

- Wise, D. R., Ward, P. S., Shay, J. E., Cross, J. R., Gruber, J. J., Sachdeva, U. M., Platt, J. M., DeMatteo, R. G., Simon, M. C., Thompson, C. B., 2011. Hypoxia promotes isocitrate dehydrogenase-dependent carboxylation of alpha-ketoglutarate to citrate to support cell growth and viability. *Proc Natl Acad Sci U S A.* 108, 19611-6.
- Wittmann, C., 2002. Metabolic flux analysis using mass spectrometry. *Adv Biochem Eng Biotechnol.* 74, 39-64.
- Wittmann, C., 2007. Fluxome analysis using GC-MS. *Microb Cell Fact.* 6, 6.
- Wittmann, C., Heinzle, E., 1999. Mass spectrometry for metabolic flux analysis. *Biotechnol Bioeng.* 62, 739-750.
- Wong, D. C. F., Wong, K. T. K., Goh, L. T., Heng, C. K., Yap, M. G. S., 2005. Impact of dynamic online fed-batch strategies on metabolism, productivity and N-glycosylation quality in CHO cell cultures. *Biotechnol Bioeng.* 89, 164-77.
- Wu, F., Yang, F., Vinnakota, K. C., Beard, D. A., 2007. Computer modeling of mitochondrial tricarboxylic acid cycle, oxidative phosphorylation, metabolite transport, and electrophysiology. *J Biol Chem.* 282, 24525-37.
- Wu, W., Zhao, S., 2013. Metabolic changes in cancer: beyond the Warburg effect. *Acta Biochim Biophys Sin (Shanghai).* 45, 18-26.
- Wu, X. M., Gutfreund, H., Lakatos, S., Chock, P. B., 1991. Substrate channeling in glycolysis: a phantom phenomenon. *Proc Natl Acad Sci U S A.* 88, 497-501.
- Wurm, F. M., 2004. Production of recombinant protein therapeutics in cultivated mammalian cells. *Nat Biotechnol.* 22, 1393-8.
- Wurm, F. M., 2007. Manufacturing of biopharmaceuticals and implications for biosimilars. *Kidney Blood Press Res.* 30 Suppl 1, 6-8.
- Wurm, M., Schopke, B., Lutz, D., Muller, J., Zeng, A. P., 2010. Microtechnology meets systems biology: The small molecules of metabolome as next big targets. *J Biotechnol.*
- Xie, G., Wilson, J. E., 1990. Tetrameric structure of mitochondrially bound rat brain hexokinase: a crosslinking study. *Arch Biochem Biophys.* 276, 285-93.
- Xie, L., Wang, D. I., 1994. Applications of improved stoichiometric model in medium design and fed-batch cultivation of animal cells in bioreactor. *Cytotechnology.* 15, 17-29.
- Xu, X., Nagarajan, H., Lewis, N. E., Pan, S., Cai, Z., Liu, X., Chen, W., Xie, M., Wang, W., Hammond, S., Andersen, M. R., Neff, N., Passarelli, B., Koh, W., Fan, H. C., Wang, J., Gui, Y., Lee, K. H., Betenbaugh, M. J., Quake, S. R., Famili, I., Palsson, B. O., Wang, J., 2011. The genomic sequence of the Chinese hamster ovary (CHO)-K1 cell line. *Nat Biotech.* 29, 735-741.
- Xu, X., Zhao, J., Xu, Z., Peng, B., Huang, Q., Arnold, E., Ding, J., 2004. Structures of human cytosolic NADP-dependent isocitrate dehydrogenase reveal a novel self-regulatory mechanism of activity. *J Biol Chem.* 279, 33946-57.
- Yan, H., Parsons, D. W., Jin, G., McLendon, R., Rasheed, B. A., Yuan, W., Kos, I., Batinic-Haberle, I., Jones, S., Riggins, G. J., Friedman, H., Friedman, A., Reardon, D., Herndon, J., Kinzler, K. W., Velculescu, V. E., Vogelstein, B., Bigner, D. D., 2009. IDH1 and IDH2 mutations in gliomas. *N Engl J Med.* 360, 765-73.

- Yang, M., Butler, M., 2000. Effects of ammonia on CHO cell growth, erythropoietin production, and glycosylation. *Biotechnol Bioeng.* 68, 370-80.
- Yang, M., Butler, M., 2002. Effects of ammonia and glucosamine on the heterogeneity of erythropoietin glycoforms. *Biotechnol Prog.* 18, 129-38.
- Yang, T., 2013. *¹³C-Based Metabolic Flux Analysis: Fundamentals and Practice*. In: Alper, H. S., (Ed.), *Systems Metabolic Engineering*. vol. 985. Humana Press, pp. 297-334.
- Yang, T. H., Bolten, C. J., Coppi, M. V., Sun, J., Heinzle, E., 2009. Numerical bias estimation for mass spectrometric mass isotopomer analysis. *Anal Biochem.* 388, 192-203.
- Yang, T. H., Frick, O., Heinzle, E., 2008. Hybrid optimization for ¹³C metabolic flux analysis using systems parametrized by compactification. *BMC Syst Biol.* 2, 29.
- Yang, T. H., Wittmann, C., Heinzle, E., 2006a. Respirometric ¹³C flux analysis, Part I: design, construction and validation of a novel multiple reactor system using on-line membrane inlet mass spectrometry. *Metab Eng.* 8, 417-31.
- Yang, T. H., Wittmann, C., Heinzle, E., 2006b. Respirometric ¹³C flux analysis, Part II: in vivo flux estimation of lysine-producing *Corynebacterium glutamicum*. *Metab Eng.* 8, 432-46.
- Yao, A., Kohmoto, O., Oyama, T., Sugishita, Y., Shimizu, T., Harada, K., Matsui, H., Komuro, I., Nagai, R., Matsuo, H., Serizawa, T., Maruyama, T., Takahashi, T., 2003. Characteristic effects of alpha1-beta1,2-adrenergic blocking agent, carvedilol, on [Ca²⁺]_i in ventricular myocytes compared with those of timolol and atenolol. *Circ J.* 67, 83-90.
- Ye, H., Aubel, D., Fussenegger, M., 2013. Synthetic mammalian gene circuits for biomedical applications. *Curr Opin Chem Biol.* 17, 910-7.
- Yoo, H., Antoniewicz, M. R., Stephanopoulos, G., Kelleher, J. K., 2008. Quantifying reductive carboxylation flux of glutamine to lipid in a brown adipocyte cell line. *J Biol Chem.* 283, 20621-7.
- Zagari, F., Jordan, M., Stettler, M., Broly, H., Wurm, F. M., 2013a. Lactate metabolism shift in CHO cell culture: the role of mitochondrial oxidative activity. *N Biotechnol.* 30, 238-45.
- Zagari, F., Stettler, M., Baldi, L., Broly, H., Wurm, F. M., Jordan, M., 2013b. High expression of the aspartate-glutamate carrier Aralar1 favors lactate consumption in CHO cell culture. *Pharmaceutical Bioprocessing.* 1, 19-27.
- Zamboni, N., 2011. ¹³C metabolic flux analysis in complex systems. *Curr Opin Biotechnol.* 22, 103-8.
- Zamboni, N., Fendt, S. M., Ruhl, M., Sauer, U., 2009. (¹³C)-based metabolic flux analysis. *Nat Protoc.* 4, 878-92.
- Zamboni, N., Sauer, U., 2009. Novel biological insights through metabolomics and ¹³C-flux analysis. *Curr Opin Microbiol.* 12, 553-8.
- Zamorano, F., Vande Wouwer, A., Jungers, R. M., Bastin, G., 2013. Dynamic metabolic models of CHO cell cultures through minimal sets of elementary flux modes. *J Biotechnol.* 164, 409-22.
- Zamorano, F., Wouwer, A. V., Bastin, G., 2010. A detailed metabolic flux analysis of an underdetermined network of CHO cells. *J Biotechnol.* 150, 497-508.

- Zara, V., Ferramosca, A., Papatheodorou, P., Palmieri, F., Rassow, J., 2005. Import of rat mitochondrial citrate carrier (CIC) at increasing salt concentrations promotes presequence binding to import receptor Tom20 and inhibits membrane translocation. *J Cell Sci.* 118, 3985-95.
- Zeng, A. P., Modak, J., Deckwer, W. D., 2002. Nonlinear dynamics of eucaryotic pyruvate dehydrogenase multienzyme complex: decarboxylation rate, oscillations, and multiplicity. *Biotechnol Prog.* 18, 1265-76.
- Zhang, F., Sun, X., Yi, X., Zhang, Y., 2006. Metabolic characteristics of recombinant Chinese hamster ovary cells expressing glutamine synthetase in presence and absence of glutamine. *Cytotechnology.* 51, 21-8.
- Zhang, Y. H., 2011. Substrate channeling and enzyme complexes for biotechnological applications. *Biotechnol Adv.* 29, 715-25.
- Zhu, Y., King, B. L., Parvizi, B., Brunk, B. P., Stoeckert, C. J., Quackenbush, J., Richardson, J., Bult, C. J., 2003. Integrating computationally assembled mouse transcript sequences with the Mouse Genome Informatics (MGI) database. *Genome Biol.* 4, R16.
- Zitova, A., O'Mahony, F. C., Cross, M., Davenport, J., Papkovsky, D. B., 2009. Toxicological profiling of chemical and environmental samples using panels of test organisms and optical oxygen respirometry. *Environ Toxicol.* 24, 116-27.
- Zupke, C., Stephanopoulos, G., 1994. Modeling of Isotope Distributions and Intracellular Fluxes in Metabolic Networks Using Atom Mapping Matrices. *Biotechnology Progress.* 10, 489-498.
- Zupke, C., Stephanopoulos, G., 1995. Intracellular flux analysis in hybridomas using mass balances and in vitro (^{13}C) nmr. *Biotechnol Bioeng.* 45, 292-303.
- Zwingmann, C., Richter-Landsberg, C., Leibfritz, D., 2001. ^{13}C isotopomer analysis of glucose and alanine metabolism reveals cytosolic pyruvate compartmentation as part of energy metabolism in astrocytes. *Glia.* 34, 200-12.

12 Supplementary material

Author contributions

Judith Wahrheit designed and performed the experiments of all chapters, analyzed and interpreted the data of all chapters, drafted and wrote the manuscripts presented as chapters 2, 3, 4 and 7, contributed to writing the manuscripts presented as chapters 5, 6, and 8.

Averina Nicolae set up the metabolic network models used in chapters 3, 4, 5, 6 and 8, performed the modeling, simulations and data analysis, drafted and wrote the manuscripts presented as chapters 5, 6, and 8.

Yannic Nonnenmacher performed the experiments of chapter 4, 7 and 8, analyzed the data of chapters 4 and 7, contributed to writing the manuscripts presented as chapters 4 and 7.

Jens Niklas set up the metabolic network model and the dynamic metabolic flux analysis method used in chapter 2.

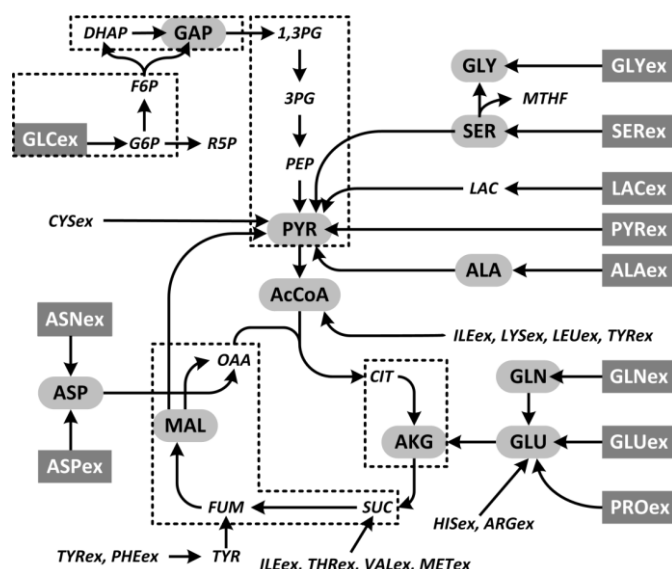
Janina Bahnemann performed the reactor cultivation of chapter 5.

Christian Weyler provided analytical support for the MALDI-TOF measurements.

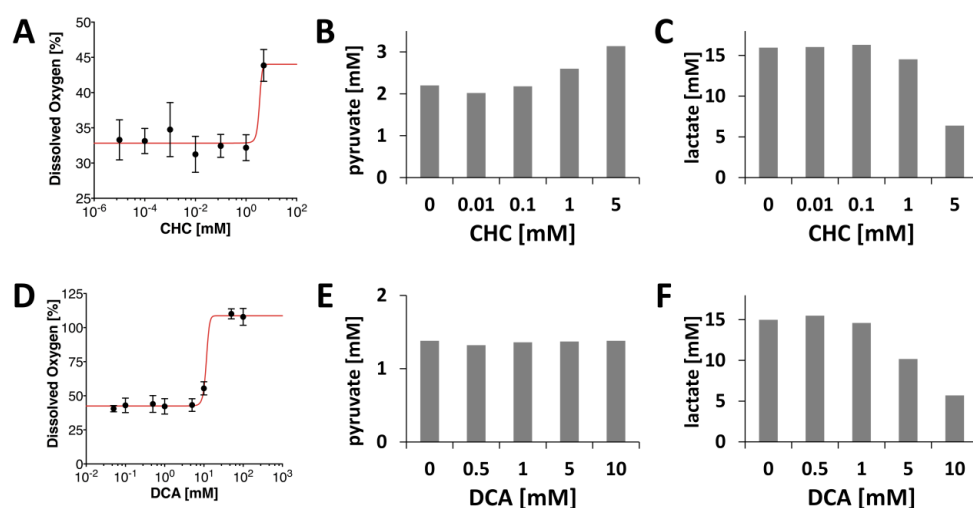
Saskia Sperber provided assistance in taking the microscopic pictures.

Elmar Heinzle was involved in the study design, provided help with the data analysis, critically revised and finalized the manuscripts.

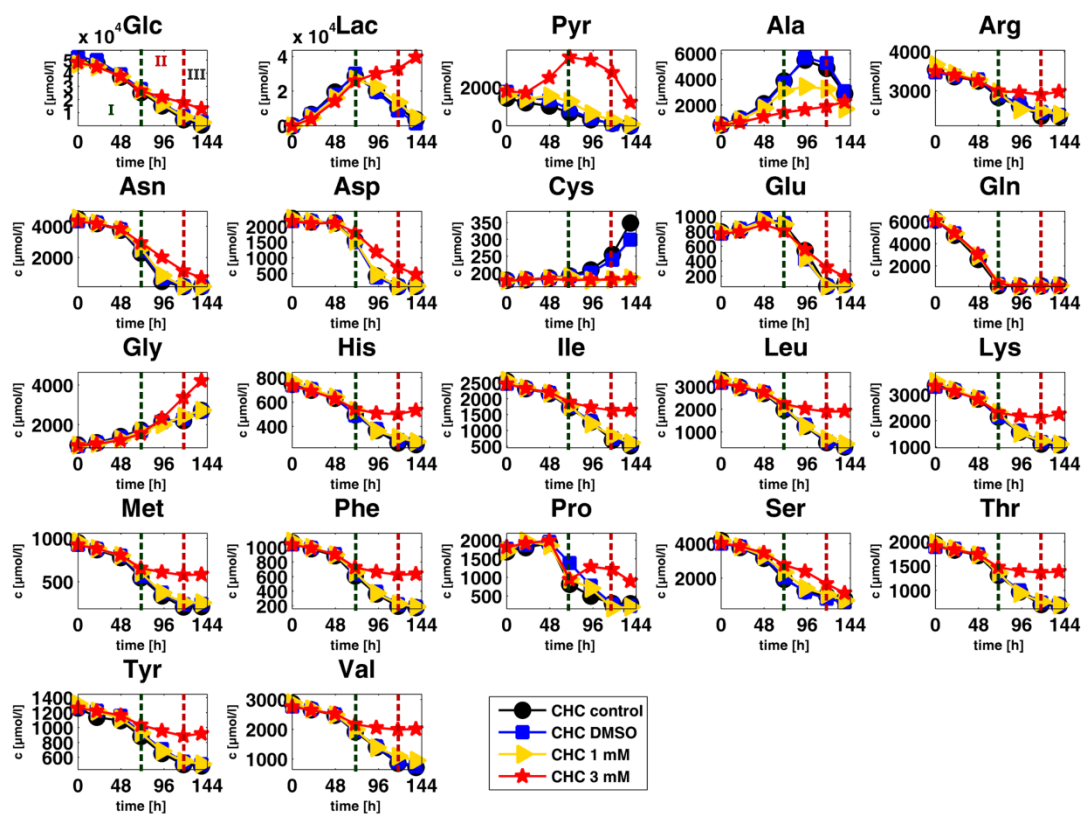
Supplementary material chapter 4



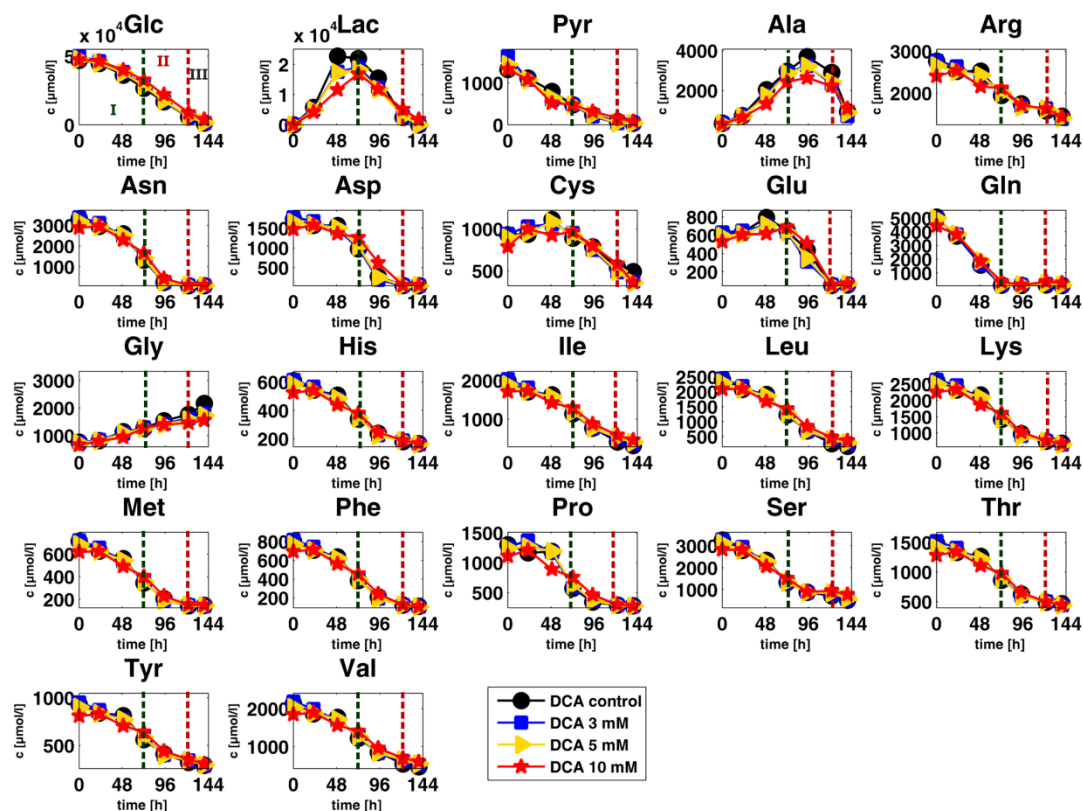
Supplementary Figure S1. Scheme of the central carbon metabolism in CHO cells. The dashed boxes indicate which metabolite pools are lumped in the condensed flux maps in Figure 4-3. Metabolites that are shown in the flux maps in Figure 4-3 are highlighted in grey



Supplementary Figure S2. Screening of CHC and DCA. (A) and (D) Concentration response curves of dissolved oxygen measurements for α -cyano-4-hydroxy cinnamic acid (CHC) and dichloroacetic acid (DCA) after 70 h of cultivation. EC₅₀ values: 3.5 mM (CHC) and 13 mM (DCA). Hill coefficients: 8.7 (CHC) and 5.4 (DCA). (B) and (E) Extracellular pyruvate concentrations after 70 h of cultivations with different CHC and DCA concentrations. (C) and (F) Extracellular lactate concentrations after 70 h of cultivations with different CHC and DCA concentrations



Supplementary Figure S3. Complete extracellular metabolite profiles of CHO-K1 cell cultures upon CHC treatment. Shown are extracellular metabolite concentrations [$\mu\text{mol/l}$] of CHO-K1 cell cultures upon treatment with 1 mM and 3 mM α -cyano-4-hydroxy cinnamic acid (CHC) compared to control cultivations without CHC and without DMSO (CHC control) and with 0.5% DMSO (CHC DMSO). Abbreviations: Glc glucose, Lac lactate, Pyr pyruvate, for amino acids the standard three letter code is used. Dashed lines indicate the different metabolic phases, phase I (0-72 h), phase II (72-120 h) and phase III (>120 h)



Supplementary Figure S4. Complete extracellular metabolite profiles of CHO-K1 cell cultures upon DCA treatment. Shown are extracellular metabolite concentrations [$\mu\text{mol/l}$] of CHO-K1 cell cultures upon treatment with 3 mM, 5 mM or 10 mM dichloroacetic acid (DCA) compared to control cultivation without DCA (DCA control). Abbreviations: Glc glucose, Lac lactate, Pyr pyruvate, for amino acids the standard three letter code is used. Dashed lines indicate the different metabolic phases, phase I (0-72 h), phase II (72-120 h) and phase III (>120h)

Supplementary Table S3. Biomass composition of CHO cells used for flux estimation.

Precursor	Yield coefficient [pmol/cell]
Ala	0.110
Arg	0.086
Asn/Asp	0.138
Gln/Glu	0.161
Gly	0.149
His	0.034
Ile	0.059
Leu	0.115
Lys	0.094
Met	0.010
Phe	0.050
Pro	0.049
Ser	0.081
Thr	0.067
Trp	0.001
Tyr	0.056
Cys	0.084
Val	0.083
G6P_carbs	0.138
lipids	0.036
R5P_DNA	0.043
R5P_RNA	0.018

Supplementary Table S4. Complete set of measured metabolic fluxes [mmol/(L × h)]. Selected fluxes are depicted in the flux maps in Figure 4-3.

flux	CHC control		CHC DMSO		CHC 1 mM		CHC 3 mM		DCA control		DCA 3 mM		DCA 5 mM		DCA 10 mM	
	0 - 72 h	72 - 120 h	0 - 72 h	72 - 120 h	0 - 72 h	72 - 120 h	0 - 72 h	72 - 120 h	0 - 72 h	72 - 120 h	0 - 72 h	72 - 120 h	0 - 72 h	72 - 120 h	0 - 72 h	72 - 120 h
glc in	217.64	54.28	224.57	55.67	176.88	52.70	245.91	42.40	179.17	55.12	173.03	47.60	177.48	60.96	161.27	71.17
lac in	-236.39	48.22	-263.05	57.27	-230.02	32.55	-292.73	-40.62	-187.90	50.13	-149.02	32.49	-166.08	42.25	-168.56	35.45
pyr in	6.13	1.48	7.68	2.07	2.35	2.70	-22.06	1.56	7.06	1.06	8.07	0.99	8.16	1.19	8.46	0.96
ala in	-29.81	-2.73	-30.00	-5.04	-22.94	-0.61	-10.73	-2.06	-22.89	-0.13	-20.95	0.46	-23.36	1.22	-21.84	0.58
arg in	6.54	2.73	6.15	2.78	6.42	2.38	5.90	1.30	6.46	2.37	6.06	1.99	6.22	2.48	6.05	2.61
asn in	19.43	5.77	18.24	6.66	16.81	6.80	16.03	8.48	17.00	3.43	16.53	3.36	16.33	3.54	14.02	4.80
asp in	6.31	3.91	6.74	4.12	6.51	4.04	4.03	5.62	6.18	2.54	6.40	2.41	5.51	2.70	2.88	3.67
cys in	6.38	2.66	5.99	2.71	6.26	2.32	5.75	1.27	5.77	2.31	5.91	1.94	6.06	2.41	5.90	2.54
glu in	-0.74	2.18	-1.01	2.32	-0.68	2.18	-0.30	2.29	-0.37	1.54	0.07	1.24	-0.44	1.58	-1.40	1.89
gln in	49.27	0.03	50.58	0.51	48.88	0.68	62.99	2.37	41.11	-0.02	38.22	-0.09	43.15	-0.18	42.80	-0.01
gly in	-6.47	-1.32	-6.54	-1.79	-6.33	-1.88	-6.91	-7.13	-4.54	-1.33	-4.47	-0.65	-5.03	-0.84	-6.15	-0.54
his in	2.56	1.07	2.40	1.09	2.51	0.93	2.31	0.51	2.31	0.92	2.37	0.78	2.43	0.97	2.36	1.02
ile in	6.89	2.72	6.42	2.68	6.54	2.56	6.24	1.49	6.65	1.91	6.54	1.55	6.17	1.78	4.81	2.14
leu in	10.77	3.82	10.15	3.94	9.79	3.81	10.13	1.96	9.61	3.15	9.28	2.66	9.11	3.30	8.06	3.47
lys in	10.58	2.99	10.63	3.04	9.69	3.04	11.25	1.43	9.73	2.59	9.61	2.18	9.55	2.71	7.67	2.86
met in	3.47	0.89	3.32	0.91	3.01	0.95	3.03	0.40	3.04	0.55	2.92	0.52	2.93	0.56	2.45	0.77
phe in	3.94	1.58	3.78	1.61	3.72	1.38	3.51	0.76	3.45	1.37	3.51	1.16	3.60	1.44	3.51	1.51
pro in	9.19	1.56	4.44	3.04	8.59	1.87	11.22	0.74	6.03	1.35	6.31	1.14	5.98	1.41	4.49	1.49
ser in	19.31	2.54	18.55	3.45	15.76	3.58	14.24	3.51	16.07	1.67	15.77	1.40	16.08	1.33	14.67	1.79
thr in	5.52	1.59	5.29	2.17	5.28	1.86	4.78	1.02	5.06	1.85	5.03	1.56	4.86	1.94	4.73	2.04
tyr in	4.26	1.78	4.01	1.81	4.18	1.55	3.85	0.85	3.86	1.54	3.95	1.30	4.05	1.61	3.94	1.70
val in	8.11	2.78	7.65	2.78	7.54	2.47	6.51	1.26	7.30	2.28	7.21	1.92	6.80	2.39	5.83	2.51
alabio	8.34	3.48	7.84	3.54	8.18	3.03	7.52	1.66	7.54	3.01	7.72	2.54	7.92	3.16	7.71	3.32
argbio	6.54	2.73	6.15	2.78	6.42	2.38	5.90	1.30	5.92	2.37	6.06	1.99	6.22	2.48	6.05	2.61
aspbio	10.47	4.37	9.84	4.44	10.28	3.80	9.45	2.09	9.47	3.79	9.70	3.19	9.95	3.97	9.68	4.18
glubio	12.21	5.09	11.47	5.18	11.98	4.43	11.01	2.43	11.04	4.41	11.31	3.72	11.60	4.62	11.29	4.87
glybio	11.32	4.72	10.64	4.80	11.11	4.11	10.21	2.26	10.24	4.09	10.48	3.45	10.76	4.29	10.47	4.51
hisbio	2.56	1.07	2.40	1.09	2.51	0.93	2.31	0.51	2.31	0.92	2.37	0.78	2.43	0.97	2.36	1.02
ilebio	4.46	1.86	4.19	1.89	4.37	1.62	4.02	0.89	4.03	1.61	4.13	1.36	4.24	1.69	4.12	1.78
leubio	8.72	3.64	8.19	3.70	8.55	3.17	7.86	1.74	7.89	3.15	8.07	2.66	8.28	3.30	8.06	3.47
lysbio	7.17	2.99	6.74	3.04	7.04	2.60	6.47	1.43	6.49	2.59	6.64	2.18	6.81	2.71	6.63	2.86
metbio	0.76	0.32	0.72	0.32	0.75	0.28	0.69	0.15	0.69	0.28	0.70	0.23	0.72	0.29	0.70	0.30
phebio	3.79	1.58	3.57	1.61	3.72	1.38	3.42	0.76	3.43	1.37	3.51	1.16	3.60	1.44	3.51	1.51
probio	3.73	1.56	3.51	1.58	3.66	1.35	3.37	0.74	3.37	1.35	3.45	1.14	3.54	1.41	3.45	1.49
serbio	6.19	2.58	5.81	2.62	6.07	2.25	5.58	1.23	5.60	2.24	5.73	1.88	5.88	2.34	5.72	2.47
thrbio	5.12	2.14	4.81	2.17	5.02	1.86	4.62	1.02	4.63	1.85	4.74	1.56	4.86	1.94	4.73	2.04
tyrbio	4.26	1.78	4.01	1.81	4.18	1.55	3.85	0.85	3.86	1.54	3.95	1.30	4.05	1.61	3.94	1.70
cysbio	6.38	2.66	5.99	2.71	6.26	2.32	5.75	1.27	5.77	2.31	5.91	1.94	6.06	2.41	5.90	2.54
valbio	6.31	2.63	5.93	2.68	6.19	2.29	5.69	1.26	5.70	2.28	5.84	1.92	5.99	2.39	5.83	2.51
g6pbio	10.50	4.38	9.87	4.46	10.31	3.81	9.47	2.09	9.50	3.80	9.73	3.20	9.98	3.98	9.71	4.19
lipids	2.71	1.13	2.55	1.15	2.66	0.98	2.44	0.54	2.45	0.98	2.51	0.83	2.57	1.03	2.50	1.08
DNA	3.25	1.36	3.06	1.38	3.19	1.18	2.94	0.65	2.94	1.18	3.01	0.99	3.09	1.23	3.01	1.30
RNA	1.35	0.56	1.27	0.57	1.33	0.49	1.22	0.27	1.22	0.49	1.25	0.41	1.29	0.51	1.25	0.54

Supplementary Table S5. Complete set of calculated fluxes [mmol/(L × h)]. Selected fluxes are depicted in the flux maps in Figure 4-3.

flux	CHC control		CHC DMSO		CHC 1 mM		CHC 3 mM		DCA control		DCA 3 mM		DCA 5 mM		DCA 10 mM	
	0 - 72 h	72 - 120 h	0 - 72 h	72 - 120 h	0 - 72 h	72 - 120 h	0 - 72 h	72 - 120 h	0 - 72 h	72 - 120 h	0 - 72 h	72 - 120 h	0 - 72 h	72 - 120 h	0 - 72 h	72 - 120 h
phgli	202.53	47.98	210.36	49.26	162.05	47.22	232.28	39.39	165.50	49.65	159.03	42.99	163.12	55.24	147.30	65.15
ald	202.53	47.98	210.36	49.26	162.05	47.22	232.28	39.39	165.50	49.65	159.03	42.99	163.12	55.24	147.30	65.15
tri	200.43	47.10	208.39	48.37	159.99	46.45	230.39	38.97	163.60	48.90	157.09	42.36	161.12	54.45	145.36	64.31
gapdh	402.95	95.08	418.75	97.63	322.04	93.67	462.67	78.35	329.11	98.55	316.12	85.35	324.24	109.69	292.67	129.46
pgk	402.95	95.08	418.75	97.63	322.04	93.67	462.67	78.35	329.11	98.55	316.12	85.35	324.24	109.69	292.67	129.46
eno	402.95	95.08	418.75	97.63	322.04	93.67	462.67	78.35	329.11	98.55	316.12	85.35	324.24	109.69	292.67	129.46
pepk	465.18	97.59	478.01	103.57	380.01	100.60	536.37	92.99	380.63	97.58	363.35	85.14	372.42	108.23	331.34	130.68
pdh	189.40	133.87	177.81	147.42	110.81	126.56	192.42	42.57	162.60	138.65	186.30	111.14	175.06	142.58	131.53	157.54
cis	158.82	115.99	150.64	129.29	76.59	113.50	169.43	34.63	135.08	122.22	155.41	97.24	141.00	125.15	91.54	139.47
icdh	158.82	115.99	150.64	129.29	76.59	113.50	169.43	34.63	135.08	122.22	155.41	97.24	141.00	125.15	91.54	139.47
akgdh	200.60	113.11	189.67	128.40	117.74	112.44	228.97	36.86	167.97	119.32	185.24	94.67	174.54	121.93	122.70	136.48
sucdh	207.94	114.14	196.71	129.88	123.78	114.23	234.51	37.72	174.97	119.89	191.54	95.15	179.48	122.29	125.13	137.31
fumarase	211.70	115.65	200.33	131.41	127.33	115.54	237.87	38.44	178.26	121.20	194.89	96.25	182.92	123.66	128.48	138.75
maldh2	211.70	115.65	200.33	131.41	127.33	115.54	237.87	38.44	178.26	121.20	194.89	96.25	182.92	123.66	128.48	138.75
c3c4	62.23	2.51	59.26	5.94	57.97	6.93	73.70	14.64	51.53	-0.97	47.23	-0.21	48.18	-1.46	38.68	1.22
ldh	236.39	-48.22	263.05	-57.27	230.02	-32.55	292.73	40.62	187.90	-50.13	149.02	-32.49	166.08	-42.25	168.56	-35.45
gdh	4.61	1.92	4.33	1.96	4.52	1.67	4.16	0.92	4.17	1.67	4.27	1.40	4.38	1.74	4.26	1.84
gpt	-38.14	-6.21	-37.84	-8.58	-31.12	-3.64	-18.25	-3.72	-30.43	-3.15	-28.67	-2.08	-31.29	-1.93	-29.55	-2.74
got	9.35	2.85	9.57	3.82	7.23	4.89	5.26	10.83	8.34	0.04	7.75	0.78	6.25	0.03	1.74	1.93
aspg	-19.43	-5.77	-18.24	-6.66	-16.81	-6.80	-16.03	-8.48	-17.00	-3.43	-16.53	-3.36	-16.33	-3.54	-14.02	-4.80
argdeg	0.00	0.00	0.00	0.00	0.00	0.00	0.00	0.00	0.54	0.00	0.00	0.00	0.00	0.00	0.00	0.00
cysdeg	0.00	0.00	0.00	0.00	0.00	0.00	0.00	0.00	0.00	0.00	0.00	0.00	0.00	0.00	0.00	0.00
glis	43.67	-2.30	45.32	-1.86	43.38	-1.35	57.94	1.25	36.04	-2.05	33.03	-1.80	37.83	-2.30	37.62	-2.24
leubcat	2.05	0.19	1.96	0.24	1.24	0.64	2.26	0.23	1.72	0.00	1.20	0.00	0.82	0.00	0.00	0.00
ilebcat	2.43	0.86	2.23	0.78	2.16	0.94	2.22	0.60	2.62	0.30	2.42	0.19	1.94	0.09	0.69	0.36
valbcat	1.80	0.15	1.72	0.11	1.36	0.18	0.82	0.00	1.60	0.00	1.37	0.00	0.81	0.00	0.00	0.00
glud	25.52	-4.48	23.38	-3.94	26.93	3.05	59.07	10.43	22.36	-5.43	19.08	-3.39	17.02	-4.76	6.82	-2.96
shmt	20.10	7.01	19.34	7.57	19.70	6.83	19.20	9.85	16.86	6.26	17.09	4.80	17.97	6.00	18.74	5.97
hisdeg	0.00	0.00	0.00	0.00	0.00	0.00	0.00	0.00	0.00	0.00	0.00	0.00	0.00	0.00	0.00	0.00
lysdeg	3.41	0.00	3.89	0.00	2.65	0.43	4.78	0.00	3.25	0.00	2.97	0.00	2.74	0.00	1.04	0.00
metdeg	2.71	0.58	2.61	0.58	2.27	0.67	2.34	0.25	2.35	0.28	2.22	0.29	2.20	0.27	1.75	0.47
phedeg	0.14	0.00	0.22	0.00	0.00	0.00	0.09	0.00	0.02	0.00	0.00	0.00	0.00	0.00	0.00	0.00
prodh	5.46	0.00	0.94	1.45	4.93	0.51	7.86	0.00	2.66	0.00	2.85	0.00	2.43	0.00	1.04	0.00
serc3	-7.38	-7.22	-7.00	-6.91	-10.41	-5.64	-10.91	-7.65	-6.75	-6.97	-7.43	-5.41	-8.16	-7.16	-10.16	-6.80
thrdg	0.40	-0.55	0.48	0.00	0.25	0.00	0.16	0.00	0.43	0.00	0.29	0.00	0.00	0.00	0.00	0.00
tat	0.14	0.00	0.22	0.00	0.00	0.00	0.09	0.00	0.02	0.00	0.00	0.00	0.00	0.00	0.00	0.00
mthsink	21.87	7.19	21.08	7.76	21.05	7.16	20.71	9.91	18.38	6.20	18.45	4.81	19.29	5.92	19.63	6.06

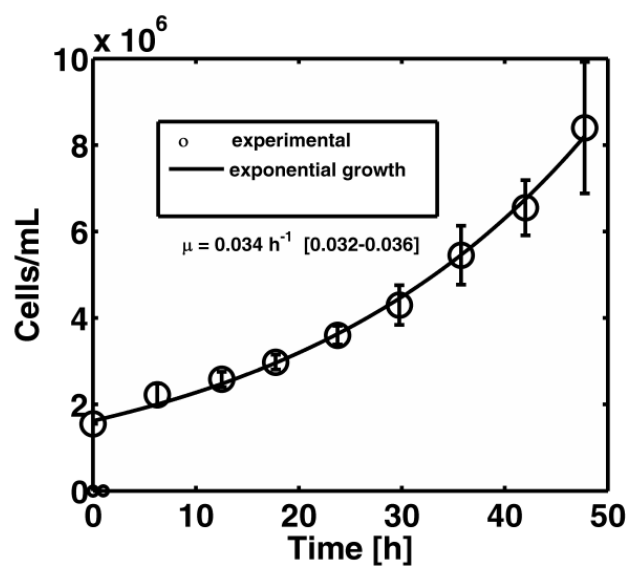
Supplementary material chapter 6

Supplementary Table S1. List of metabolic reactions, fluxes and reversibilities in the central carbon metabolism of CHO-K1 estimated for the first 2 – 18 h cultivation period. Carbon transfer rules are given in the parentheses for each reaction. Reversible reactions are indicated by double arrows. Reversibility is computed as the ratio between the reverse flux and the net flux. The 95% confidence interval was evaluated by refitting the model until the minimized objective function took the value of χ^2 (0.95, nr. experimental points – nr. parameters). Subscripts meaning: c – cytosolic; ex – extracellular; m – mitochondrial; Abbreviations: AcoA – acetyl-CoA; ALA – alanine; ASN – asparagine; ASP – aspartate; CIT – citrate; FUM – fumarate; GLC – glucose; G6P – glucose-6-phosphate; PG – phosphoglycerate; PEP – phosphoenolpyruvate; GLN – glutamine; GLU – glutamate; GLY – glycine; ICI – isocitrate; ILE – isoleucine; LAC – lactate; LEU – leucine; LYS – lysine; MAL – malate; MET – methionine; OAA – oxaloacetate; PHE – phenylalanine; PYR – pyruvate; SER – serine; SUC – succinate; THR – threonine; TYR – tyrosine; VAL – valine.

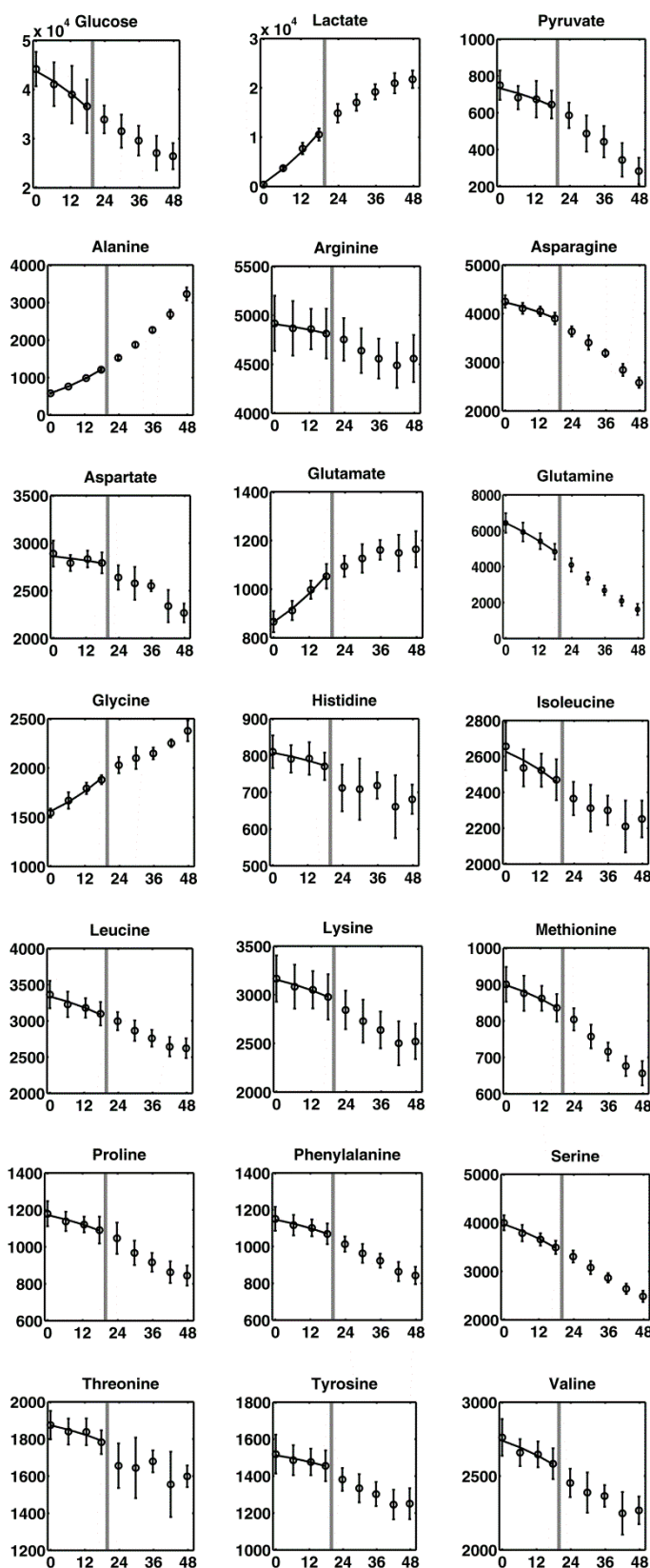
Flux	Reaction	Flux [mmol/L cell × h]	Lower boundary [mmol/L cell × h]	Upper boundary [mmol/L cell × h]	Reversibility [reverse flux/net flux]	Reversibility lower boundary	Reversibility upper boundary
v1	$GLC_{ex}(abcdef) \rightarrow G6P(abcdef)$	289.7	246.3	333.0	0	0	0
v2	$G6P(abcdef) \rightarrow PG(abc) + PG(def)$	24.3	18.6	29.2	0	0	0
v3	$3 G6P(abcdef) \rightarrow 5 PG(def) + 3 CO_2(a)$	87.4	85.4	89.6	0	0	0
v4	$G6P(abcdef) \rightarrow Biomass(DNA, RNA)$	3.3	3.3	3.3	0	0	0
v5	$PG(abc) \rightarrow PEP_c(abc)$	464.9	464.7	465.0	0	0	0
v6	$PEP_c(abc) \rightarrow PYR_{c1}(abc)$	498.2	492.3	500.2	0	0	0
v7	$PYR_{c1}(abc) \rightarrow PYR_{m2}(abc)$	118.9	113.7	119.0	0	0	0
v8	$PYR_{m2}(abc) \rightarrow AcoA_m(bc) + CO_2(a)$	77.5	77.2	77.6	0	0	0
v9	$OAA_m(abcd) + AcoA_m(ef) \rightarrow CIT_m(efbcda)$	100.8	100.6	100.9	0	0	0
v10	$CIT_m(abcdef) \rightarrow AKG_m(abcde) + CO_2(f)$	58.7	57.0	67.7	0	0	0
v11	$AKG_m(abcde) \rightarrow 0.5 MAL_m(abcd) + 0.5 MAL_m(dcba) + CO_2(e)$	105.6	105.4	105.7	0	0	0
v12	$MAL_m(abcd) \leftrightarrow OAA_m(abcd)$	191.6	185.1	198.9	10.3	10.2	11.3
v13	$PYR_{c2}(abc) \leftrightarrow LAC_{c2}(abc)$	431.7	391.0	472.3	31.9	18.6	32.0
v14	$LAC_c(abc) \leftrightarrow LAC_{ex}(abc)$	431.7	391.0	472.3	28.2	28.1	28.3
v15	$OAA_c(abcd) \rightarrow PEP_c(abc) + CO_2(d)$	66.4	61.2	68.5	0	0	0
v16	$MAL_c(abcd) \rightarrow PYR_{c1}(abc) + CO_2(d)$	5.4	0	11.0	0	0	0
v17	$OAA_c(abcd) \leftrightarrow MAL_c(abcd)$	90.5	88.6	90.7	22.7	21.7	23.0
v18	$PYR_{m1}(abc) + CO_2(d) \rightarrow OAA_m(abcd)$	23.1	15.1	24.8	0	0	0
v19	$MAL_m(abcd) \rightarrow PYR_{m1}(abc) + CO_2(d)$	8.3	5.9	9.2	0	0	0
v20	$PG(abc) \rightarrow SER(abc)$	20.5	20.4	20.5	0	0	0

Flux	Reaction	Flux [mmol/L cell × h]	Lower boundary [mmol/L cell × h]	Upper boundary [mmol/L cell × h]	Reversibility [reverse flux/net flux]	Reversibility lower boundary	Reversibility upper boundary
v21	$SER(abc) \leftrightarrow GLY(ab) + MTHF(c)$	21.9	21.9	21.9	3.8	3.2	3.8
v22	$SER_{ex}(abc) \leftrightarrow SER(abc)$	20.8	17.8	23.4	13.3	13.1	13.9
v23	$SER(abc) \rightarrow Biomass$	4.2	4.1	4.2	0	0	0
v24	$GLY(abc) \leftrightarrow GLY_{ex}(abc)$	14.3	8.7	19.9	2.9	1.9	3.1
v25	$GLY(abc) \rightarrow Biomass$	7.6	7.5	7.7	0	0	0
v26	$SER(abc) \rightarrow PYR_{c1}(abc)$	15.2	15.1	15.2	0	0	0
v27	$PYR_{c1}(abc) + GLU_c(defgh) \leftrightarrow ALA_c(abc) + AKG_c(defgh)$	5.3	4.4	6.0	0.5	0.4	0.5
v28	$ALA_c(abc) \leftrightarrow ALA_{ex}(abc)$	26.3	26.1	26.5	2.7	2.7	4.1
v29	$ALA_c(abc) \rightarrow Biomass$	5.6	5.4	5.8	0	0	0
v30	$ALA_m(abc) \leftrightarrow ALA_c(abc)$	26.6	25.9	27.5	3.7	3.5	4.7
v31	$PYR_{m1}(abc) + GLU_m(defgh) \leftrightarrow ALA_m(abc) + AKG_m(defgh)$	26.6	25.9	27.5	14.4	12.9	14.6
v32	$PYR_{ex}(abc) \leftrightarrow PYR_{c1}(abc)$	4.0	2.2	5.8	1714/time [h]	1700/time [h]	>2500/time [h]
v33	$ASP_c(abcd) + AKG_c(efghi) \leftrightarrow OAA_c(abcd) + GLU_c(efghi)$	123.8	118.8	124.0	30.0	1.9	n.d.
v34	$OAA_m(abcd) + GLU_m(efghi) \leftrightarrow ASP_m(abcd) + AKG_m(efghi)$	113.8	108.8	114.0	62.5	0	n.d.
v35	$ASN(abcd) \rightarrow ASP_c(abcd)$	13.9	11.4	16.5	0	0	0
v36	$ASP_{ex}(abcd) \leftrightarrow ASP_c(abcd)$	3.1	0.0	6.7	5.8	4.4	6.4
v37	$ASP_c(abcd) \rightarrow Biomass$	7.1	7.0	7.2	0	0	0
v38	$MAL_m(abcd) \leftrightarrow MAL_c(abcd)$	58.1	53.1	58.2	30.5	29.5	n.d.
v39	$CIT_m(abcdef) + MAL_c(ghij) \rightarrow CIT_c(abcdef) + MAL_m(ghij)$	42.1	33.1	43.7	0	0	0
v40	$CIT_c(abcdef) \rightarrow AKG_c(abcde) + CO_2(e)$	9.0	0	10.6	3.1	2.9	3.1
v41	$AKG_m(abcde) + MAL_c(fghi) \leftrightarrow AKG_c(abcde) + MAL_m(fghi)$	101.1	100.3	105.7	18.0	17.9	18.1
v42	$AKG_c(abcde) \leftrightarrow GLU_c(abcde)$	0	0	0	n.d.	-	-
v43	$GLU_m(abcde) \rightarrow GLU_c(abcde)$	156.1	155.7	156.1	2.4	0	2.7
v44	$GLU_m(abcde) \leftrightarrow AKG_m(abcde)$	7.5	7.5	7.6	9.5	7.1	9.5
v45	$GLU_c(abcde) \leftrightarrow GLU_{ex}(abcde)$	8.1	7.2	8.9	1.3	1.3	1.3
v46	$GLU_c(abcde) \rightarrow Biomass$	8.2	7.9	8.5	0	0	0
v47	$GLU_c(abcde) \rightarrow GLN_c(abcde)$	136.8	136.4	137.2	5.2	4.6	5.2
v48	$GLN_c(abcde) \rightarrow GLU_m(abcde)$	190.3	189.9	190.7	0	0	0
v49	$GLN_{ex}(abcde) \leftrightarrow GLN_c(abcde)$	53.5	51.3	55.6	0.6	0.5	0.6

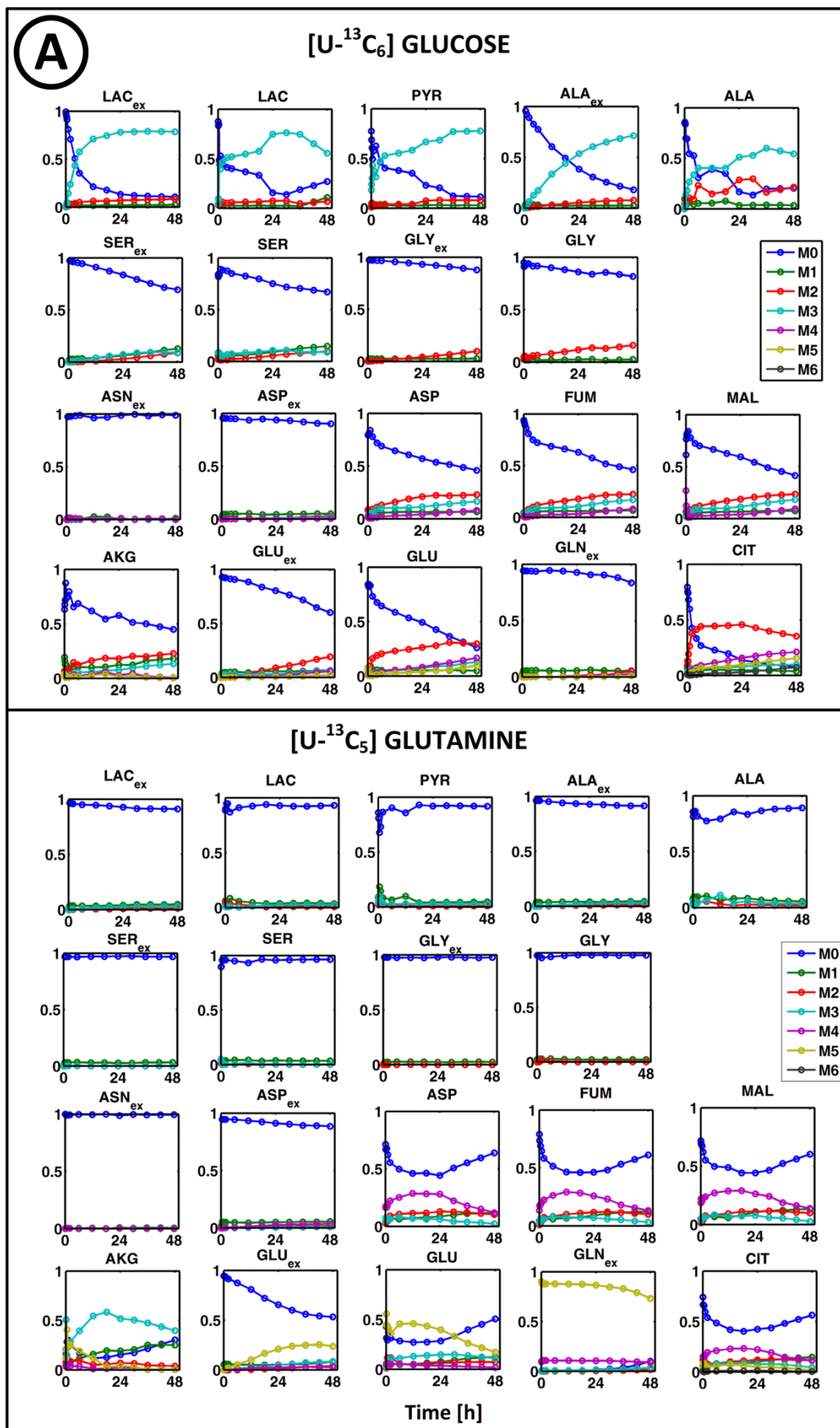
Flux	Reaction	Flux [mmol/L cell × h]	Lower boundary [mmol/L cell × h]	Upper boundary [mmol/L cell × h]	Reversibility [reverse flux/net flux]	Reversibility lower boundary	Reversibility upper boundary
v50	$CIT_c(abcdef) \rightarrow OAA_c(fcde) + AcoA_c(ab)$	33.1	32.7	33.5	0	0	0
v51	$AcoA_c(ab) \rightarrow Biomass$	33.1	32.7	33.5	0	0	0
v52	$AA_{ex}(ILE, VAL, MET, THR, TYR, PHE) \rightarrow SUC_m(AA \text{ catabolism})$	8.9	4.9	12.9	0	0	0
v53	$AA_{ex}(LEU, ILE, LYS, TYR, PHE) \rightarrow ACOA_m(AA \text{ catabolism})$	23.3	10.6	36.0	0	0	0
v54	$AKG_c(abcde) \rightarrow GLU_c(abcde)(AA \text{ catabolism})$	12.2	3.4	20.5	0	0	0
v55	$AA(PRO, HIS, ARG) \rightarrow GLU_c(AA \text{ catabolism})$	0.7	0	3.1	0	0	0
v56	$SUC_m(abcd) \leftrightarrow FUM_m(abcd)$	114.5	114.3	114.6	0	0	0
v57	$FUM_m(abcd) \leftrightarrow MAL_m(abcd)$	114.7	114.5	114.8	47.6	45.5	83.6
v58	$PYR_{c1}(abc) \leftrightarrow PYR_{c2}(abc)$	398.5	398.0	398.6	0.13	0	0.13
v59	$PEP_c(abc) \rightarrow PYR_{c2}(abc)$	33.2	33.1	33.7	0	0	0
v60	$AA_{ex}(abcd) \rightarrow FUM_m(abcd)(AA \text{ catabolism})$	0.2	0.1	0.3	0	0	0
v61	$GLU_c(abcde) + ASP_m(efgh) \leftrightarrow GLU_m(abcde) + ASP_c(efgh)$	113.8	108.8	114.0	5.6	5.6	5.6
v62	$PYR_{m2}(abc) \leftrightarrow PYR_{m1}(abc)$	41.4	36.4	41.5	0.06	0	0.06
	$PYR_{c1}(abc) \leftrightarrow LAC_{c1}(abc)$	-	-	-	60.0	59.9	60.2
	$PYR_{m1}(abc) \leftrightarrow LAC_m(abc)$	-	-	-	71.3	68.9	80.0

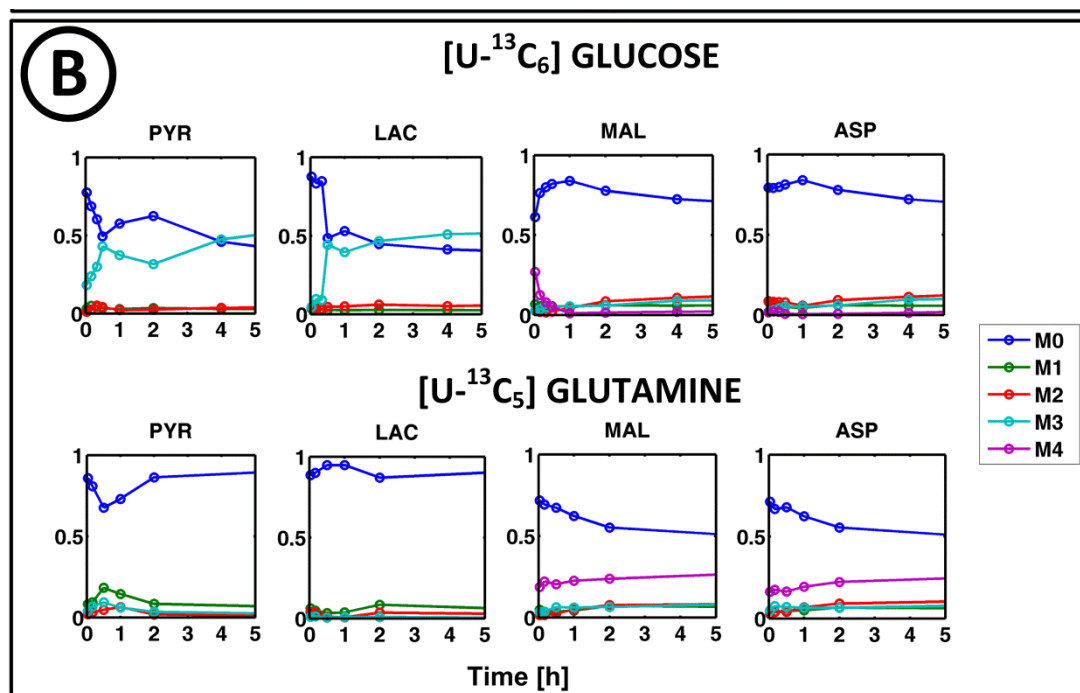


Supplementary Figure S1. Growth profile of the CHO-K1 cells in 250 ml baffled shake flask with a working volume of 120 ml and the determined specific growth rate μ . The values represent the average from 4 parallel cultivation.



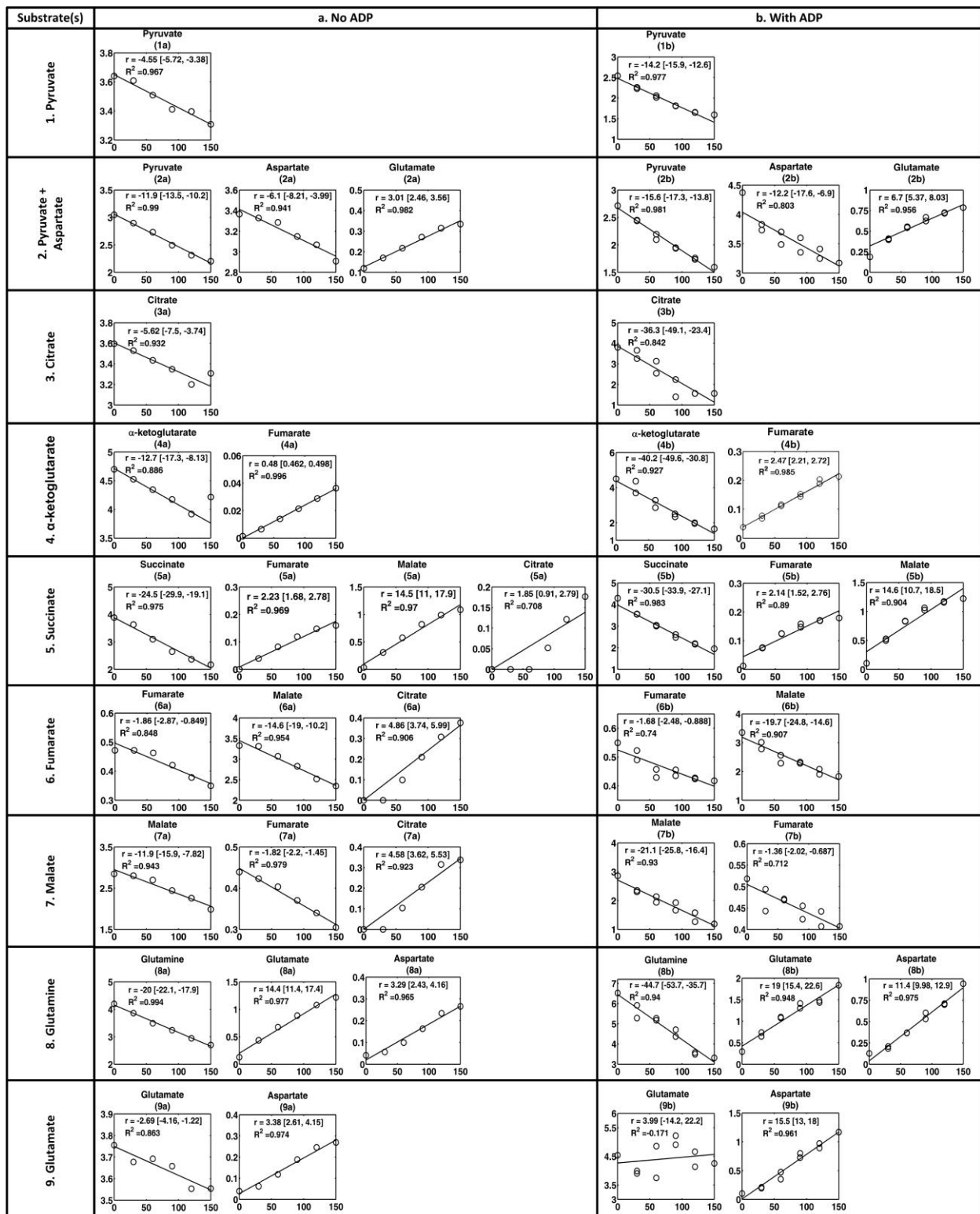
Supplementary Figure S2. Cultivation profile of the CHO-K1 cells culture during 48 h in 250 ml baffled shake flask with a start volume of 120 ml. The represented extracellular concentrations are in $[\mu\text{mol/L}]$ and the time is in [h]. The values represent the average from 4 parallel cultivations. The curves are the fitted values of extracellular concentrations simulating an exponential growth model with balanced growth (metabolic steady state) over the first 18 h.



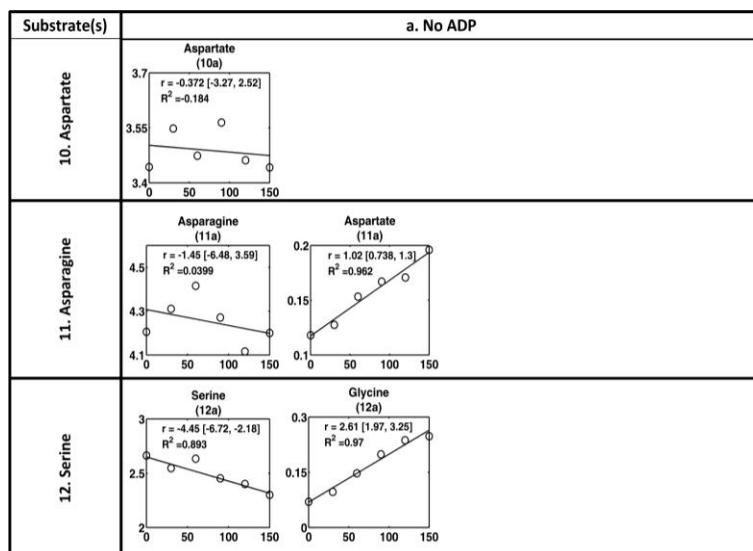


Supplementary Figure S3. (A) Experimentally determined mass isotopomer distributions of intracellular and extracellular (subscript ex) metabolites during the 48 h of the labeling experiment using $[U-^{13}C_6]$ glucose and $[U-^{13}C_5]$ glutamine as substrates. (B) The first 5 h of the labeling experiment using $[U-^{13}C_6]$ glucose and $[U-^{13}C_5]$ glutamine as substrates showing the overshooting behavior in intracellular pyruvate (PYR), lactate (LAC), malate (MAL) and aspartate (ASP). Abbreviations: AKG – α -ketoglutarate; ALA – alanine; ASN – asparagine; ASP – aspartate; CIT – citrate; FUM – fumarate; GLN – glutamine; GLU – glutamate; GLY – glycine; Lac – lactate; MAL – malate; PYR – pyruvate; SER – serine.

Supplementary material chapter 8



Supplementary Figure S1. Experimental (o) and fitted (-) extracellular concentrations in the experiments with permeabilized CHO-K1 cells. r – production rate [fmol/ (cell \times min)]. The brackets contain the 95% confidence interval for the rate.



Supplementary Figure S1. (continued)

Supplementary Table S1. Selection of the elementary modes that can describe the observed metabolite uptake and production. The modes are selected accordingly to the following criteria: u - the metabolite is taken up; p - the metabolite is produced; xu - the metabolite is not taken up; xp - the metabolite is not produced; iu - the metabolite is or is not taken up; ip - the metabolite is or is not produced.

SUBSTATE(S)	pyruvate	pyruvate, ADP	pyruvate, aspartate	pyruvate, aspartate, ADP	citrate	citrate, ADP
PRODUCT(S)	-	ATP	glutamate	glutamate, ATP	-	ATP
External Flux	1a	1b	2a	2b	3a	3b
Pyruvate	u / xp	u / xp	iu / xp	iu / xp	xu / xp	xu / xp
Malate	xu / xp	xu / xp	xu / xp	xu / xp	xu / xp	xu / xp
Succinate	xu / xp	xu / xp	xu / xp	xu / xp	xu / xp	xu / xp
Fumarate	xu / xp	xu / xp	xu / xp	xu / xp	xu / xp	xu / xp
Citrate	xu / xp	xu / xp	xu / xp	xu / xp	u / xp	u / xp
Aspartate	xu / xp	xu / xp	iu / xp	iu / xp	xu / xp	xu / xp
α -ketoglutarate	xu / xp	xu / xp	xu / xp	xu / xp	xu / xp	xu / xp
Glutamate	xu / xp	xu / xp	xu / ip	xu / ip	xu / xp	xu / xp
Glutamine	xu / xp	xu / xp	xu / xp	xu / xp	xu / xp	xu / xp
CO ₂	iu / ip	iu / ip	iu / ip	iu / ip	iu / ip	iu / ip
Serine	xu / xp	xu / xp	xu / xp	xu / xp	xu / xp	xu / xp
Glycine	xu / xp	xu / xp	xu / xp	xu / xp	xu / xp	xu / xp
C1	xu / xp	xu / xp	xu / xp	xu / xp	xu / xp	xu / xp
O ₂	iu / xp	iu / xp	iu / xp	iu / xp	iu / xp	iu / xp
NH ₃	xp / xp	xp / xp	xp / xp	xp / xp	xu / xp	xu / xp
ADP	xu / xp	u / xp	xu / xp	u / xp	xu / xp	u / xp
ATP	xu / xp	xu / ip	xu / xp	xu / ip	xu / xp	xu / ip

Supplementary Table S1. (continued)

SUBSTATE(S)	α -ketoglutarate	α -ketoglutarate, ADP	succinate	succinate, ADP	malate (fumarate)
PRODUCT(S)	-	fumarate, ATP	fumarate, malate, citrate	fumarate, malate, citrate, ATP	citrate
External Flux	4a	4b	5a	5b	6a/7a
Pyruvate	xu / xp	xu / xp	xu / xp	xu / xp	xu / xp
Malate	xu / xp	xu / xp	xu / ip	xu / ip	u / xp
Succinate	xu / xp	xu / xp	u / xp	u / xp	xu / xp
Fumarate	xu / xp	xu / ip	xu / ip	xu / ip	xu / xp
Citrate	xu / xp	xu / xp	xu / ip	xu / ip	xu / ip
Aspartate	xu / xp	xu / xp	xu / xp	xu / xp	xu / xp
α -ketoglutarate	u / xp	u / xp	xu / xp	xu / xp	xu / xp
Glutamate	xu / xp	xu / xp	xu / xp	xu / xp	xu / xp
Glutamine	xu / xp	xu / xp	xu / xp	xu / xp	xu / xp
CO ₂	iu / ip	iu / ip	iu / ip	iu / ip	iu / ip
Serine	xu / xp	xu / xp	xu / xp	xu / xp	xu / xp
Glycine	xu / xp	xu / xp	xu / xp	xu / xp	xu / xp
C1	xu / xp	xu / xp	xu / xp	xu / xp	xu / xp
O ₂	iu / xp	iu / xp	iu / xp	iu / xp	iu / xp
NH ₃	xu / xp	xu / xp	xu / xp	xu / xp	xu / xp
ADP	xu / xp	u / xp	xu / xp	xu / xp	xu / xp
ATP	xu / xp	xu / ip	xu / xp	xu / ip	xu / xp

Supplementary Table S1. (continued)

SUBSTATE(S)	malate (fumarate), ADP	glutamine	glutamine, ADP	glutamate	glutamate, ADP	serine
PRODUCT(S)	citrate, ATP	glutamate, aspartate	glutamate, aspartate, ATP	aspartate	aspartate, ATP	glycine
External Flux	6b/7b	8a	8b	9a	9b	11a
Pyruvate	xu / xp	xu / xp	xu / xp	xu / xp	xu / xp	xu / xp
Malate	u / xp	xu / xp	xu / xp	xu / xp	xu / xp	xu / xp
Succinate	xu / xp	xu / xp	xu / xp	xu / xp	xu / xp	xu / xp
Fumarate	xu / xp	xu / xp	xu / xp	xu / xp	xu / xp	xu / xp
Citrate	xu / ip	xu / xp	xu / xp	xu / xp	xu / xp	xu / xp
Aspartate	xu / xp	xu / ip	xu / ip	xu / ip	xu / ip	xu / xp
α -ketoglutarate	xu / xp	xu / xp	xu / xp	xu / xp	xu / xp	xu / xp
Glutamate	xu / xp	xu / ip	xu / ip	xu / xp	u / xp	xu / xp
Glutamine	xu / xp	u / xp	u / xp	xu / xp	xu / xp	xu / xp
CO ₂	iu / ip	iu / ip	iu / ip	iu / ip	iu / ip	iu / ip
Serine	xu / xp	xu / xp	xu / xp	xu / xp	xu / xp	u / xp
Glycine	xu / xp	xu / xp	xu / xp	xu / xp	xu / xp	xu / ip
C1	xu / xp	xu / xp	xu / xp	xu / xp	xu / xp	xu / ip
O ₂	iu / xp	iu / xp	iu / xp	iu / xp	iu / xp	xu / xp
NH ₃	xu / xp	xu / ip	xu / ip	xu / ip	xu / ip	xu / ip
ADP	xu / xp	xu / xp	iu / xp	xu / xp	u / xp	xu / xp
ATP	xu / ip	xu / xp	xu / ip	xu / xp	xu / ip	xu / xp

Table S2. Mitochondrial fluxes [fmol/cell × min] in selectively permeabilized CHO-K1 cells under various feeding conditions. The fluxes were computed using the determined extracellular rates and the stoichiometry indicated by reactions R1-R50. By addition of ADP it was assumed that the flux R44=0. Abbreviations: c - cytosolic; m - mitochondrial; AcoA – acetyl-CoA; AKG – α -ketoglutarate; ASP – aspartate; CIT – citrate; FUM – fumarate; GLN – glutamine; GLU – glutamate; GLY– glycine; MAL – malate; MTHF– methyl-tetrahydrofolate; OAA – oxaloacetate; PYR – pyruvate; SER - serine; SUC – succinate. In the column indicated with red the sampling produced fluxes without biological significance.

	Uptake	puruvate	pyruvate, aspartate	citrate	α -ketoglutarate	succinate	malate (fumarate)	glutamine	glutamate	serine	
		Production		-	glutamate	-	-	fumarate, malate, citrate	glutamate, aspartate	aspartate	glycine
		Exp. No.	Flux [fmol/cell x min]								
		1a	2a	3a	4a	5a	6a/7a	8a	9a	11a	
--> PYRc	R1	4.6	11.9	0	0	0	0	0	0	0	
<--> MALc	R2	0	0	0	0	-14.5	16.5	0	0	0	
<--> SUCc	R3	0	0	0	0	24.5	0	0	0	0	
<--> FUMc	R4	0	0	0	-0.48	-2.2	0	0	0	0	
<--> CITc	R5	0	0	5.6	0	-1.9	-4.9	0	0	0	
<--> ASPc	R6	0	6.1	0	0	0	0	-3.3	-3.38	0	
--> AKGc	R7	0	0	0	12.7	0	0	0	0	0	
<--> GLUc	R8	0	-3	0	0	0	0	-14.4	2.29	0	
--> GLNc	R9	0	0	0	0	0	0	20	0	0	
<--> SERc	R11	0	0	0	0	0	0	0	0	4.5	
<--> GLYc	R12	0	0	0	0	0	0	0	0	-2.6	
<--> ADPc	R24	0	0	0	0	0	0	0	0	0	
<--> CO2c	R10	-13.8	-45.1	-33.6	-61.58	-19.8	-36.6	-14.8	2.07	-1.9	
<--> C1c	R13	0	0	0	0	0	0	0	0	-6.4	
C1c <--> C1m	R14	0	0	0	0	0	0	0	0	-6.4	
GLYc <--> GLYm	R15	0	0	0	0	0	0	0	0	-2.6	
SERc <--> SERm	R16	0	0	0	0	0	0	0	0	4.5	
CO2c <--> CO2m	R17	-13.8	-45.1	-33.6	-61.58	-19.8	-36.6	-14.8	2.07	-1.9	
SERm <--> GLYm + MTHFm	R18	0	0	0	0	0	0	0	0	4.5	
MTHFm --> C1m + THFm	R19	0	0	0	0	0	0	0	0	6.4	
GLYm + THFm + NADm --> MTHFm + CO2m + NADHm	R20	0	0	0	0	0	0	0	0	1.9	
--> O2m	R21	11.5	34.55	25.2	49.36	27.1	27.45	15.3	0.165	0.95	
<--> NH3c	R22	0	-3.1	0	0	0	0	-22.3	1.09	0	
NH3c <--> NH3m	R23	0	-3.1	0	0	0	0	-22.3	1.09	0	
<--> ATPc	R25	0	0	0	0	0	0	0	0	0	
ADPc + ATPm <--> ADPm + ATPc	R26	0	0	0	0	0	0	0	0	0	
PYRc --> PYRm	R27	4.6	11.9	0	0	0	0	0	0	0	
FUMc <--> FUMm	R28	0	0	0	-0.48	-2.2	0	0	0	0	
MALc <--> MALm	R29	0	0	5.6	12.7	-16.4	11.6	0	0	0	
SUCc <--> SUCm	R30	0	0	0	0	24.5	0	0	0	0	
MALm + AKGc --> MALc + AKGm	R31	0	0	0	12.7	0	0	0	0	0	
ASPm + GLUc <--> ASPc + GLUm	R32	0	-6.1	0	0	0	0	3.3	3.38	0	
CITm + MALc <--> CITc + MALm	R33	0	0	-5.6	0	1.9	4.9	0	0	0	
GLNc <--> GLNm	R34	0	0	0	0	0	0	20	0	0	
GLUc <--> GLUm	R35	0	3.1	0	0	0	0	-17.7	-1.09	0	
PYRm + NADm --> ACOAm + NADHm + CO2m	R36	4.6	15	5.6	12.22	5.9	11.6	2.3	-1.09	0	
ACOAm + OAAm --> CITm	R37	4.6	15	5.6	12.22	5.9	11.6	2.3	-1.09	0	
CITm + NADm --> AKGm + NADHm + CO2m	R38	4.6	15	11.2	12.22	4	6.7	2.3	-1.09	0	
AKGm + ADPm + NADm --> SUCm + ATPm + NADHm + CO2m	R39	4.6	12	11.2	24.92	4	6.7	7.9	1.2	0	
SUCm + FADm <--> FUMm + FADHm	R40	4.6	12	11.2	24.92	28.5	6.7	7.9	1.2	0	
FUMm <--> MALm	R41	4.6	12	11.2	24.44	26.3	6.7	7.9	1.2	0	
MALm + NADm <--> OAAm + NADHm	R42	-52.9	-163.85	-120.4	-234.58	-105.1	-125.65	-70.9	1.465	-4.75	
MALm + NADPm --> PYRm + CO2m + NADPHm	R43	57.5	175.85	131.6	259.02	116.9	148.85	78.8	-0.265	4.75	
PYRm + CO2m + ATPm --> OAAm + ADPm	R44	57.5	172.75	126	246.8	111	137.25	76.5	0.825	4.75	
AKGm + ASPm <--> GLUm + OAAm	R45	0	6.1	0	0	0	0	-3.3	-3.38	0	
GLUm + NADm <--> AKGm + NH3m + NADHm	R46	0	3.1	0	0	0	0	2.3	-1.09	0	
GLNm --> GLUm + NH3m	R47	0	0	0	0	0	0	20	0	0	
2 NADHm + O2m + 5 ADPm --> 2 NADm + 5 ATPm	R48	9.2	28.55	19.6	36.9	12.85	24.1	11.35	-0.435	0.95	
2 FADHm + O2m + 3 ADPm --> 2 FADm + 3 ATPm	R49	2.3	6	5.6	12.46	14.25	3.35	3.95	0.6	0	
NADPHm + NADm <--> NADPm + NADHm	R50	57.5	175.85	131.6	259.02	116.9	148.85	78.8	-0.265	4.75	

Supplementary Table S2. (continued)

	Exp. No.	Uptake	pyruvate, ADP	pyruvate, aspartate, ADP	citrate, ADP	α -ketoglutarate, ADP	succinate, ADP	malate (fumarate), ADP	glutamine, ADP	glutamate, ADP
		Production	ATP	glutamate, ATP	ATP	fumarate, ATP	fumarate, malate, citrate, ATP	citrate, ATP	glutamate, aspartate, ATP	aspartate, ATP
		Flux [fmol/cell x min]	1b	2b	3b	4b	5b	6b/7b	8b	9b
--> PYRc	R1		14.2	15.6	0	0	0	0	0	0
<-> MALc	R2		0	0	0	0	-14.6	21.4	0	0
<-> SUCc	R3		0	0	0	0	30.5	0	0	0
<-> FUMc	R4		0	0	0	-2.5	-2.1	0	0	0
<-> CITc	R5		0	0	38	0	-1.9	-4.9	0	0
<-> ASPc	R6		0	12.2	0	0	0	0	-11.4	-15.5
--> AKGc	R7		0	0	0	40.2	0	0	0	0
<-> GLUc	R8		0	-6.7	0	0	0	0	-19	15.5
--> GLNc	R9		0	0	0	0	0	0	44.7	0
<-> SERc	R11		0	0	0	0	0	0	0	0
<-> GLYc	R12		0	0	0	0	0	0	0	0
<-> ADPc	R24		0	0	0	0	0	0	0	0
<-> CO2c	R10		-42.6	-62.1	-228	-191	-43.8	-56.2	-82.9	-15.5
<-> C1c	R13		0	0	0	0	0	0	0	0
C1c <-> C1m	R14		0	0	0	0	0	0	0	0
GLYc <-> GLYm	R15		0	0	0	0	0	0	0	0
SERc <-> SERm	R16		0	0	0	0	0	0	0	0
CO2c <-> CO2m	R17		-42.6	-62.1	-228	-191	-43.8	-56.2	-82.9	-15.5
SERm <-> GLYm + MTHFm	R18		0	0	0	0	0	0	0	0
MTHFm --> C1m + THFm	R19		0	0	0	0	0	0	0	0
GLYm + THFm + NADm --> MTHFm + CO2m + NADHm	R20		0	0	0	0	0	0	0	0
--> O2m	R21		35.5	45.45	171	153.3	48.1	42.15	81.45	23.25
<-> NH3c	R22		0	-5.5	0	0	0	0	-59	0
NH3c <-> NH3m	R23		0	-5.5	0	0	0	0	-59	0
<-> ATPc	R25		177.5	227.25	855	766.5	210	210.75	407.25	116.25
ADPc + ATPm <-> ADPm + ATPc	R26		-177.5	-227.25	-855	-766.5	-210	-210.75	-407.25	-116.25
PYRc --> PYRm	R27		177.5	227.25	855	766.5	210	210.75	407.25	116.25
FUMc <-> FUMm	R28		14.2	15.6	0	0	0	0	0	0
MALc <-> MALm	R29		0	0	0	-2.5	-2.1	0	0	0
SUCc <-> SUCm	R30		0	0	38	40.2	-16.5	16.5	0	0
MALm + AKGc --> MALc + AKGm	R31		0	0	0	0	30.5	0	0	0
ASPm + GLUc <-> ASPc + GLUm	R32		0	0	0	40.2	0	0	0	0
CITm + MALc <-> CITc + MALm	R33		0	-12.2	0	0	0	0	11.4	15.5
GLNc --> GLNm	R34		0	0	-38	0	1.9	4.9	0	0
GLUc <-> GLUm	R35		0	0	0	0	0	0	44.7	0
PYRm + NADm --> ACOAm + NADHm + CO2m	R36		0	5.5	0	0	0	0	-30.4	0
ACOAm + OAAm --> CITm	R37		14.2	21.1	38	37.7	11.9	16.5	14.3	0
CITm + NADm --> AKGm + NADHm + CO2m	R38		14.2	21.1	38	37.7	11.9	16.5	14.3	0
AKGm + ADPm + NADm --> SUCm + ATPm + NADHm + CO2m	R39		14.2	21.1	76	37.7	10	11.6	14.3	0
SUCm + FADm <-> FUMm + FADHm	R40		14.2	14.4	76	77.9	10	11.6	40	15.5
FUMm <-> MALm	R41		14.2	14.4	76	77.9	40.5	11.6	40	15.5
MALm + NADm <-> OAAm + NADHm	R42		14.2	14.4	76	75.4	38.4	11.6	40	15.5
MALm + NADPm --> PYRm + CO2m + NADPHm	R43		14.2	8.9	38	37.7	11.9	16.5	25.7	15.5
PYRm + CO2m + ATPm --> OAAm + ADPm	R44		-1.84E-15	5.5	38	37.7	11.9	16.5	14.3	0
AKGm + ASPm <-> GLUm + OAAm	R45		0	12.2	0	0	0	0	-11.4	-15.5
GLUm + NADm <-> AKGm + NH3m + NADHm	R46		0	5.5	0	0	0	0	14.3	0
GLNm --> GLUm + NH3m	R47		0	0	0	0	0	0	44.7	0
2 NADHm + O2m + 5 ADPm --> 2 NADm + 5 ATPm	R48		28.4	38.25	133	114.35	27.85	36.35	61.45	15.5
2 FADHm + O2m + 3 ADPm --> 2 FADm + 3 ATPm	R49		7.1	7.2	38	38.95	20.25	5.8	20	7.75
NADPHm + NADm <-> NADPm + NADHm	R50		-1.58E-15	5.5	38	37.7	11.9	16.5	14.3	0

Supplementary Table S3.A Stoichiometry of the modes selected using the Supplementary Table S1 using selectively permeabilized CHO-K1 cells [fmol/cell × min].

EXPERIMENT	1a	1b	2a			2b		
Substrates	pyruvate	pyruvate, ADP	pyruvate, aspartate			pyruvate, aspartate, ADP		
Total mode stoichiometry	PYR + 2.5O ₂ = 3CO ₂	PYR + 12.5ADP + 2.5O ₂ = 3CO ₂ + 12.5ATP	PYR + ASP + O ₂ = GLU + 2CO ₂	ASP + 0.75O ₂ = 1.5CO ₂ + 0.5GLU	ASP + 3O ₂ = 4CO ₂	PYR + ASP + O ₂ + 5ADP = GLU + 2CO ₂ + 5ATP	ASP + 15ADP + 3O ₂ = 4CO ₂ + 15ATP + NH ₃	ASP + 3.75ADP + 0.75O ₂ = 0.5GLU + 1.5CO ₂ + 3.75ATP
REACTION FORMULAS	Mode 1	Mode 2	Mode 3	Mode 4	Mode 5	Mode 6	Mode 7	Mode 8
--> PYRc	1	1	1	0	0	1	0	0
<--> MALc	0	0	0	0	0	0	0	0
<--> SUCc	0	0	0	0	0	0	0	0
<--> FUMc	0	0	0	0	0	0	0	0
<--> CITc	0	0	0	0	0	0	0	0
<--> ASPc	0	0	1	1	1	1	1	1
--> AKGc	0	0	0	0	0	0	0	0
<--> GLUc	0	0	-1	-0.5	0	-1	0	-0.5
--> GLNc	0	0	0	0	0	0	0	0
<--> CO ₂ c	-3	-3	-2	-1.5	-4	2	-4	-1.5
<--> SERc	0	0	0	0	0	0	0	0
<--> GLYc	0	0	0	0	0	0	0	0
<--> C1c	0	0	0	0	0	0	0	0
C1c <--> C1m	0	0	0	0	0	0	0	0
GLYc <--> GLYm	0	0	0	0	0	0	0	0
SERc <--> SERm	0	0	0	0	0	0	0	0
CO ₂ c <--> CO ₂ m	-3	-3	-2	-1.5	-4	-2	-4	-1.5
SERm <--> GLYm + MTHFm	0	0	0	0	0	0	0	0
MTHFm --> C1m + THFm	0	0	0	0	0	0	0	0
GLYm + THFm + NADm --> MTHFm + CO ₂ m + NADHm + NH ₃	0	0	0	0	0	0	0	0
--> O ₂ m	2.5	2.5	1	0.75	3	1	3	0.75
<--> NH ₃ c	0	0	0	-0.5	-1	0	-1	-0.5
NH ₃ c <--> NH ₃ m	0	0	0	-0.5	-1	0	-1	-0.5
<--> ADPc	0	12.5	0	0	0	5	15	3.75
<--> ATPc	0	-12.5	0	0	0	-5	-15	-3.75
ADPc + ATPm <--> ADPm + ATPm	0	12.5	0	0	0	5	15	3.75
PYRc --> PYRm	1	1	1	0	0	1	0	0
FUMc <--> FUMm	0	0	0	0	0	0	0	0
MALc <--> MALm	0	0	0	0	0	0	0	0
SUCc <--> SUCm	0	0	0	0	0	0	0	0
MALm + AKGc --> MALc + AKGm	0	0	0	0	0	0	0	0
ASPm + GLUc <--> ASPc + GLUm	0	0	-1	-1	-1	-1	-1	-1
CITm + MALc <--> CITc + MALm	0	0	0	0	0	0	0	0
GLNc --> GLNm	0	0	0	0	0	0	0	0
GLUc <--> GLUm	0	0	0	0.5	1	0	1	0.5
PYRm + NADm --> ACOAm + NADHm + CO ₂ m	1	1	1	0.5	1	1	1	0.5
ACOAm + OAm --> CITm	1	1	1	0.5	1	1	1	0.5
CITm + NADm --> AKGm + NADHm + CO ₂ m	1	1	1	0.5	1	1	1	0.5
AKGm + ADPm + NADm --> SUCm + ATPm + NADHm + CO ₂ m	1	1	0	0	1	1	1	0
SUCm + FADm <--> FUMm + FADHm	1	1	0	0	1	0	1	0
FUMm <--> MALm	1	1	0	0	1	0	1	0
MALm + NADm <--> OAm + NADHm	-11.5	1	-5	-4.25	-15	0	0	-0.5
MALm + NADPm --> PYRm + CO ₂ m + NADPHm	12.5	0	5	4.25	16	0	1	0.5
PYRm + CO ₂ m + ATPm --> OAm + ADPm	12.5	0	5	3.75	15	0	0	0
AKGm + ASPm <--> GLUm + OAm	0	0	1	1	1	1	1	1
GLUm + NADm <--> AKGm + NH ₃ m + NADHm	0	0	0	0.5	1	0	1	0.5
GLNm --> GLUm + NH ₃ m	0	0	0	0	0	0	0	0
2 NADHm + O ₂ m + 5 ADPm --> 2 NADm + 5 ATPm	2	2	1	0.75	2.5	1	2.5	0.75
2 FADHm + O ₂ m + 3 ADPm --> 2 FADm + 3 ATPm	0.5	0.5	0	0	0.5	0	0.5	0
NADPHm + NADm <--> NADPm + NADHm	12.5	0	5	4.25	16	0	1	0.5

Supplementary Table S3.A (continued)

EXPERIMENT	3a	3b	4a		4b	
Substrates	citrate	citrate, ADP	α -ketoglutarate		α -ketoglutarate, ADP	
Total mode stoichiometry	CIT + 4.5O ₂ = 6CO ₂	CIT + 22.5ADP + 4.5O ₂ = 6CO ₂ + 22.5ATP	AKG + 4O ₂ = 5CO ₂	AKG + O ₂ = CO ₂ + FUM	AKG + 4O ₂ + 20ADP = 5CO ₂ + 20ATP	AKG + O ₂ + 5ADP = FUM + CO ₂ + 5ATP
REACTION FORMULAS	Mode 9	Mode 10	Mode 11	Mode 12	Mode 13	Mode 14
--> PYRc	0	0	0	0	0	0
<--> MALc	0	0	0	0	0	0
<--> SUCc	0	0	0	0	0	0
<--> FUMc	0	0	0	-1	0	-1
<--> CITc	1	1	0	0	0	0
<--> ASPc	0	0	0	0	0	0
--> AKGc	0	0	1	1	1	1
<--> GLUc	0	0	0	0	0	0
--> GLNc	0	0	0	0	0	0
<--> CO2c	-6	-6	-5	-1	-5	-1
<--> SERc	0	0	0	0	0	0
<--> GLYc	0	0	0	0	0	0
<--> C1c	0	0	0	0	0	0
C1c <--> C1m	0	0	0	0	0	0
GLYc <--> GLYm	0	0	0	0	0	0
SERc <--> SERm	0	0	0	0	0	0
CO2c <--> CO2m	-6	-6	-5	-1	-5	-1
SERm <--> GLYm + MTHFm	0	0	0	0	0	0
MTHFm --> C1m + THFm	0	0	0	0	0	0
GLYm + THFm + NADm --> MTHFm + CO2m + NADHm + NH3	0	0	0	0	0	0
--> O2m	4.5	4.5	4	1	4	1
<--> NH3c	0	0	0	0	0	0
NH3c <--> NH3m	0	0	0	0	0	0
<--> ADPc	0	22.5	0	0	20	5
<--> ATPc	0	-22.5	0	0	-20	-5
ADPc + ATPm <--> ADPm + ATPc	0	22.5	0	0	20	5
PYRc --> PYRm	0	0	0	0	0	0
FUMc <--> FUMm	0	0	0	-1	0	-1
MALc <--> MALm	1	1	1	1	1	1
SUCc <--> SUCm	0	0	0	0	0	0
MALm + AKGc --> MALc + AKGm	0	0	1	1	1	1
ASPm + GLUc <--> ASPc + GLUm	0	0	0	0	0	0
CITm + MALc <--> CITc + MALm	-1	-1	0	0	0	0
GLNc --> GLNm	0	0	0	0	0	0
GLUc <--> GLUm	0	0	0	0	0	0
PYRm + NADm --> ACOAm + NADHm + CO2m	1	1	1	0	1	0
ACOAm + OAm --> CITm	1	1	1	0	1	0
CITm + NADm --> AKGm + NADHm + CO2m	2	2	1	0	1	0
AKGm + ADPm + NADm --> SUCm + ATPm + NADHm + CO2m	2	2	2	1	2	1
SUCm + FADm <--> FUMm + FADHm	2	2	2	1	2	1
FUMm <--> MALm	2	2	2	0	2	0
MALm + NADm <--> OAm + NADHm	-21.5	1	-19	-5	1	0
MALm + NADPm --> PYRm + CO2m + NADPHm	23.5	1	21	5	1	0
PYRm + CO2m + ATPm --> OAm + ADPm	22.5	0	20	5	0	0
AKGm + ASPm <--> GLUm + OAm	0	0	0	0	0	0
GLUm + NADm <--> AKGm + NH3m + NADHm	0	0	0	0	0	0
GLNm --> GLUm + NH3m	0	0	0	0	0	0
2 NADHm + O2m + 5 ADPm --> 2 NADm + 5 ATPm	3.5	3.5	3	0.5	3	0.5
2 FADHm + O2m + 3 ADPm --> 2 FADm + 3 ATPm	1	1	1	0.5	1	0.5
NADPHm + NADm <--> NADPm + NADHm	23.5	1	21	5	1	0

Supplementary Table S3.A (continued)

EXPERIMENT	5a				5b			
Substrates	succinate				succinate, ADP			
Total mode stoichiometry	SUC + 3.5O ₂ = 4CO ₂	SUC + 0.5O ₂ = MAL	SUC + 1.25O ₂ = CO ₂ + 0.5CIT	SUC + 0.5O ₂ = FUM	SUC + 3.5O ₂ + 16.5ADP = 4CO ₂ + 16.5ATP	SUC + 1.5ADP + 0.5O ₂ = MAL + 1.5ATP	SUC + 1.25O ₂ + 5.75ADP = 0.5CIT + CO ₂	SUC + 0.5O ₂ + 1.5ADP = FUM + 1.5ADP
REACTION FORMULAS	Mode 15	Mode 16	Mode 17	Mode 18	Mode 19	Mode 20	Mode 21	Mode 22
--> PYRc	0	0	0	0	0	0	0	0
<--> MALc	0	-1	0	0	0	-1	0	0
<--> SUCc	1	1	1	1	1	1	1	1
<--> FUMc	0	0	0	-1	0	0	0	-1
<--> CITc	0	0	-0.5	0	0	0	-0.5	0
<--> ASPc	0	0	0	0	0	0	0	0
--> AKGc	0	0	0	0	0	0	0	0
<--> GLUc	0	0	0	0	0	0	0	0
--> GLNc	0	0	0	0	0	0	0	0
<--> CO ₂ c	-4	0	-1	0	-4	0	-1	0
<--> SERc	0	0	0	0	0	0	0	0
<--> GLYc	0	0	0	0	0	0	0	0
<--> C1c	0	0	0	0	0	0	0	0
C1c <--> C1m	0	0	0	0	0	0	0	0
GLYc <--> GLYm	0	0	0	0	0	0	0	0
SERc <--> SERm	0	0	0	0	0	0	0	0
CO ₂ c <--> CO ₂ m	-4	0	-1	0	-4	0	-1	0
SERm <--> GLYm + MTHFm	0	0	0	0	0	0	0	0
MTHFm --> C1m + THFm	0	0	0	0	0	0	0	0
GLYm + THFm + NADm --> MTHFm + CO ₂ m + NADHm + NH ₃	0	0	0	0	0	0	0	0
--> O ₂ m	3.5	0.5	1.25	0.5	3.5	0.5	1.25	0.5
<--> NH ₃ c	0	0	0	0	0	0	0	0
NH ₃ c <--> NH ₃ m	0	0	0	0	0	0	0	0
<--> ADPc	0	0	0	0	16.5	1.5	5.75	1.5
<--> ATPc	0	0	0	0	-16.5	-1.5	-5.75	-1.5
ADPc + ATPm <--> ADPm + ATPc	0	0	0	0	16.5	1.5	5.75	1.5
PYRc --> PYRm	0	0	0	0	0	0	0	0
FUMc <--> FUMm	0	0	0	-1	0	0	0	-1
MALc <--> MALm	0	-1	-0.5	0	0	-1	-0.5	0
SUCc <--> SUCm	1	1	1	1	1	1	1	1
MALm + AKGc --> MALc + AKGm	0	0	0	0	0	0	0	0
ASPm + GLUc <--> ASPc + GLUm	0	0	0	0	0	0	0	0
CITm + MALc <--> CITc + MALm	0	0	0.5	0	0	0	0.5	0
GLNc --> GLNm	0	0	0	0	0	0	0	0
GLUc <--> GLUm	0	0	0	0	0	0	0	0
PYRm + NADm --> ACOAm + NADHm + CO ₂ m	1	0	0.5	0	1	0	0.5	0
ACOAm + OAm --> CITm	1	0	0.5	0	1	0	0.5	0
CITm + NADm --> AKGm + NADHm + CO ₂ m	1	0	0	0	1	0	0	0
AKGm + ADPm + NADm --> SUCm + ATPm + NADHm + CO ₂ m	1	0	0	0	1	0	0	0
SUCm + FADm <--> FUMm + FADHm	2	1	1	1	2	1	1	1
FUMm <--> MALm	2	1	1	0	2	1	1	0
MALm + NADm <--> OAm + NADHm	-15.5	-1.5	-4.75	-1.5	1	0	0.5	0
MALm + NADPm --> PYRm + CO ₂ m + NADPHm	17.5	1.5	5.75	1.5	1	0	0.5	0
PYRm + CO ₂ m + ATPm --> OAm + ADPm	16.5	1.5	5.25	1.5	0	0	0	0
AKGm + ASPm <--> GLUm + OAm	0	0	0	0	0	0	0	0
GLUm + NADm <--> AKGm + NH ₃ m + NADHm	0	0	0	0	0	0	0	0
GLNm --> GLUm + NH ₃ m	0	0	0	0	0	0	0	0
2 NADHm + O ₂ m + 5 ADPm --> 2 NADm + 5 ATPm	2.5	0	0.75	0	2.5	0	0.75	0
2 FADHm + O ₂ m + 3 ADPm --> 2 FADm + 3 ATPm	1	-0.5	0.5	0.5	1	0.5	0.5	0.5
NADPHm + NADm <--> NADPm + NADHm	17.5	1.5	5.75	1.5	1	0	0.5	0

Supplementary Table S3.A (continued)

EXPERIMENT	6a		6b		7a		7b	
Substrates	malate		malate, ADP		fumarate		fumarate, ADP	
Total mode stoichiometry	MAL + 3O2 = 4CO2	MAL + 0.75O2 = 0.5CIT + CO2	MAL + 3O2 + 15ADP = 4CO2 + 15ATP	MAL + 0.75O2 + 3.75ADP = 0.5CIT + CO2 + 3.75ATP	FUM + 3O2 = 4CO2	FUM + 0.75O2 = 0.5CIT + CO2	FUM + 3O2 + 15ADP = 4CO2 + 15ATP	FUM + 0.75O2 + 3.75ADP = 0.5CIT + CO2 + 3.75ATP
REACTION FORMULAS	Mode 23	Mode 24	Mode 25	Mode 26	Mode 27	Mode 28	Mode 29	Mode 30
--> PYRc	0	0	0	0	0	0	0	0
<--> MALc	1	1	1	1	0	0	0	0
<--> SUCc	0	0	0	0	0	0	0	0
<--> FUMc	0	0	0	0	1	1	1	1
<--> CITc	0	-0.5	0	-0.5	0	-0.5	0	-0.5
<--> ASPc	0	0	0	0	0	0	0	0
--> AKGc	0	0	0	0	0	0	0	0
<--> GLUc	0	0	0	0	0	0	0	0
--> GLNc	0	0	0	0	0	0	0	0
<--> CO2c	-4	-1	-4	-1	-4	-1	-4	-1
<--> SERc	0	0	0	0	0	0	0	0
<--> GLYc	0	0	0	0	0	0	0	0
<--> C1c	0	0	0	0	0	0	0	0
C1c <--> C1m	0	0	0	0	0	0	0	0
GLYc <--> GLYm	0	0	0	0	0	0	0	0
SERc <--> SERm	0	0	0	0	0	0	0	0
CO2c <--> CO2m	-4	-1	-4	-1	-4	-1	-4	-1
SERm <--> GLYm + MTHFm	0	0	0	0	0	0	0	0
MTHFm --> C1m + THFm	0	0	0	0	0	0	0	0
GLYm + THFm + NADm --> MTHFm + CO2m + NADHm + NH3	0	0	0	0	0	0	0	0
--> O2m	3	0.75	3	0.75	3	0.75	3	0.75
<--> NH3c	0	0	0	0	0	0	0	0
NH3c <--> NH3m	0	0	0	0	0	0	0	0
<--> ADPc	0	0	15	3.75	0	0	15	3.75
<--> ATPc	0	0	-15	-3.75	0	0	-15	-3.75
ADPc + ATPm <--> ADPm + ATPc	0	0	15	3.75	0	0	15	3.75
PYRc --> PYRm	0	0	0	0	0	0	0	0
FUMc <--> FUMm	0	0	0	0	1	1	1	1
MALc <--> MALm	1	0.5	1	0.5	0	-0.5	0	-0.5
SUCc <--> SUCm	0	0	0	0	0	0	0	0
MALm + AKGc --> MALc + AKGm	0	0	0	0	0	0	0	0
ASPm + GLUc <--> ASPc + GLUm	0	0	0	0	0	0	0	0
CITm + MALc <--> CITc + MALm	0	0.5	0	0.5	0	0.5	0	0.5
GLNc --> GLNm	0	0	0	0	0	0	0	0
GLUc <--> GLUm	0	0	0	0	0	0	0	0
PYRm + NADm --> ACOAm + NADHm + CO2m	1	0.5	1	0.5	1	0.5	1	0.5
ACOAm + OAAm --> CITm	1	0.5	1	0.5	1	0.5	1	0.5
CITm + NADm --> AKGm + NADHm + CO2m	1	0	1	0	1	0	1	0
AKGm + ADPm + NADm --> SUCm + ATPm + NADHm + CO2m	1	0	1	0	1	0	1	0
SUCm + FADm <--> FUMm + FADHm	1	0	1	0	1	0	1	0
FUMm <--> MALm	1	0	1	0	2	1	2	1
MALm + NADm <--> OAAm + NADHm	-14	-3.25	1	0.5	-14	-3.25	1	0.5
MALm + NADPm --> PYRm + CO2m + NADPHm	16	4.25	1	0.5	16	4.25	1	0.5
PYRm + CO2m + ATPm --> OAAm + ADPm	15	3.75	0	0	15	3.75	0	0
AKGm + ASPm <--> GLUm + OAAm	0	0	0	0	0	0	0	0
GLUm + NADm <--> AKGm + NH3m + NADHm	0	0	0	0	0	0	0	0
GLNm --> GLUm + NH3m	0	0	0	0	0	0	0	0
2 NADHm + O2m + 5 ADPm --> 2 NADm + 5 ATPm	2.5	0.75	2.5	0.75	2.5	0.75	2.5	0.75
2 FADHm + O2m + 3 ADPm --> 2 FADm + 3 ATPm	0.5	0	0.5	0	0.5	0	0.5	0
NADPHm + NADm <--> NADPm + NADHm	16	4.25	1	0.5	16	4.25	1	0.5

Supplementary Table S3.A (continued)

EXPERIMENT	8a			8b			9a		9b		11a	
Substrates	glutamine			glutamine, ADP			glutamate		glutamate, ADP		serine	
Total mode stoichiometry	GLN + 4.5O ₂ = 5CO ₂ + 2NH ₃	GLN + 1.5O ₂ = ASP + CO ₂ + NH ₃	GLN = GLU + NH ₃	GLN + 4.5O ₂ + 22.5ADP = 5CO ₂ + 2NH ₃ +	GLN + 1.5O ₂ + 7.5 = ASP + CO ₂ + NH ₃	GLN = GLU + NH ₃	GLU + 4.5O ₂ = 5CO ₂ + NH ₃	GLU + 1.5O ₂ = ASP + CO ₂	GLU + 4.5O ₂ + 22.5ADP = 5CO ₂ + NH ₃ + 22.5ATP	GLU + 1.5O ₂ + 7.5ADP = ASP + CO ₂	SER = GLY + C1	SER + 0.5O ₂ = CO ₂ + 2C1 +
REACTION FORMULAS	Mode 31	Mode 32	Mode 33	Mode 34	Mode 35	Mode 36	Mode 37	Mode 38	Mode 39	Mode 40	Mode 41	Mode 42
-> PYRc	0	0	0	0	0	0	0	0	0	0	0	0
<-> MALc	0	0	0	0	0	0	0	0	0	0	0	0
<-> SUCc	0	0	0	0	0	0	0	0	0	0	0	0
<-> FUMc	0	0	0	0	0	0	0	0	0	0	0	0
<-> CITc	0	0	0	0	0	0	0	0	0	0	0	0
<-> ASPc	0	-1	0	0	-1	0	0	-1	0	-1	0	0
-> AKGc	0	0	0	0	0	0	0	0	0	0	0	0
<-> GLUc	0	0	-1	0	0	-1	1	1	1	1	0	0
-> GLNc	1	1	1	1	1	1	0	0	0	0	0	0
<-> CO ₂ c	-5	-1	0	-5	-1	0	-5	-1	-5	-1	0	-1
<-> SERc	0	0	0	0	0	0	0	0	0	0	1	1
<-> GLYc	0	0	0	0	0	0	0	0	0	0	-1	0
<-> C1c	0	0	0	0	0	0	0	0	0	0	-1	-2
C1c <-> C1m	0	0	0	0	0	0	0	0	0	0	-1	-2
GLYc <-> GLYm	0	0	0	0	0	0	0	0	0	0	-1	0
SERc <-> SERm	0	0	0	0	0	0	0	0	0	0	1	1
CO ₂ c <-> CO ₂ m	-5	-1	0	-5	-1	0	0	-1	0	-1	0	-1
SERm <-> GLYm + MTHFm	0	0	0	0	0	0	0	0	0	0	1	1
MTHFm -> C1m + THFm	0	0	0	0	0	0	0	0	0	0	1	2
GLYm + THFm + NADm -> MTHFm + CO ₂ m + NADHm + NH ₃	0	0	0	0	0	0	0	0	0	0	0	1
-> O ₂ m	4.5	1.5	0	4.5	1.5	0	4.5	1.5	4.5	1.5	0	0.5
<-> NH ₃ c	-2	-1	-1	-2	-1	-1	-1	0	-1	0	0	-1
NH ₃ c <-> NH ₃ m	-2	-1	-1	-2	-1	-1	-1	0	-1	0	0	-1
<-> ADPc	0	0	0	22.5	7.5	0	0	0	22.5	7.5	0	0
<-> ATPc	0	0	0	-22.5	-7.5	0	0	0	-22.5	-7.5	0	0
ADPc + ATPm <-> ADPm + ATPc	0	0	0	22.5	7.5	0	0	0	22.5	7.5	0	0
PYRc -> PYRm	0	0	0	0	0	0	0	0	0	0	0	0
FUMc <-> FUMm	0	0	0	0	0	0	0	0	0	0	0	0
MALc <-> MALm	0	0	0	0	0	0	0	0	0	0	0	0
SUCc <-> SUCm	0	0	0	0	0	0	0	0	0	0	0	0
MALm + AKGc -> MALc + AKGm	0	0	0	0	0	0	0	0	0	0	0	0
ASPm + GLUc <-> ASPc + GLUm	0	1	0	0	1	0	0	1	0	1	0	0
CITm + MALc <-> CITc + MALm	0	0	0	0	0	0	0	0	0	0	0	0
GLNc -> GLNm	1	1	1	1	1	1	0	0	0	0	0	0
GLUc <-> GLUm	0	-1	-1	0	-1	-1	1	0	1	0	0	0
PYRm + NADm -> ACOAm + NADHm + CO ₂ m	1	0	0	1	0	0	1	0	1	0	0	0
ACOAm + OAAm -> CITm	1	0	0	1	0	0	1	0	1	0	0	0
CITm + NADm -> AKGm + NADHm + CO ₂ m	1	0	0	1	0	0	1	0	1	0	0	0
AKGm + ADPm + NADm -> SUCm + ATPm + NADHm + CO ₂ m	2	1	0	2	1	0	2	1	2	1	0	0
SUCm + FADm <-> FUMm + FADHm	2	1	0	2	1	0	2	1	2	1	0	0
FUMm <-> MALm	2	1	0	2	1	0	2	1	2	1	0	0
MALm + NADm <-> OAAm + NADHm	-21.5	-6.5	0	1	1	0	-21.5	-6.5	1	1	0	-2.5
MALm + NADPm -> PYRm + CO ₂ m + NADPHm	23.5	7.5	0	1	0	0	23.5	7.5	1	0	0	2.5
PYRm + CO ₂ m + ATPm -> OAAm + ADPm	22.5	7.5	0	0	0	0	22.5	7.5	0	0	0	2.5
AKGm + ASPm <-> GLUm + OAAm	0	-1	0	0	-1	0	0	-1	0	-1	0	0
GLUm + NADm <-> AKGm + NH ₃ m + NADHm	1	0	0	1	0	0	1	0	1	0	0	0
GLNm -> GLUm + NH ₃ m	1	1	1	1	1	1	0	0	0	0	0	0
2 NADHm + O ₂ m + 5 ADPm -> 2 NADm + 5 ATPm	3.5	1	0	3.5	1	0	3.5	1	3.5	1	0	0.5
2 FADHm + O ₂ m + 3 ADPm -> 2 FADm + 3 ATPm	1	0.5	0	1	0.5	0	1	0.5	1	0.5	0	0
NADPHm + NADm <-> NADPm + NADHm	23.5	7.5	0	1	0	0	23.5	7.5	1	0	0	2.5

ABBREVIATIONS: ACOA - acetyl-CoA; AKG - α -ketoglutarate; ASP - aspartate; C1 - One carbon units (methenyl, methylene, formate); CIT - citrate; FUM - fumarate; GLN - glutamine; GLU - glutamate; GLY - glycine; MAL- malate; OAA - oxaloacetate; PYR - pyruvate; SER - serine; SUC - succinate;

Supplementary Table S3.B Contribution to each mode to the total flux in each feeding experiment using selectively permeabilized CHO-K1 cells [fmol/cell × min].

EXPERIMENT	1a	1b	2a*	2b*	3a	3b	4a	4b	5a	5b*	6a/7a	6b/7b*	8a	8b	9a	9b	12a
	Contribution [fmol / cell × min]																
Mode 1	4.6	0	11.9	0	0	0	0	0	0	0	0	0	0	0	0	0	0
Mode 2	0	14.2	0	15.6	0	0	0	0	0	0	0	0	0	0	0	0	0
Mode 3	0	0	0	0	0	0	0	0	0	0	0	0	0	0	0	0	0
Mode 4	0	0	6.1	0	0	0	0	0	0	0	0	0	0	0	0	0	0
Mode 5	0	0	0	0	0	0	0	0	0	0	0	0	0	0	0	0	0
Mode 6	0	0	0	0	0	0	0	0	0	0	0	0	0	0	0	0	0
Mode 7	0	0	0	0	0	0	0	0	0	0	0	0	0	0	0	0	0
Mode 8	0	0	0	12.2	0	0	0	0	0	0	0	0	0	0	0	0	0
Mode 9	0	0	0	0	5.62	0	0	0	0	0	0	0	0	0	0	0	0
Mode 10	0	0	0	0	0	38	0	0	0	0	0	0	0	0	0	0	0
Mode 11	0	0	0	0	0	0	12.3	0	0	0	0	0	0	0	0	0	0
Mode 12	0	0	0	0	0	0	0.4	0	0	0	0	0	0	0	0	0	0
Mode 13	0	0	0	0	0	0	0	37.7	0	0	0	0	0	0	0	0	0
Mode 14	0	0	0	0	0	0	0	2.47	0	0	0	0	0	0	0	0	0
Mode 15	0	0	0	0	0	0	0	0	4.07	0	0	0	0	0	0	0	0
Mode 16	0	0	0	0	0	0	0	0	14.5	0	0	0	0	0	0	0	0
Mode 17	0	0	0	0	0	0	0	0	3.7	0	0	0	0	0	0	0	0
Mode 18	0	0	0	0	0	0	0	0	2.23	0	0	0	0	0	0	0	0
Mode 19	0	0	0	0	0	0	0	0	0	10.6	0	0	0	0	0	0	0
Mode 20	0	0	0	0	0	0	0	0	0	14.6	0	0	0	0	0	0	0
Mode 21	0	0	0	0	0	0	0	0	0	3.7	0	0	0	0	0	0	0
Mode 22	0	0	0	0	0	0	0	0	0	2.14	0	0	0	0	0	0	0
Mode 23	0	0	0	0	0	0	0	0	0	0	7	0	0	0	0	0	0
Mode 24	0	0	0	0	0	0	0	0	0	0	9.72	0	0	0	0	0	0
Mode 25	0	0	0	0	0	0	0	0	0	0	0	11.6	0	0	0	0	0
Mode 26	0	0	0	0	0	0	0	0	0	0	0	9.72	0	0	0	0	0
Mode 27	0	0	0	0	0	0	0	0	0	0	0	0	0	0	0	0	0
Mode 28	0	0	0	0	0	0	0	0	0	0	0	0	0	0	0	0	0
Mode 29	0	0	0	0	0	0	0	0	0	0	0	0	0	0	0	0	0
Mode 30	0	0	0	0	0	0	0	0	0	0	0	0	0	0	0	0	0
Mode 31	0	0	0	0	0	0	0	0	0	0	0	0	2.31	0	0	0	0
Mode 32	0	0	0	0	0	0	0	0	0	0	0	0	3.29	0	0	0	0
Mode 33	0	0	0	0	0	0	0	0	0	0	0	0	14.4	0	0	0	0
Mode 34	0	0	0	0	0	0	0	0	0	0	0	0	0	14.3	0	0	0
Mode 35	0	0	0	0	0	0	0	0	0	0	0	0	0	11.4	0	0	0
Mode 36	0	0	0	0	0	0	0	0	0	0	0	0	0	19	0	0	0
Mode 37	0	0	0	0	0	0	0	0	0	0	0	0	0	0	2.69	0	0
Mode 38	0	0	0	0	0	0	0	0	0	0	0	0	0	0	0	0	0
Mode 39	0	0	0	0	0	0	0	0	0	0	0	0	0	0	0	0	0
Mode 40	0	0	0	0	0	0	0	0	0	0	0	0	0	0	0	0	0
Mode 41	0	0	0	0	0	0	0	0	0	0	0	0	0	0	0	0	2.61
Mode 42	0	0	0	0	0	0	0	0	0	0	0	0	0	0	0	0	1.84

* In the experiments 2a and 2b it is assumed that the modes that take up ASP and PYR together are not active (Mode 3 and Mode 6) . Also, the modes that use ASP to produce only CO₂ (Mode 5 and Mode 7) are considered inactive when computing the contribution factors.

* In the experiments 5b, 6b and 7b the CIT concentration could not be determined. Mode contribution factors were computed assuming the same factors for CIT production as in 5a, 6a and 7a respectively.

* In the experiment 9b, GLU concentration could not be determined reliably, therefore the mode flux was not computed.

* The contribution of Modes 27-30 to FUM metabolism could not be determined due to extracellular conversion of FUM to MAL

Supplementary Table S4. Conclusions on mitochondrial enzymes and transporters activity and about regulation of the mitochondrial metabolism resulted by applying elementary mode analysis to the observations from feeding experiments with selectively permeabilized CHO-K1 cells. The gray areas indicate the experiments on which each corresponding conclusion was based.

Experiment No.	1a	1b	2a	2b	3a	3b	4a	4b	5a	5b	6a/7a	6b/7b	8a	8b	9a	9b	11a	
Substrate	pyruvate	pyruvate, ADP	pyruvate, aspartate	pyruvate, aspartate, ADP	citrate	citrate, ADP	α -ketoglutarate	α -ketoglutarate, ADP	succinate	succinate, ADP	malate/ fumarate	malate/ fumarate, ADP	glutamine	glutamine, ADP	glutamate	glutamate, ADP	serine	
Citrate synthase flux (TCA cycle) [fmol / cell x min]	4.6	14.2	15	21.1	5.6	38	12.22	37.7	5.9	11.9	11.6	16.5	2.3	14.3	-	-	0	
	Uptake rates increased by adding ADP. This happens because ADP stimulates PDH, IDH and AKGH																	
	In the experiments where ADP was not supplied, the highly active PCX-MDH-ME disposed of the ATP																	
	ME provides pyruvate for replenishing the TCA																	
	Reducing equivalents are transferred from NADPH to NAD+ via the NNT or using IDH isoenzymes cycling																	
	Full metabolization to CO ₂ is possible																	
	PYR and ASP had a reciprocal stimulating effect. This effect did not manifest for pyruvate in the presence of ADP. Aspartate was not taken up without pyruvate.																	
	ASP and PYR are taken up through separate modes																	
	Glutamate is re-transported into the mitochondria via the glutamate carrier																	
	PYR uptake is limited in all stimulating conditions (ADP, ASP, ASP+ADP) by the MPC. PYR uptake is in the same range with uptake in vivo by the mitochondria (Nicolae et al., 2014)																	
	Complete reuptake of malate occurs or citrate can be transported without antiport																	
	Highest complete TCA cycle flux, both with and w/o ADP																	
	High TCA cycle flux confirms that IDH and AKGDH are the bottlenecks of the TCA cycle																	
	AKG did not inhibit ME																	

Danksagung

Mein außerordentlicher Dank gilt Professor Dr. Elmar Heinzle für die Bereitstellung des Themas und das mir dabei entgegengebrachte Vertrauen. Ich danke ihm für die Möglichkeit meine Forschungsergebnisse auf Konferenzen zu präsentieren sowie für die kompetente wissenschaftliche Betreuung und die unzähligen fachlichen Diskussionen, die diese Arbeit maßgeblich mitgestaltet haben.

Bei Professor Dr. Manfred Schmitt bedanke ich mich herzlich für die ausgezeichnete Betreuung während des Studiums, insbesondere während meines Straßburg-Aufenthaltes, und für die Bereitschaft, diese Arbeit zu begutachten.

Ich bedanke mich bei Professor Dr. An-Ping Zeng und Professor Dr. Ralf Pörtner für die Projektkoordination sowie beim BMBF für die finanzielle Unterstützung des SysCompart-Projekts. Ich möchte mich besonders bei meinen Kollegen von der TUHH, Janina Bahnmann, Negar Rajabi und Uwe Jandt, für die ausgezeichnete Kooperation und Diskussionsbereitschaft bedanken. Ein großer Dank geht auch an Professor Dr. Thomas Noll (AK Zellkulturtechnik, Universität Bielefeld) für die Bereitstellung von exzellenten CHO Zellen und an Stefan Northoff von TeutoCell für die Herstellung von ebenso exzellentem CHO Zellkulturmedium, seine zahlreichen Ratschläge und sein Entgegenkommen.

Allen Mitgliedern der Technischen Biochemie, die mich auf meinem Weg begleitet haben, danke ich für eine unvergessliche Zeit, die herzliche Arbeitsatmosphäre und bereitwillige Hilfsbereitschaft. Dr. Fozia Noor danke ich für Ihre Unterstützung und die Organisation der „Zoiga“ Gruppe. Ich bedanke mich bei Veronika Witte, Robert Schmidt, Michel Fritz, Dr. Klaus Hollemeyer und Dr. Konstantin Schneider für die Hilfe im Laboralltag. Insbesondere möchte ich Michel Fritz für seine unverzichtbare technische Unterstützung danken, für die Wunder, die er bei der Analytik vollbracht hat, und die Lösungen, die er für alle kleinen und großen Probleme parat hatte. Ein besonders großer Dank gebührt außerdem Dr. Susanne Kohring für Ihre wertvolle Hilfe in unzähligen bürokratischen Angelegenheiten und für viele nette Gespräche.

Ich danke meinem ehemaligen Masterstudenten Yannic Nonnenmacher für die ausgezeichnete und humorvolle Zusammenarbeit und natürlich für seinen unschätzbaren experimentellen und kreativen Beitrag zu dieser Arbeit. Bei meinen früheren Kollegen in der Zellkultur Dr. Jens Niklas, Dr. Simone Beckers, Dr. Alexander Strigun, Dr. Daniel Müller, Dr. Georg Tascher, Richa Garg, Yeda Kaminski, Bassem Ben Yahia, sowie bei meinen früheren Kollegen aus dem Fermenterlabor, insbesondere Dr. Tobias Klein, Dr. Susanne Peifer, Dr. Andreas Neuner, Vasileios Delis, Dr. Konstantin Schneider und Dr. Karla Martinez Gomez bedanke ich mich ganz herzlich für die aufmunternden Worte, die wertvollen wissenschaftlichen Diskussionen, die uneingeschränkte Hilfsbereitschaft und die schöne Atmosphäre. Bei Dr. Tobias Klein bedanke ich mich außerdem für

seine Unterstützung und seine Geduld bei den Mikrobioreatorkultivierungen. Besonders möchte ich mich auch bei Dr. Jens Niklas für die hervorragende Zusammenarbeit bedanken.

Meinen Freunden Saskia Sperber, Malina Orsini, Christian Priesnitz, Esther Hoffmann, Sebastian Klein, Christian Weyler, Lisa Blass, Averina Nicolae, Katja Gemperlein, Stephanie Saul, Hélène Lyrmann, Dr. Elisabeth John, Lisa Wagner, Jana Schmitt, Armin Melnyk und Dr. Verena Schütz danke ich für die fortwährende Motivation, für die vielen Lacher einerseits und ernsthaften Gespräche andererseits, für die Unterstützung im wissenschaftlichen und nichtwissenschaftlichen Alltag, aber auch die Ablenkung vom Alltag durch unzählige kulinarische, sportliche, spielerische, und musikalische Ausflüge und Höhepunkte, die mein Leben bereichern, und schließlich für die Nachsicht und Geduld bei meiner mangelhaften Kenntnis der sogenannten „neuen Medien“. Vielen Dank für diese großartigen und unvergesslichen Erlebnisse! Insbesondere danke ich Averina Nicolae für die kreative und geduldige Zusammenarbeit zwischen Experimentator und Simulator, für Ihr Vertrauen, die tiefe Freundschaft und die intensiven Gespräche.

Ich bedanke mich von ganzem Herzen bei meinen Eltern, meiner Großmutter, und meiner Schwester mit Ihrer Familie. Ihr seid immer für mich da und habt mich uneingeschränkt unterstützt. Insbesondere die Zeit mit Lukas und Helene hat mir immer wieder neue Kraft geschenkt. Der größte Dank überhaupt gilt meiner Mutter, die sich mit mir gefreut hat, mit mir gelitten hat, alle Höhen und Tiefen dieser Arbeit mitgeföhlt hat und mir bedingungslos den Rücken freigehalten hat. Ohne den Rückhalt meiner Familie hätte ich das nicht geschafft.

Curriculum Vitae

Judith Wahrheit

Diplom-Biologin, geboren am 27. Februar 1985 in St. Ingbert/Saar

Werdegang

- seit 08/2014 **Biocrates Life Sciences AG** (Innsbruck, Österreich)
Biochemiker Auftragsforschung
- 01/2010-08/2014 **Promotion** im Rahmen des BMBF-Projektes “SysCompart”
Titel: *Metabolic dynamics and compartmentation in the central metabolism of Chinese hamster ovary cells*
Institut für Technische Biochemie
Universität des Saarlandes
- 12/2010 Diplomabschluss in Biologie
Diplomarbeit im Rahmen des EU-Projektes “Invitroheart”
Titel: *Physiologische Charakterisierung der HL-1 Zelllinie zur pharmazeutischen Wirkstofftestung*
Institut für Technische Biochemie
Universität des Saarlandes
- 09/2004 -11/2009 Studium der Biologie mit Schwerpunkt Human- und Molekularbiologie
Universität des Saarlandes
- 09/2006 -11/2007 Studium der Biochemie und Molekularbiologie
Université Louis Pasteur (Strasbourg, Frankreich)
im Rahmen des ERASMUS-Austauschprogramms
- 08/1996 – 06/2004 Gymnasium Johanneum in Homburg/Saar

Auszeichnungen

Posterpreis der European Society for Animal Cell Technology, Lille (2013)

Publikationen

- 2014 Nicolae A, **Wahrheit J**, Bahnemann J, Zeng A-P, Heinzle E, (2014) Non-stationary ¹³C metabolic flux analysis of Chinese hamster ovary cells in batch culture using extracellular labeling highlights metabolic reversibility and compartmentation, BMC Systems Biology, Apr 28;8(1):50

- 2014 **Wahrheit J**, Niklas J, Heinzle E, (2014) Metabolic control at the cytosol-mitochondria interface in different growth phases of CHO cells, *Metabolic Engineering*, May;23:9-21
- Wahrheit J**, Heinzle E, (2014) Quenching Methods for the Analysis of Intracellular Metabolites, In: Pörtner, R., (Ed.), *Animal Cell Biotechnology*. vol. 1104. Humana Press, pp. 211-221 (Buchkapitel)
- Wahrheit J**, Nicolae A, Heinzle E, (2014) Dynamics of growth and metabolism controlled by glutamine availability in Chinese hamster ovary cells, *Applied Microbiology and Biotechnology*, *Applied Microbiology and Biotechnology*. 98, 1771-1783
- Bahnmann J, Kayo S, **Wahrheit J**, Heinzle E, Pörtner R, Zeng A-P (2014). In search of an effective cell disruption method to isolate intact mitochondria from Chinese hamster ovary cells. *Engineering in Life Sciences*. 14, 161-169
- Wahrheit J**, Nonnenmacher Y, Sperber S, Heinzle E. High-throughput respiration screening of single mitochondrial substrates using permeabilized CHO cells (*eingereicht*)
- Wahrheit J**, Nonnenmacher Y, Nicolae A, Heinzle E. Perturbation of the Mammalian Pyruvate Metabolism and Resulting Rearrangement of Central Metabolic Fluxes in CHO Cells (*in Vorbereitung*)
- Nicolae A, **Wahrheit J**, Nonnenmacher Y, Weyler C, Heinzle E. Elementary mode analysis of the mitochondrial metabolism in selectively permeabilized CHO cells (*in Vorbereitung*)
- Nicolae A, **Wahrheit J**, Heinzle E. High resolution ¹³C metabolic flux analysis in CHO cells (*in Vorbereitung*)
- 2013 **Wahrheit J**, Heinzle E (2013) Sampling and quenching of CHO suspension cells for the analysis of intracellular metabolites, *BMC Proceedings* 7(Suppl 6):P42
- Wahrheit J**, Nicolae A, Heinzle E (2013) Investigation of glutamine metabolism in CHO cells by dynamic metabolic flux analysis, *BMC Proceedings* 7(Suppl 6):P44
- Wahrheit J**, Nicolae A, Heinzle E (2013) ¹³C labeling dynamics of intra- and extracellular metabolites in CHO suspension cells, *BMC Proceedings* 7(Suppl 6):P43
- 2012 Strigun A*, **Wahrheit J***, Niklas J, Heinzle E, Noor F (2012) Doxorubicin increases oxidative metabolism in HL-1 cardiomyocytes as shown by ¹³C- metabolic flux analysis *Toxicological Sciences* 2012 Feb;125(2):595-606.
*geteilte Erstautorenschaft.
- 2011 **Wahrheit J**, Nicolae A, Heinzle E (2011), Eukaryotic metabolism: Measuring compartment fluxes. *Biotechnology Journal* 2011 Sep;6(9):1071-85. (Übersichtsartikel)
- Wahrheit J**, Niklas J, Heinzle E (2011) Evaluation of sampling and quenching procedures for the analysis of intracellular metabolites in CHO suspension cells, *BMC Proceedings* 5(Suppl 8):P82
- Strigun A, **Wahrheit J**, Beckers S, Heinzle E, Noor F (2011), Metabolic profiling using HPLC allows classification of drugs according to their mechanisms of action in HL-1 cardiomyocytes, *Toxicology and Applied Pharmacology* 2011 Apr 15;252(2):183-91

Konferenzbeiträge

Kurzvortrag

- 2013 **Wahrheit J**, Nicolae A, Heinzle E, ^{13}C labeling dynamics of intra- and extracellular metabolites in CHO suspension cells, The European Society for Animal Cell Technology Meeting, Lille

Posterpräsentationen

- 2014 **Wahrheit J**, Nicolae A, Nonnenmacher Y, Heinzle E, Mitochondrial network analysis using high-throughput respiration screening and elementary mode analysis yields detailed information about TCA cycle activities, Conference on Systems Biology of Mammalian Cells, Berlin
- Nicolae A, **Wahrheit J**, Bahnemann J, Zeng A-P, Heinzle E, Non-stationary ^{13}C metabolic flux analysis of Chinese hamster ovary cells in batch culture using extracellular labelling, Conference on Systems Biology of Mammalian Cells, Berlin
- 2013 **Wahrheit J**, Nicolae A, Heinzle E, Investigation of glutamine metabolism in CHO cells by Dynamic Metabolic Flux Analysis, The European Society for Animal Cell Technology Meeting, Lille
- Wahrheit J**, Nicolae A, Heinzle E, ^{13}C -Labeling dynamics of intra- and extracellular metabolites in CHO suspension cells, The European Society for Animal Cell Technology Meeting, Lille
- Wahrheit J**, Heinzle E, Sampling and quenching CHO suspension cells for analysis of intracellular metabolites, The European Society for Animal Cell Technology Meeting, Lille
- 2012 **Wahrheit J**, Nicolae A, Pavanteja T, Heinzle E, High-throughput mitochondrial transport analysis in selectively permeabilized cells, Conference on Systems Biology of Mammalian Cells, Leipzig
- Wahrheit J**, Niklas J, Heinzle E, Comparison of metabolic flux dynamics and compartmental enzyme activities reveals regulatory events in CHO central metabolism, International Conference on Systems Biology, Toronto
- Rajabi N, Bahnemann J, **Wahrheit J**, Heinzle E, Zeng A-P, Müller J, Inertia-based Media Exchange and Quenching of Cells in a Continuous Flow Microfluidic Channel, EMBL Conference Microfluidics, Heidelberg
- Rajabi N, Bahnemann J, **Wahrheit J**, Heinzle E, Zeng A-P, Müller J, Selective eukaryotic cell membrane permeabilization by digitonin in a lab-on-a-chip, Biosensors, Cancun
- 2011 **Wahrheit J**, Niklas J, Heinzle E, Metabolic flux dynamics and compartmental enzyme activities of CHO cells, International Conference on Systems Biology, Mannheim/Heidelberg
- Wahrheit J**, Niklas J., Heinzle E, Evaluation of sampling and quenching procedures for the analysis of intracellular metabolites in CHO suspension cells, The European Society for Animal Cell Technology Meeting, Wien